UNIVERSITÉ DE STRASBOURG

ÉCOLE DOCTORALE de Physique et Chimie- Physique

U1121 Biomatériaux et Bioingénierie

THÈSE présentée par :

Emine BERBER

soutenue le : 21 S**eptembre 2021**

pour obtenir le grade de : **Docteur de l'université de Strasbourg**

Discipline/ Spécialité : Bioingénierie

Effet de la supplémentation par de la matrice extracellulaire de la gelée de Wharton et de l'acide tannique sur des mousses de gélatine poreuse

THÈSE dirigée par :	
M. Florent Meyer	Professeur, Université de Strasbourg
M. Nihal Engin Vrana	Docteur, Sparta Medical
RAPPORTEURS :	
Mme. Halima Kerdjoudj	Professeur, Université de Reims Champagne-Ardenne
M. Christophe A. MARQUETTE	Docteur, Université de Lyon, CNRS
AUTRES MEMBRES DU JURY :	
Mme. Wiebke Drenckhan	Professeure, Université de Strasbourg, CNRS
Mme. Fouzia Boulmedais	Professeure, Université de Strasbourg, ICS
Mme. Juliane Spohn	Docteur, Fraunhofer Institute for Ceramic Technologies and Systems

C'est la douce loi des hommes

De changer l'eau en lumière

Le rêve en réalité

Et les ennemis en frères

Paul Éluard

Dedicated to my mother…

TABLE OF CONTESTS

Acknowledgements

Fistly, I would like to thank Pierre Schaaf and Philippe Lavelle allowed me to complete my thesis in UMRS 1121.

I wish to express my special gratitude to my advisers Florent Meyer and Nihal Engin Vrana for their scientific guidance and continuous support throughout this study.

I am very grateful to Halima Kerdroudj, Celine Schneider and Marie Dubus for MIP and ELISA analysis.

I would like to thank Vincent Ball for his scientific guidance during my thesis study.

I would also want to thank Eric Mathieu for his great deal of effort for the SEM analysis.

I want to thank my colleagues Leyla Kocgozlu, Celine Muller, Gaetan Lutzweiler, Cynthia Calligaro, Dominique Vautier, Helena Knopf Marques, Cosette Betscha, Christine Affolter-zbaraszczuk and Sait Ciftci for their help and support during my thesis study.

I would like to thank the members of my thesis defense committee, Halima Kerdjoudj, Christophe A. Marquette, Wiebke Drenckhan, Juliane Spohn and Fouzia Boulmedais for accepting to evaluate this study.

My warmest thanks to my dear, Victor. Thank you so much McBlay! for being always on my side with your love. And to remind me the beauties of the future waiting for me on the finish line.

And a big thank to my nephew, Sadık, who has just joined us last year. Son, I'm glad you came, just in time, to give me strength, with your two teeth smile.

Finally, but in the first place of my life, I thank to my parents, Yıldız Berber and Hasan Berber for their endless support, trust and love. And my sister Hatice Berber, my brother Şerif Berber, they were always on my side in the ups and downs that involved in this work. I owe my deepest thanks to my family.

List of main abbreviations

BMSCs : Bone Marrow Mesenchymal Stem Cells

CLSM : Confocal Laser Scanning Microscopy

DAPI : 4',6 diamidino-2-phenylindole

ECM. : Extracellular Matrix

FBS. : Fetal Bovine Serum

GAGs. : Glycosaminoglycans

HUCMSCs. : Human umbilical cord mesenchymal stem cells

RP-HPLC: Reverse Phase High Performance Liquid Chromatography

MIP: Mercury Intrusion Porosimetry

MSCs. : Mesenchymal stem cells

SDS PAGE: Sodium dodecyl sulfate polyacrylamide gel electrophoresis

SEM: Scanning electron microscopy

TA: Tannic acid

WJ: Wharton`s Jelly

Résumé français de la thèse

Introduction

L'ingénierie tissulaire est le développement de substituts tissulaires fonctionnels qui peuvent être utilisés pour reconstruire des tissus ou des organes endommagés. Le principal objectif de l'ingénierie tissulaire est de développer des biomatériaux capables d'imiter les caractéristiques essentielles de la matrice extracellulaire (MEC), le microenvironnement tridimensionnel qui entoure les cellules dans les tissus et les organes du corps. Dans ce contexte, la MEC dérivée de tissus humains tels que le placenta et le cordon ombilical pourrait être une source idéale pour la construction de matrices naturelles. La gelée de Wharton (WJ) est un tissu conjonctif présent dans le cordon ombilical. La MEC de ce tissu a montré des effets bénéfiques sur la cicatrisation. Cependant, bien que les échafaudages dérivés de la MEC offrent des réponses régénératrices prometteuses dans de nombreux contextes, leur disponibilité et leurs propriétés mécaniques sont limitées pour façonner ces matrices afin d'obtenir des structures plus robustes et durables. De plus, la composition et la libération de certains composés en fonction des modes de fabrication sont primordiales par leur influence sur les processus cellulaires tels que la différenciation et la migration. Le sujet de cette thèse était donc l'étude de l'interaction entre les protéines et les glycosaminoglycanes de la matrice extracellulaire de la gelée de Wharton avec des mousses de gélatine qui servent de squelette pour former un échafaudage d'ingénierie tissulaire qui serait stable dans les conditions physiologiques dans les délais requis pour la régénération et la croissance cellulaire. Dans cette étude, nous avons développé un échafaudage poreux à base de gélatine complété par des microparticules d'ECM dérivées de WJ ou de l'acide tannique (TA). Dans le cadre de cette thèse, l'échafaudage poreux proposé, complété par des microparticules d'ECM dérivées de WJ, a été évalué pour des études in vitro en réponse à des cellules souches mésenchymateuses de cordon ombilical humain (HUCMSC) et des cellules immunitaires THP-1. Les interactions cellule-échafaudage ont été évaluées par un test de viabilité cellulaire et l'imagerie MEB. L'AT a été incorporé à l'échafaudage de gélatine vierge pour évaluer l'efficacité antimicrobienne et anti-biofilm de la formulation définie contre les bactéries Gram-positives, Staphylococcus aureus. Les échafaudages ont été fabriqués en utilisant la technique de lyophilisation. La transglutaminase microbienne

(TGA) a été utilisée pour réticuler les hydrogels composites et pour adapter leurs propriétés mécaniques. La stabilité des mousses de gélatine vierges réticulées a été évaluée dans des conditions physiologiques et enzymatiques. La taille des pores et l'étendue de la porosité ont été évaluées respectivement par microscopie électronique à balayage (MEB) et par porosimétrie à intrusion de mercure (PIM).

Résultats

Afin de définir la concentration optimale de gélatine, des mousses avec des concentrations variables de gélatine de 1,4, 2,8, 5,6, 11,2 et 16,8 % *p/v* ont été examinées pour la morphologie des pores et leur porosité. Par commodité, ces cinq conditions ont été appelées 1,4 %, 2,8 %, 5,6 %, 11,2 % et 16,8 % dans les parties suivantes. La morphologie des pores et l'étendue de la porosité de la même série de mousses ont été évaluées respectivement par microscopie électronique à balayage et par analyse porosimétrique à intrusion de mercure. La figure 1.1 montre les images SEM des mousses de gélatine réticulées par TGA. Les images révèlent que les mousses préparées avec les concentrations de gélatine de 11.2 et 16.8 % ne montrent aucune formation de pore distincte (Fig. 1.1. d et e). Une morphologie poreuse claire a été obtenue avec les mousses aux valeurs de concentration entre 1.4 et 5.6 % (Fig. 1.1 a, b et c). Cependant, la morphologie des pores des mousses à 1.4 et 2.8 % était un mélange de pores irréguliers, elliptiques et sphériques alors que l'échantillon de mousse à 5.6 % a montré une formation de pores plus régulière, presque hexagonale. La mesure du diamètre des pores des mousses à 11.2 et 16.8 % n'a pas été effectuée à partir des images MEB car aucune formation de pores n'a été observée.

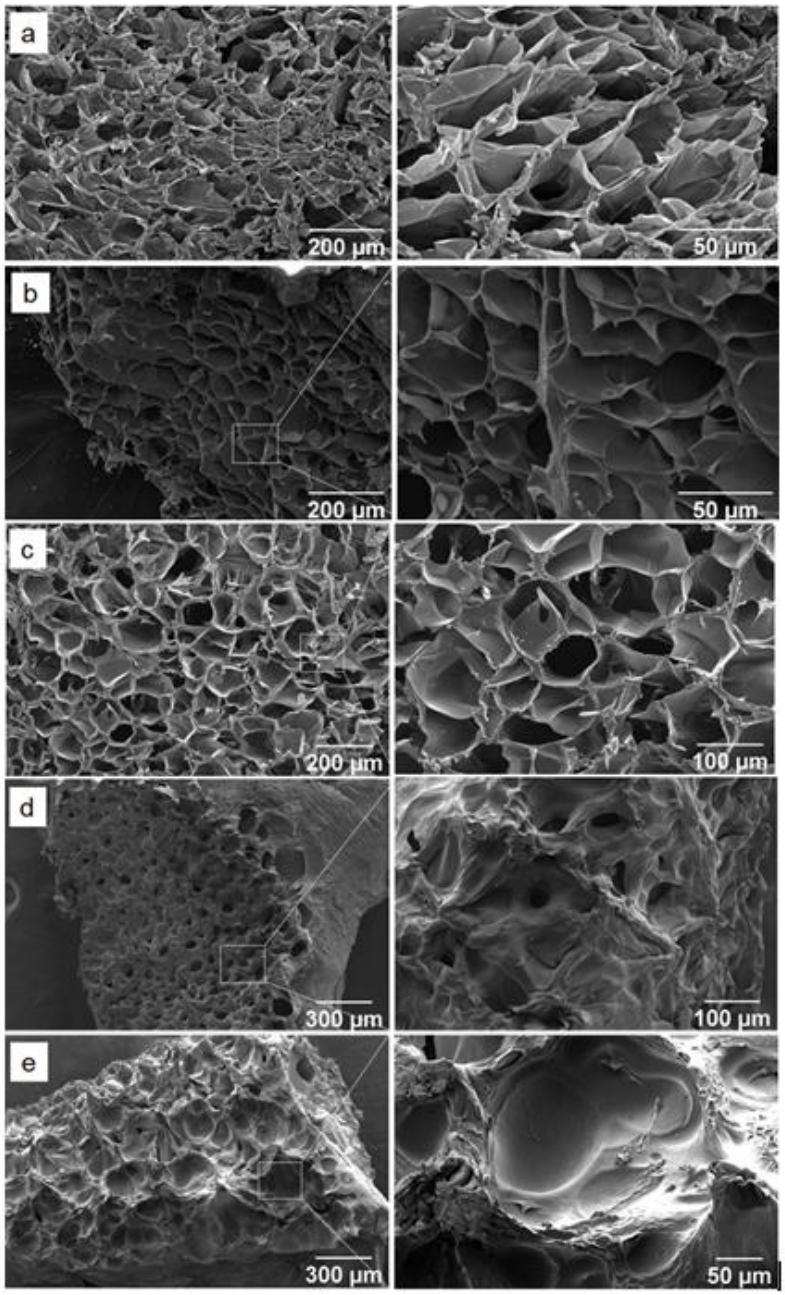

Figure 1.1 Images SEM des mousses de gélatine préparées à des concentrations de 1,4 (a), 2,8 (b), 5,6 (c) 11,2 (d) et 16,8 %.

Le diamètre moyen des pores de la mousse de gélatine à 1,4, 2,8 et 5,6 % a été mesuré à 46,24 ± 36, 45,09 ± 20 et 54,8 ± 27,5 µm respectivement. La porosité de cinq mousses respectives a été évaluée par la méthode de porosimétrie par intrusion de mercure [403]. Les porosités des mousses ont été déterminées à 95,5 %, 93,5 %, 88,8 %, 83,3 % et 69,1 % pour les mousses de gélatine à 1,4, 2,8, 5,6, 11,2 et 16,8 %, respectivement.

La taille des pores du même ensemble d'échantillons a également été examinée par MIP. La figure 1.2a montre le rayon des pores des échafaudages correspondant au pic principal sur la courbe incrémentale. L'augmentation de la concentration de gélatine a entraîné une augmentation de la taille des pores jusqu'à la valeur de concentration de 5,6 %. Au-delà de cette valeur, la taille des pores des échafaudages était négligeable. Les résultats du MIP (figure 1.2b) ont également révélé que l'augmentation de la concentration de gélatine entraîne une réduction de la porosité des échafaudages.

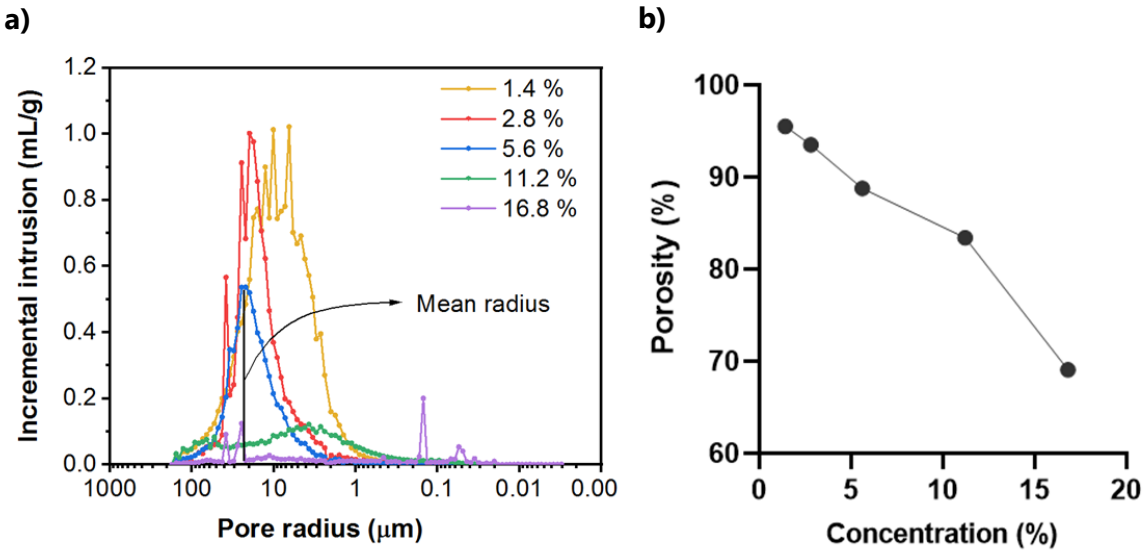

Figure 1.2 a) Rayon des pores MIP des échafaudages correspondant au pic principal sur la courbe incrémentale, b) Porosité des échafaudages obtenus par MIC.

Après avoir déterminé que la concentration optimale de gélatine était de 5,6 % p/v, les mousses non réticulées, réticulées et réticulées/complémentées en TA ont été caractérisées par MEB pour évaluer l'effet de la réticulation TGA et de la supplémentation en TA sur la taille des pores. Les images SEM sont présentées dans la Figure 1.3.

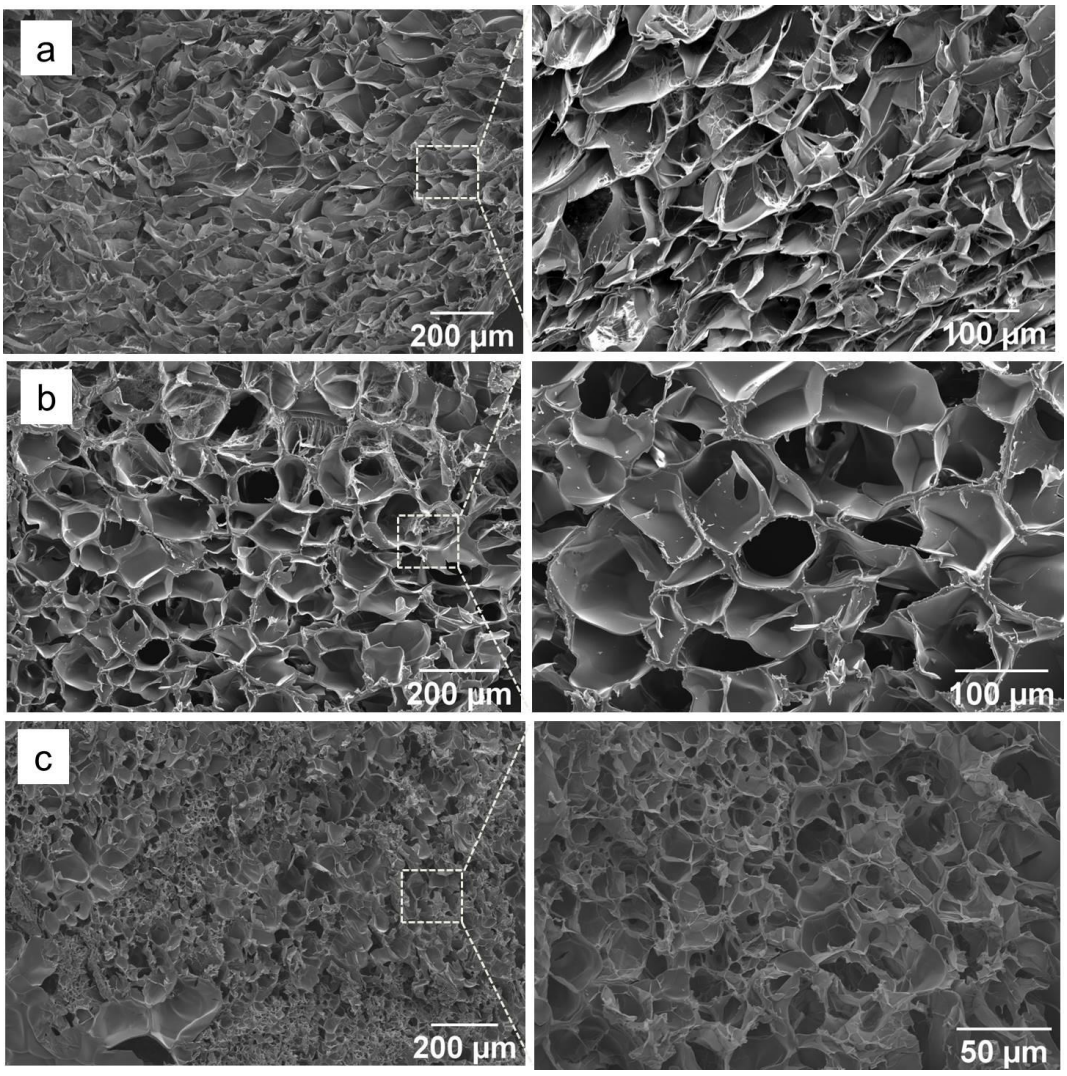

Figure 1.3 Images SEM en coupe transversale de mousses de gélatine à 5,6 % a) non réticulées, b) réticulées et c) réticulées/complémentées en acide tannique à différents grossissements.

La figure 1.4 montre le diagramme en boîte à moustache de chaque traitement obtenu à partir de l'analyse d'image MEB. Les mousses non réticulées, réticulées par TGA et supplémentées en AT présentent des tailles de pores de 70 ± 40.6, 54.8 ± 27.5, et 32.8 ± 25.4 μm, respectivement, et les valeurs montrent des différences significatives. De plus, avec la réduction de la taille des pores entre les groupes, un profil de distribution de taille plus homogène est observé.

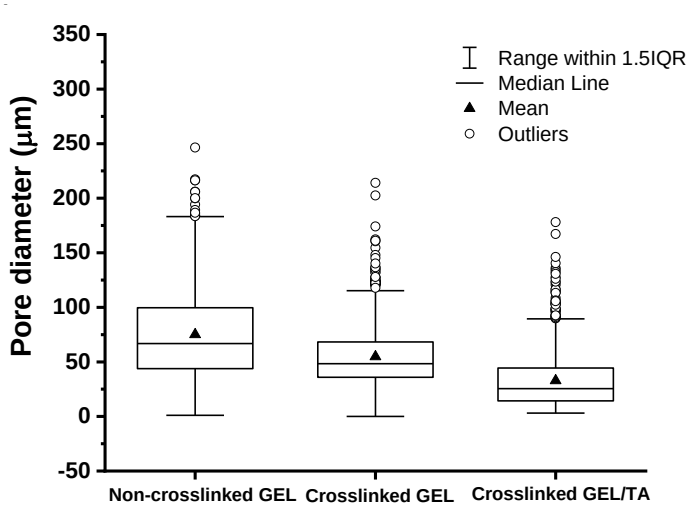

Figure 1.4 Tracé en boîte et moustache (b) de mousses de gélatine non réticulées, réticulées et réticulées/acide tannique à 5,6 %.

Afin d'analyser si la réaction de réticulation entraîne des effets cytotoxiques, les tests de cytotoxicité indirecte ont été examinés selon la norme ISO 10993/5. Le test au bleu d'Alamar a été utilisé pour l'analyse quantitative de la viabilité des HUCMSCs cultivées dans des mousses de gélatine non réticulées et réticulées par TGA et les résultats ont été exprimés en nombre de cellules. La figure 1.5 montre les résultats de cytotoxicité de toutes les mousses de gélatine non réticulées. En l'absence de réticulation, aucun effet cytotoxique n'a été observé et la viabilité cellulaire n'était pas statistiquement différente des conditions de contrôle (Fig 1.5a). La viabilité cellulaire de tous les échafaudages était supérieure à 70% (Fig 1.5b).

Dans un deuxième temps, afin de voir l'effet de la réaction de réticulation TGA sur le comportement cytotoxique des mousses, les mêmes tests ont été effectués après réticulation. La figure 1.6 montre les résultats de cytotoxicité des mousses de gélatine réticulées. Aucun effet cytotoxique n'a été observé jusqu'à une concentration de mousses de 5,6 %. A des concentrations plus élevées de gélatine, une diminution statistiquement significative du nombre de cellules a été observée (Fig. 1.6a), même si elle est restée au-dessus du niveau de cytotoxicité, 70% de viabilité (Fig. 1.6b).

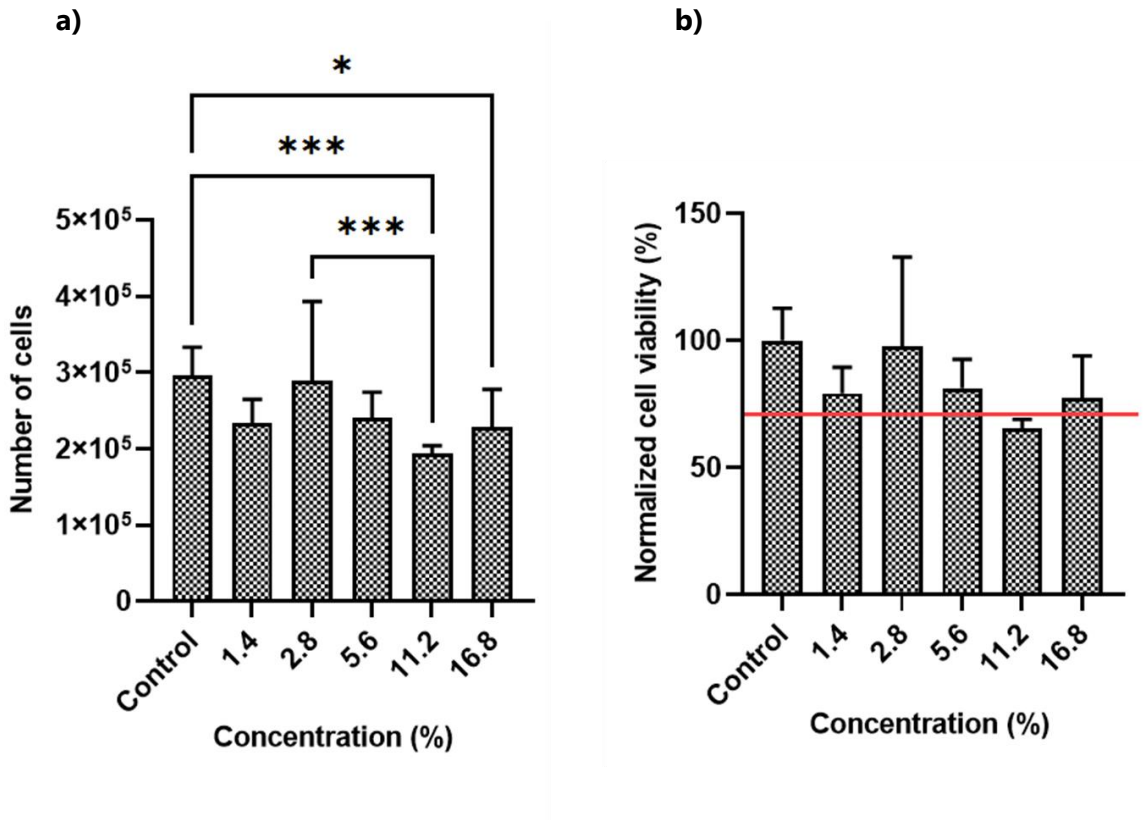

*Figure 1.6 a) Cytotoxicité indirecte des mousses de gélatine réticulées b) Viabilité cellulaire normalisée (*p<0.05, ***p<0.001).*

Afin de voir comment l'acide tannique est libéré du système de mousse et d'établir un lien avec ses propriétés antimicrobiennes, un test de libération a été effectué sur une période de 4 jours. Les résultats sont présentés sous forme de libération cumulée d'acide tannique dans la Figure 1.8 comme (a) la quantité d'acide tannique libéré et (b) le pourcentage d'acide tannique libéré.

Dans la période initiale, variant entre 1 et 24 h, une libération rapide a lieu ; la quantité d'acide tannique libérée est faible, environ 40% du polyphénol incorporé.

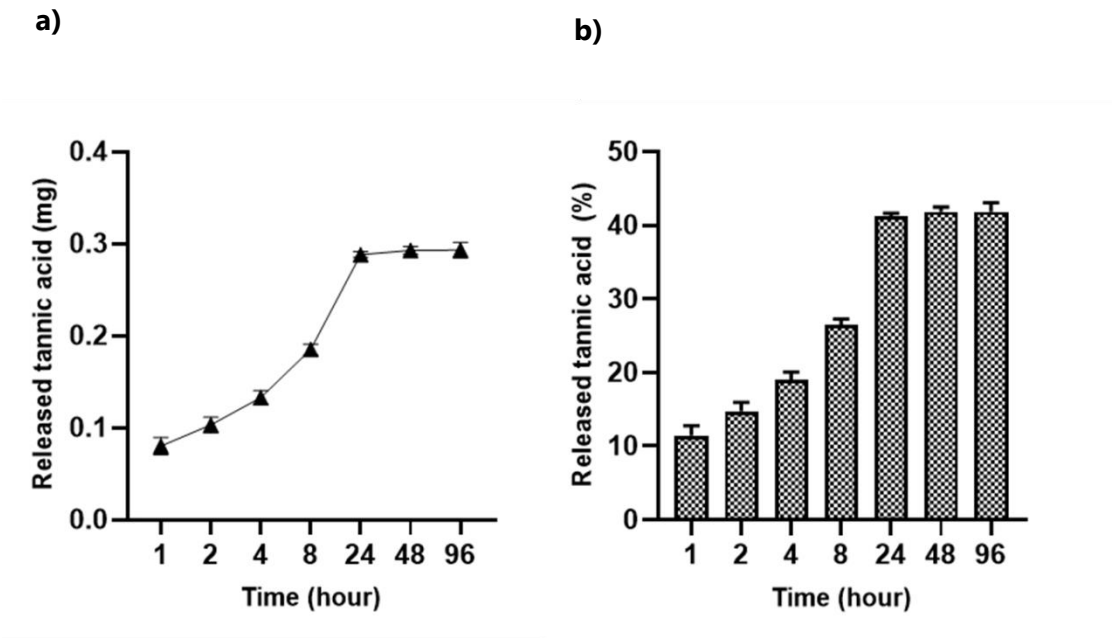

Figure 1.7 a) Libération de l'acide tannique de la mousse de gélatine à 5,6 % au cours du temps : a) quantité et b) pourcentage.

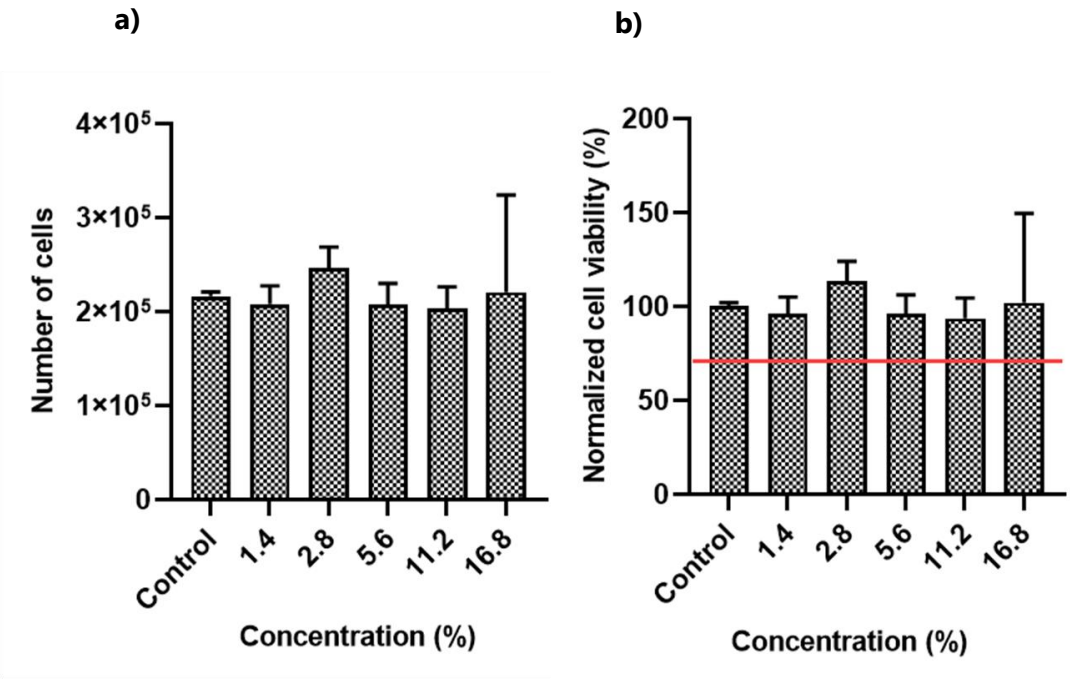

Figure 1.8 a) Cytotoxicité indirecte des mousses de gélatine non réticulées b) Viabilité cellulaire normalisée.

La cytotoxicité des échafaudages en gélatine réticulés par TGA et supplémentés en AT a été testée sur des HUCMSC en suivant le même protocole de test de contact indirect que celui décrit précédemment. Dans ce cas, il a été observé que le premier extrait était cytotoxique, puis des extraits d'échafaudages prélevés à 24 heures d'intervalle ont été utilisés. L'objectif ici est de tester s'il est possible d'atteindre un niveau non cytotoxique en rinçant les mousses. La figure 1.9 montre les résultats sous la forme a) du nombre de cellules et b) de la viabilité cellulaire normalisée pour 3 extractions consécutives pendant 24 heures. Une diminution significative de la viabilité cellulaire, inférieure à 60 %, a été observée pour le milieu extrait des mousses GEL/TA au 1er et au 2ème cycle d'incubation de 24 heures.

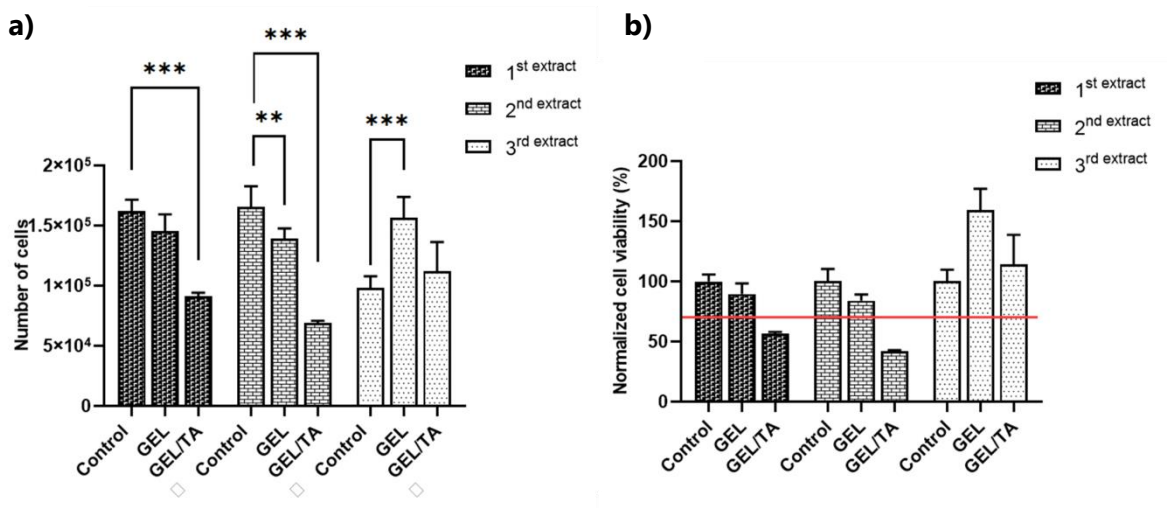

*Figure 1.9 a) Cytotoxicité indirecte des mousses de gélatine supplémentées en acide tannique b) Viabilité cellulaire normalisée. (**p<0.01, ***p<0.001).*

L'activité antimicrobienne *in vitro* des mousses complétées par 5,6 % de TGA réticulé/TA a été évaluée contre une bactérie Gram-positive, *S. aureus*, en utilisant le test du nombre de cellules viables. La croissance de *S. aureus* a été évaluée en présence de la mousse enrichie en TA. La mousse réticulée TGA a été utilisée comme contrôle négatif et la Tetracycline/Cefotaxime a été utilisée comme contrôle positif en contact avec la mousse réticulée TGA. La figure 1.10 montre la croissance normalisée de *S. aureus* après 24h. L'efficacité d'inhibition de la mousse supplémentée en AT a été observée autour de 70 %.

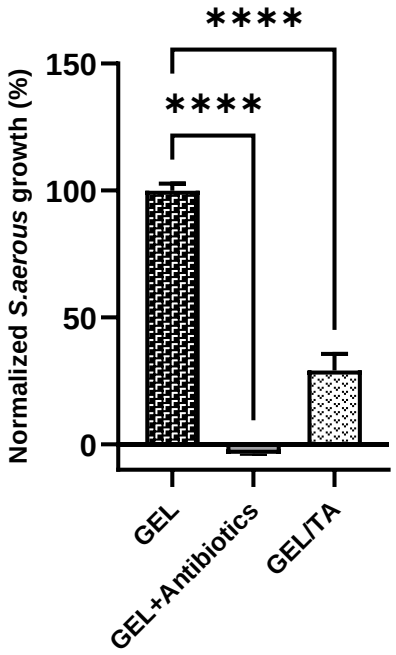

*Figure 1.10 Croissance normalisée de S. aureus sur une mousse de gélatine supplémentée en acide tannique (****p<0,0001).*

Trois méthodes différentes ont été utilisées pour produire une forme particulaire de WJ. La figure 1.11 montre les images MEB de fragments de gelée de Wharton lyophilisés après dissociation, pulvérisation et broyage et la distribution de la taille des particules. Les échantillons dissociés avaient une morphologie de type fibrille et la taille des fragments était d'environ 1 mm. Comparativement à la méthode de dissociation, les méthodes de pulvérisation et de broyage ont généré des particules plus petites. De plus, les particules broyées avaient une distribution de taille plus uniforme avec un maximum de 370 μm. Par conséquent, les particules produites par la méthode de broyage ont été utilisées pour des examens ultérieurs.

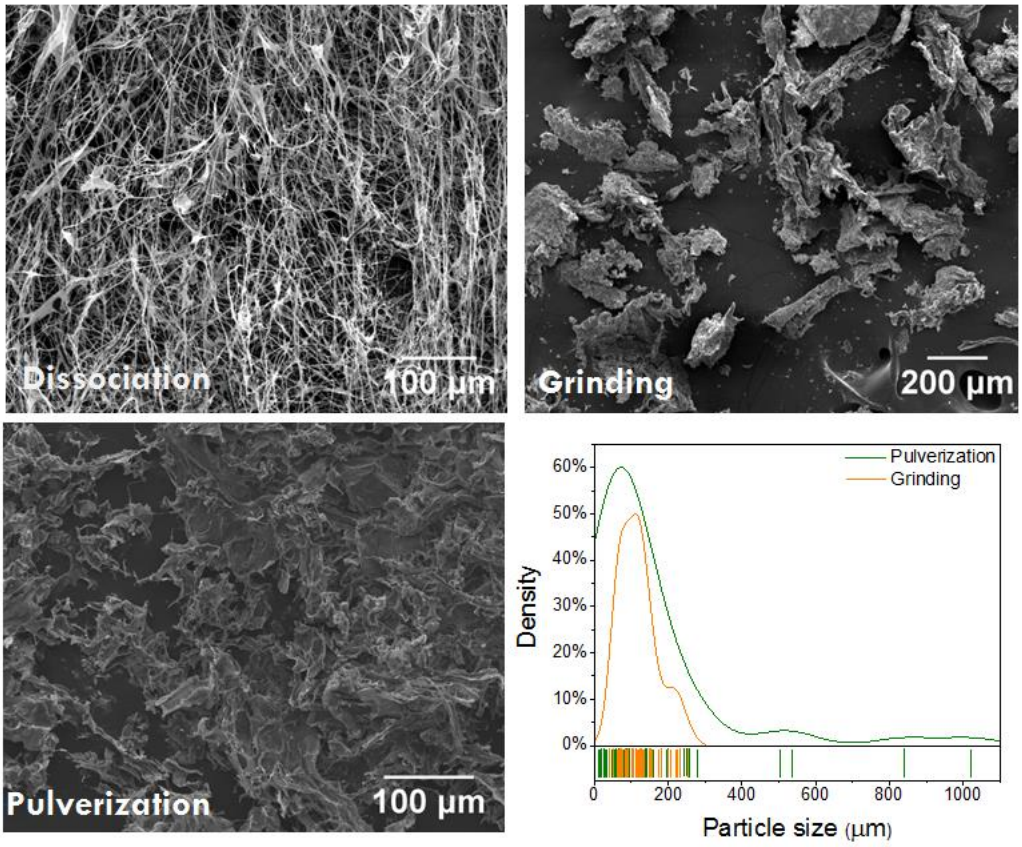

Figure 1.11 Images SEM des particules obtenues par dissociation, pulvérisation, méthode de broyage et distribution granulométrique des échantillons pulvérisés et broyés.

Après avoir défini la taille optimale des particules, les particules broyées ont été ajoutées aux échafaudages de gélatine. La figure 1.12 montre les images MEB des échafaudages de gélatine enrichis de particules Wj. Les particules étaient attachées autour et à l'intérieur des pores et la taille des particules observée sur l'échafaudage était cohérente avec la distribution de taille des particules observée précédemment, indiquant que les particules ont maintenu leur phase dispersée pendant la lyophilisation.

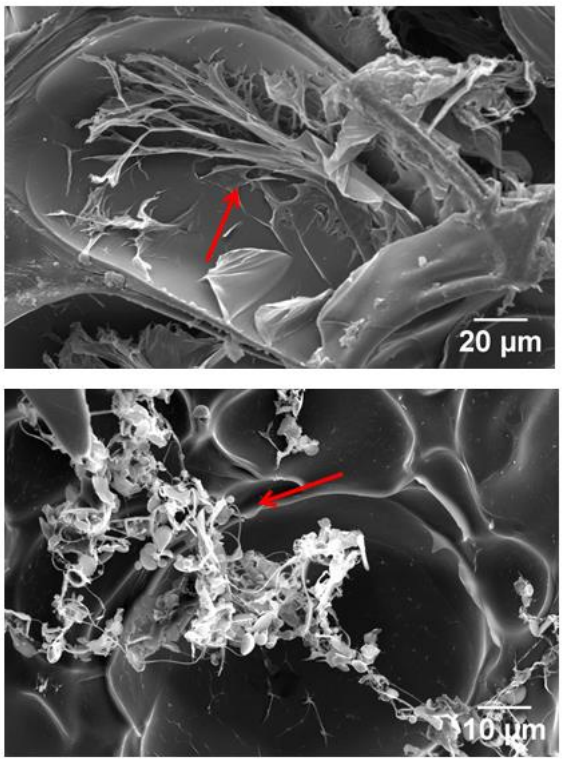

Figure 1.12 Images SEM de l'échafaudage complété par des microparticules de WJ. Les particules de WJ sont attachées et distribuées autour de l'échafaudage, (les flèches indiquent les microparticules de WJ).

Dans une dernière étape, les échafaudages de gélatine et de gélatine/WJ ont été évalués *in vitro* pour la réponse immunitaire et la réponse des cellules souches. La figure 1.13a montre l'activité métabolique de macrophage (lignée de Thp-1) sur la période de 1, 4, 6 jours. Tout d'abord, compte tenu du nombre de cellules ensemencées sur les échafaudages, qui était d'environ 100 000/échafaudage, les cellules restantes détectées au jour 1 étaient nettement inférieures, ce qui peut être attribué à la plus faible affinité des cellules pour les échafaudages. Deuxièmement, comme les macrophages ne se divisent pas, la différence significative au jour 4 entre les groupes peut s'expliquer par la plus faible affinité des macrophages pour les échafaudages en gélatine vierge. La figure 1.13b montre les conditions de culture en 3D des échafaudages ensemencés de macrophages aux jours 1 et 6. En accord avec les résultats du MEB, beaucoup moins de macrophages se sont attachés aux échafaudages de gélatine vierges au jour 1 et au jour 6, l'attachement cellulaire était minimal dans les deux cas.

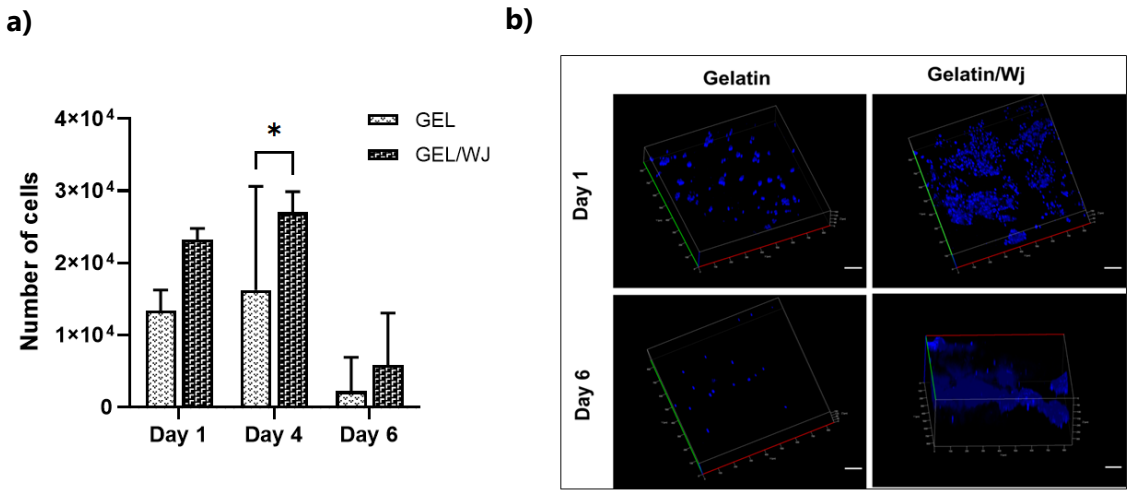

Figure 1.13 a) Activité métabolique des macrophages THP-1 ensemencés sur les échafaudages. b) Conditions de culture 3D des macrophages THP-1 ensemencés sur les échafaudages, (barre d'échelle = 100 µm, p<0.05).*

Les échafaudages ont également été examinés *in vitro* pour la réponse cellulaire afin d'évaluer l'effet du WJ sur la prolifération des HUCMSC. La figure 1.14 a montre l'activité métabolique des cellules à 1, 4 et 6 jours. Après 1 jour de culture, aucune différence significative sur la viabilité des cellules n'a été observée entre les groupes. Au jour 4, une augmentation significative de la viabilité cellulaire a été observée pour les deux types d'échafaudages par rapport au jour 1, indiquant que la matrice supplémentée en WJ a permis aux cellules souches de proliférer au moins autant que l'échafaudage en gélatine vierge. Après 6 jours de culture, aucune différence n'a été observée sur la viabilité cellulaire pour les deux types d'échafaudages par rapport au jour 4. La figure 1.14 b montre les images de microscopie confocale des échafaudages aux jours 1 et 6. Les images ont révélé que l'attachement et la pénétration des cellules étaient plus élevés en présence de microparticules de WJ sur les échafaudages.

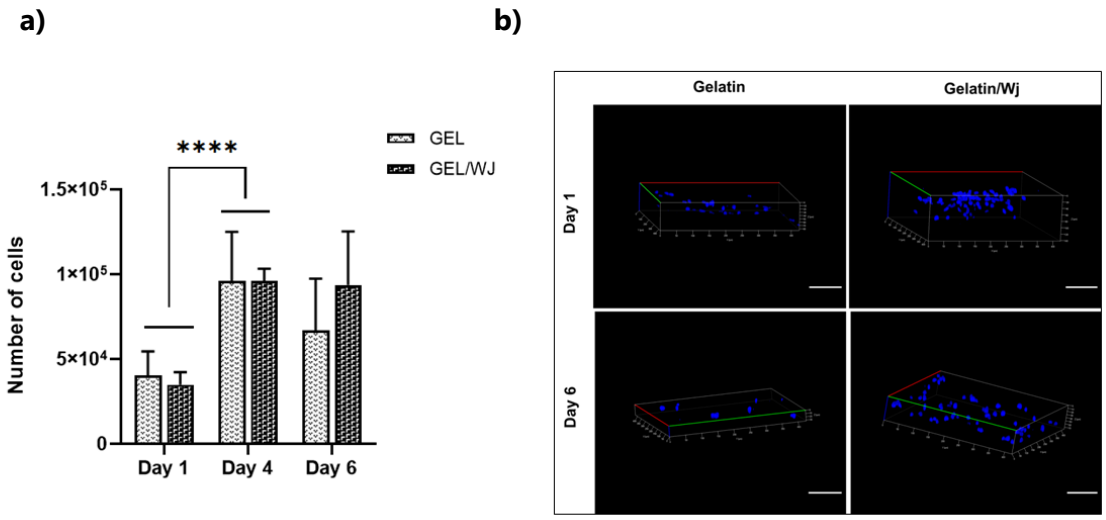

*Figure 1.14 a) Activité métabolique des HUCMSCs ensemencées sur les échafaudages. b) Conditions de culture 3D des HUCMSCs ensemencées sur les échafaudages, (barre d'échelle = 100 µm, ****p<0.0001).*

Conclusion

Dans cette étude, nous avons montré la faisabilité de l'incorporation de microparticules de gelée de Wharton en combinaison avec de la gélatine pour réaliser une matrice poreuse 3D en utilisant la technique de lyophilisation. La taille des pores et la porosité des échafaudages étaient dans une gamme appropriée pour la croissance cellulaire et le remodelage des échafaudages.

La réticulation par la transglutaminase microbienne a permis à la gélatine de se dégrader de manière contrôlée sans perdre sa biocompatibilité. Cependant, l'ajout d'acide tannique a rendu la structure cytotoxique, sans toutefois pouvoir fournir une inhibition bactérienne complète.

La taille des microparticules de gelée de Wharton se situait dans une plage appropriée pour l'induction de la régénération tissulaire. L'échafaudage composite Gélatine/WJ obtenu présentait une dispersion homogène de microparticules de gelée de Wharton et aucune différence significative n'a été observée sur la taille des pores avant et après l'ajout de gelée

de Wharton. La réponse des monocytes THP-1 et des macrophages à l'échafaudage supplémenté en microparticules de gelée de Wharton était minimale, tout comme l'échafaudage vierge en gélatine, ce qui montre que la gelée de Wharton n'a pas d'effet spécifique sur les cellules immunitaires innées. Bien que la supplémentation en microparticules de gelée de Wharton n'ait pas eu d'effet significatif sur la prolifération des HUCMSC, on a observé que la pénétration des cellules était améliorée en présence de gelée de Wharton. Sur la base des résultats présentés, les deux matrices composites, la gélatine supplémentée en microparticules de gelée de Wharton et la gélatine supplémentée en acide tannique, pourraient être évaluées pour la conception de nouveaux échafaudages qui répondent aux caractéristiques antimicrobiennes et biocompatibles pour les applications d'ingénierie des tissus mous.

Liste des publications

1. Muller C.; **Berber E**, Lutzweiler G.; Ersen O.; Bahri M.; Lavalle P. ; Ball V. ; Vrana N.E.; Barthes J. Polyarginine decorated Polydopamine nanoparticles with antimicrobial properties for functionalisation of hydrogels, 2020. 8(982).

2. Reitzer F.; **Berber E**.; Halgand J.; Ball V.; Meyer F. Use of Gelatin as Tannic Acid Carrier for Its Sustained Local Delivery. Pharmaceutical Frontiers, 2020. 2(1): p. e200002.

3. Gokyer S.; Yilgor E.; Yilgor I.; **Berber E**.; Vrana N.E.; Orhan K.; Monsef Y.A.; Oto C.; Yilgor Huri P Novel 3D Printed Biodegradable Polyurethane-Urea Elastomer Recapitulate Skeletal Muscle Structure and Function. Submitted to ACS Biomaterials Science & Engineering, Revised 01.10.2021.

Introduction

Tissue engineering is the development of functional tissue substitutes that can be used for reconstructing damaged tissues or organs. The main focus in the field of tissue engineering is to develop biomaterials that able to mimic critical features of the extracellular matrix (ECM), the three-dimensional microenvironment surrounding cells in the tissues and organs of the body. In this context, ECM derived from human tissue such as placenta and umbilical cord could be an ideal source for the construction of natural matrices. Wharton's jelly (WJ) is a connective tissue found in the umbilical cord. The ECM of this tissue has shown beneficial effects in healing. However, despite ECM derived scaffolds offer promising regenerative responses in many settings it is limited in availability and mechanical properties for shaping such matrices to obtain more robust and long-lasting structures. In addition, composition and the release of certain compounds as a function of the modes of fabrication are primordial by their influence on the cellular processes such as differentiation and migration. The subject of this thesis was therefore the investigation of the interaction between the proteins and glycosaminoglycans of the Wharton jelly extracellular matrix with gelatin foams which acts as a backbone to form a tissue engineering scaffold that would be stable in the physiological conditions within the timeframe required for regeneration and cellular in-growth. In this study, we developed a gelatin based porous scaffold supplemented with WJ derived ECM micro-particles or Tannic acid (TA). Within the scope of the thesis study, proposed porous scaffold supplemented with WJ derived ECM micro-particles was assessed for *in vitro* studies in response to Human umbilical cord mesenchymal stem cells (HUCMSCs) and THP-1 immune cells. Cell-scaffold interactions have been assessed by cell viability assay and SEM imaging. TA was incorporated to the blank gelatin scaffold for the assessment of antimicrobial and anti-biofilm efficiency of defined formulation against Gram-positive bacteria, *Staphylococcus aureus*. Scaffolds were fabricated by using freeze-drying technique. Microbial transglutaminase (TGA) was used to crosslink the composite hydrogels and to tailor their mechanical properties. Stability of crosslinked blank gelatin foams were evaluated in physiological and enzymatic conditions. Pore size and the extent

of the porosity were evaluated by Scanning electron microscopy (SEM) and Mercury intrusion porosimetry (MIP) analysis, respectively.

Structurally, this thesis study consists of four chapters. *Chapter 1* presents a general introduction to the basic concepts of tissue engineering and background information based on the fundamental aspects of the field of tissue engineering. *Chapter 2* describes the detailed experimental stages of the study. In *Chapter 3,* results of the study were given and discussed. *Chapter 4* presents the conclusion and the outlook of the study.

CHAPTER 1

GENERAL INTRODUCTION

1.1 Tissue engineering: Definition and clinical need

Tissue engineering is the development of functional tissue substitutes that can be used for reconstructing damaged tissues or organs**.** In 1993, Langer and Vacanti defined tissue engineering as "an interdisciplinary field that applies the principles of engineering and life sciences toward the development of biological substitutes that restore, maintain, or improve tissue function or a whole organ" [1]. In human body, there are tissues with limited repair/regeneration capability, therefore the loss or failure of an organ or tissue is posing a major healthcare challenge. Currently used treatments are based on the use of auto/allografts or xenografts, implantable materials or surgical repair [2]. However, each of these solutions has some inconveniences. Harvesting of autografts is expensive, painful and moving tissue from one position to another position causes abnormal tissue interactions in new location and donor site morbidity. For example, diversion of urine to colon can induce fatal colon cancer after 20-30 years. Similarly, producing oesophageal tubes from skin can let the formation of skin tumors 30 years later [3]. Transplantation from one individual to another (allograft), although lifesaving, it has severe constraints. The major limitation is donor organ shortage. The number of patients waiting for organ transplantation over exceeds the number of donors available. According to the report of the Organ Procurement and Transplantation (OPTN) and U.S. Scientific Registry of Transplant Recipients (SRTR), there were 112, 568 patients waiting for organ transplantation and 19,267 donors available in the United States, in 2019 [4]. Besides, need for immunosuppression to avoid the rejection of transplanted tissue causing the transmission of infections or diseases from the donor to patient, limit the impact of transplantation. Major problems also exist with the use of implantable materials such as dislodgment or migration of implanted material, infection at the tissue/material interface and fracture in long term [3].

In this context, there is a growing need for new therapeutic solutions and tissue engineering is emerging as a significant potential alternative. The idea behind the tissue engineering approach was if the cells are cultured under appropriate reactor conditions in three dimensions, they could be able to organize into tissues and eventually organs [5]. In this sense, general aspect of tissue engineering is the use of biomaterial based scaffolds that accurately mimic the *in vivo* extracellular matrix (ECM) providing the encapsulation of

cells and bioactive molecules, to regenerate functional tissue. Figure 1.1 illustrates the general steps of tissue engineering methodology. First, cells are isolated from the patient and expanded *in vitro*. Then, proliferated cells are seeded on the scaffold and cultured under static cell culture conditions or dynamic bioreactor systems such as perfusion [6], rotating-wall vessel [7] or spinning-flask reactors [8] to provide the necessary transport conditions for cell growth. In the final step, engineered tissue or organ is transplanted back into the patient.

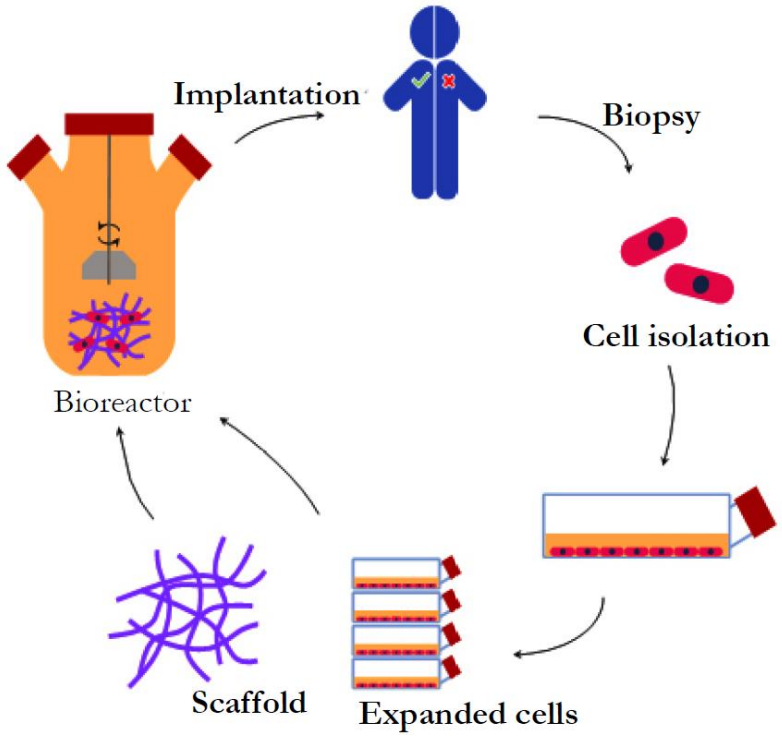

Figure 1.1 General steps of tissue engineering: Cells are isolated from the patient and expanded in vitro. Proliferated cells are seeded on the scaffold and cultured. In the final step, engineered tissue or organ is transplanted back into the patient (Fortunata et al., 2017).

Therefore, from a clinical perspective, a great number of patients can be treated with a small tissue supply by expanding the isolated cells to a considerable mass. To date, a significant progress has been achieved in the field of tissue engineering. Developed tissue constructs have been used successfully in patients in the areas of skin [10], bone [11], bladder[12] and airway [13]. For example, Interpore's (Irvine, CA) Pro-Osteon coral-derived bone graft material was introduced in 1993. Then, in 1996 Integra's (Plainsboro, NJ) Artificial Skin was approved for as an in vivo tissue regeneration product [2].

The basic premise of tissue engineering is to combine the appropriate cells with the appropriate materials under the conditions that permit the tissue formation. Accordingly, tissue engineering research is based on the combination of three fundamental components referred as a tissue engineering triad: Scaffolds, cells, and signals (Fig. 1.2).

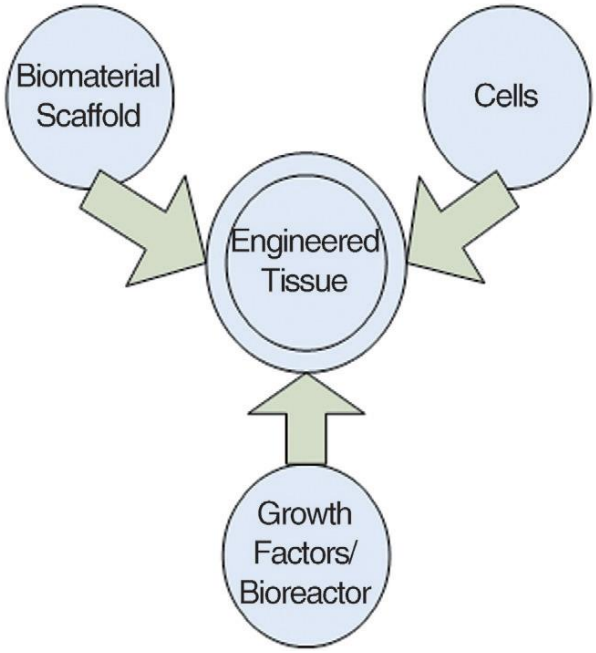

Figure 1.2 Tissue engineering triad: Tissue engineering research is based on the combination of three fundamental components: cells, scaffold and signals (O`Brien et al., 2017).

While the scaffold provides a 3D template for the cells, signals (biochemical or physical stimuli) allow the creation of appropriate chemical and physical environment, by the addition of growth factors or in the form of a bioreactor system respectively [14].

1.2 Scaffolds

Scaffold can be defined as a temporary structure that provides a template for cell adhesion, proliferation, differentiation, extracellular matrix deposition and finally new tissue formation. 3D scaffolds are biocompatible, porous and biodegradable structures manufactured from natural or synthetic biomaterials. These structural properties intend to permit diffusion of nutrients/ waste products, promote cell interaction, viability and extracellular matrix deposition with minimum toxicity while the scaffold is degrading in a certain rate [15]. Accordingly, in consideration of these functional properties, there are some pre-requisites to determine the suitability of a scaffold for use in tissue engineering:

(i) Biocompatibility:

Biocompatibility refers the nature and interaction degree between host tissue and biomaterial [16]. In 1987, biocompatibility was formally defined as ”the ability of a biomaterial to perform with an appropriate host response in the specific application” [17]. It is one of the critical concerns in biomaterial research and thereby in the field of tissue engineering. Tissue engineered construct or its degradation by products must be non-toxic and after implantation, it must not induce a long-term, adverse immune reaction in the body. The host response to an implanted biomaterial in many cases leads to foreign body response. Regardless of the origin (biologic or synthetic), all biomaterials or implantable devices induce an immune response in the body [18]. When the inflammation is not resolved and foreign body response is triggered, the biological process is characterized by chronic inflammation, progressing with the formation of a collagenous, avascular fibrous capsule which is typically 50–200 μm surrounding the foreign material (Fig. 1.3) [19, 20]. Fibrous capsule forms within three to four weeks after implantation, acts as an impenetrable wall and prevent the device-host tissue communication. Depending on the device, long term exposure to chronic inflammation leads to degradation or corrosion of the biomaterial

which induces further immune reaction thus creating a vicious cycle. [21]. Implant longevity significantly depends on the behavior of cells at the material-tissue interface. Following the initial injury, macrophages play an important role in wound healing and cellular response to implants [22]. These macrophages are generally categorized by two distinct polarization states: M1 type macrophages which induces the inflammatory process in the early stage of wound healing and M2 type macrophages which are involved in pro-regenerative processes including cell proliferation and tissue healing [18, 23]. Accordingly, common feature of pro-regenerative biomaterials is that they stimulate macrophages from M1 to M2 polarization state or aid in the resolution of the inflammation around them [24].

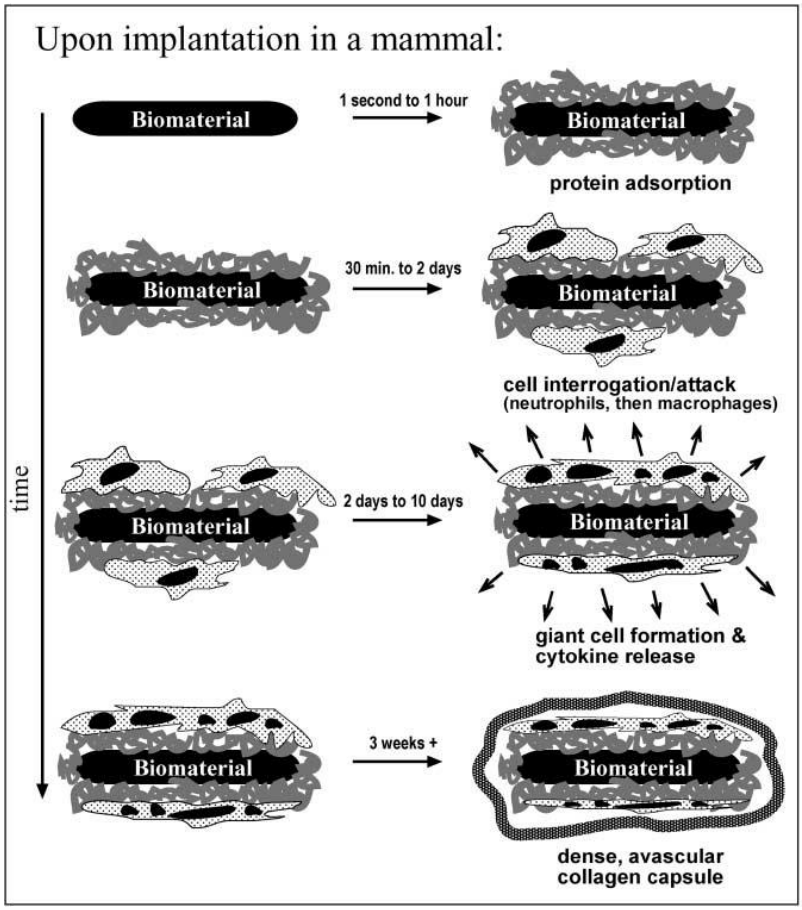

Figure 1.3 Schematic depiction of in vivo foreign body response (FBR): Upon implantation, a biomaterial elicits a nonspecific protein adsorption immediately. A number of different cells adhere to the biomaterial surfaces and lead to upregulation of cytokines and subsequent pro-inflammatory processes. Chronic inflammation at the biomaterial interface ensues and the frustrated macrophages fuse together to form multinucleated foreign body giant cells. At the final stage, device is walled off by an avascular fibrous tissue that is typically 50–200 μm thick (Ratner et. al., 2004).

Form and the surface properties of biomaterial have a critical effect in modulating the foreign body reaction. Buoen *et al*. [25] demonstrated that the same material in solid or porous form heals differently with more blood vessels around the porous material after implantation. Such porous materials with 30–40 micron pores were showed nonfibrotic, vascularized, reconstructive healing properties in skin [26] and cardiac tissue applications [27]. Thus control of the porosity of tissue engineering scaffolds would have a significant effect on their in vivo performance due to the specific immune cell reaction as a function of

pore size. In another study, Sussman *et al.* [28] quantified macrophage polarity to compare the foreign body response at the sites of subcutaneously implanted hydrogel scaffolds with non-porous, 34 μm and 160 μm pore sizes. Their results showed that 34 μm pore implants show thinner and less dense fibrous capsule formation and mostly cellular pore infiltration revealing a strong pro-healing effect in subcutaneous tissue (Fig. 1.4).

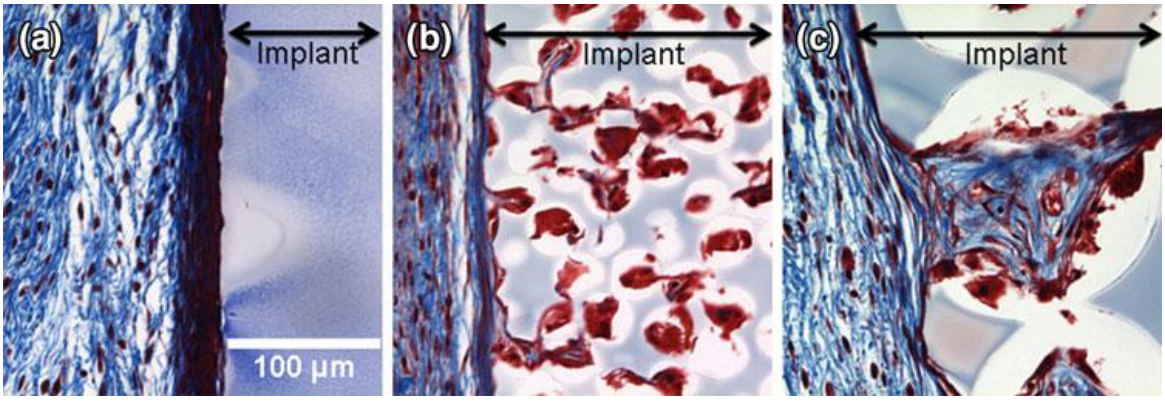

Figure 1.4 Cellular and collagen composition of the foreign body reaction to solid (a) and porous (b) 34 μm (c) 160 μm implants. Implants with 34 μm pore size show thinner and less dense fibrous capsule formation (Sussman et. al., 2013).

On the other hand, B.D. Ratner [29] recently suggested the following equation to quantitatively express biocompatibility:

$$\beta = (\mathrm{A})\left(\frac{1}{\mathrm{C_T}}\right)\left(\frac{1}{\mathrm{C_D}}\right)(\mathrm{M})\left({}^{\mathrm{M_2}}/_{\mathrm{M_1}}\right)(\mathrm{O}) \tag{1.1}$$

where β is the biocompatibility number, A is the blood vessel density or angiogenesis, C_T is the capsule thickness, C_D is the capsule collagen density, M is the number of macrophages, $M_2/\ M_1$ is the ratio of M_2 polarization to M_1 and O represents the other cell types (complex term). This quantification approach might enable the prediction of the implant performance and guide the development of new biomaterials. An in vitro

approximation of this formula based on endothelial cell and macrophage behavior would be a useful tool for biomaterial assessment.

(ii) Biodegradability: The aim of tissue engineering is to permit the body`s own cells and ECM secretion to replace the implanted construct, therefore scaffold must be biodegradable and eventually be eliminated to allow the cells to produce their own extracellular matrix [30]. By definition, biodegradable materials change their chemical and physical form on contact with a biological environment. Biodegradation of polymeric materials involves the cleavage of bonds in the structure hydrolytically (erosion) or enzymatically (biodegradation) leading to polymer degradation [31]. Depending on the type of this degradation process polymeric materials can classified as hydrolytically degradable polymers and enzymatically degradable polymers. Naturally occurring polymers generally undergo enzymatic degradation. The first stage of degradation, cleavage of molecular linkages, results in a decrease in molecular weight, change in morphology and mechanical behavior by conserving the total mass of the polymer [32]. In the second stage of degradation a considerable mass loss occurs when the molecular weight decrease reaches to a point that the chain cleavage produces oligomers which are small enough to be solubilized and diffuse out of from the polymer network. These oligomers are released into the adjoining tissues and thus should be biocompatible [33]. In addition, in vivo degradation rate of polymer has a critical effect on the long-term performance of a cell/scaffold construct. In principle, there must be synchronization of polymer degradation with the new tissue formation. Degradation rate should be as close as possible to tissue growth rate to provide constructive stability during the regeneration process. Figure 1.5 shows the effect of hydrolytic degradation on material appearance [34].

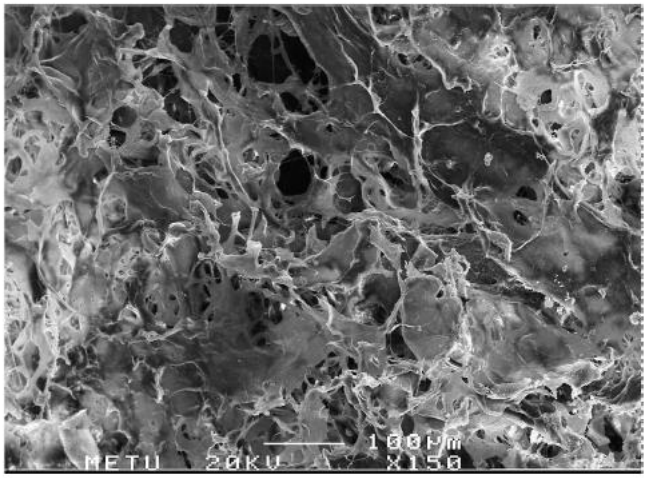

(a)

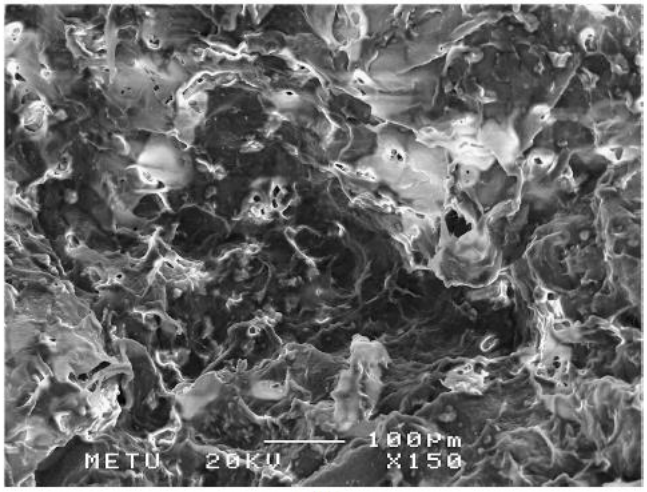

(b)

Figure 1.5 SEM images of Collagen based porous scaffold (a) before and (b) after 4 weeks of hydrolytic degradation. Degradation causes formation of holes and depressions on the foam surface and increase in the pore size (Vrana et al., 2007).

(iii) Mechanical properties

Ideally, a scaffold has to withstand the external forces caused by new tissue formation and maintain the mechanical properties close to the surrounding tissue. In consideration of tissue specific requirement, mechanical properties of scaffold should match the in vivo native tissue. For example, scaffolds designed for bone tissue applications should have comparable resistance to the native bone tissue to withstand physiological loadings and to prevent stress shielding [35]. From the mechanical standpoint, Young's modulus (modulus

of elasticity, E) is the main parameter determining mechanical properties of a tissue engineered scaffold. Young's modulus is a measure of stiffness. Material stiffness for Newtonian solids is defined by a linear relationship between the stress (σ) acting on the surface of a particle and the strain (Ɛ) measured in the same direction as the stress acts. These variables are determined by a uniaxial tensile or compression test [36]. The stiffness of a material is defined by the relationship:

$$E = \frac{\sigma}{\varepsilon} \tag{1.2}$$

where E is Young`s modulus (modulus of elasticity), σ is the uniaxial stress and ε is the strain. For hard and soft tissue application, modulus of the scaffold can range between 10-1500 MPa [37] and 0.4–350 MPa [38] respectively as a function of the target . Specifically, it has been reported that the compressive/tensile strength of human trabecular bone to be around 7-10 MPa/10-20 MPa and 170-193 MPa/50-150 MPa for cortical bone respectively [39]. Apart from the material properties used for scaffold fabrication, the porous architecture of scaffold has a critical effect on mechanical properties of the overall structure. The mechanical properties of the scaffolds are compromised because of the large amount of void volume. Therefore, an optimum balance between mechanical strength and the porosity of the scaffold is another challenge in the field of tissue engineering. The use of materials with high inherent mechanical strength could be a solution to this problem [40].

(iv) Scaffold architecture:

Cell behavior is directly affected by scaffold architecture. Interconnected pore structure and porosity enable cellular penetration and sufficient diffusion of nutrients and waste product in and out of the cellular matrix [41]. Moreover, a porous interconnected structure allows the diffusion of scaffold degradation products out of the body without interference with the surrounding tissues and organs [14]. In thick scaffolds, necrotic cores (the presence of necrotic cells in the central part of the scaffolds), result from lack of vascularization and insufficient waste removal from the center of scaffold, which is a major challenge in the

field of tissue engineering [42, 43]. In addition to porosity, another important component is the mean pore size of the scaffold. Cells predominantly interact with scaffold via ligands (chemical groups) on the surface of the material. Scaffolds fabricated from native extracellular materials such as collagen, inherently possess these ligands such as Arg-Gly-Asp (RGD) binding sequences (Fig. 1.6). However, scaffolds fabricated from synthetic materials require the incorporation of these ligands or the presence of adsorbed proteins and the ligand density is altered by the specific surface area of the scaffold which is available for the adhesion of the cells. And, the surface area is dependent on the mean pore size. Consequently, the pores should be large enough to permit the cell to migrate into the scaffold and eventually bind to the ligands but also small enough to generate high specific surface area providing low ligand density to allow the binding of critical number of cells [10, 44]. Therefore, for each type of scaffold, there is a specific range of pore size and this range may diverge depending on the cell type and tissue being engineered.

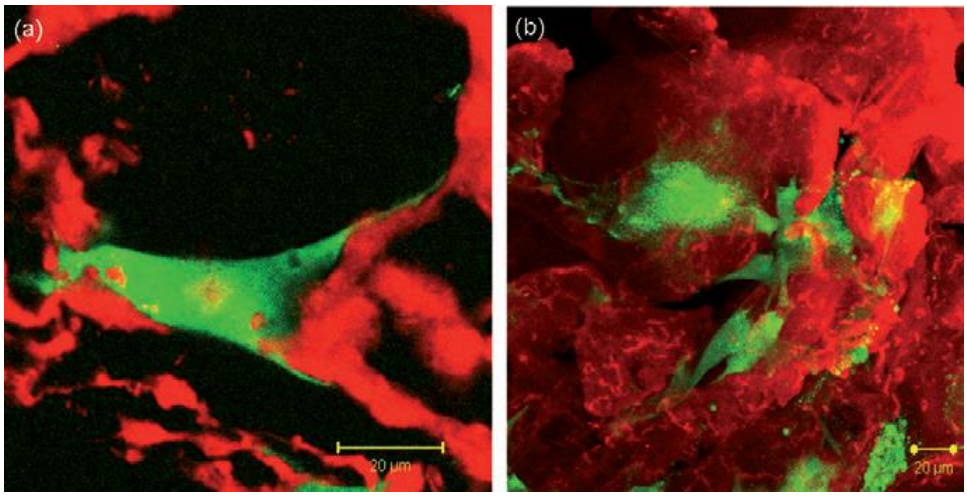

Figure 1.6. Confocal images showing osteoblast cells (green) attached to a highly porous collagen-GAG scaffold (red) (O'Brien et al. 2011).

In bone tissue engineering, there are conflicting reports about the optimum pore size for osteoblast activity. Commonly, scaffolds having pore sizes of 20-1500 µm have been used [45, 46]. In a research by Akay et al [47], osteoblast activity was studied in porous

PolyHIPE polymer (PHP) foam scaffolds, fabricated by high internal phase emulsion (HIPE) polymerization. Three types of foam matrices with pore sizes of 40, 60, 100 µm were studied. Higher osteoblast migration was observed in smallest pore size matrices (40 µm), while the largest pore size matrices (100 µm) demonstrated increased rates of cell penetration depth. Additionally, no significant pore size dependent effect on cell viability or differentiation has been observed for these pore size ranges. In another study, Collagen-glycosaminoglycan scaffolds were used to investigate the effect of pore size on MC3T3-E1 pre-osteoblastic cell line. The results showed that the scaffolds with mean pore sizes larger than 300 µm facilitate the cell proliferation and infiltration. On the other hand, in scaffolds with the mean pore size of 120 µm, an additional early stage peak was observed revealing that the high specific surface area (provided by smaller pores) enhance the initial cell attachment [45].

1.2.1 Porous scaffold fabrication techniques

In the last decade, various porous scaffolds have been developed for tissue engineering and regenerative medicine. Porous network of these scaffolds simulates the native architecture of extracellular matrix allowing cells to interact with their environment. Figure 1.7 represents some examples of porous scaffolds. Foaming approach has several advantages, such as (i) it provides a physical surface allowing the cells to lay their own ECM (ii) may inhibit early cell growth of adherent contact-inhibited cells, (iii) provides efficient nutrient transport to the center of the device through the interconnected porous network, and (iv) can limit the cluster size to the pore size of the foam and thereby prevent the formation of clusters that can potentially develop a necrotic center [48]. A porous surface also serves to facilitate mechanical interlocking between the scaffolds and surrounding tissue to improve the mechanical stability of the implant [49]. Various techniques have been developed for the fabrication of 3D porous scaffolds such as salt leaching, gas forming, phase separation, electrospinning, freeze-drying and particulate leaching. These techniques have been discussed in the following sections.

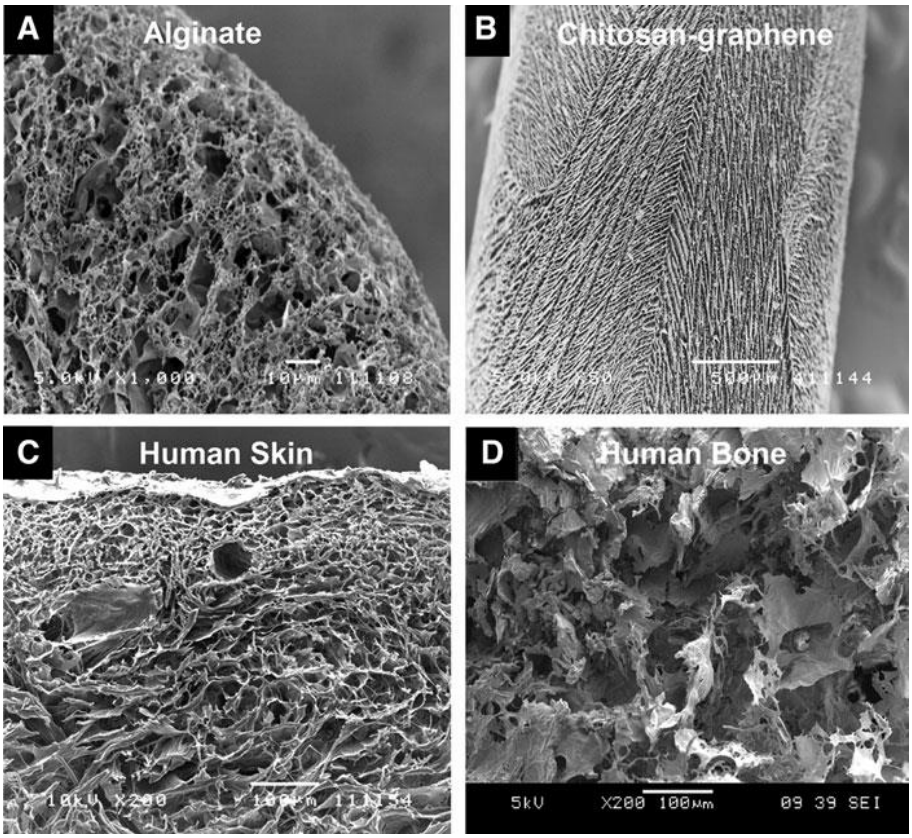

Figure 1.7 SEM images of (A, B) porous scaffolds and (C, D) human tissues with interconnected pores. Tissue engineered scaffolds ideally should mimic the porosity, pore size and function of targeted native human tissue (Loh et. al. 2012).

1.2.1.1 Freeze-drying

Freeze-drying is a technique based on the removal of ice or related frozen solvents from a material by sublimation which is resulted in pore formation. Freeze-drying is processed at temperatures below 0°C and at pressure values lower than the saturation vapor pressure of the ice. Because of the low drying temperature (between -20 °C and -40 °C) biochemical and physiological characteristics of resulted product does not change [51]. Theoretical basis of freeze-drying technique can be explained by a phase–state diagram of water (Fig. 1.8). At atmospheric pressure, the pure water boils at 100 °C. At higher pressure levels, this boiling point is increased. If the pressure is higher than 6.1 hecto Pascal, water passes

through three states (solid → liquid → gas) while the temperature increases and under this point, water passes directly from the solid to the gas state [51].

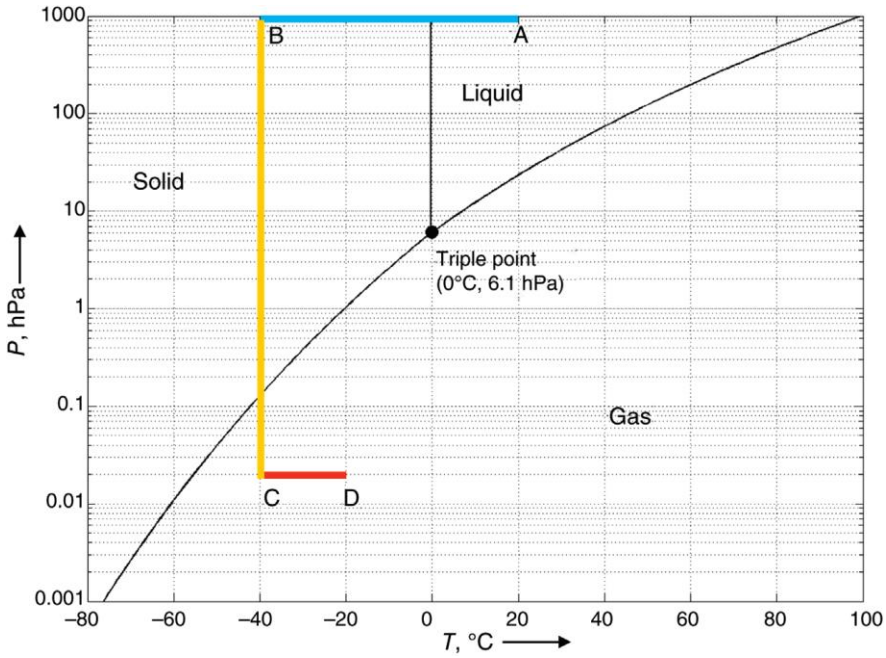

Figure 1.8 Phase diagram of pure water. (A→B) Liquid water freezes into ice, (B→C) drying phase with decrease in pressure, (C→D) increase in temperature enabling the sublimation of ice (Kharaghani et. al., 2017).

Based on this phase diagram, the progress of freeze-drying can be analyzed: AB direction refers the freezing step: temperature is reduced and water passes to the ice state. After freezing, primary drying starts: decrease in the pressure (BC) and increase in temperature (CD) allow the sublimation of ice. After sublimation, secondary drying starts with a gradual increase in the temperature which initiates desorption of the remaining unfrozen water [51]. A typical freeze-dryer consists of four main components: drying chamber, ice condenser, vacuum pump and the compressor (Fig. 1.9).

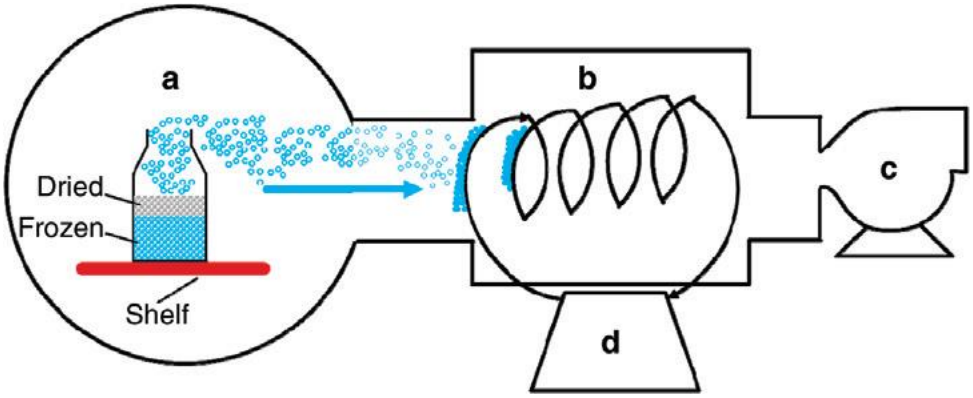

Figure 1.9 Schematic diagram of a typical shelf freeze-dryer: a) drying chamber, b) ice condenser, c) vacuum pump and d) compressor. Shelves are heated to supply latent heat for sublimation. Vacuum pump evacuates non-condensable air from the drying chamber. Ice condenser attracts water vapor from the chamber and compressor cools the ice condenser (Kharaghani et. al., 2017).

Briefly, shelves are heated by conduction to supply latent heat for sublimation. Vacuum pump evacuates non-condensable air from the drying chamber. Ice condenser attracts water vapor from the chamber and compressor cools the ice condenser [51]. Freeze-drying technique was first used by Whang et al. to fabricate polyglycolic acid (PLGA) scaffolds [52] and in the last decades, it has been widely investigated for the fabrication of porous scaffolds for tissue engineering applications. For example, Autissier et. al. [53] developed a freeze-drying/cross-linking process to prepare porous polysaccharide-based (pullulan/dextran) scaffolds. Sodium trimetaphosphate (STMP) was used as a crosslinker and cross-linking process was performed during freeze-drying process on the frozen (-80°C) polysaccharide solutions. Their results revealed that i) crosslinking of bio-macromolecules could be processed during freeze-drying. ii) freeze-drying pressure modulates the pore size and degree of porosity; High freeze-drying pressure (6.5 mbar) leads to smaller porosity and smaller pore formation (33 ± 12%, 55 ± 4 µm), and low pressure (0.1 mbar) resulted in larger porosity and pore formation (68 ± 3%, 243 ± 14 µm). iii). MSCs penetrated deeper (300 µm) into scaffolds with larger pores (Fig. 1.10).

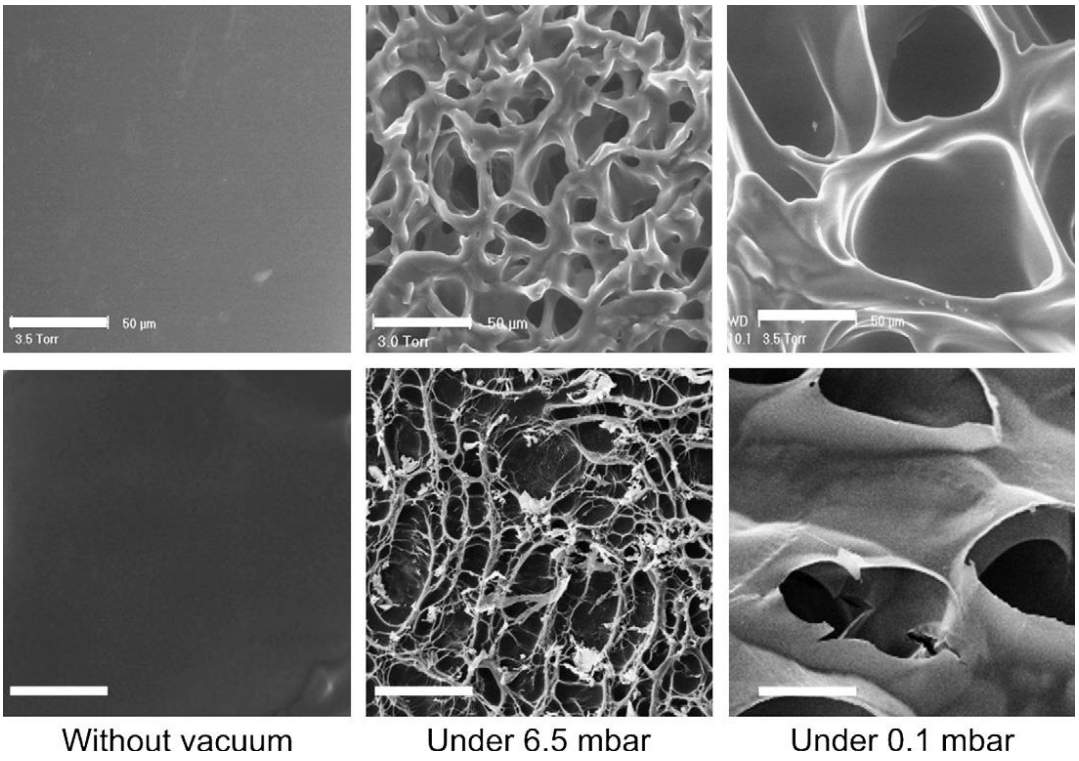

Figure 1.10 ESEM images of hydrated pullulan–dextran polysaccharide scaffolds (top) and SEM images of dehydrated scaffolds (bottom) fabricated under different process conditions. High freeze-drying pressure leads to smaller porosity and smaller pore formation and low pressure resulted in larger porosity and pore formation. Scale bar= 50 µm (Autissier et. al., 2010).

In another study, O'Brien et al.[54] developed a modified freeze-drying technique to obtain more homogeneous type I collagen-glycosaminoglycan (CG) scaffold specified by less variation in mean pore size. In conventional freeze-drying, rapid and uncontrolled quench freezing process (freezing rate: 4.1 °C/min, liquid–solid transition time: 2 min) results in space and time variable heat transfer through the suspension, leading to scaffold heterogeneity. Also, to modulate the heat transfer between the pan and the freeze-dryer shelf, the size of the pan was reduced to increase the pan stiffness and reduce the effects of warping. Their results showed that, freezing rate of 0.9 °C/min (liquid–solid transition time: 10.5 min) resulted in more homogeneous pore size distribution than the conventional quenching protocol (Fig. 1.11) Also, no significant difference in mean pore size was found between the scaffolds processed in reduced pan size.

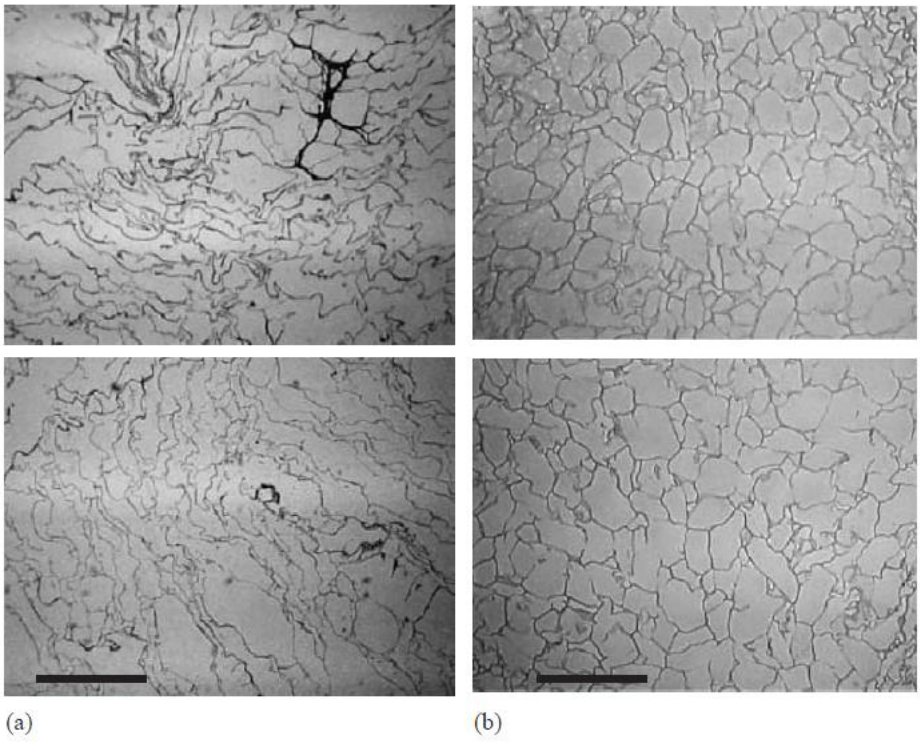

Figure 1.11. Longitudinal images taken via the fixed selection protocol from a single sheet of collagen-glycosaminoglycan scaffold produced using the (a) quenching (4.1 °C/min) and the (b) constant cooling rate technique (0.9 C/min). Decrease in freezing rate results in more homogeneous pore size distribution. Scale bar=300 μm (O'Brien et. al., 2003).

1.2.1.2. Electrospinning

Electrospinning is a technique used for the fabrication of fibers with diameters in nanoscale (<1000 nm) or microscale (>1 μm) range [55]. In electrospinning process, a syringe pump, a high voltage source, and a collector are used (Figure 1.12). Firstly, a high voltage is applied to a capillary tube filled with polymer solution or melt, which is held at the tip of the capillary via surface tension. Secondly, a mutual charge repulsion caused by application of an electrical field is induced within the polymer solution or melt, which directly opposes the surface tension of the polymer solution. When the intensity of the electrical field is increased, the charge repulsion will overcome the surface tension to form a jet. Finally, solvent evaporates to form fibers while the jet travels to the collector. Fibers

in various diameter sizes ranging from nanometers to micrometers can be obtained by adjusting the process parameters such as concentration and flow rate of the solution, , strength of the applied electrical field and tip to collector distance [56] **.** Pham *et al.* [57] demonstrated that the average pore size of electrospun poly(epsilon-caprolactone) scaffolds increased with increasing fiber diameter.

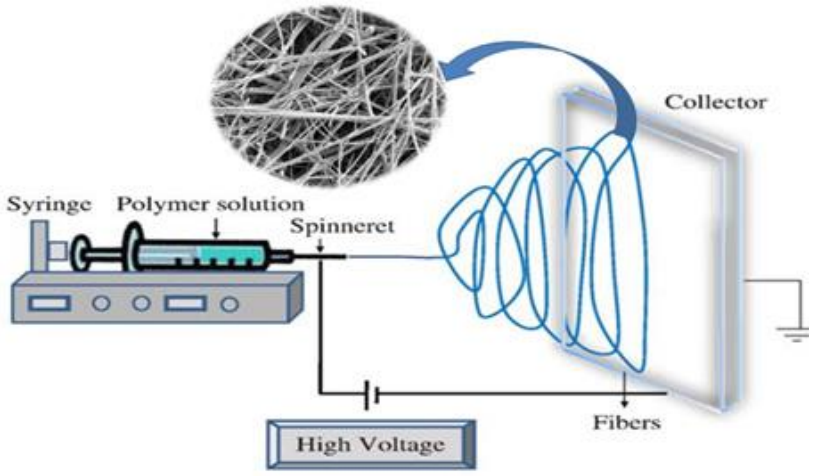

Figure 1.12 Schematic of an electrospinning set-up. A Syringe containing polymer solution connected to a high voltage source and loaded into a syringe pump for controlled flow. When the intensity of the electrical field is increased, the charge repulsion overcomes the surface tension of polymer solution and forms a jet. Finally, solvent evaporates and fibers form in various diameter sizes ranging from nanometers to micrometers (Faki et. al. 2006).

Rho *et al*. [59] developed a biomimetic nano-fibrous, type I collagen scaffold with average fiber diameter of 460 nm and the scaffold was found to enhance cell attachment and proliferation after coating with extracellular matrix proteins (type I collagen or laminin). The main advantage of electrospun scaffolds is that the presence of high surface area for cell attachment and high porosity facilitating the nutrient and waste exchange [60]. In addition, a variety of natural (collagen, silk fibroin, chitosan) and synthetic polymers (polylactic acid, polyglycolic acid, polylactic-co-glycolic acid, polycaprolactone) can be

processed by electrospinning technique [61, 62]. However, the main disadvantage of electrospinning is the involvement of toxic organic solvents to the scaffold that can be harmful for cells. Therefore, melt electrospinning is an alternative to solution electrospinning. In melt electrospinning, instead of using a solvent, polymer is heated above its melting point. However, due to the lower charge density and high viscosity comparing to its solution phase, fibers obtained from melt electrospinning are thinner than the ones obtained from solution electrospinning [63].

1.2.1.3 Porogen leaching

In this technique, pores are generated by the use of a porogen. Porogens are soluble particles such as sugar, salt, wax, paraffin or gelatin [64-67]. Leaching technique was first used by Mikos et al. to fabricate composite scaffolds [68]. During the fabrication process, porogens are blended with a polymer solution and the mixture is casted in a mold. Then, the solution is hardened (via gelation and or polymerization) and the porogen is leached out by dissolution of a porogen specific solvent. After the solvent is removed by evaporation, a porous structure is obtained [69]. Figure 1.13 shows the general steps of porogen leaching. Pore size and porosity can be controlled by modulating the size and quantity of the porogen, respectively [70]. This technique is easy to carry out and able to processed with small amounts of polymer. However, some critical variables such as pore interconnection and pore shape are not controllable. Also, long leaching period, residual porogen contamination and poor mechanical properties constitute the other drawbacks of this technique. To overcome these drawbacks, porogen leaching has been used in combination with other techniques such as freeze-drying [71], compression molding [72, 73] and gas foaming [73].

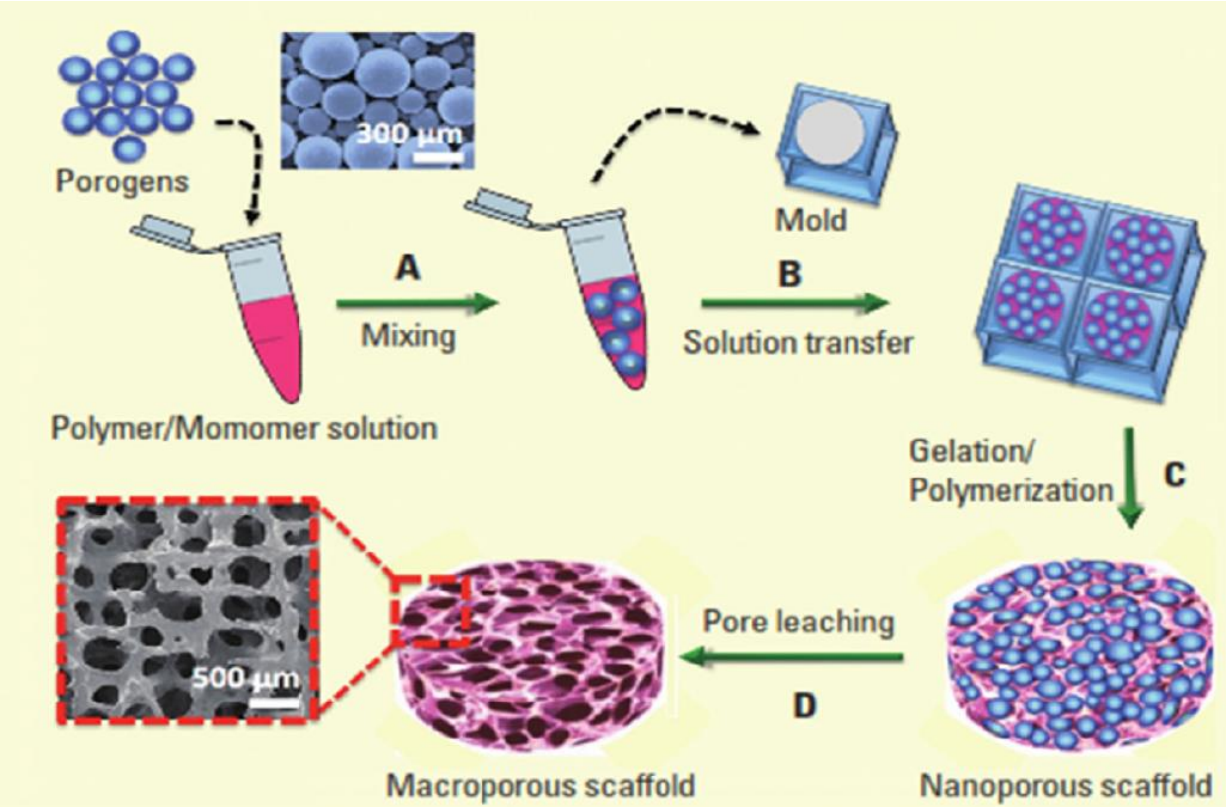

Figure 1.13 Schematic representation of porogen leaching: porogens are blended with a polymer solution and the mixture is casted in a mold. Then, the solution is hardened (via gelation and or polymerization) and the porogen is leached out by dissolution of a porogen specific solvent. After the solvent is removed by evaporation, a porous structure is obtained (Bencherif et al., 2013).

Modaress et. al. [71] developed a gelatin/chitosan porous scaffold through salt leaching/lyophilization (SLL) to improve scaffold pore uniformity and interconnectivity. In addition to the leaching step which provides the formation of pores, lyophilization step was used to facilitate phase separation at the walls of the pore resulted in interconnected pore formation. They compared the efficiency of this combined method with the conventional phase separation method (PS) performed by the lyophilization / crosslinking/ lyophilization of gelatin/chitosan solution. Their results revealed that scaffolds fabricated by SLL method show higher pore uniformity, interconnectivity and surface porosity (Fig. 1.14). Scaffolds with different salt/polymer ratios and salt crystal size, showed a porosity and mean pore size rage of 91–97 % and 94–190 µm respectively.

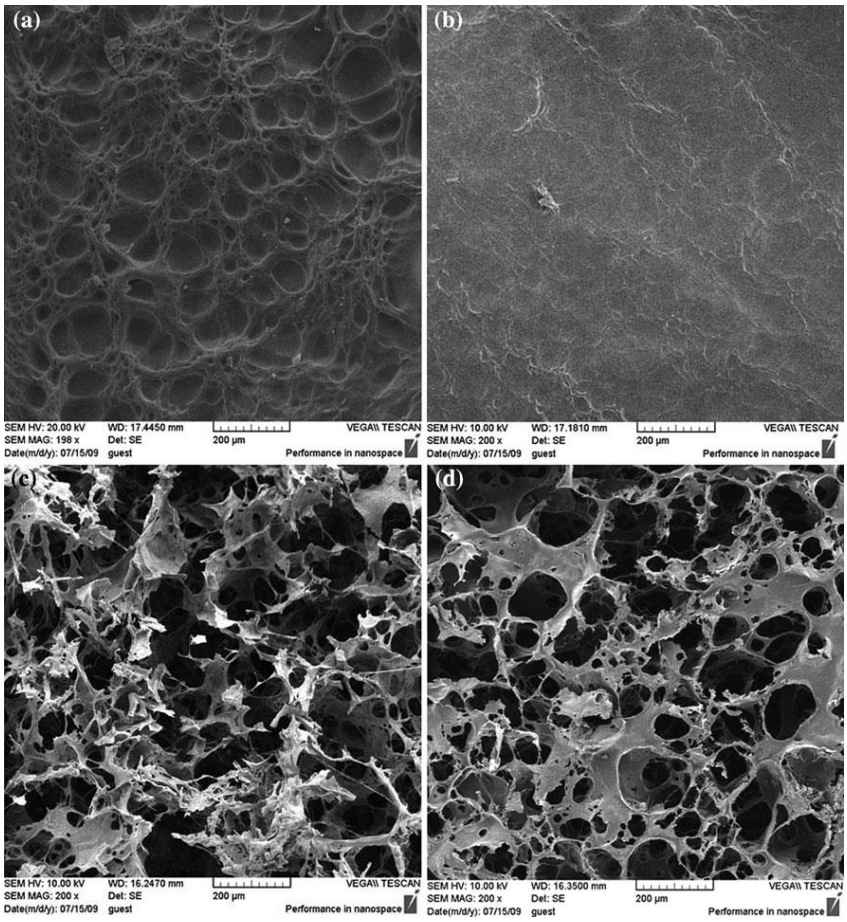

Figure 1.14. Surface morphology of gelatin/chitosan scaffolds fabricated by a) PS: 0.05 g/mL, b) PS: 0.05 g/mL, pre-freezing at -20 °C, c) SLL: prepared using ten times NaCl with particle size 57–150 µm and d) SLL: prepared using five times NaCl with particle size 57–150 µm. SLL method results in higher pore uniformity, interconnectivity and surface porosity (Modaress et. al., 2012).

1.3 Cells for tissue engineering

Tissue engineering generally fall into two strategies: use of acellular matrices, depending on the body's natural ability to regenerate for proper orientation and direction of new tissue growth, and the use of matrices with cells. Acellular tissue matrices are usually prepared by manufacturing artificial scaffolds or by removing cellular components from tissues by mechanical and/or chemical treatments to generate collagen-rich matrices [74, 75]. These matrices tend to slowly degrade on implantation and are generally replaced by the

extracellular matrix (ECM) proteins that are secreted by the growing cells.

In vitro fabrication of a cell-based engineered tissue requires the use of cells to populate matrices and eventually generate the native tissue like matrix. The cell source has an important effect on the success of engineered tissue construct. Cells applicable to tissue engineering can be classified as autologous (patient's own cells), allogenic (cells from another human) and xenogenic (cells from an animal). Autologous cells are primarily preferred because the use of these cells does not cause an immune response following the implantation. Allogenic and xenogenic cells are immunogenic and therefore use of these heterogenous cells requires immunosuppressive therapy [76]. Also, transmission risk of infectious agents such as viruses is the other limitation for the use of xenogenic cells. For instance, after publishment of reports revealing the presence of porcine endogenous retrovirus in pigs, the use of pigs as the cell source has reduced [77]. The main shortcoming associated with the use of autologous cells is the difficulty in harvesting sufficient amount of cells especially in diseased cases or with aged patients [78]. For example, to harvest cells from a patient suffering from myocardial infarction is extremely difficult [76]. If the amount of harvested cells is not enough for clinic application, cells are expanded by cell culture, but this procedure is time consuming and has contamination risk. Furthermore, differentiated primary cells such as chondrocytes often lose their tissue-forming ability in vitro and therefore they are unable to support tissue repair or regeneration [79]. In consideration of these shortcomings, stem cells have become the main cell source for tissue engineering applications by meeting the several cell therapy requirements that differentiated primary cells cannot meet.

1.3.1 Stem cells

A stem cell is defined as an undifferentiated cell that is capable of asymmetrical cell division; generating one differentiated cell type while remaining in the tissue of origin as a stem cell (self-renewal) [80]. Typically, stem cells generate an intermediate cell type before the development of their differentiated state (Fig. 1.15). The intermediate cell is called a

precursor or progenitor cell. These cells are partly differentiated cells that can divide and generate differentiated cells [81].

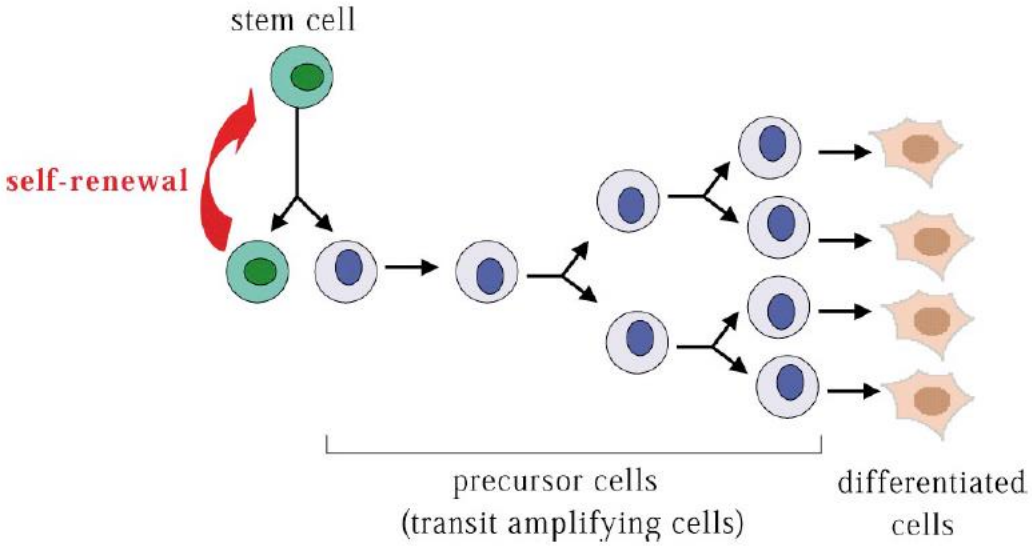

Figure 1.15 Differention pathway of a stem cell: Cell generates one intermediate (precursor) cell while remaining in the tissue of origin as a stem cell (self-renewal). Then, intermediate cells are developed to their differentiated state (Raff et al., 2003).

Stem cells mediate diverse roles in development and tissue repair processes (and also in disease progression in certain cases) in all tissue and organ system of the body. On the basis of differentiation potential, stem cells are classified as totipotent, multipotent, pluripotent and unipotent (Fig. 1.16).

i) Totipotent stem cells: Zygote is the only totipotent stem cell in human body. These cells have the highest differentiation potential and thereby they are able to form whole organism through the process of differentiation. These cells can later develop into any of the three germ layers or form the placenta. After approximately 4 days, the blastocyst's inner cells mass (ICM) become pluripotent. This structure is the source of pluripotent cells [82].

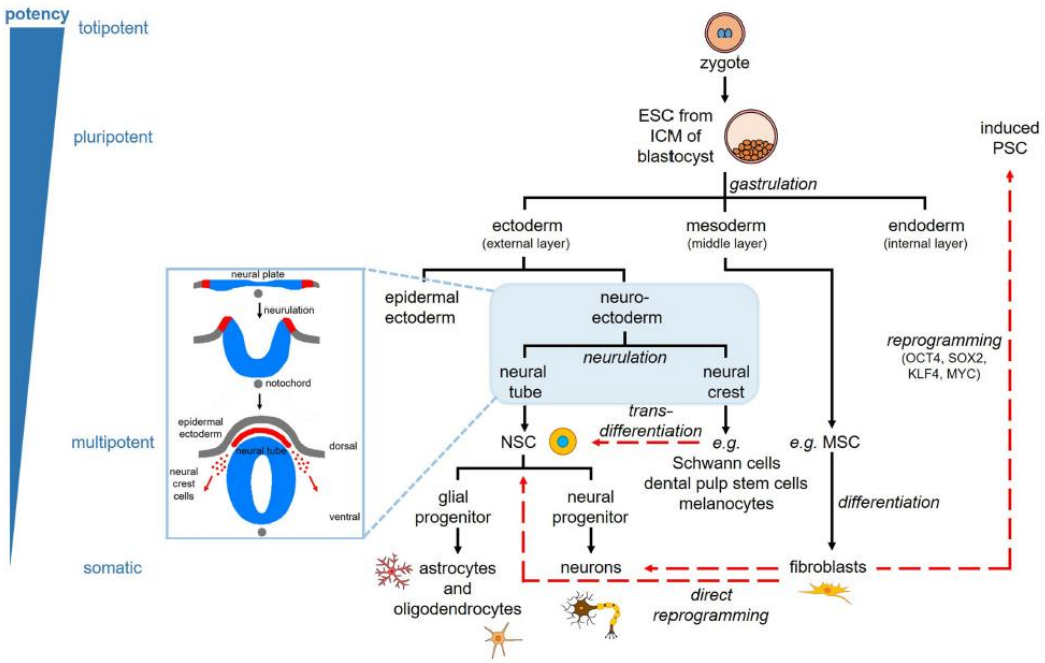

Figure 1.16 Stem cell lineage and reprogramming. Pluripotent embryonic stem cells (ESC) are derived from the inner cell mass (ICM) of the blastocyst. Three germinal layers (ectoderm, mesoderm and endoderm) are specified through the process of gastrulation. Ectoderm generates the nervous system and skin; mesoderm generates blood, bone, muscle and fat; endoderm generates the respiratory, gastrointestinal and urogenital tracts (Gancheva et al., 2019).

ii) Pluripotent stem cells: Cells are described as pluripotent, if they can form all the cell types of the adult organism [84]. Pluripotent cells generate all germ layers except extraembryonic structures, such as placenta. Embryonic stem cells (ESCs) are an example to pluripotent stem cells. ESCs are derived from the inner cell mass (ICM) of pre-implantation embryos. Although pluripotency can occur naturally only in embryonic stem cells, it is possible to induce differentiated cells to become pluripotent again. The process of direct reprogramming converts differentiated somatic cells into iPSC lines that can form all cell types of an organism [82].

iii) Multipotent stem cells: These cells develop into multiple specialized cell types present in a specific tissue or organ. They can form to all cell types of a particular germ layer, but

not all three germ layers, unlike pluripotent cells [82]. The main function of an adult stem cell is to maintain and repair the tissue in which they are found. These cells usually remain quiescent i.e. they do not actively divide nor differentiate. They maintain the stem cell pool and await signals for activation. Most adult stem cells are multipotent stem cells and best exemplified by mesenchymal stem cells (MSCs) [85]. MSCs will be discussed in more detail in section 1.3.1.1 under the title of *Mesencymal Stem Cells (MSC).*

iv) Unipotent stem cells: Unipotent stem cells are characterized by narrowest differentiation capabilities. These cells such as dermatocytes can only generate one type of cell [82].

1.3.1.1. Mesencymal Stem Cells (MSC)

Mesenchymal stem cells (MSCs) are multipotent, self-renewing progenitors that can be differentiated into adipocytes, chondrocytes, and osteocytes. The criteria that identify MSCs was defined by International Society for Cellular Therapy (ISCT) [86]. These criteria describe the MSC as a cell population which possess;

- adherence to plastic: the cells, must be plastic-adherent when cultured under standard culture conditions using tissue culture flask.
- expression/ lack expression of specific markers: 95% of the cell population must express CD105, CD73 and CD90 and lack of expression of HLA class II and hematopoietic markers CD45, CD34, CD14 or CD11b, CD79a or CD19.
- multipotency: the cells must be able to differentiate to chondroblasts, osteoblasts and adipocytes under standard *in vitro* induction conditions.

However, at present, identification of MSCs on specific markers that define the cell types is controversial. New studies have been reported MSCs from various human tissues, which possess the positive expression of CD29, CD44, CD146, CD140b in addition to the earlier

reports mentioned above. Expression of CD34 which is negative for MSCs is also still controversial [87]. Another example of this exception is human amniotic fluid-derived MSCs. These cells are positive for CD29, CD44, CD90, CD105, HLA-ABC (major histocompatibility complex class I) but they are negative for HLA-DR (MHC II) [88]. Also, Stro-1, which is considered as a stemness marker for MSCs was found to be expressed in dental [89] and bone marrow [90] while not to be expressed in adipose derived MSCs [91]. Table 2.1 summarizes hMSC sources and their surface markers basing on current researches.

Table 1.1 *hMSCs sources and their cell surface markers (Repreduced from Ullah et al.,2015)*

Source	Cell surface markers		Ref.
	Positive	Negative	
Bone marrow	CD73,CD90, CD105, STRO-1	CD14, CD34, CD45, HLA-DR	**[92, 93]**
Adipose tissue	CD73, CD090, CD29, CD44, CD71, CD105, CD13, CD166, STRO-1	CD14, CD31, CD34, CD45	**[94]**
Amniotic fluid and membrane	CD29, CD44, CD90, CD105, CD, SH2, SH3, HLA-ABC	CD10, CD14,CD34, HLA-DR	**[95]**
Dental tissue	CD29, CD44, CD90, CD105, STRO-1	CD14, CD34, CD45	**[96]**
Endometrium	CD73, CD90, CD105, CD146	CD34, CD45	**[97]**
Limb bud	CD13, CD29,CD90, CD105, CD106	CD3, CD4, CD14, CD15, CD34, CD45, HLA-DR	**[98]**
Peripheral blood	CD44, CD90, CD105, HLA-ABC	CD45, CD133	**[99]**
Placenta, fetal membrane	CD29, CD73, CD90, CD105	CD34, CD45	**[100]**
Salivary gland	CD13, CD29, CD44, CD90, STRO-1	CD34, CD45	**[101]**
Skin, foreskin	CD44, CD73, CD90, CD105, CD166, SSEA-4, Vimentin	CD34, CD45, HLA-DR	**[102]**
Synovial fluid	CD44, CD90, CD105, CD147, STRO-1	CD31, CD34, CD45, CD106	**[103]**
Wharton`s jelly	CD73, CD90, CD105	CD14, CD34, CD45, CD79, HLA-DR	**[104]**

MSCs are diversely distributed *in vivo* and currently they are able to be isolated from bone marrow (assumed as an efficient population) and the other sources including adipose tissue, amniotic fluid, amniotic membrane, dental tissues, endometrium, limb bud, menstrual blood, peripheral blood, placenta and fetal membrane, salivary gland, skin and foreskin, sub-amniotic umbilical cord lining membrane, synovial fluid and Wharton's jelly [105-107] (Table 1.2). Despite the mentioned classical trilineage differentiation that functionally identifies MSCs, also, MSCs have been shown to be differentiated into ectoderm and endoderm derived cell lineages under specific in vitro conditions [108]. In vitro differentiation of MSCs into different cell linages is induced by incubating a monolayer of cells with various differentiation media.

In general, differentiation of MSCs into chondrocytes, osteocytes and adipocytes is confirmed by the expression of type I and II collagen, formation of mineralized matrices and oil droplets, respectively. Figure 1.17 shows MSCs and their differentiation after exposed to osteogenic, adipogenic and chondrogenic media. According to the first standard protocol for chondrogenesis established by Mackay et al. [109], cells are cultured in insulin transferrin selenium, linoleic acid, selenious acid, pyruvate, ascorbate 2-phosphate, dexamethasone and transforming growth factor-β III (TGF-βIII) supplemented medium. Differentiation of cells resulted in formation of pre-chondrocytes and the expression of type I and type II collagens. In the final stage, pre-chondrocytes differentiate to the mature chondrocytes and express chondrogenic transcription factors such as Sox9, L-Sox5 and Sox6 [110]. Osteogenic differentiation is generally assessed by the use of differentiation medium containing dexamethasone, ascorbic acid and β-glyceralphosphate for 3 weeks. Osteogenic induction of MSCs initiated mineral aggregation and leads to increase in alkaline phosphatase activity at 3th week of differentiation. These mineralized structures are positive for von Kossa and Alizarin red staining [92]. Osteogenesis is initiated by osteoprogenitors which then differentiate into pre-osteocytes and finally into mature osteoblasts. Expression of runt-related transcription factor 2 (Runx2) is the most important indicator of osteogenesis [111]. For adipogenesis, MSCs are cultured in dexamethasone, indomethacine, insulin and isobutyl methyl xanthine supplemented medium for 3 weeks. In addition to the formation of lipid droplets, other indication of adipogenesis is the expression of adipocyte-specific genes such as peroxisome proliferator activated receptor γ (PPARγ).

Initiation of adipogenesis is characterized by two stages: determination and terminal phase. In determination phase, cells are in pre-adipocytes form and presents fibroblast like morphology. In terminal phase, pre-adipocytes become mature adipocytes and express adipocyte specific proteins and begin to accumulate lipid droplets [92]. At the molecular level, induction into one lineage, prevent the MSCs to differentiate to the other linages. A converse relationship between adipogenesis, osteogenesis and chondrogenesis was reported [112, 113]. Expression of PPARγ counteracts expression of Runx2 and Sox9 inhibits Runx2 activation.

As mentioned above, along with the mesodermal differentiation ability, MSCs have the capacity of differentiation into ectodermal lineages. MSCs isolated from various sources have shown differentiation into neuronal specific phenotypes such as oligodendrocytes, cholinergic and dopaminergic neurons under neural induction culture medium supplemented with growth factors [114, 115]. For example, Barzilay et al. [116] demonstrated that the transcription factor neurogenin-1 is efficient in the trans-differentiation of MSCs into neuronal protein expressing cells. In another work, Naghdi et al. [114] showed that β-Mercaptoethanol (BME) and nerve growth factor (NGF) treated MSCs differentiated into cholinergic neuronal cells.

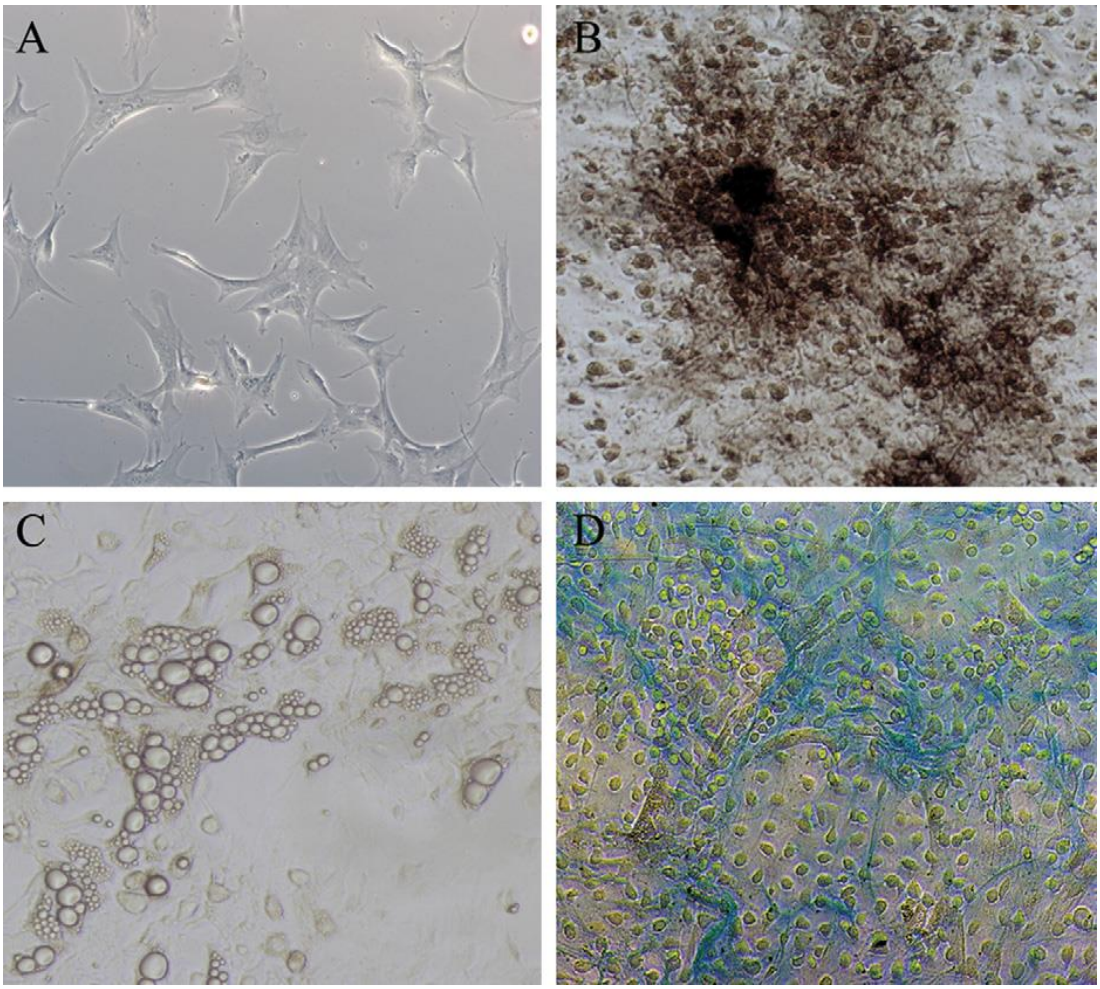

Figure 1.17 Mesenchymal stem cells (MSCs). Differentiation of MSCs into chondrocytes, osteocytes and adipocytes is confirmed by the expression of type I and II collagen, formation of mineralized matrices and oil droplets, respectively. (A) Undifferentiated MSCs grown in monolayer culture, (B) MSCs exposed to osteogenic medium; cells expressed alkaline phosphatase at the 21st day, (C) MSCs exposed to adipogenic medium; lipid droplets can be detected after 2 weeks induction, (D) Chondrocytes observed by Alcian Blue staining, which stains matrix which is secreted by chondrocytes (Chen et al., 2008).

MSCs have also revealed to be able differentiate into endodermal derived linages such as hepatocytes and pancreocytes by the modulation of conditioning media. Lee et al. [117] demonstrated the differentiation of human BM-MSCs and umbilical cord derived blood MSCs into functional hepatocyte-like cells by using two steps protocol defined as differentiation and maturation. In differentiation step, cells were cultured in growth medium supplemented with bFGF (fibroblast growth factor-basic) and nicotinamide for a week. During maturation step, cells were cultured in growth medium supplemented with oncostatin M, dexamethasone and ITS+ (insulin, transferrin, selenium). They confirmed the differentiation of the cells into hepatocyte like cells with the expression of liver specific transcription markers: albumin, α-fetoprotein and nuclear factor 4 α (HNF-4α). In another study, An et al. [118] demonstrated valproic acid (VPA) induces an increase in the expression of hepatic markers HNF-1β (hepatocyte nuclear factor-1 beta), c-MET (hepatocyte growth factor receptor) and FOXA1 (forkhead box A1) in human umbilical cord derived MSCs (hUCMSCs).

Recently, hMSCs derived from adipose, umbilical cord, amnion, Wharton`s jelly, placental and dental tissue have differentiated into pancreatic linage [107, 119]. For example, in a study of Govindasamy et al. [120] dental pulp stem cells (DPSCs) differentiated into pancreatic cell lineage by inducing the conditioning medium with acitvin A, sodium butyrate, taurine and nicotinamide. They confirmed the differentiation as islet-like cell aggregates (ICAs) by using dithiozone-positive staining and by the expression of Isl-1, Pax4, Pax6, Pdx-1, Ngn3 and C- peptide. At day 10, ICAs released insulin and C-peptide, showing *in vitro* functionality of the cells. In another study, Kim et al. [121] differentiated human amniotic mesenchymal stem cells (hAMs) into insulin-secreting cells *in vitro* by using nicotinamide, activin A and glucagonlike peptide-1 containing induction medium and transplanted to immunocompetent mice with type 1 diabetes. Their results revealed that following the transplantation, cells were able to normalize blood glucose level of the mice over the secretion of their own human insulin.

High regeneration ability of MSCs was attributed to the presence of soluble factors secreted by these cells such as transforming growth factor-1, hepatocyte growth factor, stem cell factor, Fms-like tyrosine kinase 3 ligand, interleukin-1 (IL-1), IL-1β, IL-3, IL-6, IL-7 and

IL-11. It is suggested that these soluble factors may stimulate proliferation and differentiation of endogenous stem-like progenitors found in most tissues, decrease inflammatory and immune reactions [122]. MSCs repress many T cell, B cell and NK cell functions, thus they are generally considered to be weakly immunogenic. Additionally, MSCs produce various cytokines, growth factors, proteases and chemokines that are likely modulate their migration and immunomodulatory ability. In this sense, MSCs have been shown to express a narrow pattern of chemokine receptors permitting them to migrate to tissues upon the stimulation of certain chemotactic triggers [123]. Recent studies propose that these cells are selectively migrating to injury/inflammation or tumor microenvironment where they contribute to the tissue repair and tumor-associated stroma formation. Figure 1.18 represents the steps of proposed phenomena.

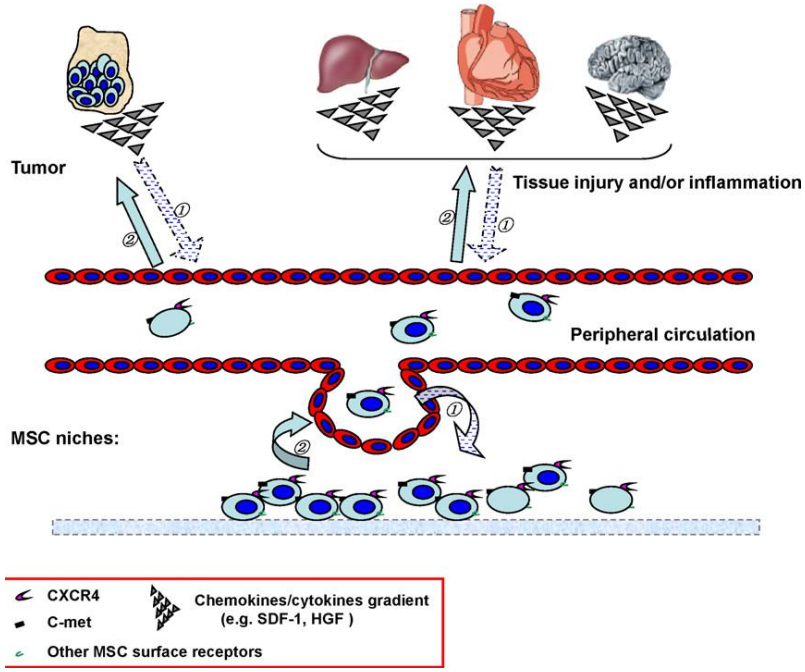

Figure 1.18 Model showing the migration selectivity of MSCs. They contribute to the tissue repair and formation of tumor-associated stroma. (1) Secretion of chemokines/cytokines from injured tissue or tumors (2) Migration of MSCs migrate to the sites of injury/inflammation and tumors (Chen et al., 2008).

Because of their immunomodulatory properties, MSCs have been used in treatment of many human autoimmune disorders such as Alzheimer disease, Because of their immunomodulatory properties, MSCs have been used in treatment of many human autoimmune disorders such as Alzheimer disease, Rheumatoid arthritis and Type 1 diabetes. After the realization of the fact that human BM-MSCs can protect the hematopoietic precursor from inflammatory damage [124], other MSCs such as human cord blood-derived mesenchymal stem cells (CB-MSCs) [125] and adipose-derived mesenchymal stem cells (AD-MSCs) [126].

On the basis of their sources, three types of stem cells exist: embryonic stem cells (ESCs), adult stem cells (ASC) and umbilical cord stem cells (UCSCs). Each type will be discussed in the next sections.

1.3.1.2 Embryonic stem cells (ESCs)

Embryonic stem cells are harvested from the inner cell mass of a blastocyst which forms several days after fertilization [127]. The cells in this line are pluripotent and thereby they are able to differentiate under appropriate culture conditions into the cells of all three embryonic germ layers [128]. ESCs were first isolated from mice in 1981 by Evan et al. [129] and since then, they have been derived from rodents [129, 130], primates [131] and human [132, 133]. Figure 1.19 depicts the isolation steps of ESC.

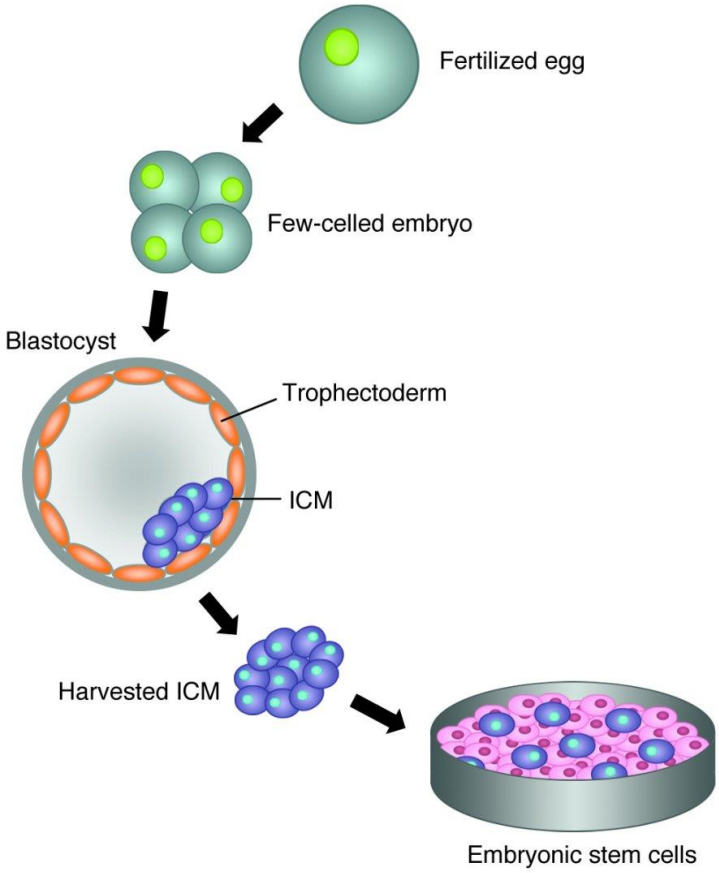

Figure 1.19 Isolation of embryonic stem cells: Following the sperm and egg join, the egg is fertilized and starts to develop. About one week after the fertilization, inner cell mass (ICM) of blastocyst is removed and cultured. By changing the culture conditions, cells can be stimulated to differentiate into various cell types such as skin, skeletal muscle and neural cells (Landry et al. 2004).

Various tissue engineering strategies have been developed for the generation of specialized cell types from ESCs such as keratinocytes [135], osteoblasts [136], chondrocytes [137], endothelial cells [138] , β-islets [139], hepatocytes [140] and corneal epithelia [141]. The common approach for these different strategies is to direct the cells to a pure population of the desired cell types by modulating the culture conditions.

For example, Bielby et al. [142] showed the osteogenic differentiation of human H1 ESC by supplementing the culture medium with ascorbic acid, β-glycerophosphate, and dexamethasone. H1 line was propagated *in vitro* and shown to be pluripotent by expression of the markers Oct-4 and SSEA-4. In vivo efficiency were assessed by implanting the cells into SCID (severe combined immunodeficient) mice on a poly-D, L-lactide (PDLLA) scaffold and the results revealed that the cells had the capacity to generate mineralized tissue *in vivo*. Also, they shown that the culture methodology established for differentiation of murine ESC [143] was totally transferable to human ESC. Hwang et al. studied the chondrogenic differentiation ability of murine ESCs [137]. Embryoid bodies (EBs) encapsulated in poly(ethylene) glycol (PEG) based hydrogel and EBs plated on conventional monolayer were cultured in vitro chondrogenic medium in the presence of transforming growth factor (TGF)-β1 or bone morphogenic protein (BMP)-2. Their results showed that PEG hydrogel culture upregulates the cartilage relevant markers such as aggrecan and type II collagen and induction of chondrocytic phenotype is stimulated by (TGF)-β1. In another study, Baharvand et al. examined the differentiation potential of human ESCs into hepatocytes in 2D and 3D culture systems. Embryoid bodies (EBs) were cultured in a collagen scaffold or on collagen-coated dishes and stimulated with exogenous growth factors to induce hepatic histogenesis. Expression of endodermal and hepatocyte specific markers such as hepatocyte nuclear factor 3β (HNF3β), α-fetoprotein (AFP), albumin (ALB), glucose-6-phosphatase (G6P) and transthyretin (TTR) was observed during ESCs differentiation. Briefly, their results showed that the 3D collagen scaffold culture exhibits earlier and higher expression of ALB, AFP and G6P indicating the differentiation of ESCs into functional hepatocyte-like cells. Also, morphology analysis of differentiated ESCs confirmed the hepatocyte-like ultrastructure specified by glycogon granules, well developed Golgi apparatuses, rough and smooth endoplasmic reticuli and intercellular canaliculi.

However, moral and legal controversies concerning ES cells` use for clinical and therapeutic application, have prompted active examination of the reservoirs of progenitor cells harbored within the adult organism [144].

1.3.1.3 Induced pluripotent stem cells (iPSCs)

Although pluripotency can occur naturally only in ECMs, it is possible to induce differentiated cells to become pluripotent again. Direct reprogramming process converts differentiated somatic cells into iPSC lines that can generate all cell types of an organism (Fig. 1.20) Reprogramming based on the expression of oncogenes such as Myc and Klf4 (Kruppel-like factor 4) and this process is supported by a downregulation of genes promoting genome stability, such as p53 [82]. Also, cell reprogramming involves histone alteration. Since pluripotent cells can propagate indefinitely and differentiate into any kind of cell, they can be an unlimited source for replacing lost or diseased tissues bypassing the need for embryos in stem cell therapy. Because they are made from the patient's own cells, they are autologous and do not generate any risk of immune rejection. At first, fibroblasts were used as a source of iPSCs [145]. Because a biopsy was needed to achieve these types of cells, the technique underwent further research. Researchers investigated if more accessible cells could be used in the method. Further, other cells were used in the process: peripheral blood cells, keratinocytes, and renal epithelial cells found in urine. An alternative strategy to stem cell transplantation can be stimulating a patient's endogenous stem cells to divide or differentiate, occurring naturally when skin wounds are healing. In 2008, pancreatic exocrine cells were shown to be reprogrammed to functional, insulin-producing beta cells [146]. Limitation of iPSC is potential mutagenic risk and later lead to an increased number of mutations. However, in human iPSCs teratoma formation rate was observed to be elevated compared to hESCs [147]. Teratomas are benign tumours. They are capable of rapid growth in vivo and are able to develop into tissues of all three germ layers simultaneously [148]. This difference is connected to different differentiation methods and cell origins.

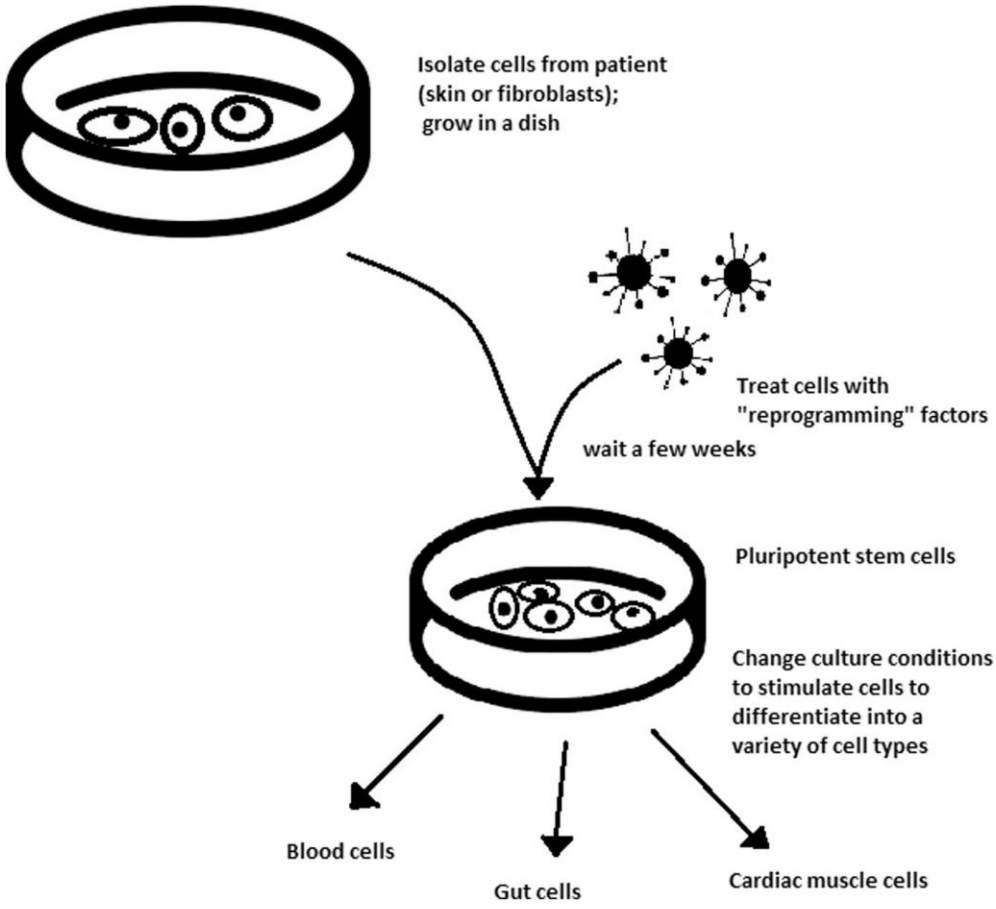

Figure 1.20 Induced pluripotency in isolated patient somatic cells. Target cells lose their role as somatic cells and once again, become pluripotent and can differentiate into any cell type of human body (Zakrzewski1 et al. 2019).

1.3.1.3 Adult stem cells (ASCs)

Adult stem cells (also known as somatic or tissue stem cells) are a rare population of undifferentiated cells, located in a differentiated organ, in a specialized structure, called niche which maintain the local microenvironments to regulate the growth and development of stem cells [149]. The adult stem cells have the capacity to self-renew themselves, and they can be differentiated into a limited number of mature cell types [150]. For example, skin stem cells can only produce different cell types of the skin, but not nerve or blood cells. ASCs are normally maintained in a quiescent state, but, upon the loss of cells or

injury, they are activated to proliferate and differentiate into the required type of cells to promote the tissue repair [151].

ASCs were first identified in the 1960 when it was realized that the bone marrow stroma and blood have cells which can treat the bone marrow failure in humans and animals [152]. Subsequently, the presence of adult stem cells in a broad majority of adult tissues was recognized including muscle [153], subcutaneous adipose tissue [154], articular cartilage [155], synovium [156], trabecular bone [157], the gastrointestinal (GI) tract [158] nervous tissue [159], periosteum [160], infrapatellar fat pad [161]. Figure 1.21 shows the locations of ASCs [150].

1.3.1.4 Bone marrow stem cells (BMSCs)

Bone marrow stem cells (BMSCs) are the first adult stem cells identified [162]. In the bone marrow, there is approximately one stem cell for every 100 000 bone marrow cells [163] and cell populations derived from bone marrow are heterogeneous mix of subpopulations including bone marrow hematopoietic stem cells (BMHSCs), mesenchymal stem cells (BMMSCs) [164] and endothelial progenitor cells [165]. BMHSCs generate the three class of circulating blood cells: thrombocytes (platelets), erythrocytes (red blood cells) and leukocytes (white blood cells. Human BM-HSCs express CD34 antigen, however, it has limited use for the isolation of cells when used alone, as it is also expressed on hematopoietic and non-hematopoietic progenitors [166]. Hence, these cells extensively have been used in direct therapy, for instance for the replacement of the bone marrow system following the radiation treatment causing the destruction of bone marrow [150].

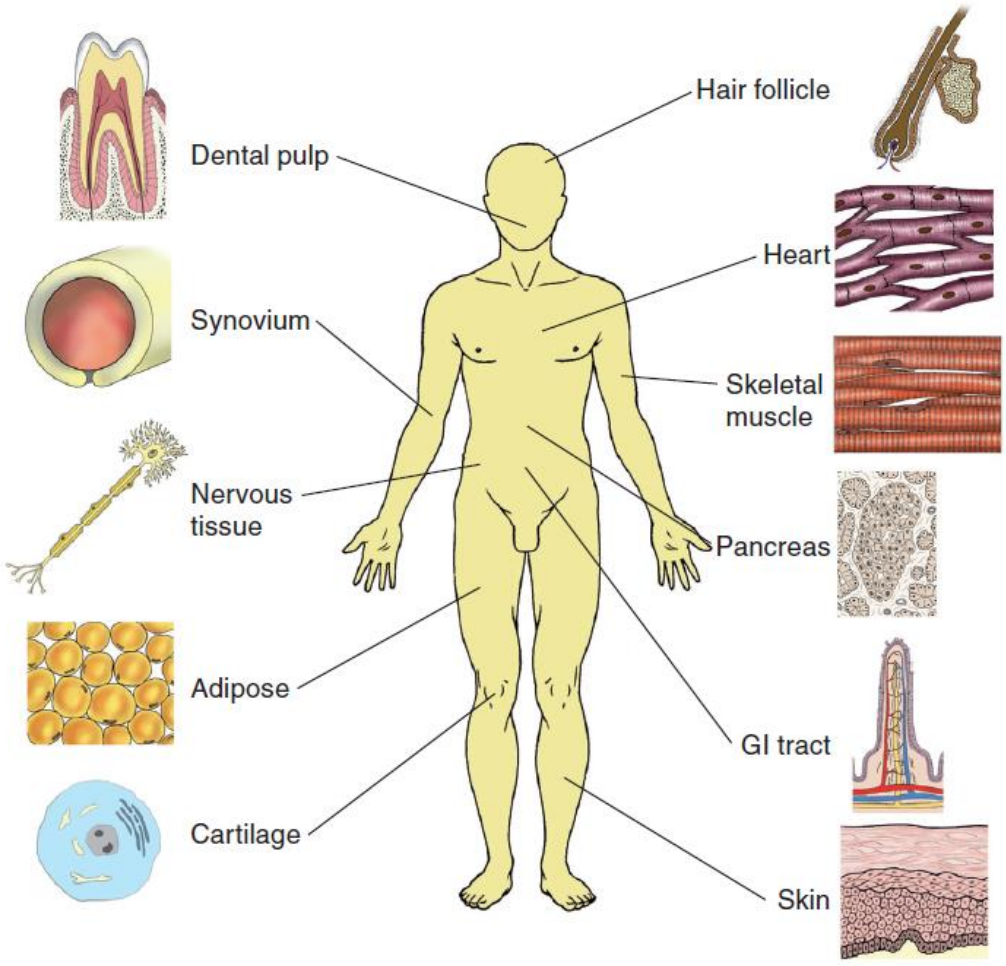

Figure 1.21 Selected locations of human adult stem cell populations (Hodgkinson et al., 2009)

BMMSCs are able to generate several distinct phenotypic lineages including chondrogenic, osteogenic, tenogenic, adipogenic and myogenic *in vitro* by the alteration of culture conditions (Fig. 2.22) [167]. BMMSCs have been used for the *in vitro* fabrication of bone, particularly via bioreactor technology and porous 3D scaffolds.

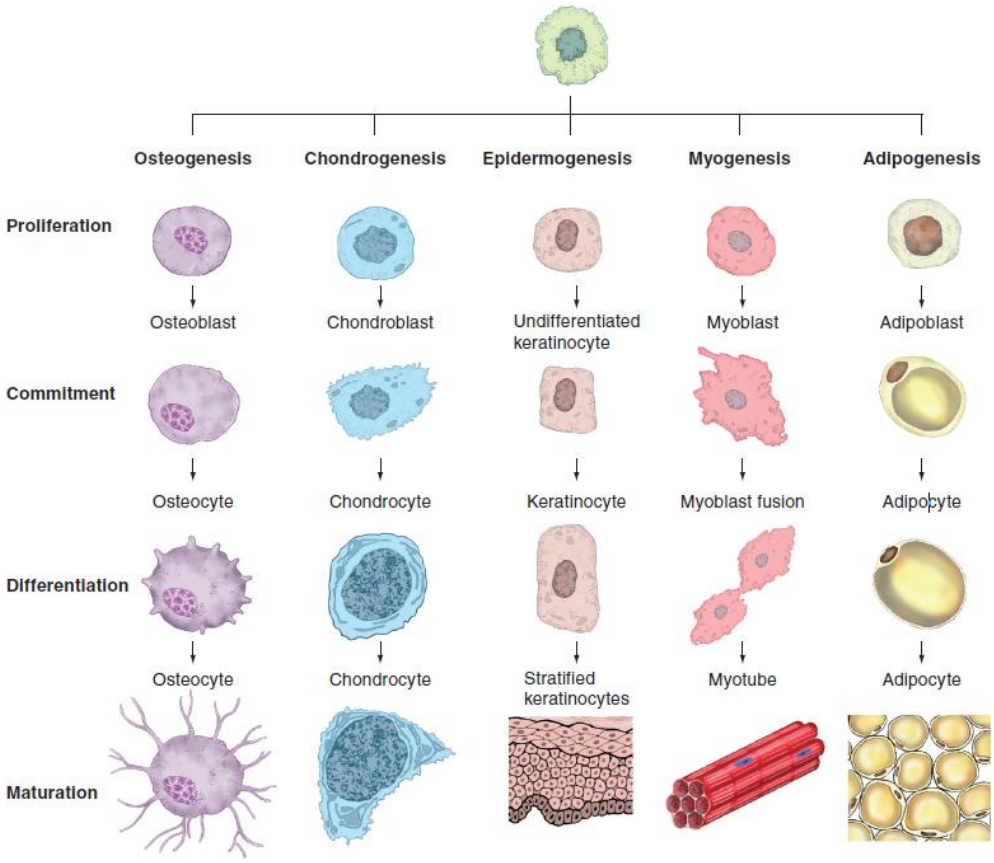

Figure 1.22 In vitro differentiation potential of bone marrow mesenchymal stem cells, hair follicle-derived stem cells and adipose-derived stem cells (Hodgkinson et al., 2009).

Marracci *et al.* [168] used autologous BMMSCs seeded onto porous hydroxyapatite (HA) ceramic scaffolds to treat long bone diaphysis defects in a clinical trial. They observed no detrimental effects from the stem cells' used and a progressive new bone formation inside the bio-ceramic pores and progressive vascular ingrowthhave been identified. Complete fusion between the host bone and the implant occurred 5 to 7 months after surgery. The bias of their method was the low resorbability of porous HA bioceramics, thus the scaffold had not degraded during 6–7 years post implant. In similar studies, BM-MSCs have also been used to repair cranial bone defects with the conjunction of collagen- hydroxyapatite-polylactic [169] and titanium [170] scaffolds. In another study, Vojtaššák *et al.* investigated the use of autologous BMMSCs in combination with an autologous biograft composed of autologous skin fibroblasts on biodegradable collagen-hyaluronan membrane (Coladerm)

for the treatment of diabetic ulcer (chronic non-healing wound) [171]. Briefly, BM-MSCs was injected on the wound and covered with prepared autologous biograft. The wound was analyzed after 29 days and it was reported that the size of wound was reduced and vascularization of the dermis was increased. However, BM-MSCs have a low number density as ~1 MSC per 5000 bone marrow mononuclear cells [172]. BM-MSCs are mostly cultured to obtain the required cell quantities for clinical applications. But, it has been proposed that the *in vitro* culturing can induce alterations in stem cell characteristics and loss of multipotentiality and may drive the cells into senescence [173]. Also, because of the painful invasive extraction process and the low cell numbers in aspirates, BM-MSCs are not considered an ideal candidate population for tissue engineering applications.

1.3.1.5 Adipose-derived mesenchymal stem cells (A-MSC)

Adipose-derived mesenchymal stem cells (A-MSCs) have been also shown to have similar properties to BMMSCs. They can differentiate *in vitro* toward osteogenic, adipogenic, myogenic, chondrogenic lineages and have several advantages over BM-MSCs. For instance, they can be extracted relatively in high numbers from a less invasive surgical procedure called as liposuction and the quantity of A-MSCs obtained from a lipoaspirate is approximately 400,000 cells/ml that is usually discarded as waste [150, 174]. In addition, A-MSCs can be easily isolated and rapidly expanded in culture conditions [174].

Kakudo *et al.* investigated the osteogenic capacity of A-MSCs cultured on 3D honeycomb collagen scaffold for bone tissue engineering. In vitro osteogenic ability of A-MSCs was confirmed by histologic characterization and measuring the expression of transcription factor cbfa-1. A-MSCs loaded collagen scaffolds were subcutaneously transplanted into nude mice, and excised after 8 weeks. In vivo bone formation was assessed using osteocalcin immunostaining, HE stain and von Kossa stain. These histological analyses revealed that there are significant positive stains in the samples of osteogenic medium in the three types of stain suggesting that the used collagen based scaffold is suitable for the differentiation of A-MSCs and as a three-dimensional bone tissue engineering scaffold in vitro and in vivo [175]. There are also various studies reporting successful cartilage

formation using A-MSCs. Betre et *al.* [176] studied the ability of elastin-like polypeptide (ELP) hydrogel to induce the chondrocytic differentiation of human A-MSCs in the absence of additional exogenous chondrogenic media supplements such as TGF-β, dexamethasone and ascorbate). ELP hydrogel and A-MSCs construct were cultured in a standard or chondrogenic media and assessed for the biochemical composition, immunostaining and histological anlaysis. The results revealed that the human A-MSCs loaded on ELP hydrogel shows similar chondrogenic properties regardless of the culture media conditions.

1.3.1.6 Dental pulp stem cells

Dental pulp is a non-mineralized tissue, composed of connective tissue, nervous and vascular lymphatic elements that fill the central pulp cavity of each tooth [177]. Pulp cavity elongates through the root of the tooth, and the root canal opens into the periodontium via apical foramen. Vessels, nerves and blood of dental pulp enter and leave the tooth through this foramen (Fig. 2.23). Blood vessels and nerves provide nutrition and form a responsive sensory system, respectively [178].

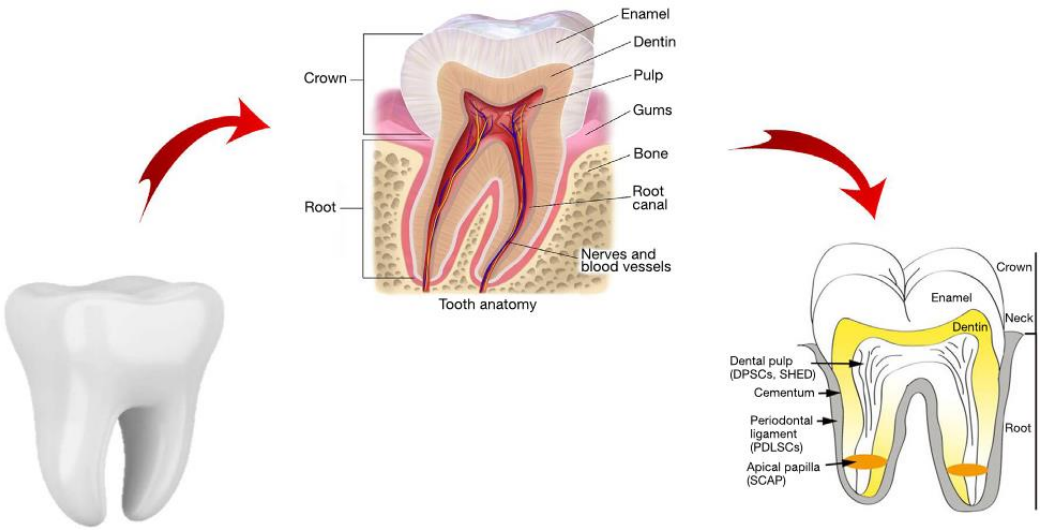

Figure 1.23 Tooth anatomy and location of dental stem cells (Manivasagam et al. 2019).

The main function of dental pulp is to produce dentin and maintain the biological and physiological vitality of the dentin [179]. However, unlike bone, which can repair itself, teeth do not possess complete regeneration ability; they show limited reparative processes [178]. After the formation of crown, ameloblasts go through a programmed cell death and they lose their ability to repair enamel *in vivo* [180]. Even though, odontoblasts cannot repair dentin, their stem cells are able to migrate to the dentin surface and differentiate into odontoblast to generate reparative dentin. However, this reparative dentin is not well organized like primary dentin, but it supplies a barrier for the dental pulp [181]. This ability to create a new odontoblast in response to damage, suggested a stem cell source in dental pulp and for the first time in 2000, Gronthos *et al.* [182] isolated and characterized these stem cells and identified them as dental pulp stem cells (DPSCs). They used impacted human third molars as the tissue sources. For the isolation of stem cells, the pulp was removed from the root and crown and subsequently exposed to dispase and collagenase. Single cells in suspension were then generated by physical straining of the digested tissue. Colony-forming cells were obtained at a frequency of 22–70 colonies/104 cells plated which is higher compared with the stem cell quantity isolated from bone marrow.

DPSCs are heterogeneous MSC population originated from migrating neural crest cells (Fig. 1.23) and they are able to differentiate into chondrogenic, odontogenic, osteogenic, adipogenic, neurogenic, and myogenic lineages [183, 184]. These cells exhibit similar and different characteristics when compared to (BMMSCs). For instance, DPSCs and BMMSCs have similar matrix proteins (osteocalcin, osteopontin and alkaline phosphates which is involved in formation of mineralized tissue) and surface markers such as CD44 (mesenchymal cell marker), CD 105 (vascular endothelial marker), Oct4 (embryonic stem cell marker) and E2F2, PTTG1, TWIST 1 (mesenchymal transcription factors) [183, 185]. On the other hand, Shi *et al.* [183] showed that a high number of DPSCs expressed the pericyte marker 3G5 in contrast to less expression in BMMSCs. In another study, Karaöz *et al.* [186] demonstrated that DPSCs show higher expression of cytokeratin (CK)-18 and -19, in contrast to BMMSCs which involve in odontoblast differentiation and dentine repair. Also, they showed the ability of expressing some epithelial and neural stem cell markers facilitating the in vitro differention of these cells into vascular endothelial and neural cell linages. In addition, DPSCs have been shown to express Nestin (central nervous system

progenitor cell marker), LANGFR- low affinity nerve growth factor receptor (receptor for neurotrophins which is responsible for neural development), EphB (transmembrane receptor responsible for cell-cell interaction in neural tissue embryogenesis) which is not expressed by BMMSCs [187].

Recently, MSC-like populations can be isolated from different perioral structures such as gingival tissue (GMSCs) [188], periodontal ligament (PDLSCs) [189], root apical papilla (SCAP) [190], human exfoliated deciduous teeth (SHED) [191] and dental follicle progenitor cells (DFPCs) [192]. However, DPSCs are the most used dental stem cell source in tissue engineering because of their easy surgical accessibility, higher dentin tissue production capacity compared to the non-dental stem cell sources, cryopreservation facility and their anti-inflammatory ability [193].

Periodontal disease (PD) is considered as the most common chronic infectious disease to be present in 90 % of world population and it is the most common cause of tooth loses in adults [194]. Periodontal disease is defined as having at least one periodontal site with 3 mm or more loss of attachment and 4mm or more pocket depth [195]. In the developed countries, 7% of population has lost one or more teeth by the age of 17 and over 50, an average of 12 teeth have been lost [196]. Current treatment methods to repair these defects are based on mechanical solutions including metal implants and artificial dentures. However, these non-biological structures have many disadvantages such as insufficient biocompatibility, damage to the surrounding tissue, uncomfortable sensation, and unpredictable long-term therapeutic performance [197]. Thus, there is a need for new strategies for tooth replacement in the field of dental research.

“Bio-tooth” refers a kind of biological tooth which is regenerated and re-integrated into the jaw of a human having tooth loss. An appropriate bio tooth must meet several conditions [197]: i) Cells must be easy to isolate from old individuals, the major population for tooth loss, ii) Cells must be expandable *in vitro* to provide sufficient cell population for the tooth reconstruction, iii) odontogenic microenvironment must facilitate the cells to form a 3D tooth structure in vivo or in vitro, iv) newly formed bio-tooth must have the ability to continue its development, generate functional root–periodontal complex, and perform

directional eruption at the jaw environment, v) Size and shape of the bio-tooth must be controllable in order to match the patient's own teeth.

Although tooth-like structures have been experimentally constructed, at present, whole tooth regeneration has not been achieved. Reconstruction of a tooth is complicated by the facts that, i) tooth is composed of various soft (dental pulp and periodontal ligament) and hard (cementum, dentin, and enamel) tissues with different biological and mechanical features; ii) tooth development maintains by the complex interactions between ectoderm and ectomesenchyme; and (iii) there are different types of teeth (incisor, premolar, canine, and molar) with different function [96, 197]. For these reasons two populations of stem cells are considered in the development of the tooth: epithelial (EpSC) and mesenchymal stem cells (MSC). EpSCs differentiate into ameloblasts while MSCs are generating odontoblasts, cementoblasts, osteoblasts and fibroblasts of the periodontal ligament [198, 199]. Currently, various approaches have been developed to create tooth-like structures, such as scaffold based tooth regeneration, assembly of different bioengineered components, recombination experiments, cell pellet engineering, induction of third dentition, gene-manipulated tooth regeneration and chimeric tooth engineering [197]. However, among these approaches, scaffold based regeneration is currently the most promising and accepted strategy. Figure 1.24 summarizes the steps of a scaffold-based tooth regeneration approach. Recent studies carried out in animal models, consider DPSCs as a potential candidate for tooth regeneration.

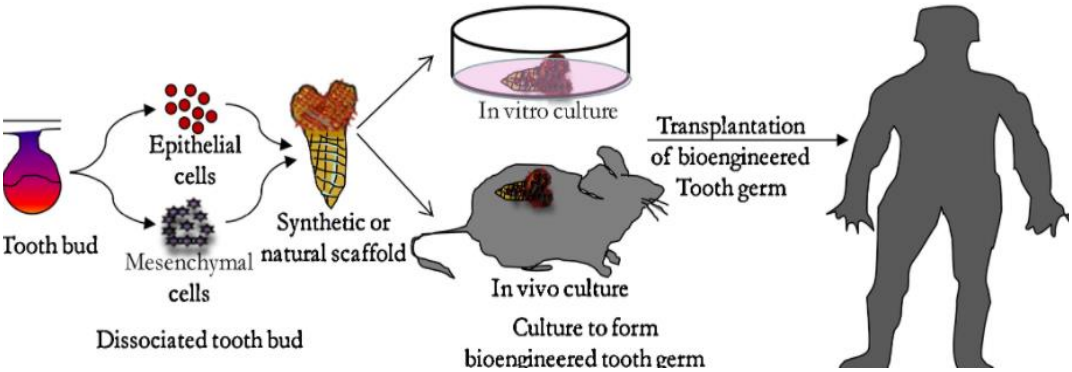

Figure 1.24 Scaffold-based approach to engineer a whole tooth (Neel et al. 2014)

Gonçalves et al. [200] evaluated periodontal regeneration efficiency of DPSCs on electrospun poly (isosorbide succinate-co-L-lactide) (PisPLLA) and poly(L-lactide) (PLLA) based scaffolds. Both polymers were combined with hydroxyapatite (HA), collagen (COL) and growth factor bone morphogenetic protein-7 (BMP7). Their osteoinductive capacity was assessed in vitro via cell proliferation/bone differentiation and in vivo by evaluating regeneration of periodontal defects in rats. Their results revealed that both PLLA/COL/HA and PisPLLA/COL/HA scaffolds induced periodontal regeneration and new bone formation. However, PLLA/COL/HA scaffold was observed to have higher osteoconductive and extracellular mineralization capacity while PisPLLA/COL/HA scaffold show better osteoinductive properties.

In a similar study, Khorsand *et al.* [201] examined the effect of DPSCs on regeneration of periodontium defect of a canine model. The scaffold used in this study was a bovine bone mineral (Bio- Oss®) showing the same crystalline size (10–60 nm) and interconnected pore structure (300-1500 μm) with normal human bone. Autologous DPSCs combined with Bio-Oss® and Bio- Oss® scaffold alone were compared for the cementum and periodontal ligament (PDL) regeneration on 3-walled periodontal defect. Histomorphometric analysis showed that the amount of cementum and PDL regenerated in DPSC seeded Bio-Oss® scaffold was significantly higher than the blank Bio-Oss® scaffold as 2.42 ± 1.40 mm and 1.77 ± 1.27 mm, respectively.

In another study, Wang et al. [202] investigated in vitro and vivo odontogenic differentiation of human DPSCs on nanofibrous (NF)-poly(l-lactic acid) (PLLA) scaffolds in the absence and presence of odontogenic inductive factors Dexamethasone (DXM) or DXM + bone morphogenetic protein 7 (BMP-7). The diameter of obtained nanofibers ranged from 50 to 500 nm which is the same as natural collagen fiber bundles, and the size of pores were ranged from 250 to 420 μm. Their results showed that all three groups of scaffolds were filled with connective tissue like tissue structures with vascular growth and the DXM + BMP-7 group better induced odontogenic differentiation and hard tissue formation than the DXM alone group both *in vitro* and *in vivo.*

In another study similar to Wang *et al*., Yang *et al*. [203] examined the odontoblastic behavior of DPSCs in vitro and in vivo seeded on electrospun poly(epsilon-caprolactone) (PCL)/gelatin scaffolds without (F1) or with (F2) the addition of nano-hydroxyapatite (nHA). Average diameter of F1 and F2 electrospun scaffolds were found to be 161 nm and 281 nm respectively indicating that the addition of nHA increases the fiber diameter. In vitro assessments revealed the presence of nHA upregulated ALP (alkaline phosphatase) activity and promoted OC (osteocalcin) expression. For in vivo examination, both scaffolds seeded with DPSCs were implanted into immunocompromised nude mice. Scaffolds with nHA but without cells were implanted as control. Histological evaluation revealed that all implants were surrounded by a thin fibrous tissue capsule without any adverse effects. Cell scaffold composites showed in vivo hard tissue formation, but no tissue ingrowth. Morover, the combination of nHA in scaffolds upregulated the expression of specific odontogenic genes concluded that the incorporation of nHA in nanofibers facilitated DPSCs differentiation towards an odontoblast-like phenotype in vitro and in vivo. DPSCs have been also shown to be able to repair periodontal tissue, diabetic critical limb ischaemic tissue, bone damage caused by osteonecrosis, skin lesions caused by burns, liver, neuronal tissue, skeletal muscle tissue and blood vessels [89, 178, 204, 205].

1.3.1.7 Umbilical cord mesenchymal stem cells (UCMSCs)

In placental mammals, umbilical cord (UC) connects the fetus and the placenta during pregnancy [206]. Its primary function is to provide the blood flow between the mother and the fetus. UC is formed of a vein and two arteries embedded in a gelatinous substance known as Wharton's jelly (WJ), which prevents strangulation of umbilical vessels (Fig. 1.25) [207].

Stem cells have been identified in UC blood [208] and UC matrix. UC blood contains haematopoietic, mesenchymal and non-haematopoietic stem cells and currently, UC blood transplantation is an accepted practice for haematological malignancies [209]. UC matrix stem cells can be obtained from: 1) whole UC [210], 2) UC WJ or UC vessels [211, 212],

3) UC sub-amnion region of lining membrane [213], (4) UC perivascular region [214] (Fig 1.25).

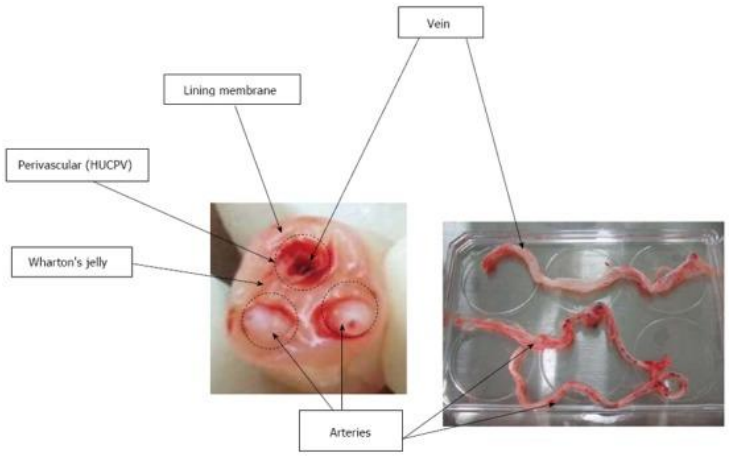

Figure 1.25 Compartments of UC which MSCs can be isolated. HUCPV: Human umbilical cord perivascular (Nagamura-Inoue et al. 2014).

In this study, WJ and Human umbilical cord mesenchymal stem cells (HUCMSCs) are used as ECM source and supporting niche cells, respectively. Here, the details of the both elements will be discussed as a sub-section.

1.4 Extracellular Matrix (ECM)

Extracellular matrix (ECM) is a complex network of macromolecules generated by resident cells in every tissue and organ in a cell/tissue-specific manner. ECM components are arranged in a 3D organization contributing to mechanical stability of tissues. In addition to its structural aspect, ECM is also a reservoir of bioactive molecules and growth factors. ECM is a dynamic body which is subjected to a continuous turnover through a cross-talking process with the cells termed as "dynamic reciprocity". That is, ECM affects the phenotype and the behavior of the cells (proliferation, adhesion, migration, polarity, differentiation, and apoptosis) and in turn, these cells produce, remodel and degrade the ECM [215].

ECM is mainly composed of fibrillary proteins, glycosaminoglycans (GAGs) and proteoglycans. Major fibrous proteins of ECM are collagen, elastin, fibronectin and laminin (Fig. 1.26 a) [216]. Other important components of ECM are growth factors (GFs) and integrins [217]. These components are discussed briefly below.

Collagens are most abundant protein in the body and they are predominantly found in connective tissues such as tendons and skin [218]. Collagen is formed into fibrils and this fibril formation is restricted to collagen types I, II, III, V and XI. Fibrous construction provides tensile strength to the tissue to withstand mechanical forces such as shear, tension and pressure [219]. In addition to its structural aspect, collagen influences other cellular processes such as adhesion and migration [220]. In tissue engineering, collagen type I is frequently used as coating material on gel scaffolds to promote cell addition and to stimulate osteogenic and myogenic differention of stem cells [221].

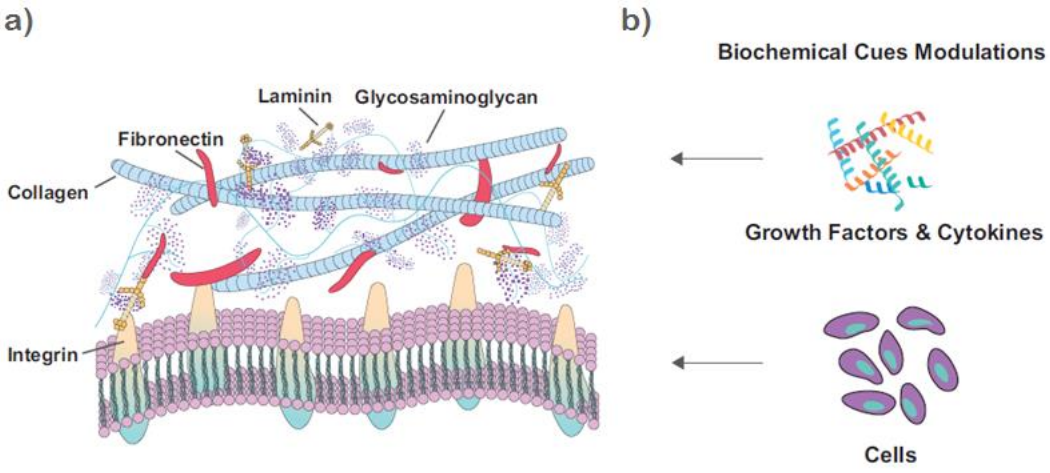

Figure 1.26. a) Schematic of ECM composition and assembly, b) Modification of constructed ECM scaffolds with cells, growth factors and cytokines (Yi et al., 2017).

Elastin is the other structural protein which is closely linked to collagen with its function. It provides elasticity to tissue subjected to repeated stretch, such as lung and vascular vessels. It is composed of single tropoelastin subunits which are cross-linked with an outer layer of fibrillin microfibrils that form an elastic fibrous structure [223]. Due to this inter-chain crosslink, elastin has a half-life of 70 years and is one of the most stable proteins known. Elastin has been suggested for various tissue engineering applications including skin substitute, vascular grafts, heart valves, and elastic cartilage [224].

Fibronectin is a glycoprotein that is assembled into a fibrillar matrix in all tissues. It is a disulphide-bonded dimer that can be broken down into subunits forming three different types (types I, II and III) [225]Fibronectin fibrils generate linear and branched networks around cells and provide connection to neighboring cells [226]. Fibronectin matrix is related with the actin cytoskeleton of cells through integrin activity and this relation has been considered as a key for a successful matrix formation therefore in wound healing [227].

Laminins are major components of basal membrane of ECM influencing cell differentiation, migration, and adhesion [228]. Similarly to fibronectin, laminins have the cell binding ability and used as an alternative to fibronectin to enhance cell adhesion in culture conditions [229].

Growth factors are secreted, soluble proteins which stimulate the growth of specific tissue by instructing specific cellular responses such as migration, differentiation and proliferation. Secreted growth factors initiate a transmission mechanism through binding to specific transmembrane receptors on the target cells. The instructions are translated into the cell through complex signal transduction networks resulting in a specific biological cellular response [230]. Thus, enabling the control over growth factor is a consideration for tissue engineering to achieve tissue regeneration. Currently, two different strategies have been used for biomaterial presentation of growth factors in tissue engineering. The former approach is based on chemical binding or affinity interaction between growth factor-polymer substrate and a cell or a tissue. The other approach is involved encapsulation, diffusion and pre-programmed release of growth factor from substrate into the surrounding tissue. The efficacy of growth factor delivery can be increased by 3D patterning of the growth factors on scaffolds [231, 232]. Basic fibroblast growth factor (bFGF), bone morphogenetic protein (BMP), epidermal growth factor (EGF), vascular endothelial growth factor (VEGF) and insulin like growth factors are examples of growth factor used on tissue engineering.

Integrins are a class of mechanosensors that facilitate cell-cell and cell-ECM adhesion. They are also involded in apoptosis, cell cycle progression, migration and cytoskeletal organization [233]. Integrins can be modulated by extracellular forces such as shear stress or intracellular signaling pathways such as Rho, Rac, R-Ras, Rho GTPases [234]. In tissue engineering, various approaches have been developed to induce cellular responses such as increased cell migration, proliferation and differentiation by using integrin-targeting biomaterials. These approaches are based on the modification scaffold materials with ECM-derived proteins. Collagen [235], gelatin [236], laminin [237] and osteolectin [238] are commonyl used ECM proteins that interact with integrins involved in tissue regeneration.

GAGs are linear chains of repeating disaccharide units. Currently, six main types of GAGs have been identified in mammals: hyaluronic acid (HA), heparan sulfate (HS), heparin (Hep), keratan sulfate (KS), dermatan sulfate (DS) and chondroitin sulfate (CS) and they are predominantly isolated from cartilage, lung, and intestines [239]. GAGs play an important role in ECM assembly including collagen, elastin, and laminin polymerization [240] as well as physical properties including tissue hydration, compression and lubrication [241]. GAGs have been incorporated into biomaterials for use in tissue engineering, drug delivery and regenerative medicine [242-244]. Proteoglycans are proteins that are post-translationally modified with one or more GAGs except HA because HA is synthesized at the cell membrane via HA synthases and does not get involve in protein core of a proteoglycan [245]. Proteoglycans are the essential members of ECM by instructing various vital functions such as embryogenesis, ECM formation, tissue turnover and also known to bind growth factors, cytokines, chemokines, morphogens, enzymes, and lipases through their GAG chains [246]. Thus, incorporation of proteoglycans into biomaterials has been shown to offer additional functionality over the use of blank GAGs. For example, protein core of proteoglycans can be functional in cell adhesion, such as the α2β1 integrin binding site in perlecan [247] extracellular matrix interactions, such as decorin and biglycan mediating collagen fibrillogenesis [248] and growth factor signaling, such as the protein core of perlecan supporting FGF7 signaling [249].

1.4.1 ECM scaffolds

Based upon these key functions of ECM mentioned above, it has been shown that, when appropriately prepared, ECM derived substrates consisting of individual ECM components can act as an inductive templates for tissue regeneration. Composition and the ultrastructure of ECM are not still well understood and there is controversy concerning the importance of the composition vs. structure of these materials. In addition to its mechanical aspect, signaling pathways and ECM-cell interaction mechanism are discovered, thus to separate these mechanical and functional aspects of these components is quite difficult and it is hardly possible to mimic this complex structure. In various studies it has been attempted to

mimic these structures using artificial approaches. For example, use of electrospun fiber materials is one of these approaches [250, 251]. By this technique, it is possible to fabricate interconnected and randomly distributed fibers on the size of fibrillary components of ECM. However, varied size distribution and the composition including hundreds of components of the ECM cannot be accounted by this and similar synthetic approaches revealing the key role of topography, structure, and mechanics of ECM. In this sense, ECM is considered as a feasible alternative to these synthetic approaches. ECM can be harvested from allogeneic and/or xenogeneic whole tissue and organ. These scaffolds remain the main components of ECM, mimic the natural structure of target tissues and/or organs, and thus provide a structural framework and biochemical signaling platform for tissue regeneration. Also, modification of the constructed ECM scaffolds with cells, growth factors, and cytokines further provides biochemical cues, and helps the construction of natural microenviroment niche [222] (Fig. 1.26 b). Currently, ECM has been obtained from heart valves [252], blood vessels [253], skin [254], nerves [255], tendons [256] urinary bladder [257] and UCWJ [258-260]. However, the use of xenogeneic sources faces with some concerns [14]. For example, if they are not completely eluted or internalized, in addition to the xenogeneic infectious agents, the xenogeneic antigens could trigger an immune response. Therefore, the use of these sources required humanizing processes like genetic manipulation to produce compatible human-like structures [261]. On the other hand, animal experimentation requires a rational moral foundation and making moral decisions and evaluate a proper protocol is a sensitive task for researchers and ethics committees [262]. On the contrary, as an allogeneic source, human UCWJ does not pose these potential risks and their isolation is not associated with any moral concern since it is discarded as a waste material after birth. Furthermore, compared with the other human derived sources, its isolation is not invasive and it presents a limitless source for the large scale production for clinical applications.

1.4.1 Wharton`s Jelly (WJ)

WJ is a mucoid, porous connective tissue of UC and is derived from the embryonic and extraembryonic mesoderm [263]. It was firstly identified by Thomas Wharton in 1656 and for the first time the cells from WJ was isolated by McElreavey *et al.* in 1991 [264]. The cells of Wharton's jelly were previously described as myofibroblasts, which exhibit the structural characteristics of fibroblasts and smooth muscle cells [265]. WJ contains high amounts of ECM components such as, collagen (types I,III, IV and V), hyaluronic acid (HA), sulfated glycosaminoglycans (GAGs), growth factors, cytokines and low number of cells [266]. The presence of excess ECM versus low cell number has been interpreted as high stimulation of cells to produce large amount of ECM [267]. Biosynthesis of ECM components is promoted by several growth factors primarily insulin-like growth factor (IGF) [268], fibroblast growth factor (FGF) [269] and transforming growth factor b (TGF-b) [270]. The large amount of ECM content of WJ has been also associated with the presence of these growth factors.

In tissue engineering applications, sulfated GAG chains have been incorporated into scaffolds to enhance cell growth, adhesion, intracellular signaling, tissue remodeling [271], controlled growth factor delivery [272] and drug delivery with nanoparticles [273]. Correspondingly, HA based polymers have been also used in numerous applications such as wound healing [274], articular cartilage [275] and cardiac tissue [276] repair. Umbilical cord, primarily WJ contains high amount of HA and some sulfated GAGs, immobilized in an insoluble collagen fibril network [277]. Because of its high HA content, WJ is highly hydrated and viscos, thus it is considered as a natural hydrogel-like biomaterial characterized by permeability to water-soluble metabolites, facilitating diffusion of nutrients and ability for self-organization in situ [278].

As mentioned earlier, recently, ECM has been derived from various allogeneic and/or xenogeneic whole tissue and organs. However, the most comprehensive studies have been reported for porcine urinary bladder (UBM) [257, 279] and small intestinal submucosa (SIS) [280, 281]. Although promising results have been obtained with these studies, the

ongoing challenge is to produce them cost-effective and timely way in particular with allogeneic sources, to obtain more practicable clinical outcomes.

Among the ECMs used for tissue engineering, few numbers of studies have examined the feasibility of WJ matrix. However, currently, new studies towards the use of WJ are being suggested. In these studies, WJ has been used in blank or composite form reinforced by polymers or as a source of individual ECM components for dermal [260] and chondral repair [282]. WJ has been mainly used in cartilage tissue repair applications because of its structural and functional similarities to cartilage tissue associated with stem cell chondrogenesis and cartilage ECM deposition [283]. Lin et al. [284] fabricated an electrospun nanofiber scaffold composed of decellularized WJ and poly (e-caprolactone) (PCL) and evaluated it is *in vitro* chondroinductive ability of adipose-derived mesenchymal stem cells (A-MSCs). In this study, WJ processed to obtain suspension slurry and lyophilized to prepare WJ/PCL composite solution for electrospinning. After 4 weeks of culture, higher expression of cartilage-specific genes including collagen II, aggrecan and SOX 9 was identified in WJ/PCL group compared to PCL group. Also, chondrogenic-like cells with a round structure were observed in the WJ/PCL group, while cells with a spindle shape (specific to A-MSCs) were observed in the PCL group. Stocco et al [285] fabricated a film formed hybrid ECM scaffold composed of decellularized WJ or articular cartilage (AC) and poly (vinylalcohol) (PVA) to evaluate the feasibility of WJ as an alternative to AC. In this study, decellularized ECMs were homogenized with acid treatment to form as a cast film and lyophilized. ECM/ PVA composite scaffolds were prepared placing a thin layer of WJ or AC film upon PVA solution. Prepared scaffolds assessed for AC chondrocyte adhesion and proliferation *in vitro*. Their results showed that, while PVA itself was not able to facilitate cell proliferation and adherence, PVA/WJ scaffold revealed a similar profile to PVA/AC scaffold to sustain cell proliferation and adhesion despite its aspecific origin. In similar studies proposed for the cartilage regeneration, Xiao et al. produced WJ scaffolds by freeze-drying and explored cartilage ECM component gene expression and secretion [286]. Herrero-Mendez et al. [287] prepared hydrogels by extracting hyaluronic acid (HA) and glycosaminoglycans (GAGs) from WJ and examined the feasibility of the resulting hydrogel scaffolds in inducing stem cell chondrogenesis for chondral and dermal repair. As another example of dermal repair, Beiki et al. [260]

designed a pores decellularized WJ scaffold using freeze-drying and assessed its i*n vivo* wound healing efficiency. *In vivo* studies showed that designed scaffold has an accelerated wound closing efficiency. In scaffold implanted group, the wound area at day 12 was significantly decreased (4.5 ± 1.69%), compared to control group (17.31±1.96). In addition to this wound healing efficiency, no inflammatory responses observed.

Consequently, these studies confirmed the hypothesis regarding the possibility to use WJ as a feasible ECM source that is easily accessible, abundant and lack of ethical restrictions.

1.4.1.2 Wharton`s jelly mesenchymal stem cells (WJMSCs)

In appearance, WJMSCs display a spindle-shaped morphology like fibroblasts or myofibroblasts. From a single donor, $4-5x10^9$ cells can be obtained in 5 to 6 passages [288]. Because of their high ex vivo proliferation index and short population doubling time, they can expand to 300 fold within 6-7 passages without any abnormal karyotype [289]. ESCs are considered as a leading candidate for tissue engineering applications because of their high self-renewal capacity and pluripotency *in vitro* and *in vivo*. However, in addition to ethical restrictions, use of ESCs in clinical applications is limited because of teratoma formation caused by the depletion of mature cells. Although WJMSCs are also of embryonic origin and show ESC characteristics such as having ESC-like antigens (e.g. Tra-1-60, Tra-1-81, SSEA-1) and pluripotency genes (e.g. Oct-4, Nanog, SSEA-4, and SOX-2), the use of WJMSCs is not ethically controversial since this anatomical structure, UC, is usually considered as waste and discarded after birth [290]. In addition, compared to other MSCs sources such as bone marrow and adipose, WJ has advantages such as unlimited availability, low cost, easy and noninvasive isolation procedure. Moreover, previous studies showed that WJMSCs were less immunogenic and not rejected 4 months after transplantation as xenografts without the need for immunosuppressive drugs [291].

In this context, WJMSCs are considered as an appealing source in the treatment of different diseases or tissue regeneration. Recently, WJMSCs have been used for neurological disorders [292], kidney injury [293], lung injury [294], orthopaedic injury [294], liver

injury [295] and cancer therapy [263]. Here, some examples of WJMSC based tissue engineering strategies will be discussed.

Millan-Rivero et al. [296] investigated the wound healing effeciency of electrospun silk fibroin (SF) scaffolds seeded with human WJMSCs using a murine excisional wound splinting model. WJMSCs based SF scaffold showed significant effect in re-epithelization and vascularization of wound with reduced scar formation by decreasing myofibroblast proliferation. In another study, Chen et al.[297] examined the chondrogenic potential of human WJMSCs embedded into collagen hydrogel for cartilage repair. Their results revealed that, WJMSCs embedded in collagen hydrogel possessed ability to undergo chondrogenesis characterized by increased expression of cartilage-specific matrix proteins, such as collage type II, aggrecan and COMP, and early chondrogenic transcription factor sox 9. For bone regeneration, Jamalpoor et al. [298] designed a porous nano-hydroxyapatite/chitosan/gelatin (nHA/CS/Gel) scaffold and evaluated the interaction of human WJMSC on this scaffold for the fabrication of an ideal bone substitute. Their results indicated that nHA/Cs/Gel scaffolds are able to facilitate WJMSC to attach, proliferate, migrate and 3-week culture of WJMSCs on scaffolds, immersed in osteogenic medium, rendered the microenvironment in favor of stem cell differentiation into osteoblast-like cells and extracellular matrix secretion. Li et al. [299] used Poly (3-hydroxybutyrate-co-3-hydroxyvalerate-co-3-hydroxyhexanoate) (PHBVHHx) 3D scaffold to induce differentiation of WJMSCs into hepatocyte-like cells for hepatic tissue engineering. PHBVHHx scaffolds loaded with WJ-MSCs were transplanted into liver injured mice to investigate their effects on the recovery of hepatic functions. Their results showed that after 30 days of transplantation, WJMSCs-PHBVHHx scaffold construct significantly improved hepatic tissue regeneration, decreased collagen fiber formation and hepatic lesions were significantly healed.

1.5 Scaffold Materials

Biomaterials that have been used in tissue engineering can be classified as metals, polymers and ceramics. In medical field, ceramics and metals have major advances especially in orthopedic tissue replacement. However, the processability of these materials is limited and they are not biodegradable, therefore polymer materials are widely used for tissue engineering applications because of their easy control over processability and biodegradability [300].

There are two kinds of polymer materials: natural and synthetic polymers. Polyesters, polycarbonate, polyorthoester, polycaprolactone, polyanhydride and polyfumarate are main biodegradable synthetic polymers [301]. Polyesters such as poly(glycolic acid) (PGA), poly(lactic acid) (PLA) and their copolymer of poly[lactic-co-(glycolic acid)] (PLGA) are commonly used polymers. Natural polymers can be classified as polysaccharides (glycosaminoglycans, cellulose, chitin, amylose and dextran,) proteins (gelatin, silk, collagen, fibrinogen, elastin, actin, myosin and keratin) and polynucleotides (DNA, RNA) [302]. They have been frequently used in tissue engineering because they are the components of, or have similar properties to, ECM, such as biodegradability, water-binding capacity, gelation ability and pseudoplastic behavior [303]. In addition, because of their functional groups presents in the structure (amino, carboxyl, hydroxyl) they can be modified or conjugated by enzymatic [304] or chemical processes such as hydrolysis, oxidation, reduction, esterification, and cross-linking reactions [305] which allows the production of various products with tailorable properties. On the other hand, protein materials have additional advantages compared to other natural sources since they are able to interact with cells through their specific recognition domains.

1.5.1 Collagen

Collagen is the most abundant protein in human body. It is the major component of bone and skin which constitutes approximately 25% of the total dry weight of mammals [306]. Collagen can be extracted from almost every living animal. However, in tissue engineering,

common sources of collagen are bovine skin and tendons, porcine skin and rat tail among the others. Until now, 29 collagen types have been characterized in which a typical triple helix structure and collagen types I, II, III, V and XI are shown to form collagen fibers. Fibril-forming collagens are the most commonly used ones for the fabrication of collagen-based biomaterials. Collagen molecules consist of three α chain that assemble together due to their molecular structure. Every α chain is composed of more than a thousand amino acids based on Gly-X-Y- sequence [307]. The presence of glycine in every third amino acid position provides a tight packaging of the three α chains in the tropocollagen molecule and the X and Y positions are generally filled by proline and 4-hydroxyproline [308]. Assembled tropocollagen units constitute collagen fibril ranging from 10 to 300 nm in diameter. A collagen fiber with a diameter ranging between 0.5 to 3 μm is formed by the aggregation of collagen fibrils (Fig. 1.27).

Collagen is extensively used for various medical applications, primarily for tissue engineering scaffolds. Collagen-based scaffolds have shown favorable results in skin [309], nerve tissue [310, 311], bone/cartilage tissue [312, 313], tendon/ligament tissue [314, 315] and vascular graft [316, 317] applications. However, the status of collagen as an animal-derived biomaterial raise concerns regarding its potential to trigger immune response [318]. An immune response against collagen mainly targets epitopes in the telopeptide region at each end of the tropocollagen molecule [319]. Also, the conformation of the helical part and the amino acid sequence on the surface of collagen fibril, also influence the immunologic characteristics of collagen molecule [320]. Therefore, type I collagen is highly preferred one in tissue engineering because of its low immunogenicity comparing to the other fibril forming collagen types.

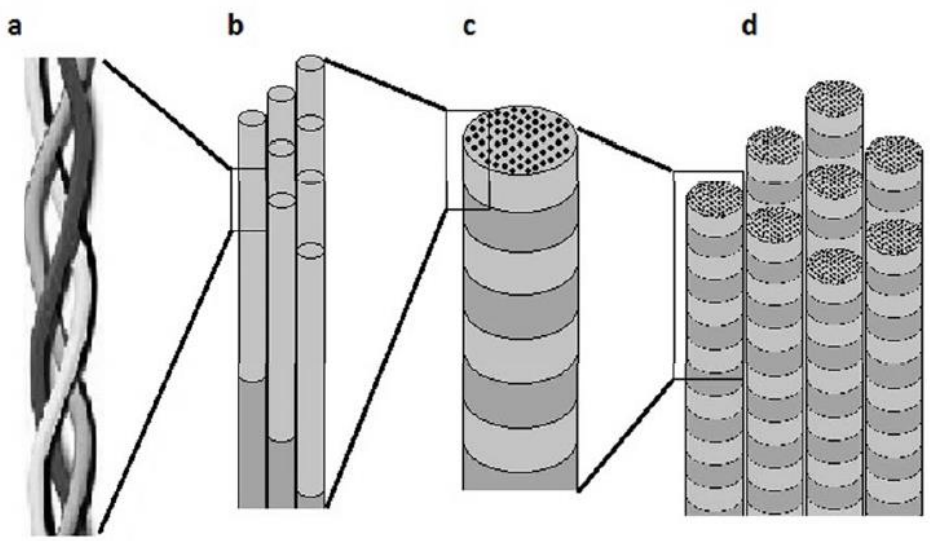

Figure 1.27 Schematic of a) a collagen α chain triple helix b) Assembled tropocollagen molecules c) Collagen fibrils 10-300 nm in diameter d) collagen fibers with a diameter ranging from 0.5 to 3 μm (Zata et al., 2020).

1.5.1 Gelatin

Gelatin is a polypeptide derived from collagen hydrolysis. As natural biopolymer, gelatin has desirable properties such as good biocompatibility and water solubility, low immunogenicity, plasticity, adhesiveness, promotion of cell adhesion, growth, and availability in low cost, as well as the ability to form transparent gels under specific conditions [322]. The most abundant sources of gelatin are fish, pig skin, bovine hides, pig and cattle bones [323]. Triple helix structure of collagen is denatured during the hydrolysis to form gelatin in a random coil conformation [324]. Depending on hydrolysis type (Fig. 1.28), gelatin manufacturing is classified as acid or base hydrolysis process. In acid hydrolysis process, collagen is hydrolyzed by using an acid solution and the obtained product is called type A gelatin. In base hydrolysis process, protein structure is hydrolyzed by alkalis and this process yields type B gelatin. Isoelectric point of Type A gelatin is between 6 and 9 and that of Type B gelatin is between 4.7 and 5.4 [323, 325].

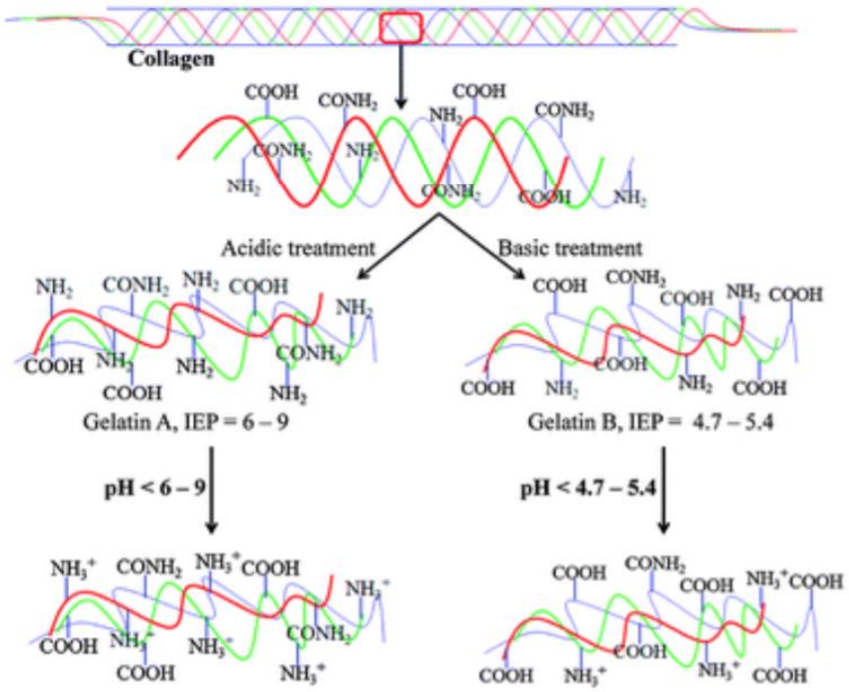

Figure 1.28 Preparation of two different gelatins from hydrolysis of collagen from acidic treatment and basic treatment (Wahab et al. 2012).

The approximate amino acid composition of gelatin is as follows: glycine 21%, proline 12%, hydroxyproline 12%, glutamic acid 10%, alanine 9%, arginine 8%, aspartic acid 6%, lysine 4%, serine 4%, leucine 3%, valine 2%, phenylalanine 2%, threonine 2%, isoleucine 1%, hydroxylysine 1%, methionine and histidine < 1%, and tyrosine < 0.5%. These values vary depending on the source of the raw material and processing technique [327] The structure of gelatin unit is given in Figure 1.29.

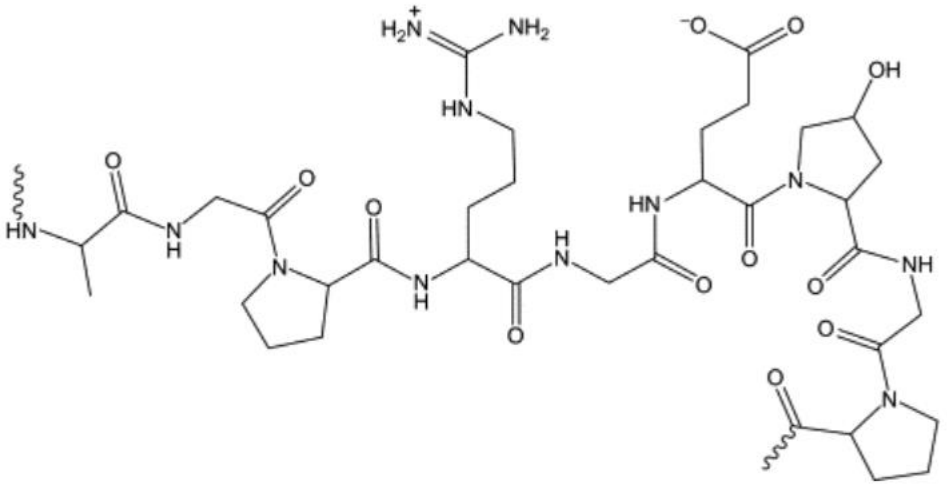

Figure 1.29 Structure of gelatin (Kariduraganavar et al 2014).

Gelatin consists of many glycine-X-proline or glycine-X-hydroxyproline residues, where X is a charged amino acid [2-4]. In preparation of gelatin hydrogels, these residues provides the partial reformation of triple helices into secondary helix structures, which are presumed as a driving force behind the sol–gel transition of gelatin [328]. Compared to its precursor, gelatin has lower antigenicity and it retains some of the properties of collagen, such as Arg–Gly–Asp (RGD) sequence recognized by cells as an adhesion sequence, which partially enhance the cell-adhesive activity [329]. As a scaffold material, gelatin has been used in the form of foam, hydrogel [330], fibrous matrices [331], 3D printed structure [332], and membranes. For the fabrication of three-dimensional (3D) scaffolds, gelatin has been combined with other organic or inorganic biomaterials by different approaches for skin [333], cartilage [334], ophthalmic [335], hepatic [336] and bone [337] tissue engineering applications.

Frazier *et al.* [324] fabricated gelatin-based foams with aligned pore structures via liquid-to-gas vaporization method. In the presented method, water was thermally vaporized instead of using freeze drying, gases or salts as conventional techniques. Four gelatin film samples with varying gelatin-water concentrations were studied namely 5% (G5), 10% (G10), 20% (G20), and 30% (G30). Briefly, the films were dehydrated at ambient conditions and foamed at a constant temperature of 150 C using an oven. The pore

structures of the foams were vertically aligned with the top and bottom and similar in pore diameter varying between 100 and 600 μm with an average of ~350 μm regardless of gelatin concentration. To elucidate the mechanism of foaming process, they investigated the secondary structure, molecular interactions, and water content of gelatin films before and after foaming. They identified the helical structures in the film, but not in the foamed samples after vaporization (~150 °C) revealing that the primary foaming mechanism is governed by the vaporization of water that is tightly bound in secondary structures (i.e., helices, β-turns, β-sheets) that are present in dehydrated gelatin films.

In another study, Vlierberghe *et al.* [338] used a combination of phase separation and freeze-drying to induce pore formation within gelatin hydrogels. Phase separation process was achieved by using a developed cryo-setup to vary the cryogenic parameters such as cooling rate, temperature gradient and freezing temperature prior to freeze-drying. Gelatin was chemically crosslinked by the modification with methacrylamide side groups with a degree of substitution of 60 % and gelatin concentration was varied from 5% (w/v), 10% (w/v) to 15% (w/v). Scanning electron microscopy (SEM), helium pycnometry (He pycnometry), and microcomputed tomography (μ-CT) analysis were used to characterize pore size, pore geometry and porosity of gelatin scaffolds. Pore analysis results revealed that the porosity and pore size are both decreased with the increased concentration of gelatin interpreted to the increased nucleation rate of higher gelatin concentrations caused by the higher decrease of the freezing temperature of the water. The second possible explanation was that the decreased heat and protein transfer of high concentration gelatin hydrogel causes formation of smaller pores. Also, the effect of cooling rate was studied and they observed that decreasing the cooling rate from 0.83 to 0.15 °C/min resulted in an increase in the average pore diameter from 65 to 135 μm of 10% (w/v) gelatin hydrogels. On the other hand, the porosities of both types of hydrogels were identical and the pores were interconnected. The effect of temperature gradient was also observed by applying temperature gradients of 10 and 30 °C during the freezing step. The results showed that the temperature gradient causes a pore size gradient through the scaffold (from top to bottom, highest to lowest temperature) in an average pore diameter distribution of 116 and 330 mμ for temperature gradients of 10 and 30 °C respectively. As the last part of the work, final

freezing temperature was varied (-10 vs -30 °C) and the results showed that the freezing temperature does not have a significant effect on pore size and porosity of the structures.

1.5.2 Tannic acid (TA)

Tannic acid is a specific form of tannin, a type of polyphenol. Polyphenols are secondary metabolites of plants and are mainly involved in protection against ultraviolet radiation or aggression by pathogens [339]. Structurally, polyphenols contain at least one phenol unit attaching with one or more hydroxyl groups. Depending on the amount and the combination of phenol unit, more than 8000 kinds of polyphenols have been identified [340]. Figure 1.30 depicts a polyphenol, TA. TA is composed of a glucose core and ester-linked gallol groups. It is the most complex phenolic structure with the highest number of OH group, so it is highly hydrophilic. Its water solubility is about 2 g/mL and molecular weight is 1701.198 Da [341]. A number of natural phenolic compounds have been reported to be interactive or reactive with proteins and resulted in improved anti-oxidant, anti-inflammatory and anti-bacterial properties. In tissue engineering, as scaffolds or supplements, polyphenols can be used to maintain normal recovery conditions by scavenging free radicals, inhibiting inflammatory responses, devitalizing microorganisms and preventing coagulation. Specifically, incorporating polyphenols into biomimetic scaffolds for their antioxidant properties which have a significant effect on ordered and expected tissue repair [342]. Therefore, polyphenols are intensively used in wound healing, bone repair, nerve repair and cardiovascular tissue engineering. Here, the research status of polyphenols in the field of tissue engineering will be discussed in TA specific manner.

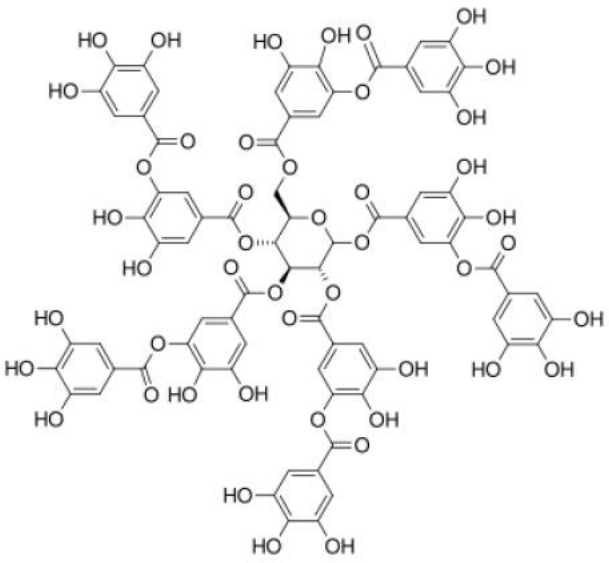

Figure 1.30 Chemical structure of Tannic acid (Kaczmarek et al., 2020)

Antioxidant ability of phenols arises from the capacity of scavenging ROS (Reactive oxygen species), referring to free radicals and non-free radicals such as superoxide anions (O_2^-), hydrogen peroxide (H_2O_2), hydroxyl radicals (HO) and ozone (O_3) [343]. Depending on the structure of phenolic units, polyphenols have direct antioxidant properties through hydrogen atom transfer (HAT), single electron transfer (SET) and transition metal chelation (TMC) (Fig. 1.31). Electrostatic effect of phenolic oxygen atoms, hydrophobicity of aromatic ring, hydrophilicity of the phenolic hydroxyl groups facilitate the high affinity between polyphenols and proteins [344].

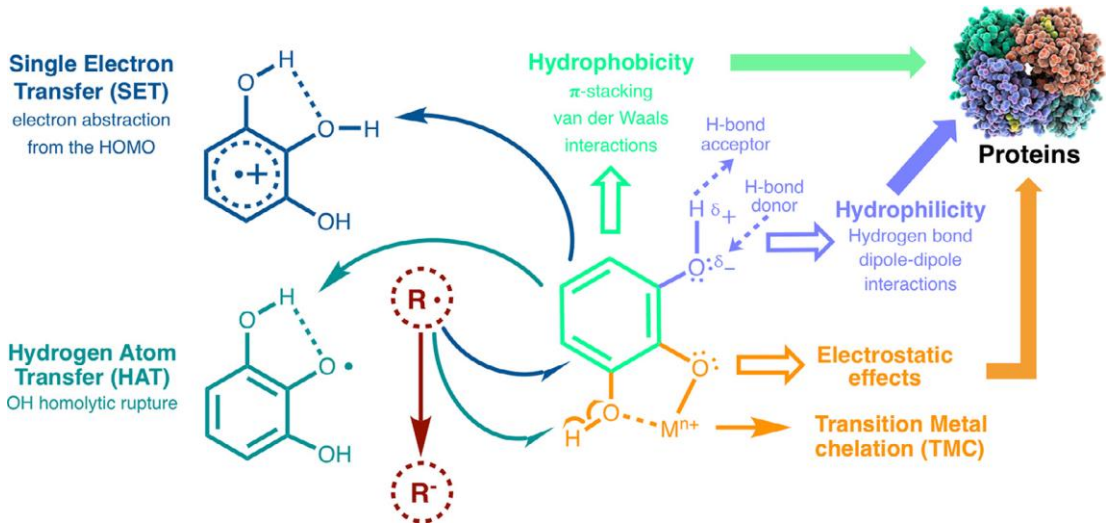

Figure 1.31. Mechanism of the direct antioxidant effect of polyphenols and the interactions between polyphenols and proteins (Gao et al., 2021).

Chen et al. [345] investigated the antioxidant activities of porcine plasma protein hydrolysates modified with oxidized chlorogenic acid or oxidized tannic acid. They reported that DPPH and ABTS scavenging activity, chelating activity and ferric reducing antioxidant power of both conjugates were significantly increased with increasing concentrations of oxidized polyphenols. In a similar study, Aewsiri et al [346] grafted cuttlefish skin gelatin and tannic acid under alkaline condition. Their results also revealed that scavenging activity and ferric reducing antioxidant power of gelatin increased with the tannic acid incorporation. In a study of Thi et al. [347] gallic acid-conjugated gelatin was introduced into gelatin-hydroxyphenyl propionic hydrogels to create an injectable ROS scavenging hydrogel for tissue repear releated to ROS overexpression. Obtained conjugate significantly suppressed the oxidative damage of human dermal fibroblast (hDFBs), preserved their viability by reducing intracellular ROS production and accelerated the wound healing process. In other study, Kim et al. developed a polyphenol incorporated anti-inflammatory and tissue adhesive hydrogel composed of Epigallocatechin gallates grafted hyaluronic acid (HA_E) and tyramine grafted hyaluronic acid (HA_T). They

reported that HA_TE hydrogel exhibited high tissue adhesiveness and closed a skin wound with insignificant host tissue response.

In addition to their antioxidant properties, many phenolic compounds have been shown to exhibit significant antibacterial activity [348]. Antimicrobial activity can be described as the ability of an agent to inhibit the growth of bacteria and prevent the formation of microbial colonies without being toxic to neighboring tissues. Scaffold-related infections are one of the main failure mechanism of tissue engineering [349]. Complex porous morphology of many scaffolds can facilitate bacterial attachment. Because of their small individual cell volume (~0.4–3 μm^3, e.g. *S. aureus, E. coli*) bacteria able to penetrate the scaffold interior and adhere which is less accessible for larger tissue cells which are around 4000 μm^3 in volume [350]. In addition to the this structural aspect, since the ECM components are attractive targets for bacteria [351], scaffold materials such as natural polymers (e.g. gelatin, collagen) can induce the adherence and growth of bacteria.

Bacterial adhesion and subsequent growth mostly result in biofilm formation. Bacterial biofilms are clusters of bacteria that are adhere to a surface and/or to each other and embedded in a self-produced polymeric matrix. Biofilm mode of growth increases the resistance of bacteria against external stresses such as antibiotics, disinfectants, phagocytosis and make the organism less perceptible to the host immune system [352]. Excessive and inappropriate use of antibiotics in clinical practice has facilitated the selection and expansion of resistant bacterial strains and consequently increased the treatment failure ratio [353]. For example, staphylococcal strains are one of the major public health problems in worldwide because of their increasing resistance to macrolide, lincosamide, and streptogramin B antibiotics as a result of their extensive use against Gram-positive bacteria [354]. In terms of tissue regeneration, pathogen invasion is an important problem. Wound healing involves three stages: inflammation, proliferation and remodeling [355]. But if, this repair process is exposed to an invasion of external pathogens or a disorder of internal environment, it leads to a disorder or interruption on these reparative stages which cause a transition from an acute wound to a chronic wound [356]. Therefore, there is a need for effective antibacterial agents which reveals more efficient

bactericidal mechanisms. In this regard, polyphenols are postulated as an alternative to current antibiotic based medical practice.

The mechanism behind the antibacterial activity of polyphenol is explained as i) modification in permeability of cell membranes, ii) changes in various intracellular functions induced by hydrogen binding of the phenolic compounds to enzymes or iii) modification of the cell wall rigidity with integrity losses due to different interactions with the cell membrane [357-359].

Antibacterial activity of TA is mainly attributed to their ability to increase the membrane permeability or inhibit the enzymes by interacting with bacterial proteins [360]. Also, TA can chelate metal ions such as magnesium (Mg), iron (Fe) and copper (Cu) which are vital almost for all bacteria and inhibit their availability or activity [361, 362].
In addition to this destructive effect on bacteria, TA inhibits bacterial biofilm formation by blocking quorum sensing (QS) which is a signaling system for intra and interspecies bacterial communication [363]. TA has been studied in both Gram-negative (primarily *E. coli*) and Gram-positive (primarily S. *aureus*) bacteria.

Reitzer et al. [364] developed a gelatin based delivery system for the controlled release of TA for potential antibacterial wound dressing applications. In this work, gelatin has been used as a carrier for TA and paraformaldehyde was used to crosslink final structure. Obtained matrices showed a sustained TA release profile for 4 days (at pH=7) and released TA showed antibacterial activity against *S. aureus* and E. coli. Growth inhibition efficiency against both types of bacteria increased in the case of increased content (strain specific content) of TA in the material and more than 90 % growth inhibition was achieved at 50 and 15 molar ratio values (TA/gelatin) for *E. coli and S. aureus*, respectively. In a similar study, Ninan et al. [365] fabricated a carboxylated agarose/TA hydrogel scaffolds cross-linked with Zn^{2+} for pH-controlled release of TA for wound healing applications. This study proposed that the pH responsive characteristics of the scaffold could allow more controlled and sustained release of TA. That is, TA's ability to form metal complexes is predominantly pH dependent [366]. At low pH, the phenolic groups of TA are highly protonated and therefore less phenolate binding sites are available to form complex with

metal ions. And reversely, at high pH, the degree of deprotonation of TA increases and more phenolate binding sites become free to form complex with metal ions. Based on this phenomenon, they assessed the release of TA from carboxilated agarose/TA/Zn (CTZ2) and carboxilated agarose/TA (CT) composite hydrogels at pH 3, 5.5 and 7.4. For CTZ2 hydrogel, minimal TA release, less than 5%, was observed at pH 7.4 and maximal TA release, ~20 %, occurred at pH 3. This pH dependent variation was not observed for CT hydrogel showing stable TA release, ~20 %, for each pH value. They examined the antibacterial activities of the hydrogel against E.coli. Hydrogel CTZ2 showed similar anti-bacterial activity to gentamycin. The diameter of the zone of inhibition (ZOI) for CTZ2 and gentamicin was 8 mm and 9 mm, respectively. Dabbaghi et al. [367] designed a superabsorbent polymer (SAP) based hydrogel, crosslinked with functionalized TA and assessed the antibacterial activity of the final hydrogels against *S. aureus and E. coli* and compared with the conventional SAP. Their results indicated that the average of the inhibitory zone that formed around the internal and external cross-linked SAPs were about 9.4 and 5.7 mm, respectively, as no inhibition zone was observed for conventional SAP revealing that the antimicrobial effect of TA highly depended on the content of phenolic hydroxyl groups as described Liu et al. [368]. Also, they showed that increased concentration of internal cross-linked SAP to 2000 ppm, increased the antibacterial activity against *S. aureus* and *E. coli* up to 81% and 76%, respectively.

In tissue engineering, chemical crosslinking of proteins is required to enhance mechanical strength and water/enzyme resistance of the final protein-based constructs. The most common crosslinker used in tissue engineering is glutaraldehyde because of its high availability, low cost and solubility in aqueous solutions. However, there are some limitations associated with the use of glutaraldehyde as a crosslinker. For example, depending on the concentration, over 8%, glutaraldehyde was shown to be toxic [369]. Also, glutaraldehyde is not able to crosslink elastin which is the main component of blood vessels and valve matrix. After implantation, degradation of elastin is considered to initiate implant calcification [370]. Because of their high biocompatibility and wide sources, polyphenols have become an alternative crosslinking agent in the field of tissue engineering.

It is generally accepted that there are four potential interactions between polyphenols and proteins such as covalent bonding, hydrogen bonding, ionic and hydrophobic interactions [371, 372]. The type of these interactions highly depends on environmental conditions such as temperature, type of polyphenol or protein and predominantly pH because of the effect of pH on protein conformation and polyphenol structure. At low pH (pH<7.0), proteins dissociate and this facilitates the exposure of binding sides of protein for electrostatic interactions with polyphenols [373]. Alkaline conditions (pH>7.0) leads polyphenols to oxidize to quinones and these reactive compounds interact with proteins via covalent interactions [374]. Covalent interactions result in more rigid and stable material organization [375]. Possible chemical reactions between polypeptides and phenolic compounds have been postulated by Strauss et al. [376] (Fig. 1.32): Diphenol moiety of a phenolic structure **1)** oxidized to an orthoquinone (enzymatically or by molecular oxygen). Generated quinone **2)** forms a dimer in a side reaction or reacts with reactive group of polypeptides such as amine group of lysine and arginine, amide group of asparagine and glutamine and sulfuhydryl group of cysteine to form covalent C-N or C-S bonds. Generated hydroquinone **3)** reoxidized and binds a second polypeptide, causing a crosslink. In an alternative way, **4)** two quinones can dimerize and form a cross-link.

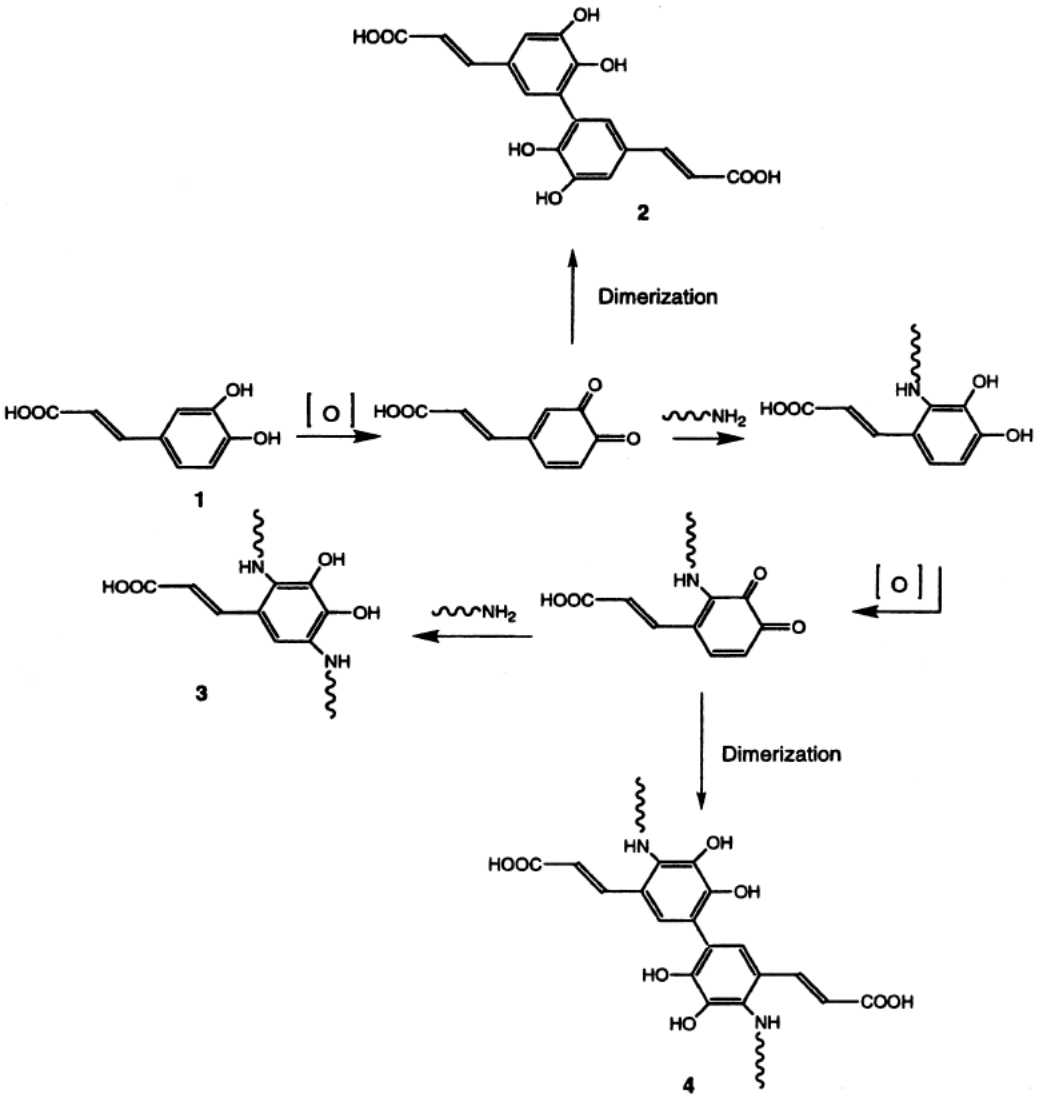

Figure 1.32 Reaction pathways of a phenolic acid with amino side chains of polypeptides (Strauss et al., 2003).

Crosslinking chemistry of TA/gelatin systems has been studied. Zhang et al. [377] modified gelatin by TA (at pH 8) and examined the chemical and physical properties of resulted gelatin materials. They showed that increased TA content (0.75-1.00 wt %) resulted in a significant molecular weight increase as 7-11M. Optimum TA concentration for an efficient crosslinking found to be approximately 3 wt %. At this concentration, thermal stability of the films was maximum, attributed to the high number of covalent linkages. When the TA

concentration reached to 10 wt %, tensile strength and modulus of the films decreased to the lower levels of non-crosslinked gelatin, but the elongation of the films continued to increase due to the the plasticization effect TA additive.

1.6 Pore size and porosity measurement techniques

The total porosity is related to the extent of pore space in a structure. Physical properties such as material or bulk density of the scaffolds can be used to calculate the total porosity. Fluid intrusion methods are also used to indirectly measure the porosity. Apart from these physical characterization methods, imaging techniques are employed for porosity measurements [50].

1.6.1 Gravimetric method

The total porosity (π) of a scaffold can be determined by gravimetric method as shown in equations 1.3 and 1.4 [378, 379].

$$\rho_{\text{scaffold}} = \frac{\text{mass}}{\text{volume}} \tag{1.3}$$

$$\text{Total porosity } (\pi) = 1 - \frac{\rho_{\text{scaffold}}}{\rho_{\text{material}}} \tag{1.4}$$

Where, $\rho_{scaffold}$ is the apparent density of the scaffold and $\rho_{material}$ is the density of scaffold material. Apparent density is determined by measuring the weight and the volume of the scaffold. Although this method is simple and fast, it provides a rough estimation of the actual porosity because of the possible errors on determining the actual volume of the scaffold [378]. However, this method is generally preferred for materials such as nanofiber mats that cannot withstand the high pressures used in other porosity determination methods [380].

1.6.2 Mercury Intrusion porosimetry

This method allows the measurement of average pore diameter, pore size distribution and pore volume fraction of a 3D material [381]. In this method, porous material is placed in a mercury penetrometer and then infused with mercury under increasing pressure up to a maximum of 414 MPa (Fig. 1.33). Mercury is a non-wetting liquid thus it only fills the pores when the applied pressure is higher than the tension forces of the surface meniscus. Since the smaller pores have higher tension forces due to the greater curvature of the surface meniscus, more pressure is required to force the mercury inside the pores. This inverse relationship between pore size and pressure is called Washburn equation (Eq. 1.5) assuming that the pore is cylindrical and the opening is circular in cross-section;

$$D = -4\gamma cos(\theta)/P \quad (1.5)$$

Where D is the diameter of the pore, γ is the surface tension of the mercury, P is the applied pressure and θ is the contact angle. By this equation, under a known pressure applied to a container of mercury covering the porous material, mercury is intruded to the pores of a certain size of D or larger. At the maximum pressure value of 414 MPa, mercury can be forced to enter the pores as small as 0.003 µm. This technique has been used to evaluate the pore characteristics of various scaffold types, for example, hydroxyapatite scaffolds, poly (a-hydroxy acid) foam scaffold, and electrospun poly (e-caprolactone) nano- or micro-fiber scaffolds [57, 382-384].

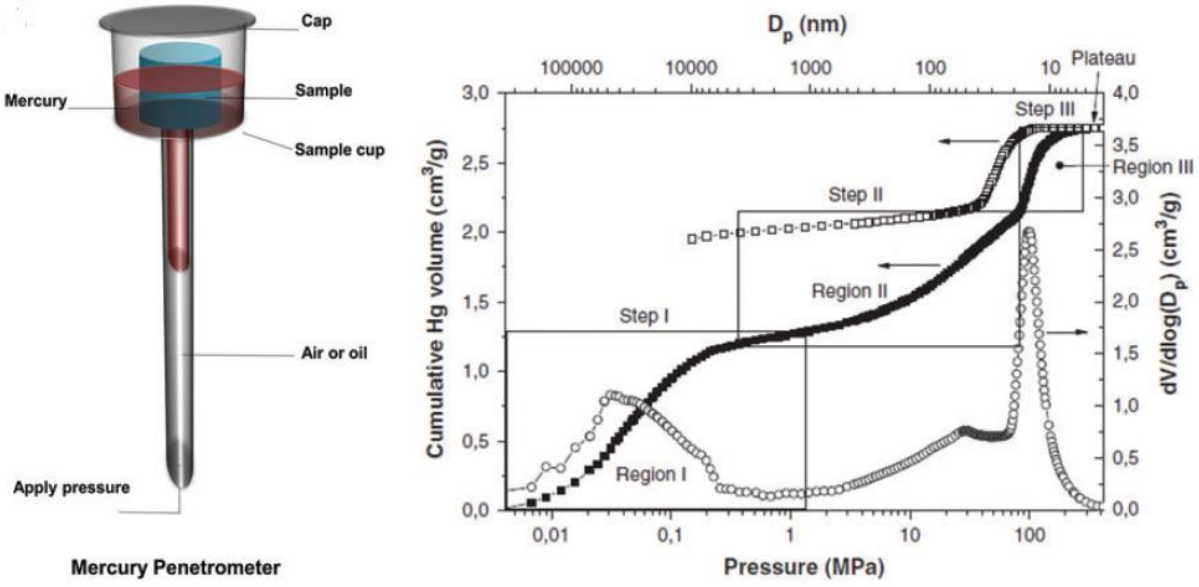

Figure 1.33 Schematic illustration of mercury porosimetry (Karageorgiou et al., 2005)

Although this method is more reliable than the other method requiring manual measurements that may vary depending on individuals, it has some shortcomings such as compressing or collapsing the material, for example hydrogels [385], because of the high pressure applied. In addition, materials with thin cross sections may be destroyed if they are examined at high pressures [380]. Another drawback of this method is the toxicity and cost of mercury used during the analysis.

1.6.3 Liquid displacement method

Scaffold porosity is determined by using a displacement liquid which is not a solvent of the scaffold material and capable of penetrating into the pores without inducing the size shrinkage or swelling of the material [386]. In this method, the scaffold is immersed into a cylinder, containing a known volume of displacement liquid (V_1) and pressed to force the air from the scaffold and the liquid to fill the pores. The total volume of displacement liquid and liquid impregnated scaffold was recorded as V_2. Liquid impregnated scaffold is removed from the cylinder and the remaining liquid volume is recorded as V_3 (Fig. 1.34) [387]. The porosity of the scaffold is expressed using the following equation (Eq. 1.6) [388].

$$\text{Porosity} = \frac{V_1 - V_3}{V_2 - V_3} \tag{1.6}$$

Liquid displacement is a simple method that can be carried out easily, but it is an indirect way to measure the porosity.

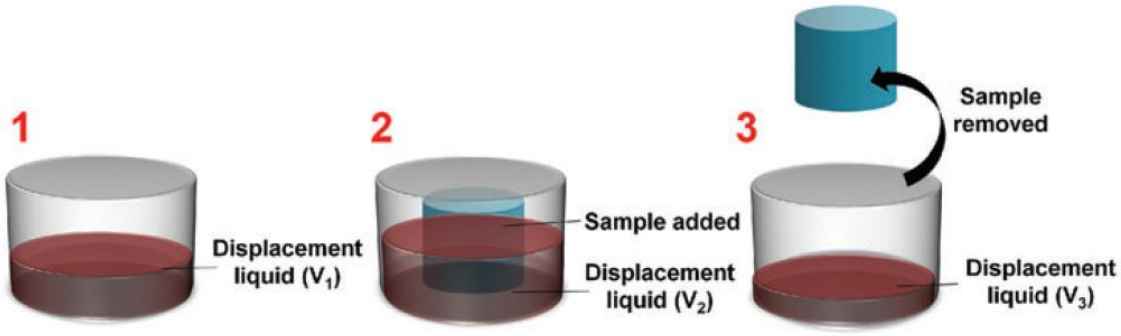

Figure 1.34 Three-step liquid displacement process (Zhang et al., 2001)

1.6.4 Scanning electron microscopy analysis

SEM 2D image analysis is considered as the "gold standard" for porosity and particularly pore size measurements because of its widespread use and its wide availability. Morphological characteristics such as cross-sectional area, wall thickness and interconnectivity can also be obtained by using image processing programs such as ImageJ and SemAfore [389, 390]. The manual mode of the program can be used for the measurement of pore size. For statistical analysis, defined numbers of pores (e.g. from 10-40 pores [391] to a minimum of 100 [392]) are analyzed for the measurement. Porosity is determined as the ratio between the area of the pores and the total area of the sample (Eq. 1.7)

$$P\% = \frac{Pores\ Area}{Total\ Ares}\ x\ 100 \qquad (1.7)$$

The major benefit of SEM is high spatial resolution providing the better detection of thin pore walls compared to other 2D analysis technique such as 2D micro-computed tomography (micro-CT) (Fig. 1.35 a, b) [393].

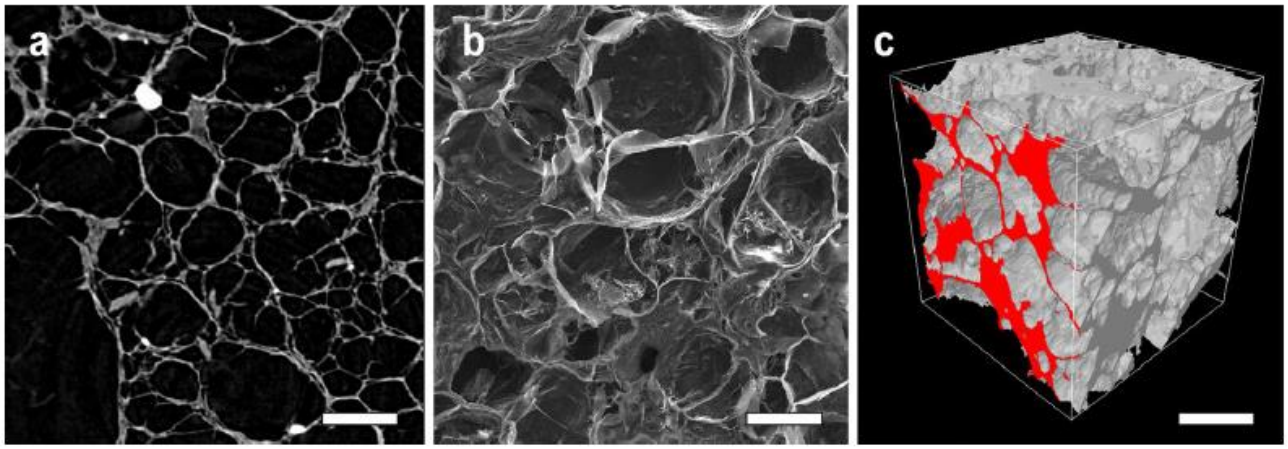

Figure 1.35 Collagen-based composite scaffolds, ***a)*** *Micro-CT 2D section,* ***b)*** *SEM section,* ***c)*** *Micro-CT 3D section. Scale bars = 400 µm (Bartos et. al. 2018).*

The major disadvantage of SEM is the inability to directly assess the 3D structure of the sample and limitation of the analysis to limited number of sections. For example, bone-like structures are not totally isotropic, so the results are dependent on the orientation of the sections [393]. Since the SEM is based on the mechanical sectioning and special treatment, structural alterations may occur during the preparation of the sample which is laborious and time consuming. In addition, manual measurement of pore sizes limits the random selection of the analyzed pores. For example, smaller pores (e.g.10–50 μm in diameter) which significantly contribute to the total pore area of the analyzed section, tend to be neglected by the observer resulted in higher value of pore size than the other analysis method such as Micro-CT 2D section and (MIP) Mercury Intrusion porosimetry [393].

1.6.5 Microcomputed tomography (Micro-CT)

Micro-CT is an X-ray based imaging method which provides non-destructive 2D and 3D analysis for structure visualization and quantification (Fig. 1.35 a,c) [394]. During the imaging process, X-rays are used to divide the scaffold into a series of 2D thin sections. Emerged X-rays are captured by a detector array that calculates the X-ray path and attenuation coefficients. This attenuation coefficient is correlated to the material density to obtain a 2D map which shows the various material phases within the scaffold. Subsequently, with the aid of a 3D modeling program, such as Anatomics, Velocity and Mimics, 3D models are created from the individual 2D maps obtained before [395]. There are many advantages of micro-CT application. This method provides direct 3D analysis (without orientation dependency), whole specimen evaluation and time efficacy. Also it does not require any physical sectioning or chemical treatment which enables the specimen to be reused for other analysis after scanning [49, 395].

However, there are some shortcomings. Analyzed virtual object based on micro-CT scans is not exactly identical to the real specimen. The partial volume effect, the structure below resolution limits and low X-ray density may cause the loss of the virtual structure and these result in reduction of volume, changes in surfaces and higher degree of

interconnection between the pores and increase in pore size [396]. In addition this technique is not suitable for scaffolds that contains metals since the X-rays are heavily attenuated by them, which results in bright and dark grainy scan images that causes loss of details [395].

1.6.6 Permeability-based method

Scaffold permeability is the other parameter that can be used for the determination of scaffold`s pore properties. This method has been used by Sell *et al*. to determine the pore size and fiber diameter of electrospun fibrinogen scaffolds [397].) In this method, using a flowmeter (Fig. 1.36), the amount of fluid that passes through the scaffold area over time is determined. The permeability (T) is calculated using the following equations (Eq. 1.8-9)

$$p = \rho g h \tag{1.8}$$

$$\mathrm{T} = \frac{Q \eta h_s}{Ftp} \tag{1.9}$$

where p is the applied head pressure (Pa), ρ is the density of water, g is the gravitational force, h is the total height of the system, Q is volume of fluid that passed through the scaffold over a period of time (t), η is the viscosity of the fluid, h_s is the thickness of scaffold, and F is the cross-sectional area of the scaffold perpendicular to the fluid flow. After calculating the scaffold permeability, the pore radius (r) of the scaffold can be calculated according to Eq. 1.10:

$$\mathrm{r} = \frac{0.5092}{\mathrm{T}^{-1/2}} \tag{1.10}$$

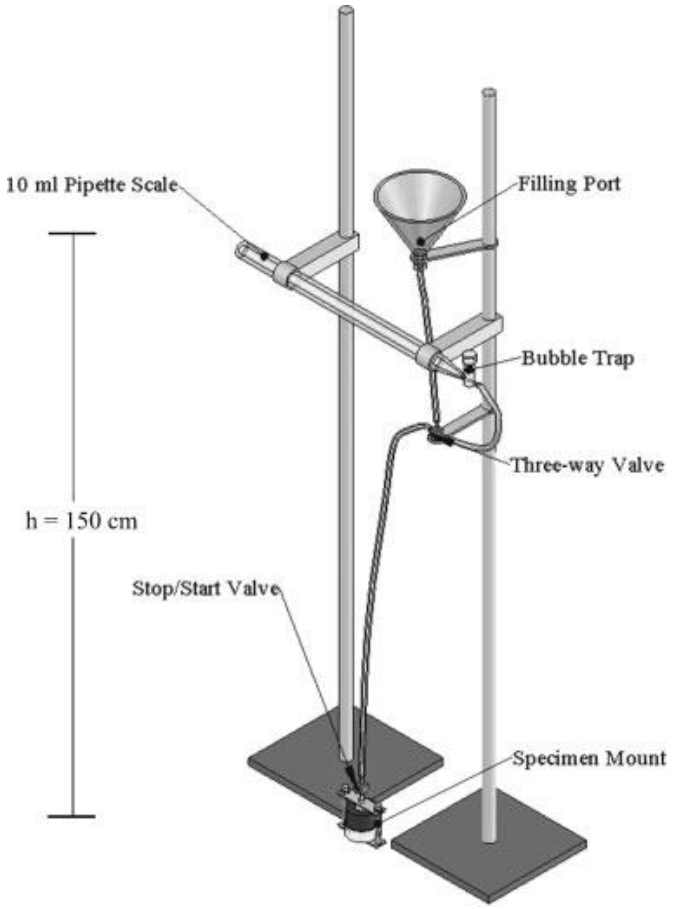

Figure 1.36.Diagram of a simple flowmeter used for permeability-based method (Sell et al. 2007).

1.6.7 Capillary flow porometry

This is a nondestructive method that can be used to measure the pore size and distribution of scaffolds within a range of about 1 to 50 μm [398]. Working principle of capillary flow porometry is based on saturating small samples of the media with a wetting liquid, and then "blowing out" pores with air by increasing the differential pressure Δp across the sample [399]. Assuming the pores have an ideally circular cross-section, the relationship between the differential pressure Δp and the smallest empty pore d_{pore} is calculated by the following equation (Eq. 1.11)

$$d_{pore} = 4\frac{\gamma\cos(\theta)}{\Delta p} \quad (1.11)$$

Where γ is the surface tension of the wetting liquid and θ is the contact angle of the wetting liquid. This technique utilizes low pressure during the process, thus it is suitable for measuring the porous structure of fibrous membranes.

CHAPTER 2

MATERIALS AND METHODS

2.1 Materials

Gelatin Type A from porcine skin (Mw: 5-10 x 10^4 Da, CAS: 9000-70-8), Tannic Acid (Mw: 1701.19 g/mol, CAS: 1401-55-4), Glutaraldehyde (Grade II, 25% in H_2O, CAS: 111-30-8), Cefotaxime sodium salt (CAS: 64485-93-4), Tetracycline (CAS: 60-54-8), Collagenase from *Clostridium histolyticum* (Type IA, 0.5-5.0 FALGPA units/mg) Poly(2-hydroxyethyl methacrylate) (pHEMA, CAS: 25249-16-5), PMA (Phorbol-12-myristate-13-acetate), BSA (Bovine Serum Albumin), Acetic acid (≥99.7%, CAS: 64-19-7) and Trifluoroacetic acid (CAS Number 76-05-1) were purchased from Sigma-Aldrich. Microbial-Transglutaminase (86-135 units/g) was kindly provided by Ajinomoto Inc. Phosphate Buffer Saline (PBS, 1X), Fetal Bovine Serum (FBS), Trypsin-EDTA (0.05% trypsin, 0.02% EDTA), RPMI 1640 Medium, Penicillin-streptomycin (10000 U/mL) and freezing medium (DMEM 70%, FBS 30%, DMSO 10 %) were obtained from Dutscher. DAPI (4',6 diamidino-2-phenylindole) was purchased from PromoKine. Phalloidin (Alexa Fluor™ 568), Trypan blue solution (0.4%) and 2-Mercaptoethanol (50 mM) and NuPAGE 4–12% Bis–Tris gradient gels were supplied by Life Technologies. AlamarBlue™ assay, Hexamethyldisilazane (HMDS, Alfa Aesar™), Mueller-Hinton Broth (BD^{TM}DIFCO^{TM}), Mueller-Hinton agar (BD^{TM}DIFCO^{TM}) and Coomassie brilliant blue R 250 were purchased from Thermo Fisher. Alpha MEM Eagle and Penicillin-streptomycin, Amphotericin B (100x) were obtained from Lonza. MES SDS running buffer (20X) and SeeBlue™ Plus2 Pre-Stained Standard were purchased from Fisher Scientific. Paraformaldehyde (16%, CAS: 30525-89-4) was supplied by Electron Microscopy Sciences. Acetonitrile / 2-propanol was supplied by Applied Biosystems. Laemmli Sample Buffer 4x and Bio-Rad DC protein assay were purchased from Bio-Rad. THP-1 cells (human monocytic leukemia cell line, Catalog ID: TIB-202) and Staphylococcus aureus strain (*S. aureus*, 25923) were obtained from ATCC.

2.2 Methods

2.2.1 Preparation of Wharton's jelly micro particles from human umbilical cord

Human umbilical cords (HUCs) were obtained from the maternity service of Medico-Surgical and Obstetric Center of Schiltigheim (Strasbourg/France) with the informed consent of the parents and the study was approved by the ethical board of Inserm ITMO Santé Publique Pôle Recherche Clinique (PRC), (authorization number: DC-2015-2364). UCs were transferred to the laboratory in PBS with 1% (v/v) streptomycin and penicillin. The average length of the cords was 50 cm and 2 cm in diameter. Cords were rinsed several times with PBS to remove excess blood cells and cut into 3-4 cm pieces. Each piece was split and the vessels were removed. Gelatinous tissues were collected and immersed in PBS. Then, tissues were rinsed with ultrapure water (Milli Q-plus system, Millipore) to prevent the precipitation of salts and centrifuged at 1200 rpm for 5 min two times. Three different methods have been assessed to produce powder form of WJ. In the first method, after dissection, WJs were particulated by using a dissociater (gentleMACS™ Dissociator) in PBS, rinsed with ultrapure water and frozen overnight at −80 °C. Following freezing, WJs were lyophilized 24h at -56 °C, 0.5 mBar by using a CHRIST Alpha 1-4 LD plus lyophilizator. In the second method, dissected and rinsed WJ fragments were freeze and lyophilized at the same conditions as described for dissociation method. Then, lyophilized fragments were particulated by using a pulverizator (Pulverisette 0, Fritsch, France). In the third method, lyophilized WJ fragments were particulated by using a salt grinder (Peugeot Elis Sense Electric Salt Mill, 20 cm) and sieved through 500 µm pore size strainer. Obtained WJ powders produced from three different methods were stored at +4 °C and used without further modifications.

2.2.2 Preparation of Scaffolds

In this study**,** three different scaffold groups were examined for their ability in sustaining Umbilical cord mesenchymal stem cells (UCMSC) and THP-1 derived macrophage adhesion and proliferation: Gelatin (GEL), gelatin supplemented with WJ micro-particles

(GEL/WJ) and gelatin supplemented with tannic acid (GEL/TA. All supplemented gelatin scaffold experiments used solutions with a final gelatin concentration of 5.6 %. The scaffolds were fabricated using a freeze-drying (lyophilisation) process. Final temperatures of freezing of -80 °C were used and ice phase was then sublimated under vacuum (0.5 mBar) at -56 °C for a period of 24 h by using a freeze-dryer (CHRIST Alpha 1-4 LD plus, Germany). Lyophilized samples were then stored at +4 °C until use.

2.2.2.1 Crosslinked Gelatin and Tannic acid supplemented scaffold preparation

To prepare crosslinked gelatin scaffolds, gelatin was dissolved in demineralized water to obtain a final concentration of 6.72 % at 50°C for 1h to ensure complete dissolution. Microbial Transglutaminase (mTGA) was prepared in demineralized water at 20 % and filtered with 0,2 µm strainer and added into gelatin solution in a volume ratio of 1:5. After a mixing step, 600 µL crosslinked gelatin solutions were poured into 20 mm diameter size molds and kept at RT for 1 h and at +4°C for 30 min. to provide complete crosslinking and gelation respectively. The solidified samples were then removed from the molds, frozen overnight at −80 °C and lyophilized for 24 h at -56 °C, 0.5 mBar.

To prepare TA supplemented gelatin scaffolds, TA and gelatin solutions were prepared separately; TA solution was prepared by dissolving TA powder (0.25 %) in demineralized water and stirring at RT for 1h. Gelatin solution was prepared in demineralized water at a concentration value of 12.3 % (w/v) by heating at 50°C for 1h. To prevent TA precipitation, two solutions were mixed in a mole ratio of 1:1. After mixing by pipetting, GEL/TA solution was crosslinked by mTGA in a volume ratio of 5:1. Following crosslinking, composite hydrogels were molded, frozen and lyophilized as described previously. Figure 2.1 shows the overall fabrication steps of two different scaffolds.

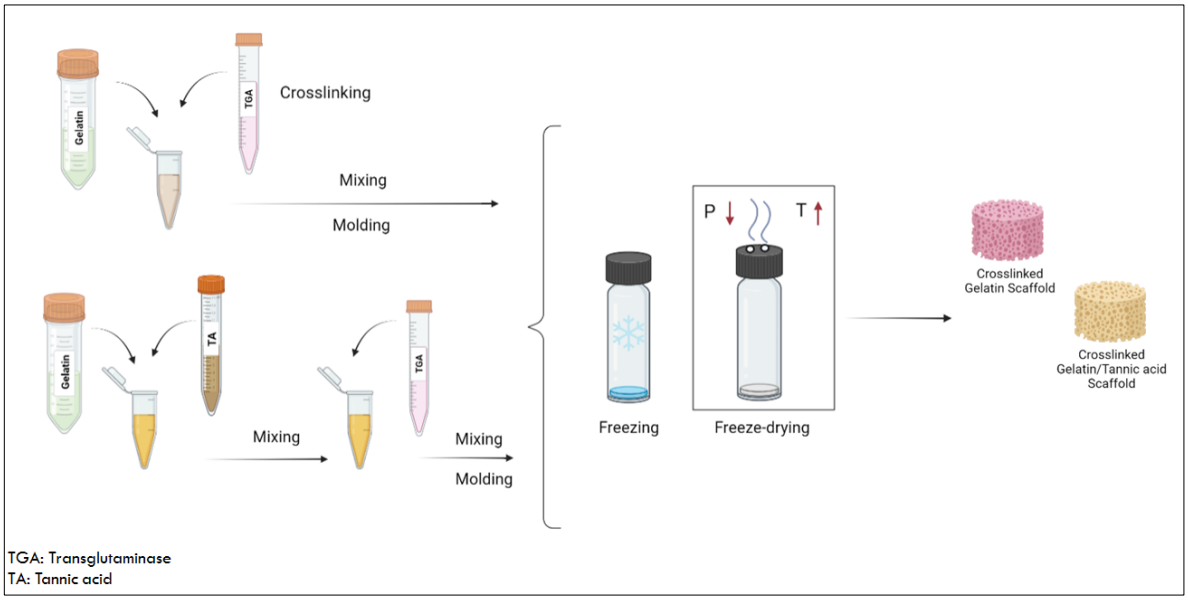

Figure 2.1 Fabrication steps of crosslinked and Tannic acid supplemented gelatin scaffolds

2.2.2.2 Wharton`s Jelly microparticle supplemented gelatin scaffold preparation

Gelatin/ Wharton`s Jelly (GEL/WJ) hydrogels were prepared by mixing gelatin (67.2 mg/mL) and WJ micro particles (2.4 mg/mL) in demineralized water and heating at 37°C for 1h. After complete dissolution of gelatin, GEL/WJ suspension was crosslinked with mTGA in a volume ratio of 5:1 (GEL/WJ: mTGA, v:v). After crosslinking, composite hydrogels were molded, frozen and lyophilized as described in section 2.2.2.1. Figure 2.2 shows the general preparation steps.

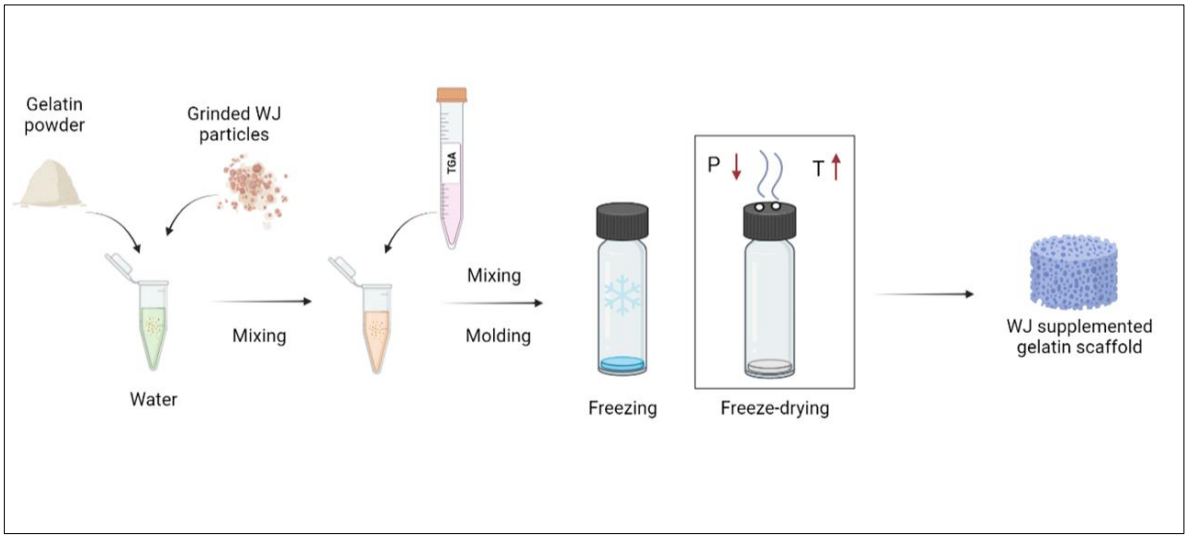

Figure 2.2 Fabrication steps of Wharton`s Jelly microparticle supplemented scaffolds

2.2.3 Characterization of Scaffolds

2.2.3.1 Pore size distribution

Pore size distributions of the scaffolds were determined by Scanning Electron Microscopy (SEM) (Hitachi SU8010, Japan). Surface and cross-section morphology was studied with an accelerating voltage of 15 kV. Samples were mounted on adhesive metallic tape and coated with gold under vacuum with a sputter coating device (Hummer JR, Anatech, USA) at 7.5 mA for 4.5 min to obtain a thin (~84 nm) conducting layer before SEM examination. Diameter of 1000 (from 10 different SEM images) pores were measured using image visualization software (ImageJ 1.50 b, NIH Image, USA).

2.2.3.2 Wharton`s Jelly micro particle size distribution

Size distribution of WJ micro particles was analyzed using SEM. A thin layer of powder was mounted on adhesive metallic tape and excess of the powder was discarded with a pipette bulb. The powder was sputter coated with gold as described in section 2.2.3.1.

Samples were studied with an accelerating voltage of 10 kV. The average particle size was determined from 100 measurements on two SEM images.

2.2.3.3 Quantification of the released proteins from gelatin and WJ supplemented gelatin scaffolds

Total protein concentration of gelatin and WJ supplemented gelatin scaffolds were estimated using the Bradford protein assay. Scaffolds were sterilized with 70% ethanol for 1h following two times PBS washing and treated with UV for 30 min. Three experiment groups were prepared in triplicates for each type of scaffold to assess the protein release at time points of 1, 7 and 14 days. Release experiments was performed in PBS (pH = 7.4). Sterilized scaffolds were incubated in 500 µL PBS at 37°C and extracts were collected from the related experiment group at determined time intervals. Extracts were stored at -20 °C until analysis. To perform protein assay, frozen samples were thawed at 25°C and BSA standards were prepared by performing serial dilutions from a 10 mg/ml stock solution in PBS. Working reagent A` was prepared according to the manufacturer's instructions. Five micro liter of each protein standard or sample was transferred into a 96-well plate in triplicates prior to the addition of 25 µL reagent A` and 200 µL reagent B. After 15 min incubation at room temperature, absorbance was read at 720 nm using a spectrophotometer, SAFAS (FLX-Xenius).

2.2.3.4 Determination of the released protein components of gelatin and WJ supplemented gelatin scaffolds

After determination of protein concentrations, the same set of gelatin and WJ supplemented gelatin scaffolds (day 1, 7 and 14) were analyzed for their protein content according to Laemmli's sodiumdodecyl sulfate/polyacrylamide gel electrophoresis (SDS/PAGE) method [400]. Protein samples (20 mg of total protein) were loaded into NuPAGE 4–12% Bis–Tris gradient gels and electrophoresed in 1X Novex MES SDS running buffer at 200 V, 125 mA for 1.5 h at room temperature. Then after, gel was stained

for 1h in a solution containing 0.1 % (v/v) Coomassie brilliant blue R 250, 30 % (v/v) ethanol and 10 % (v/v) acetic acid in MilliQ water. Afterwards, gels were washed with MilliQ water and visualized under UV light.

2.2.3.5 Chromatography of gelatin and Wharton`s Jelly supplemented gelatin scaffolds extracts

Gelatin and WJ supplemented gelatin scaffold day 14 extracts were evaluated by reverse-phase high-performance liquid chromatography (RP-HPLC) (Dionex system, Germerong, Germany), using a Nucleosil 300-5 C18 column (4×250 mm, particle size 5 μm, porosity 300 Å; Macherey Nagel, Düren, Germany). The solvent system consisted of 0.1% (v/v) trifluoroacetic acid in water (solvent A) and 0.09% (v/v) trifluoroacetic acid in 70% acetonitrile in milliQ water (solvent B). Elutions were performed at a flow rate of 1 mL/min using the gradient indicated on the chromatogram. Extracts were centrifuged at 13000 rpm for 10 min at room temperature and 0.002 % (v/v) solution of supernatant in solvent A was used. Fractions (~500 μL) were collected (Fraction Collector FC204, Gilson, Middleton, WI, USA) in eppendorf tubes and stored at −20 °C.

2.2.3.6 Porosity of scaffolds

Porosity of 5.6 % crosslinked gelatin foams was assessed using a mercury intrusion porosimeter (MIP) (Micromeretics AutoPore IV 9500, Hexton, UK) with a measured pore access radius ranged between 165 μm (0.005 MPa) and 0.003 μm (274 MPa). Hence, pores smaller or larger than these sizes are not detectable by this technique. The same analysis was carried out for 1.2, 2.4, 11.2, 16.8 % crosslinked gelatin foams to examine the effect of gelatin concentration on porosity of foams. One sample was analyzed for each type of foam.

2.2.3.7 Quantification of TA release from the scaffolds

TA release studies were adapted from a protocol described by Reitzer *et al*. [364]. TA supplemented gelatin scaffolds were placed in a 24-well plate (n=5) and incubated in 1 mL PBS (pH = 7.4) at 37 °C. At time points 1, 2, 4, 8, 24, 48, 72, 96 h, 100 µL supernatant were withdrawn, transferred in a 96-well plate (UV star, ref 655801, Greiner Bio-One) and absorbance was read at 277 nm using a spectrophotometer, SAFAS (FLX-Xenius). At each time point, after withdrawal of the supernatant, the elution medium was completed to 1 mL by the addition of 100 µL fresh PBS. Concentration of TA in release media was calculated from a calibration curve, constructed using the same protocol.

2.2.3.8 Stability of Foams

Stability of crosslinked blank gelatin foams were evaluated in physiological (pH 7.4) and enzymatic conditions.

2.2.3.8.1 In vitro hydrolytic stability

Pre-weighted foams were placed in 24-well plate and incubated in 1 mL PBS 1X (1% streptomycin/penicillin) under culture conditions (37 °C, 5% CO_2). At time points 0, 1, 2 and 4 weeks, remaining foams were dried under vacuum for 2h and weighed. Degradation rates were determined by calculating the percentage of remaining weight compared with the initial weight.

2.2.3.8.2 In vitro enzymatic stability: Collagenase Assay

Collagenase type IA (0.1 mg/mL in PBS) was used to study the resistance of gelatin foams to enzymatic degradation. Lyophilized, dry foams were first soaked in PBS for 1h at +4°C. Water saturated samples were then gently dried with filter paper to remove the excess water

and weighed. After that, samples were placed in 24-well plate and incubated in 1 mL collagenase solution under culture conditions (37 °C, 5% CO_2). At specified time points of 30, 60, 90, 120, 150, 180, 210, 240, 270, 300, 330 and 360 min, remaining foams were collected, excess water was removed and foams were weighed. The extent of degradation was determined by calculating the percentage of remaining weight versus the initial weight of foams.

2.2.4 In vitro Studies

2.2.4.1 Cell Culture

Both cell types, HUCSCs and THP-1 monocytes were stored in liquid nitrogen until use in a freezing medium. After thawing, cells were passaged once before they were seeded onto the scaffolds. All cell culture experiments were performed under standard culture conditions. Cells were incubated at 37°C with 5% CO_2 in a humidified chamber.

2.2.4.1.1 Human umbilical cord mesenchymal stem cell culture

HUCMSCs were harvested from one consenting patient in accordance with ethical regulations with a procedure previously described by Smith *et al*. [401] in our laboratory. Cells were suspended in T175 tissue culture flasks, in α-MEM Eagle culture growth medium supplemented with 20 % (v/v) of decomplemented FBS, 1 % (v/v) of L-glutamine and 1 % (v/v) pen/strep /amphotericin and passaged with a 1:4 split ratio using trypsin-EDTA when the cell population reached 70-80 % confluence. Cells between passages 2-6 were used for seeding on scaffolds.

2.2.4.1.2 THP-1 monocyte culture

THP-1 cells (human monocytic leukemia cell line) were cultured in suspension in T75 tissue culture flask with RPMI-1640 culture growth medium supplemented with 10% (v/v) decomplemented FBS, 1% (v/v) pen/strep and 0.05mM of β-mercaptoethanol to avoid the monocyte attachment to the surface of the flask. Cell culture medium was renewed in every 2 days and cells were passaged in a density of $2x10^5$ cells/mL when the cell concentration reached around $8x10^5$ cells/mL. Medium renewal and passaging were done with centrifugation at 1100 rpm for 5 min. In all experiments, cells between passages 2-30 were used.

2.2.4.1.3 THP-1 macrophage culture

Macrophage-like state was obtained by resuspending THP-1 monocytes after centrifugation in 50 ng mL^{-1} phorbol 12-myristate 13-acetate (PMA) containing medium for 24h in T75 tissue culture flask in a density of $2x10^5$ cells mL^{-1}. PMA activation induces the macrophage-like behavior and causes the attachment of THP-1 cells to the surface of the flask [402].

2.2.5 Cell Seeding onto Scaffolds

Scaffolds, 3 mm height and 15 mm in diameter were placed in a 24-well plate in triplicates and sterilized under UV light during 30 min for each side just before cell seeding. Two identical plates were prepared for each experimental group to evaluate the growth profile on day 1 and day 7 by CLS microscopy and SEM in addition to the Alamar blue assay. All cell culture experiments that were performed with adherent cell types (HUCSCs) and THP-1 macrophages were conducted in poly(2-hydroxyethyl methacrylate) (pHEMA) coated hydrophobic 24-well plates to prevent the attachment of the cells to the plate surface. To coat the plates, 1 mL 0.5% (w/v in ethanol) poly(2-hydroxyethyl methacrylate) (pHEMA) solution was poured into the wells and plates were incubated at 40°C for 2 days to evaporate the excess ethanol. Coated plates were sterilized under UV light for 15 min

before using. Adherent cells were first washed with PBS and then treated with trypsin-EDTA solution for 5 min at 37 °C to be detached from the flask surface. Then, trypsin was inactivated by the addition of culture medium containing serum to the flask and the cell suspension was centrifuged for 5 min at 1200 rpm. Cells were then counted with a hemocytometer. After counting, cell suspension was diluted to obtain the defined number of cells in 50 µL and seeded onto scaffolds. Depending on the experiment, cell seeding density was varied between 0.5 and 5 $\times 10^5$ cells per scaffold. Cell seeded scaffolds were then incubated for 15 min to facilitate the attachment of the cells onto the scaffold. Then, culture medium was completed to 1 mL and cells were incubated. The same seeding protocol was followed for THP-1 monocyte (suspension phase) seeding without trypsinization step.

2.2.6 Assessment of cell viability/metabolic activity

Viability/metabolic activity of both HUCMSCs and THP-1 cells on the scaffolds was assessed by Alamar Blue assay. The assay is based on the reduction of resazurin in living cells to resorufin which is red and highly fluorescent. Metabolic activity of the cells was measured at day 1, day 3 and day 7. For each time point, scaffolds were transferred to a new well plate and 10 % (v/v, in supplemented culture medium), 500 µL of Alamar Blue solution was added to the wells (24-well plate) and the plates were incubated for 2 h at 37°C, 5 % CO_2. All Alamar blue experiments were performed in the dark. After incubation, 100 µL of Alamar blue solution in triplicate was poured in 96-well plate and the fluorescent intensity of the solutions was measured with a spectrophotometer, SAFAS (FLX-Xenius) with excitation/emission ($\lambda_{exc}/\lambda_{em}$) wavelengths of 560/590nm respectively. Cell number on scaffolds was defined using a calibration curve prepared with known number of related cells.

2.2.7 Microscopy of the cell seeded scaffolds

2.2.7.1 Laser confocal scanning microscopy (LCSM)

Visualization of f-actin filaments and nuclei of seeded cells was performed by fluorophore conjugated phalloidin (Alexa-Fluor 568 conjugated) and DAPI (4',6 diamidino-2-phenylindole) stainings respectively. Prior to staining, scaffolds were fixed with 4% (v/v) paraformaldehyde (PFA) solution in PBS, for 15 min at RT. After two PBS washing for 5 min, cells were permeabilized with 0.1 (v/v) % Triton X-100 solution in PBS for 10 min at room temperature, followed by two PBS washing for 5 min. After this step, samples were protected from light until the end of staining. After washing, samples were incubated in 1/40 (v/v) Phalloidin solution in BSA (1/100 v/v in PBS) for 30 min. Then, samples were washed two times with PBS for 5 min and incubated in DAPI solution at a dilution of 1/100 in PBS for 5 min. Finally, samples were washed with PBS again to remove the unbound phalloidin and DAPI and preserved at 4°C in PBS until microscope observation. Confocal images were taken after the staining of the cells using an inverted Zeiss LSM 710 microscope. Objectives x10 and x20 or x40 were used to visualize the cells within the scaffolds.Excitation/emission wavelengths were 578/600 nm and 360/460 nm for Alexa Fluor™ 568 Phalloidin and DAPI respectively.

2.2.7.2 Scanning Electron Microscopy (SEM)

SEM analysis was performed to observe the three dimensional distribution of cells within day 1 and day 7 cell seeded scaffolds. Scaffolds were fixed with PFA as described previously.. After PFA fixation, samples were fixed with 4% (v/v) glutaraldehyde solution (in PBS) for 1h at room temperature, then, washed with PBS once and three times with demineralized water. For dehydration, samples were treated with graded series of ethanol (70, 95, 100 %, v/v, in water) and 50 % (v/v, in ethanol) of hexamethyldisiloxane solution 30 min. Then after, samples were washed with pure hexamethyldisiloxane for 1h and then let dry under a fume hood for 24 h.

2.2.8 Biological assays

2.2.8.1 Cytotoxicity assay

Prepared scaffolds were tested for their cytotoxicity toward human umbilical cord stem cells by indirect contact method according to a protocol adapted from ISO 10993-5 guidelines [403]. Prior to the analysis, 0.53 cm^3 cylinder shaped scaffolds were sterilized under UV light for 1 h (30 min/side). After sterilization, scaffolds were conditioned with 1 mL supplemented α-MEM in triplicate at 37°C for 24h. In parallel, pre-culture of HUCMSCs were prepared in 24-well plate in an initial density of $6x10^4$ cells/well in order to obtain a cell layer of 80% confluency after 24 hours incubation. On the following day, medium of cultured cells was replaced with the liquid extract of scaffolds and cells were incubated at 37°C with 5% CO_2 for 24h. Alamar Blue assay was used to evaluate the metabolic activity of the cells and thus to determine the percentage of viability. Viability was normalized with a growth control group which is cultured for 48h in culture medium without contact with scaffold extract. For a viability value less than 80 %, the sample was considered cytotoxic.

2.2.8.2. Antibacterial assay

Staphylococcus aureus strain was used to assess antibacterial efficiency of TA supplemented gelatin scaffolds. Bacterial strain was cultured aerobically at 37 °C in a Mueller Hinton Agar (BD), pH 7.4 at 37°C for 24 h. Then, a single bacterial colony on the agar was transferred to 10 mL of Mueller Hinton Broth (BD) and grown at +37°C for 24h in an incubator shaker to obtain bacteria in the mid logarithmic phase of growth. After 24h, the absorbance of bacteria suspension was read at 600 nm and OD value was adjusted to 0.001, corresponding to final density of 8.10^5 $CFU.mL^{-1}$. Scaffolds (0.53 cm^3 disk shaped) were sterilized by UV light exposure for 1 h (30 min/side) and deposited in 24-well plates with 300 µL of *S. aureus* suspension, A_{600} = 0.001. Then after, suspension was completed to 1mL with Mueller Hinton Broth (BD) medium and incubated under agitation for 24 h at 37 °C. For negative control, TGA crosslinked gelatin foams were incubated with *S. aureus*

using the same method. For positive control, tetracycline (10 μg·mL^{-1}) and Cefotaxime (0.1 μg·mL^{-1}) were added into *S. aureus* solution in contact with blank gelatin scaffolds. All tests were performed in triplicates. In order to quantify bacteria growth or inhibition after 24 h, the absorbance of the supernatant was measured at 620 nm. Results were compared to blank gelatin growth condition defined as 100% growth. The percentage of normalized growth was measured according to the following equation:

$$\text{Bacterial growth } (\%) = \left(\frac{OD(Sample) - OD(Positive\ control)}{OD(Negative\ control) - OD(Positive\ control)}\right) \times 100 \quad (2.1)$$

After absorbance reading, scaffolds were washed with PBS two times and fixed with 4% (v/v) PFA followed by two times PBS washing.

2.2.9 Statistical analysis

Data was analyzed with statistically significant values defined as $p < 0.05$ based on one-way analysis of variance (ANOVA) followed by Tukey's test for determination of the significance of difference between different groups ($p \leq 0.05$).

CHAPTER 3

RESULTS AND DISCUSSIONS

3.1 Characterization of Scaffold

3.1.1 Characterization of gelatin foams

In order to define the optimum gelatin concentration, foams with varying gelatin concentrations 1.4, 2.8, 5.6, 11.2, and 16.8 % *w/v* were examined for their pore morphology and porosity. For convenience, these five conditions were referred as 1.4 %, 2.8 %, 5.6%, 11.2 % and 16.8 % in further parts. Figure 3.1 shows the optic images of TGA crosslinked gelatin foams. There is not a distinct difference in appearance of the foams 1.4, 2.8, 5.6 and 11.2 %. They are white and have an opaque appearance. But, comparing to the first three foam type, 11.2 % foam has a more smooth surface morphology due to the formation of a thicker skim layer which clogged the pores. Foam with highest gelatin concentration, 16.8 %, has a translucent appearance.

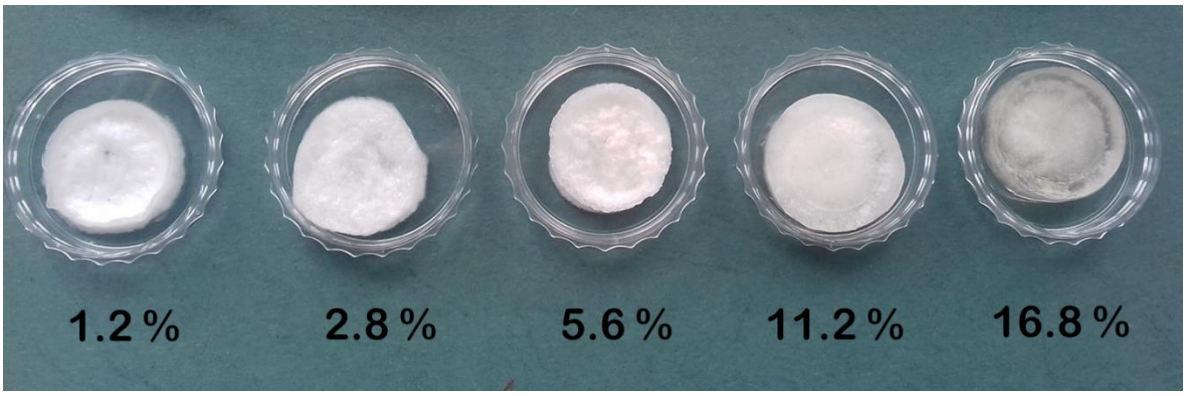

Figure 3.1 Material appearance of gelatin foams prepared in different concentrations (%). There is not a distinct difference in appearance of the foams 1.4, 2.8, 5.6 and 11.2 %. They are white and have an opaque appearance. Foam with highest gelatin concentration, 16.8 %, has a translucent appearance.

Pore morphology and the extent of the porosity of the same set of foams were evaluated by Scanning electron microscopy and Mercury intrusion porosimetry analysis, respectively. Figure 3.2 shows the SEM images of TGA crosslinked gelatin foams. The images reveal that the foams prepared with the gelatin concentrations of 11.2 and 16.8 % show no distinct

pore formation (Fig 3.2. d and e). A clear porous morphology was obtained with the foams at the concentration values between 1.4 and 5.6 % (Fig. 3.2 a, b and c). However, pore morphology of 1.4 and 2.8 % foams was a mixture of irregular, elliptical and spherical pores whereas the 5.6 % foam sample showed more regular, nearly hexagonal pore formation. The pore diameter measurement of 11.2 and 16.8 % foams was not performed from SEM images as no pore formation was observed.

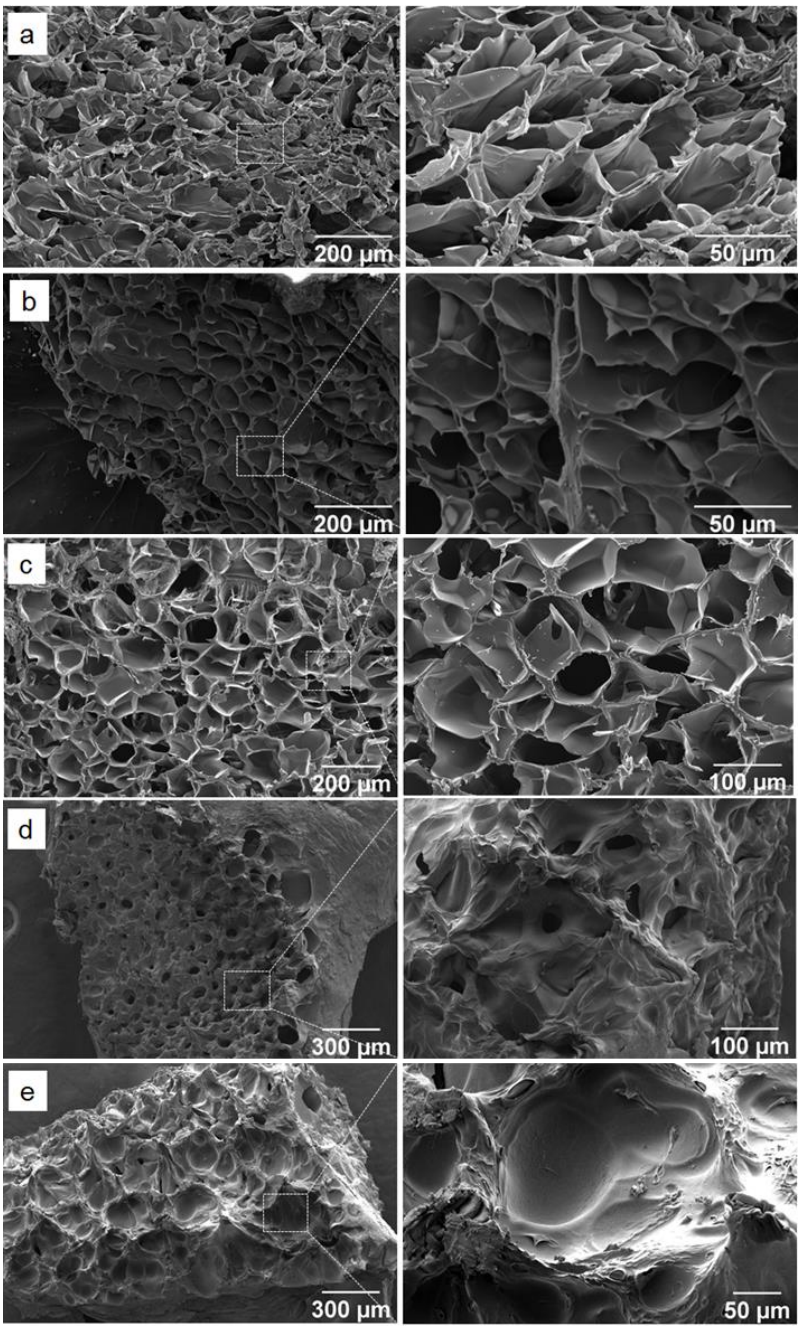

Figure 3.2 SEM images gelatin foams prepared in concentration values of 1.4 (a), 2.8 (b), 5.6 (c) 11.2 (d) and 16.8 %.

Average pore diameter of 1.4, 2.8 and 5.6 % gelatin foam was measured to be 46.24 ± 36, 45.09 ± 20 and 54.8 ± 27.5 μm respectively. The porosity of five respective foams was assessed by Mercury Intrusion Porosimetry Method [404]. The porosities of the foams were determined to be 95.5 %, 93.5 %, 88.8 %, 83.3 %, and 69.1 % for 1.4, 2.8, 5.6, 11.2, and 16.8 % gelatin foams, respectively (Fig. 3.3.). These results indicate that the increased gelatin concentration resulted in reduced foam porosity in agreement with the previous studies [405-408]. The concentration of 5.6% both allowed a well-defined pore structure and a nearly 90% porosity, both are enabling features for cellular in-growth and scaffold remodeling.

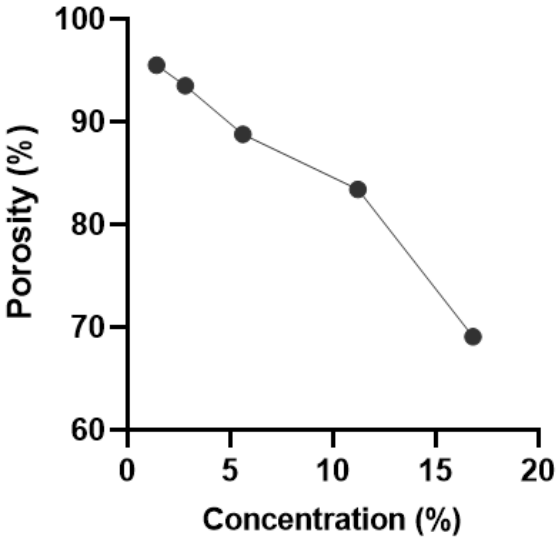

Figure 3.3 Porosity of porosity of five respective gelatin scaffolds assessed by Mercury Intrusion Porosimetry Method

Table 3.1 Pore size and porosity of Gelatin foams

Gelatin concentration (%)	**Pore diameter (µm) (SEM)**	**Pore Radius (µm) (MIP)**	**Porosity % (MIP)**
1.4	*46 ± 36*	6.5	95.55
2.8	45 ± 20	19.7	93.50
5.6	54 ± 27	22	88.88
11.2	——	3.7	83.36
16.8	——	0.14	69.13

Figure 3.4 shows the pore size distribution of the foams obtained by MIP representing the mean radius on the incremental curve (a) and the pore threshold on the cumulative curve (b). The incremental curve gives the mean pore radius where the intrusive volume is maximal. The cumulative curve indicates the pore threshold that corresponds to the pore access allowing the filling of the main part of the porous network. When the both values are close, the pore distribution is considered as unimodal.

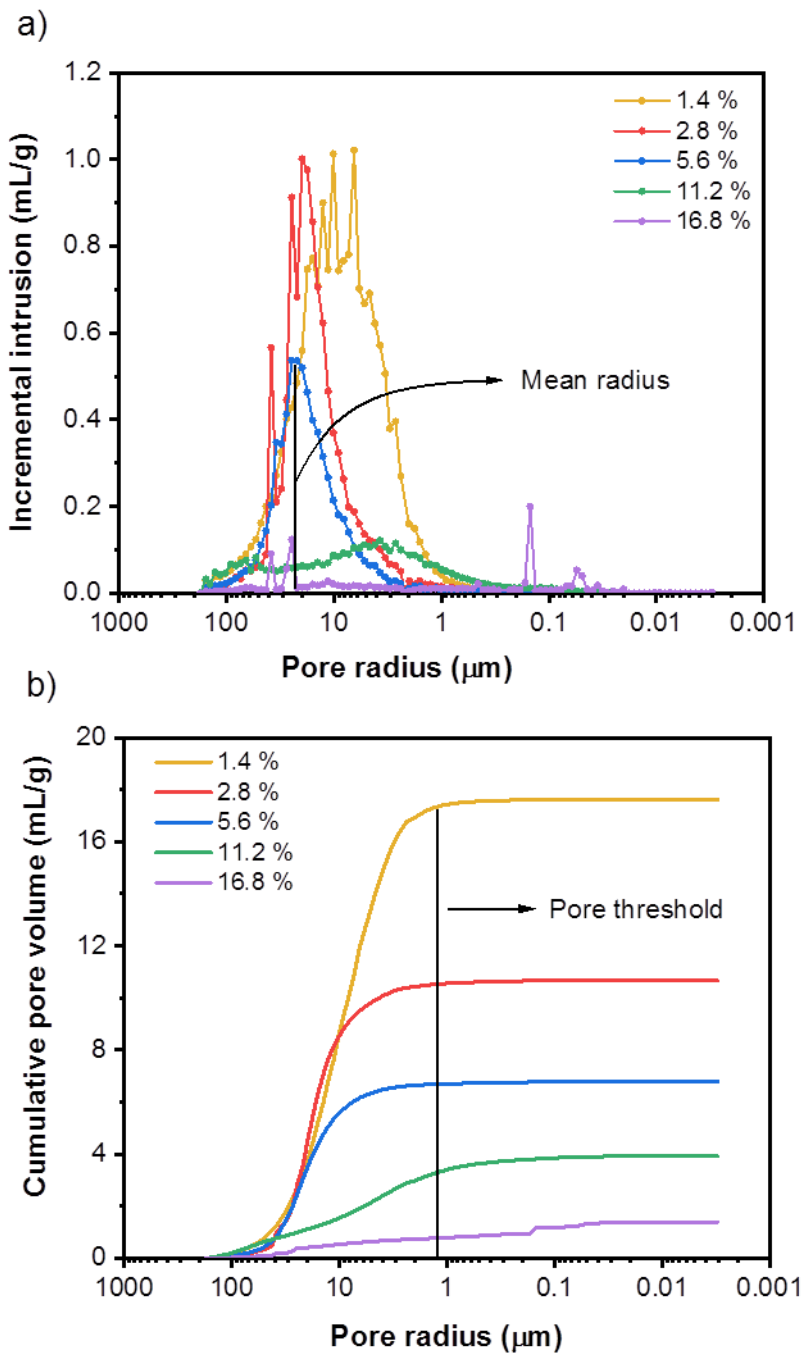

Figure 3.4 Incremental (a) and cumulative (b) pore size distributions of foams obtained by MIC. Increased gelatin concentration resulted in an increase in pore diameter till a concentration value of 11.2 % w/v which after the pore size decreased with increasing polymer concentration.

The mean pore radius of foams corresponding to the main peak on incremental curve (Figure 3.4. a) of around 6.5 µm, 19.7 µm, 22 µm, 3.7 µm and 0.14 µm and the pore thresholds determined by the intersection of the two tangents of the cumulative intrusion curves were around 2.8 µm, 8.6 µm, 11 µm, 0.5 µm and 0.03 µm, respectively. For 5.6 % foam, these two values were closer to each other showed that the porous network was more unimodal compared to the other foam structures. On the other hand, scaffolds size distributions obtained by MIP technique are quite consistent with 2.8 and 5.6 % foam size distributions obtained by SEM image analysis (Table 3.1). However, for 1.4 %, MIP pore diameter result was not consistent with the SEM image analysis. This can be explained by the smaller pore acces radius of MIP which is around 0.003 µm. That is, pores which were not visible in SEM images were detected by MIP providing the consideration of smaller pores. Another reason could be the lower gelatin concentration leading to the compression of the smaller pores during sample cross-sectioning.

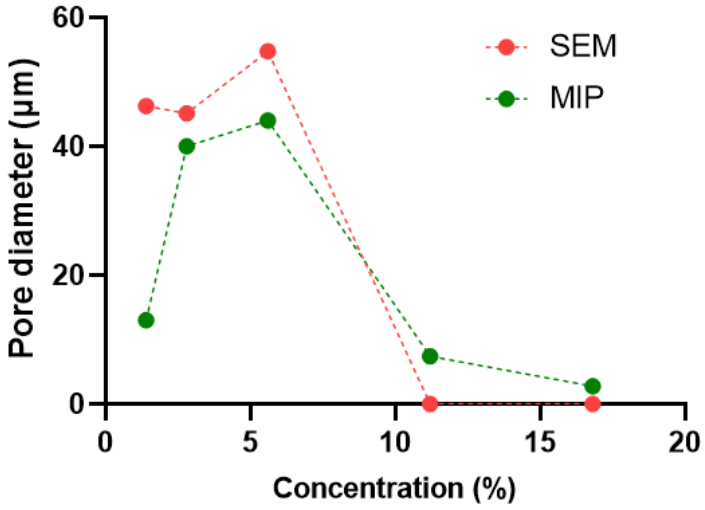

Figure 3.5 Pore diameters of the scaffolds obtained by SEM and MIP analysis.

Thus, MIC results have been considered to evaluate the pore size distribution of the scaffolds. MIC results revealed that the increased gelatin concentration resulted in an increase in pore diameter till a concentration value of 11.2 % which after the pore size decreased with increasing polymer concentration. This concentration dependent variation in pore size has been explained on the basis of ice crystal growth during freeze drying process by O'Brien et al. [54]. The structure of the gelatin gel is made of macromolecular strands which are soluble in water above approximately 40°C. Below this temperature, they generate local junctions between themselves, which gradually forms a three-dimensional network characteristic of the gel structure. Higher gelatin concentration enhance the rigidity of these gel strands due to a greater junction density and this induces a higher mechanical resistance on the gelatin fibers and so on the ice crystal, to push and to grow inside the network which is unfavorable to move in the solution [409]. Therefore, with higher polymer concentration, smaller ice crystals are formed leading to a smaller pore size following sublimation. In a similar study, Enrione et al. [410] designed a gelatin/chitosan/hyaluronic acid scaffold using freeze-drying technique. They evaluated the effect of gelatin concentration on the microstructure of scaffolds prepared with gelatin solutions of 0.8, 1.0 and 1.2 % cross-linked with 1-ethyl-(3,3-dimethyl-aminopropyl)-carbodiimide (EDC). Their results showed that the scaffold prepared with the solution of 0.8 % gelatin has higher porosity (95.9 ±0.05) and pore size (120.6 ±15.95). In another study, Zhang et al. [411] fabricated gelatin/hyaluronic acid (GE/HA) scaffolds by freeze-drying technique. Scaffolds with varying porous morphology prepared by modulating the blending ratious (w/w) of 5 w/v% gelatin/HA aqueous solution as 100:0, 80:20, 60:40, 40:60, 20:80, 0:100 (named as GH0, GH2, GH4, GH6, GH8 and GH10 respectively) and 1-ethyl-(3,3-dimethyl-aminopropyl)-carbodiimide (EDC) was used as crosslinker. They observed that the increased HA content resulted in a significant increase in the pore size. Average pore size of GH0 (pure gelatin) scaffold was found to be 137±40 μm and it increased to 189±61μm for GH2 scaffold which has a HA content of 20%. And when the HA concentration was 60 %, pore size increased to 205±46 μm in width and 415±144 μm in length. And the pore size of pure HA scaffold (GH10) was found to be as 103±26 μm which is smaller than pure gelatin scaffold (GH0, 137±40 μm). This result was attributed to the effect of high hydroxyl group content of pure HA, which facilitates the gather of water

molecules and induces the larger ice crystal formation. Thus, the increase of the HA content favors the formation of larger pore size in the high content HA scaffolds.

In consideration of the obtained pore size ranges in our study, different scaffold designs have been reported with similar range of pore size to facilitate different types of cellular activities such as adipogenesis (6-70 μm) [412], osteogenesis (2-100 μm) [413], skin regeneration (20-125 μm) [10] and smooth muscle cell differentiation (50-200 μm) [414]. Thus, the obtained foams are suitable for soft tissue applications, such as gingival tissue engineering.

3.1.2 Characterization of non-crosslinked and crosslinked/TA supplemented gelatin foams

After the optimum gelatin concentration was determined to be 5.6 % w/v, 5.6 % w/v non-crosslinked, crosslinked and crosslinked/ TA supplemented foams were characterized by SEM to evaluate the effect of TGA crosslinking and TA supplementation on pore size. SEM images are shown in Figure 3.6 and 3.7.

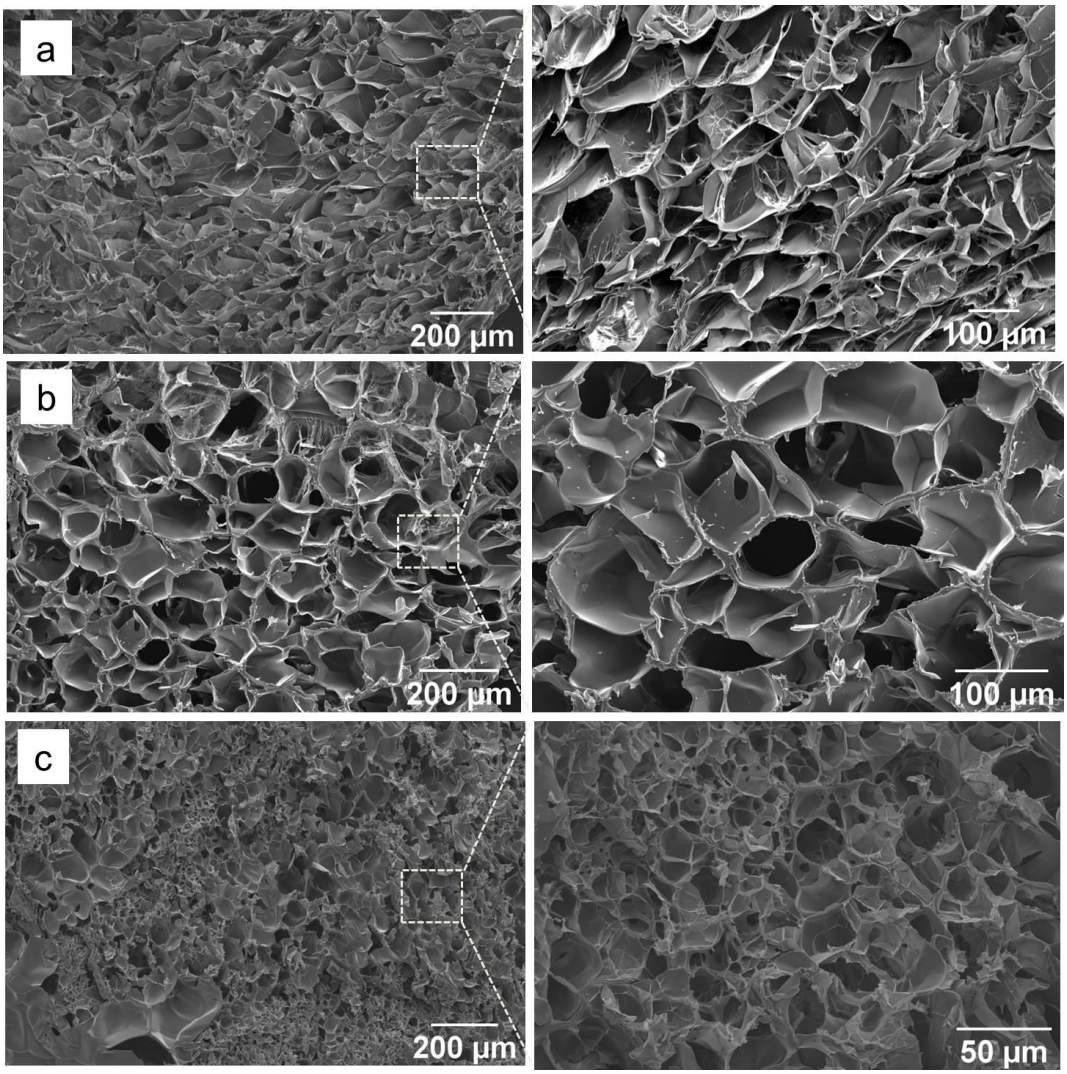

Figure 3.6 Cross-section SEM images of 5.6 % a) non-crosslinked, b) crosslinked and c) crosslinked/tannic acid supplemented gelatin foams in different magnifications.

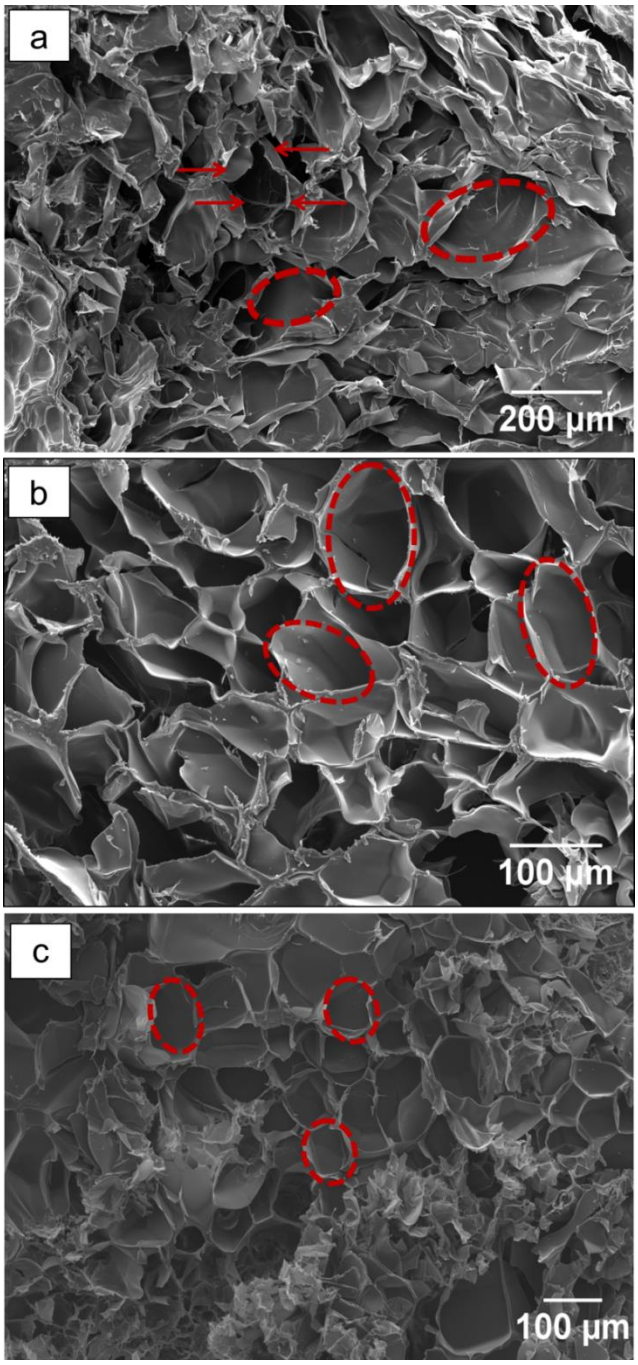

Figure 3.7 Cross-section SEM images of 5.6 w/v % a) non-crosslinked, b) crosslinked and c) crosslinked/tannic acid supplemented gelatin foams. Pore morphology was altered after TGA and TA modification resulting in more regular pore structure compared to non-crosslinked foams which showed a collapsed pore formation (Circles represent pore shape, arrows show pores).

In general, after TGA or TA treatments, foams maintained their porous architecture. However, pore morphology was altered after TGA and TA modification resulting in more regular pore structure compared to non-crosslinked foams which showed a collapsed pore formation. This result can be attributed to the effect of crosslinking in material viscosity. Belyadi et al. [415] explained this effect as the influence of cross-linker which is significantly increases the viscosity of gelling agents by linking multiple molecules together, which is resulted in an increase in molecular weight of base polymer (Fig. 3.8).

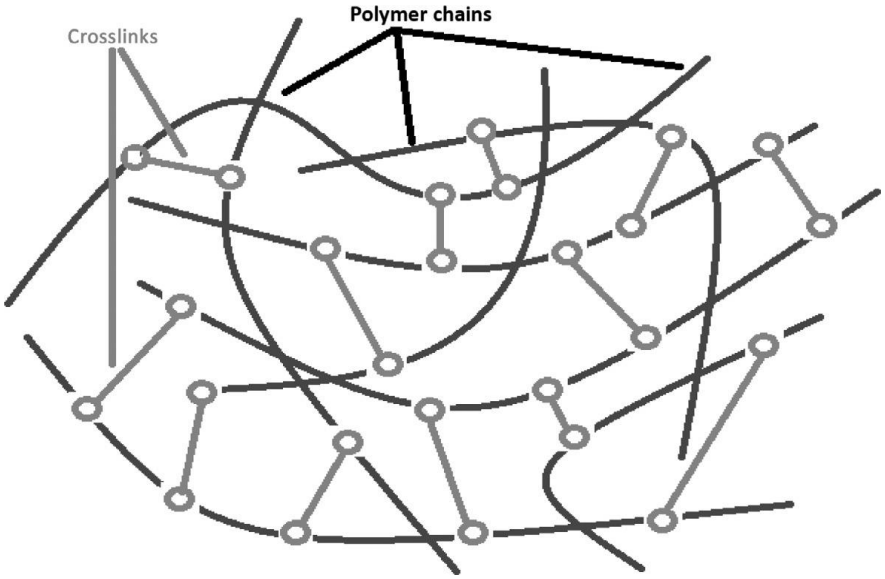

Figure 3.8 Crosslinked gel. Cross-linker increases the viscosity of gelling agents by connecting the separate gel polymers together. (from Belyadi et al., 2019)

In consideration of materials subjected to the freeze-drying process, collapse of the structure can be explained by the increased viscosity as suggested by Krokida et al. [416]. That is, in freeze-drying process, as the frozen ice crystal is sublimated, the concentrated solution tends to collapse due to the surface tension of the capillaries. The opposite force, which tends to keep the matrix non-collapsed is the complex viscosity of the matrix. Therefore, at relatively higher viscosity, material becomes too stiff and difficult to collapse.

Figure 3.9 shows the pore size (a) and box and whisker plot (b) of each treatment obtained from SEM image analysis. Non-crosslinked, TGA crosslinked and TA supplemented foams exhibited the pore sizes of 70 ± 40.6, 54.82 ± 27.5, and 32.84 ± 25.4 μm, respectively and the values showed significant differences ($P<0.05$). Also, with the reduction in pore size between the groups, a more homogeneous size distribution profile is observed. In consideration of TGA results, these data is consistent with the previous studies revealing that the crosslinking causes a decrease in pore size of collagen based materials [417-419]. Also, in a specific manner, obtained pore size value for defined gelatin and TGA concentration is consistent with the previously reported works based on TGA crosslinked gelatin porous material [420, 421]. In the case of TA supplemented foams, as mentioned earlier, in addition to its antibacterial and antiviral properties, it has been also shown that TA is an effective crosslinking agent for collagen based materials primarily for gelatin [422-424]. Moreover, as observed for collagen [417] and poly(vinyl alcohol) PVA [425] derivative hydrogels, there is an inverse relationship between degree of crosslinking and pore size. Therefore, considering these observations, higher decrease in pore size of TGA crosslinked/TA supplemented foams compared to TGA crosslinked foams, can be interpreted as the effect of increased degree of crosslinking by TA supplementation. As TGA is an enzymatic crosslinking reaction acting on specific amino acid residues, unlike EDC or GA which works on all available -COOH and -NH3 groups; there is availability of pendant groups in the current configuration for further crosslinking via TA.

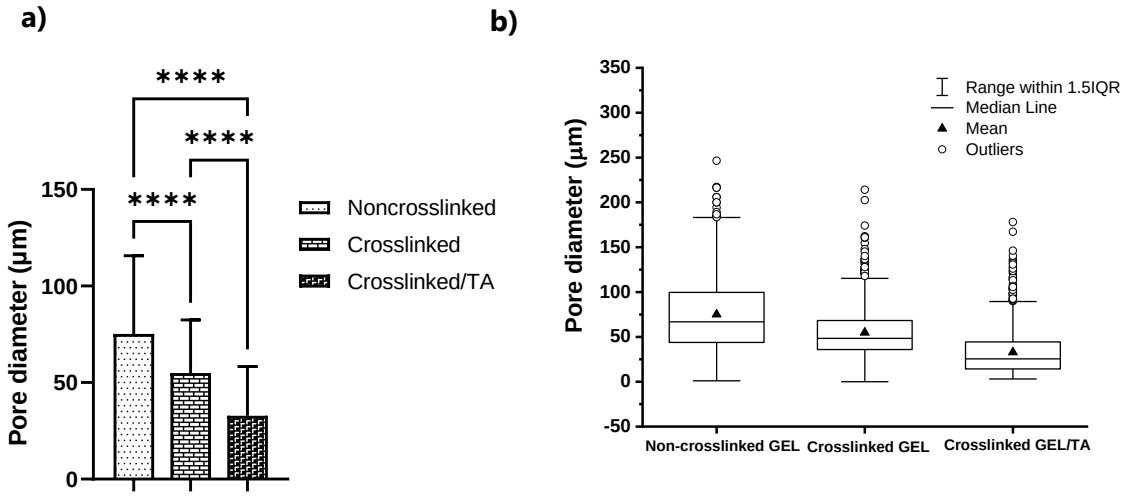

*Figure 3.9 Pore size (a) and box and whisker plot (b) of 5.6 % non-crosslinked, crosslinked and crosslinked/tannic acid supplemented gelatin foams. Transglutaminase crosslinking and TA supplementation resulted in a significant decrease in pore diameter (****p < 0.00001).*

3.1.3 Degradation profiles of Scaffolds

Scaffolds for tissue engineering applications should be degradable at a rate which matches ECM production and tissue remodeling [426]. Effect of scaffold degradation on the fate of cells has been studied previously. For example, MSCs encapsulated in a non-degradable hyaluronic acid gel showed adipogenic differentiation while the cells encapsulated in a degradable gel differentiated to the osteogenic lineage [427]. The rate of scaffold degradation is also of crucial importance. For instance, while blood vessel formation and angiogenesis require a fast (few days) degradation rate, mineralization and osteogenesis need relatively slow (few weeks) degradation rate [428, 429]. In biological environments, degradation of scaffolds is water and enzyme induced process. Although degradation makes changes in geometry, physical and chemical properties of the material, direct measure of degradation is mass loss [430]. In this work, hydrolytic and enzymatic degradation studies were assessed for crosslinked gelatin foams in various gelatin concentrations at 37 °C, in PBS (pH=7.4) and collagenase, respectively. Degradation behavior was examined by observing the percent weight loss as a function of time. Hydrolytic degradation profiles of 1.4, 2.8, 5.6, 11.2 and 16.8 % crosslinked gelatin foams are presented in Figure 3.10. At the

end of 2 weeks, foams 1.4, 2.8 and 5.6 %, lost 76, 72 and 62 % of their initial weight, respectively and maintained their bi-phasic state in the following 3 weeks. It has been previously shown that the rate of degradation decreases as the concentration of gelatin solution increases [431]. Accordingly, observed variation in degradation rates is consistent with the gelatin concentration of the foams. However, this concentration dependent degradation rate was not observed for 11.2 and 16.8 % foams. This weak hydrolysis resistance despite the higher gelatin concentration can be explained by the lower or heterogeneous crosslinking density of the hydrogels. As described earlier, Gelatin/TGA hydrogels were prepared by mixing gelatin solution in various concentrations (corresponding to the aimed final concentration) and TGA (20 %) solution at a volume ratio of 5:1. Therefore, the amount of TGA might be insufficient to provide the crosslinking of whole structure resulting in higher degradation rate. Another reason might be the increased viscosity of the hydrogel preventing the homogenous dispersion of TGA solution through the hydrogel and caused the formation of non-crosslinked local points which are accelerating degradation rate.

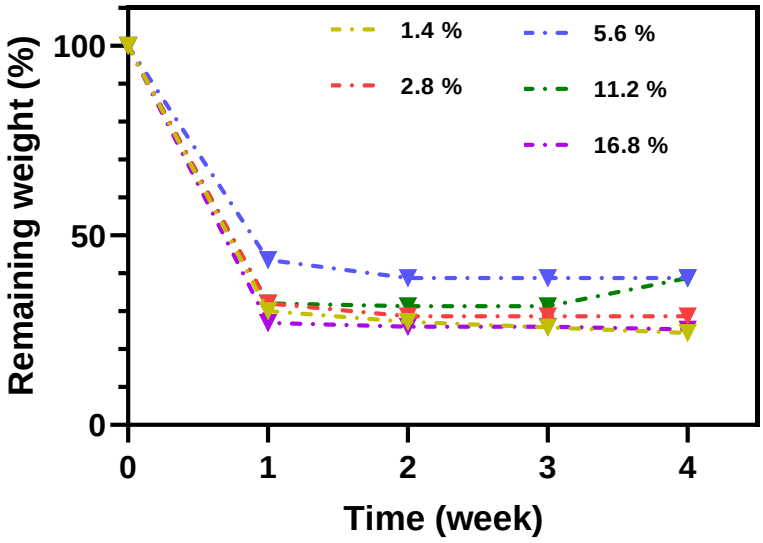

Figure 3.10 In vitro hydrolyticc degradation profiles of the gelatin foams over the period of 4 weeks at 37°C in PBS (pH 7.4).

Since the cells seeded in a tissue engineered scaffold secrete several proteases, such as collagenase, trypsin and pepsin which could lead to material degradation, the enzymolitic degradation performance of a scaffold should be evaluated to provide a basis for cellular inoculation and digestion. In this evaluation, although the enzyme concentration is different between in vitro and in vivo conditions, degradation mechanism is the same. Collagenase has been previously used as a mimic for some of the protease which is secreted by hMSCs [432, 433]. Figure 3.11 shows collagenase degradation behaviors of 1.4, 2.8, 5.6, 11.2 and 16.8 % crosslinked gelatin foams. Remaining weights of the foams after enzymatic treatment was measured at each half hour. Unlike the hydrolysis, enzymolitic degradation rates of the foams show a concentration dependent variation. Foams 1.4, 2.8 and 5.6 % completely degraded after 60, 90 and 120 min of enzymatic degradation. Gelatin foams above 5.6 % were found to be more resistant to collagenase degradation. Complete degradation of 11.2 and 16.8 % foams required 5 and 6.5 h, respectively.

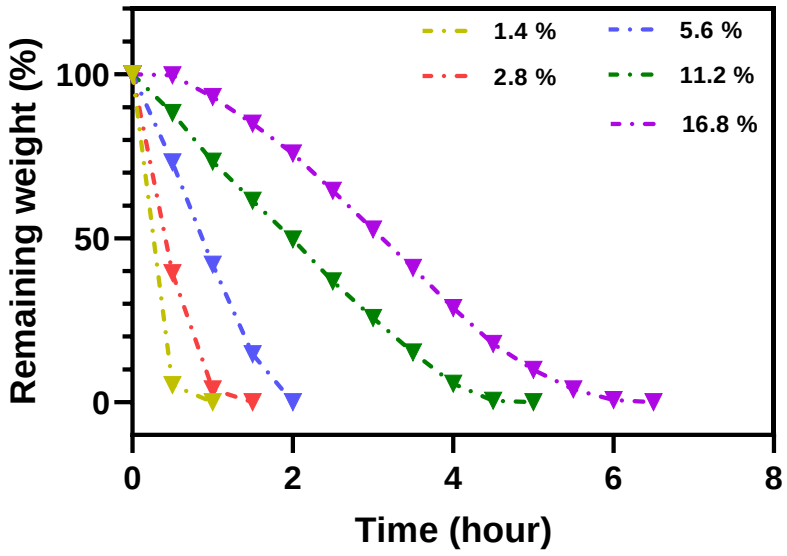

Figure 3.11 In vitro enzymatic degradation of the gelatin foams in the presence of 0.1 mg/ml collagenase Type IA (0.5-5.0 FALGPA units/mg) solution in PBS (pH 7.4) at 37 °C.

Structural disintegration of noncrosslinked gelatin materials and the hydrolytic/enzymatic degradation resistance of TGA crosslinked equivalents have been shown previously [421, 434]. In literature, similar results were found based on gelatin/TGA system with comparable degradation rate profiles for 5.6 % gelatin formulation. For example, Muller at al. [435] developed a TGA crosslinked gelatin-based hydrogel loaded with polydopamine (PDA) nanoparticles decorated with polyarginine (PAR) as a model of tissue engineering scaffold with antimicrobial ability and improved mechanical properties. In a study of Ciftci et al. [436], TGA crosslinked gelatin based bi-layered film structures were designed to produce respiratory epithelium for the purpose of fast epithelialization of large implant surfaces. Designed substrate was attached to titanium implants and the epithelial patch was stable under in vitro conditions for 7 days without deterioration.

3.1.5 Cytotoxicity of non-crosslinked and TGA crosslinked gelatin foams

In tissue engineering, use of biomaterials requires a cytotoxicity evaluation to test cell response to the used material. Here, in order to analyze whether the crosslinking reaction results in any cytotoxic effects, the indirect cytotoxicity tests have been examined according to ISO 10993/5. The indirect cytotoxicity method was selected as it is more suitable with respect to the mode of action of the foams, degradation and remodeling. Alamar blue assay was used for quantitative analysis of HUCMSCs viability cultured in non-crosslinked and TGA crosslinked gelatin foams and results were expressed in number of cells. Figure 3.12 shows the cytotoxicity results of all non-crosslinked gelatin foams. In the absence of crosslinking, a significant amount of gelatin is extracted, however as expected, there were no cytotoxic effects due to the presence of gelatin in the cell culture media, and the cellular viability was not statistically different from control conditions (Fig. 3.12 a). Cell viability of all the foams was higher than 70% (Fig. 3.12 b). According to ISO/EN 109935 a material is considered as cytotoxic if it causes at least 30% decrease in cell viability Cytocompatibility of gelatin has been examined in various studies and it has been shown that gelatin does not induce toxicity and other adverse effects in human cells

[437-439]. However, cytotoxicity can arise depending on the reagent used to crosslink gelatin solutions [440, 441].

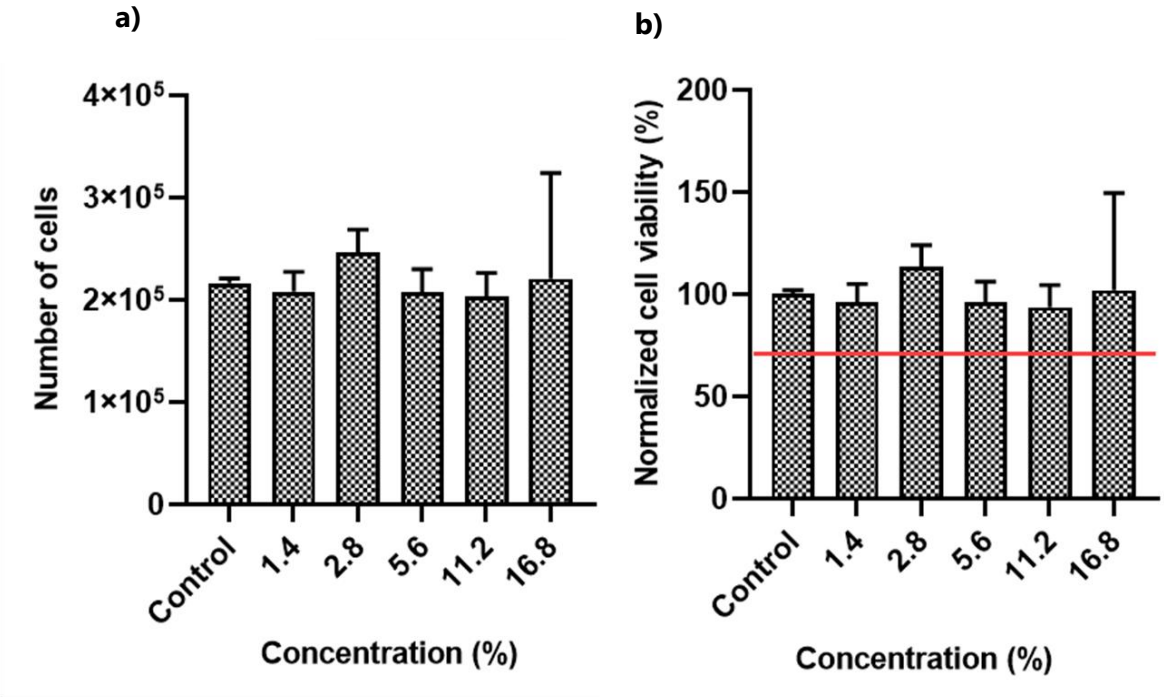

Figure 3.12 a) Indirect cytotoxicity of non-crosslinked gelatin foams b) Normalized cell viability

Thus, as a second step, in order to see the effect of the TGA crosslinking reaction on the cytotoxic behavior of the foams, same tests were carried out after crosslinking. Figure 3.13 shows the cytotoxicity results of crosslinked gelatin foams. No cytotoxic effect was observed up until the concentration of foams of 5.6 %. At higher gelatin concentrations, a statistically significant decrease in cell numbers was observed (Figure 3.12 a), even though it stayed above the cytotoxicity level, 70% viability (Fig. 3.13 b). This effect might be due to several parameters such as the impurities in TGA solution, the potential cytotoxic effect of TGA at high concentration due to the unwanted crosslinking of cellular components, high viscosity of high concentration of gelatin solutions, heterogenous distribution of added

TGA which has led to non-homogeneous crosslinking and the release of unreacted TGA residues. However, the system is stable at the optimized concentration of 5.6%.

As explained earlier, Gelatin/TGA hydrogels were prepared by mixing gelatin solution in various concentrations (corresponding to the aimed final concentration) and TGA (20 %) solution at a volume ratio of 5:1. That is, for varying gelatin concentrations, the amount of TGA was kept stable. Although the same amount of TGA was introduced, cytotoxic effect is observed for increased gelatin concentrations. Thus, in the case of increased gelatin concentrations, cytotoxic effect can be attributed to the presence of the unreacted TGA residues. Generation of these unreacted residues can be explained by the high gelatin concentration not allowing the homogeneous dispersion of crosslinker resulted in formation of unreacted TGA clusters. Here, the toxic effect can be considered indirectly as the effect of high crosslinker concentration as reported in literature. For example, Halloran et al. [442] evaluated the relative cytocompatibility of different concentrations of microbial TGA crosslinked collagen Type II scaffolds using 3T3 fibroblasts. Although there was no significant difference in cell viability between the control and cross-linked, for TGA concentrations above 0.01 %, a reduction in viability was observed compared to scaffolds with lower enzyme concentrations, attributed to the some level of toxicity associated with higher concentrations of the enzyme. However, the general consensus is that the microbial TGA is not cytotoxic [434, 440, 443, 444]. Apart from the effect of TGA, another variable, viscosity of the scaffold extracts may affect the cell viability. Viscosity is the property of resistance which opposes the relative motion of the adjacent portions of a liquid and it is regarded as a type of internal friction [445]. However, the same effect was not observed for non-crosslinked foams for the same gelatin concentration. This can be explained by the effect of crosslinking which increases the viscosity of gelling agents by linking multiple molecules together, which is resulted in an increase in molecular weight of base polymer [415]. Correspondingly, Bryant Chase [446] suggested that increased viscosity of a solvent decreases chemical reaction kinetics. Correspondingly, decreased cell viability in a high viscosity medium was attributed to the limited nutrient transport. . Taking into account these proposed explanations, obtained cell viability results are comparable with the literature. However, further examinations are required to identify the toxic effect of TGA in

defined conditions, in terms of the source of microbial TGA and the type of the cells examined.

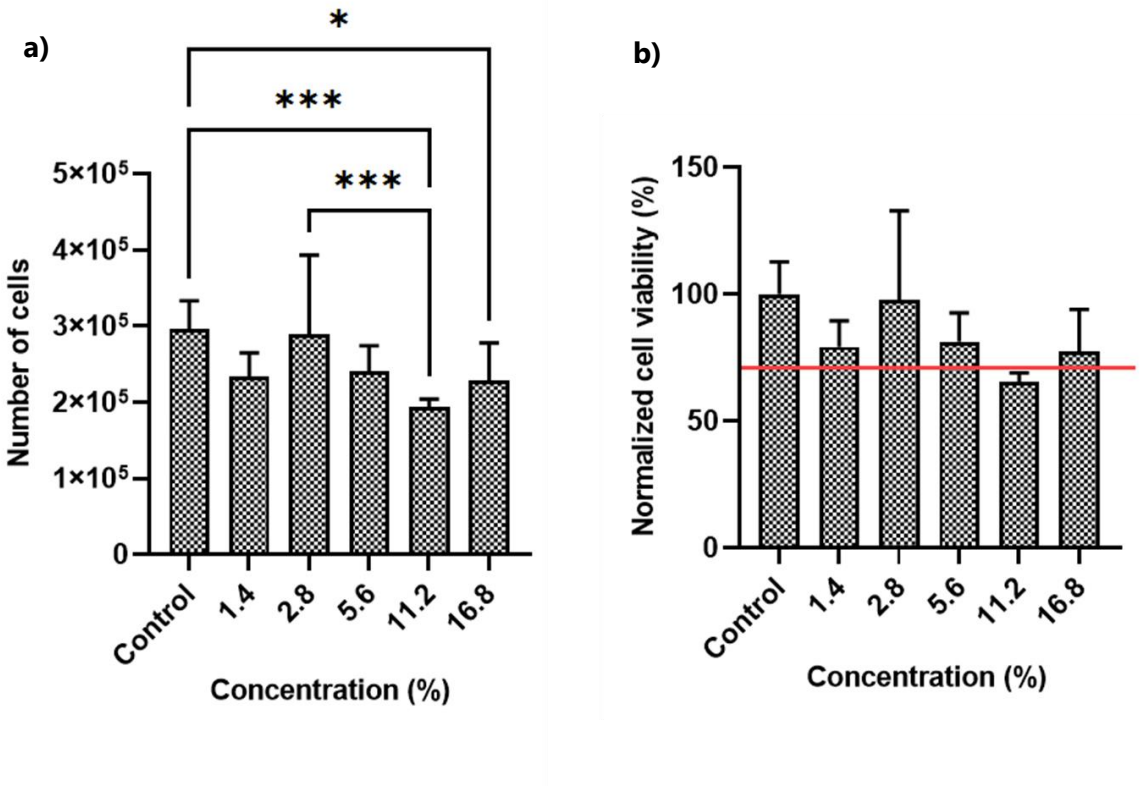

*Figure 3.13 a) Indirect cytotoxicity of crosslinked gelatin foams b) Normalized cell viability (*p<0.05,***p<0.001).*

3.1.5 Quantification of TA release from the scaffolds

In order to see how Tannic acid is released from the foam system and to be related to its antimicrobial properties, a release test was carried out over the course of 4 days. No longer tests were carried out as a plateau was observed on 3 consecutive days, meaning that the release has stopped. The results are presented as cumulative tannic acid release in Figure 14 as (a) the amount of released tannic acid and (b) the percentage of released tannic acid. In the initial period, varying between 1 and 24 h, a rapid release takes place; the amount of

released tannic acid is low, around 40% of the incorporated polyphenol. This can be explained the fact that the main portion of encapsulated tannic acid is chemically bonded and the small amount is physically included in the complex. This result is consistent with the previous results which revealed the crosslinking effect of TA on pore size of the foam referring the specific interactions (hydrogen bonding and hydrophobic interactions) between gelatin and TA.

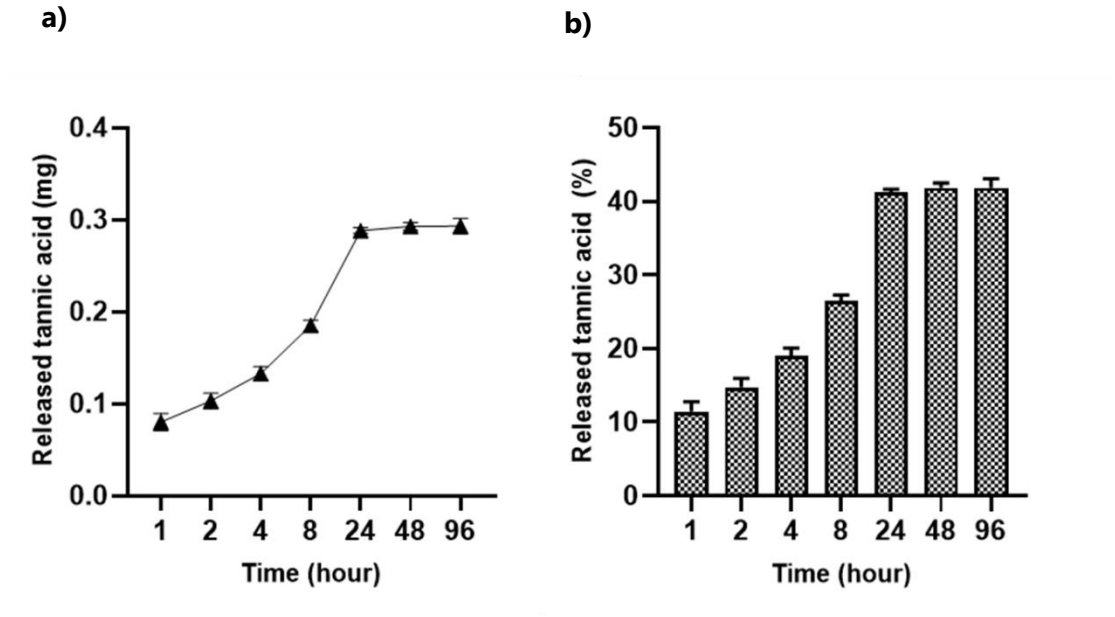

Figure 3.14 Tannic acid release from 5.6 % gelatin foam over the time: a) amount and b) percentage.

Depending on the aggregation state of tannins, two distinct processes have been identified between tannins and proteins. Under the critical micellar concentration (CMC) of tannin, a specific interaction takes place between the tannin and the peptide. Above the CMC, nonspecific interactions dominate and tannins form aggregates [447]. In our case, corresponding to 1:1 molar ratio of gelatin TA complex, concentration of tannic acid was $6.8\,x10^{-4}$ M which is above the CMC of tannic acid ($3.1\,x10^{-4}$ M, i.e., 0.53 mg/mL)

[448]. Figure 3.15 shows the macroscopic images of gelatin/TA hydrogels prepared in molar ratio of 1:1 and 1:2.

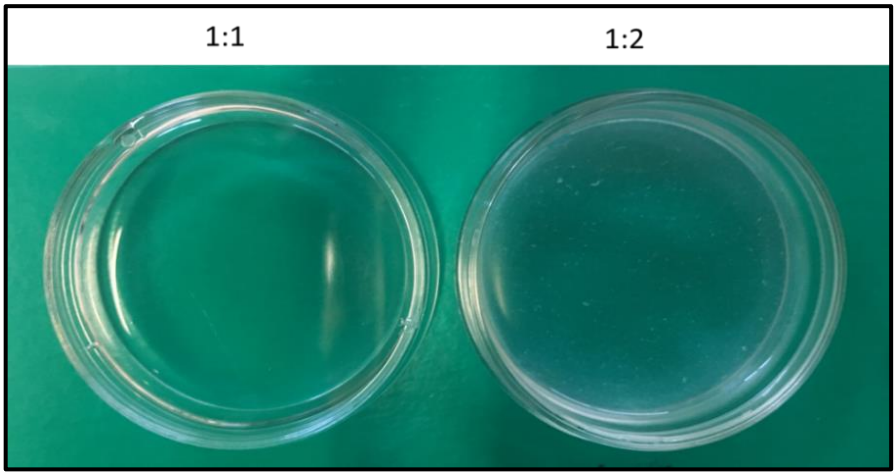

Figure 3.15 Macroscopic image of gelatin/TA hydrogels prepared in molar ratio of 1:1 and 1:2.

Aggregation began to be observable at the molar ratio of 1:2, which TA concentration reached to $1.4x10^{-3}$ M. But on the other hand, the other possibility is that the aggregation did not occur at this molar ratio because of the presence of other additive in the complex, TGA. That is, gelatin was exposed not only to TA but also to TGA. On preparation step, solutions have been mixed at the same time, that is, the reactions occurred simultaneously. Thus, aggregation could not be occurred since all the gelatin in the matrix did not react with TA. However, for the further examinations, 1:1 molar ratio has been chosen to obtain a matrix with no particle formation, which may interfere with the WJ particles in the further steps of scaffold preparation.

3.1.5 Cytotoxicity of TGA crosslinked/TA supplemented foams

TGA crosslinked/TA supplemented gelatin scaffolds were tested for their cytotoxicity using HUCMSCs following the same protocol as described in 3.1.5 for indirect contact test. However, in this case, it was observed that the first extract was cytotoxic and then foam extracts taken at 24 hour intervals were used. The aim here is to test whether it is possible to reach a non-cytotoxic level by rinsing the foams. Figure 3.16 shows the results as a) number of cells and b) normalized cell viability for 3 consecutive extractions for 24 h. A significant decrease in cell viability which is less than 60 % has been observed for medium extracted from GEL/TA foams at 1st and 2nd cycle of 24h incubation. If we recall the results of TA release experiment of the same foams (Fig 15.a), in the first 24 h, the concentration of released TA was 300 µg/ mL.

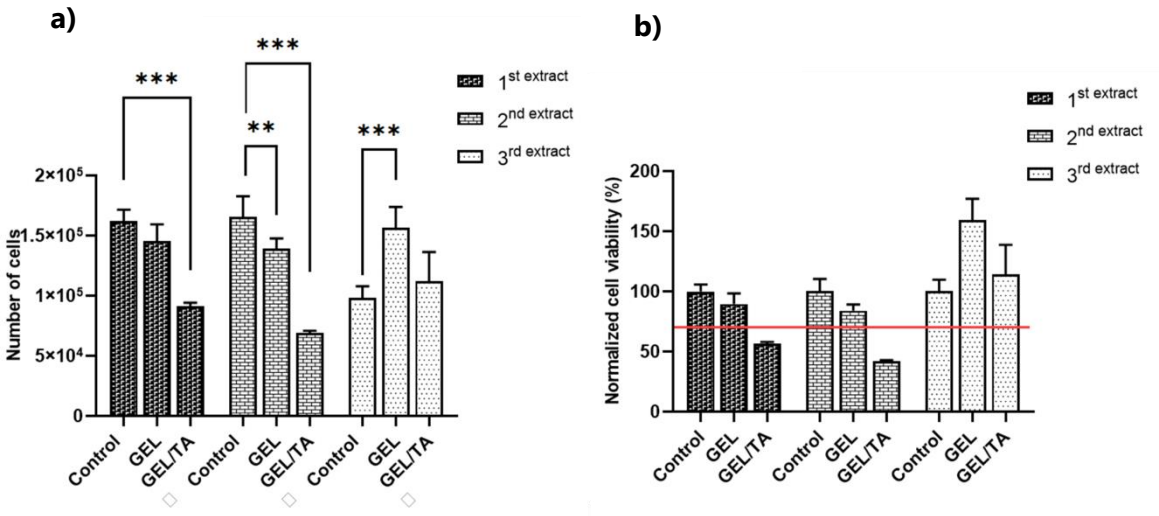

*Figure 3.16 a) Indirect cytotoxicity of Tannic acid supplemented gelatin foams b)Normalized cell viability. (**p<0.01,***p<0.001)*

Cytotoxic effect of tannins is revealed in the literature [449-451]. In terms of concentration dependent cytotoxic effect of TA, obtained cytotoxicity result is consistent with the previous studies. For example, Chen et al. [452] showed that TA less than 10 µg/ mL did

not influence bovine aorta endothelial cell (BAEC) proliferation. But as concentration reached to 50 µg/ mL, tannic acid almost completely inhibited BAEC proliferation. In another study, Cass et al. [453] designed a TA cross-linked collagen scaffold for minimally-invasive breast reconstruction. For this aim, they assessed the TA concentration that would kill MCF-7 tumor cells while allowing D1 mesenchymal stem-like stromal cells. They examined the cytotoxic effect of TA in condition of 5, 25 and 50 µg/ mL TA. A significant difference in the metabolic activity of MCF-7 cells was detected at 48 h at the 25 µg/ mL condition while a significant change was observed in the D1 culture at 24 h in the 5 µg/ mL experimental condition. However, actual decrease in metabolic activity was observed at 50 µg/ mL TA concentration within both cell types over a period of 72 h. To sum up, in consideration of these similar studies, decrease in cell viability for the 1st cycle (24 h) extraction can be attributed to the increased TA concentration which was found to be 300 µg/ ml. In the 2nd cycle (48 h) extraction conditions, although the all released TA was removed and medium was renewed, cell viability did not begin to increase until 3th cycle extraction (72 h). This result can be explained by the residual TA in the foam that cannot be removed during renewal of cell culture media. Due to the presence of proteases in the culture medium, a slight degradation of the foams during the incubation might have resulted in continued release of TA entangled within the matrix. Consistent with the TA release at 72 h, no significant difference was observed between control and the 3th cycle extraction conditions showing that the all residual TA was removed from the structure.

3.1.6 Antimicrobial activity of TGA crosslinked /TA supplemented gelatin foams

Antimicrobial activity of TA involves different modes of action such as enzyme inhibition, increased permeability of the membrane or destabilization of the cytoplasmic membrane by interacting with bacterial proteins [454] and these various modes of action are efficient to decrease the risk of developing antibacterial resistance. In vitro antimicrobial activity of 5.6 % TGA crosslinked/TA supplemented foams was evaluated against Gram-positive bacteria *S. aureus* using viable cell count test. This bacterial strain used for the study as it is a major pathogen causing a variety of clinical infections in human [455]. *S. aureus* growth was

evaluated in the presence of TGA crosslinked/TA supplemented foam. TGA crosslinked foam was used as negative control and Tetracycline/Cefotaxime was used as positive control in contact with TGA crosslinked foam. Figure 3.17 shows the normalized *S. aureus* growth after 24h.

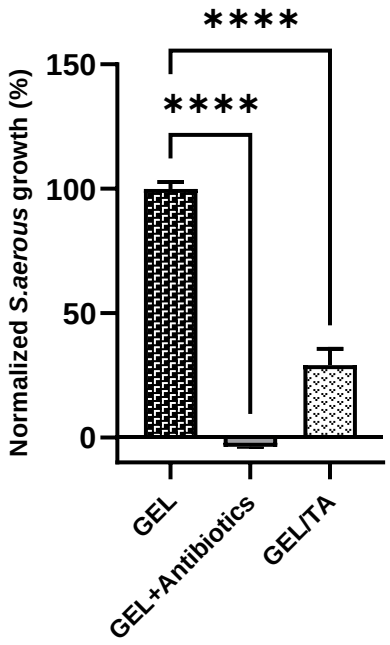

*Figure 3.17 Normalized S. aureus growth on Tannic acid supplemented gelatin foam (****p<0.0001).*

Inhibition efficiency of TA supplemented foam was observed around 70 %. However, the cytotoxicity of TA supplemented gelatin foam was elevated at 24h and this is not suitable for tissue engineering even though there is an antimicrobial activity. Therefore, in terms of antimicrobial activity with complete inhibition and in terms of biocompatibility, a proper Gelatin-TA formulation that meets both conditions should be considered.

3.2 Characterization of WJ particles and GEL/ WJ composite foam

Three different methods have been used to produce particulate form of WJ. Figure 3.18 shows the SEM images of lyophilized WJ fragments following the dissociation in PBS. Obtained material shows a fibrillary structure with partially uniform fiber morphology. However, the majority of the material was longitudinal mesh formed fragments around 1mm size not passing through 500 µm pore size strainer. As mentioned earlier, ECM is a rich source of growth factors and other bioactive molecules. Increased release of these molecules is a way to enhance the inductive potential of ECM based scaffolds. Thereby, particle size of ECM matrix is an important parameter for the efficient release of growth factors and other bioactive molecules. Thus, it has been suggested that reducing the particle size could promote release of these biological key factors in ECM materials [456]. However, it is also indicated that the use of spherical carriers with diameters less than 50–70 µm resulted in a significant cell growth reduction [457]. On the other hand, large particle size has disadvantages, such as diffusion limits and higher shear stress on the outer surface of the particle [458]. In different studies, it has been shown that the optimum size of ECM particles to promote tissue regeneration ranges from 100-400 µm [459, 460]. Therefore, the other methods have been evaluated in order to reduce WJ particle size.

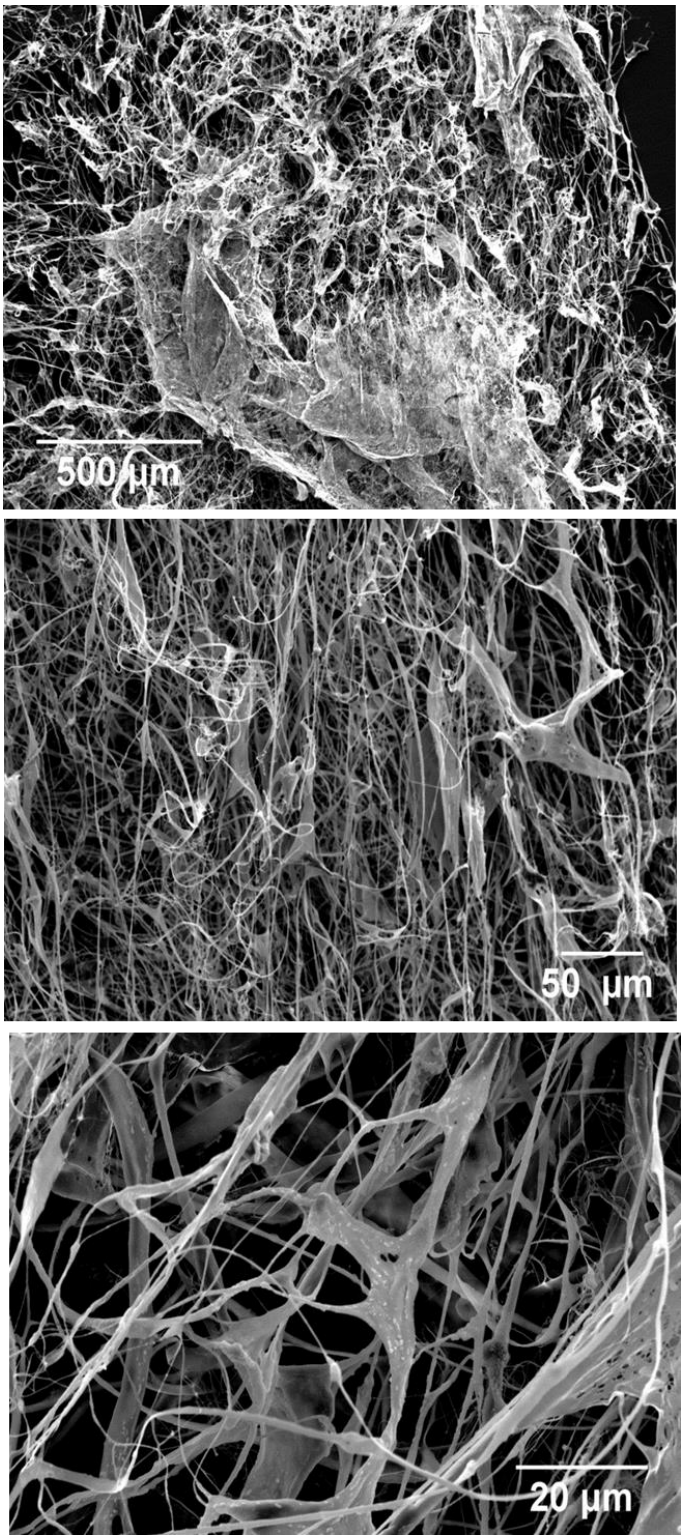

Figure 3.18 SEM images of lyophilized WJ fragments following the dissociation in PBS. Material shows a fibrillary structure with partially uniform fiber morphology.

Figure 3.19 shows the SEM images of WJ particles produced by pulverization method. Compared to the dissociation method, a larger portion of the obtained matrix fragments were small enough to be able to sieve by 500 µm pore size strainer. Also, surface ultrastructure of the particles showed a different morphology. Pulverized particles have a relatively smooth surface but fibrous morphology was preserved. The mean particle size (Fig. 3.20), based on maximum of 1019 µm was found to be 143.8 ±192.7 µm. Although the fragments were sieved by 500 µm pore size strainer, the fraction of particles with a size of more than 500 µm was around 4 % of the total volume. This result can be explained by the folding of the particles during sieving or clumping and agglomeration during powder preparation stage of SEM imaging. The distribution and the average size of the particles obtained by this method were within the limits in the literature for the induction of regeneration.

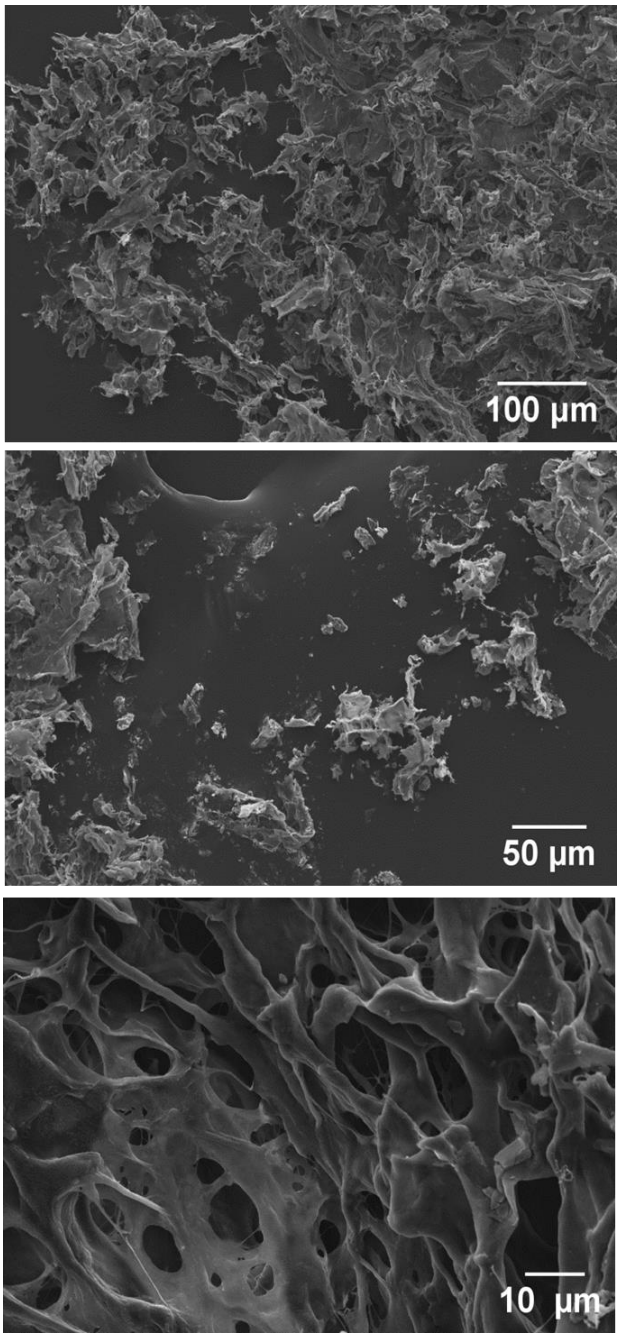

Figure 3.19 SEM images of WJ particles produced by pulverization method. Particles have a relatively smooth surface but fibrous morphology was preserved. Comparing to the dissociated samples, smaller fragments have been obtained.

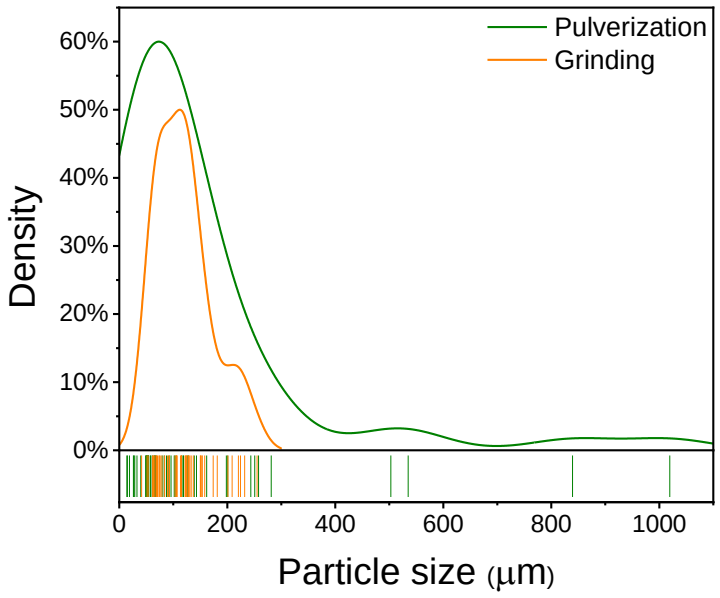

Figure 3.20 Particle size distributions of WJ particles produced by pulverization and grinding methods obtained from SEM image analysis.

Powder form of ECM matrix was obtained by grinding method. Figure 3.21 shows the optic images of obtained ECM powder. Powder was light yellow in color. In macroscopic scale, obtained particles were suitable for the preparation of Gelatin/WJ colloidal gel.

Figure 3.21 Optic image of WJ powder produced by grinding method. Particles had a sheet like appearance with a yellowish color.

Figure 3.22 represents the SEM images of WJ particles obtained by grinding method. Particles showed irregular-shaped convoluted forms with low porous microstructure without a fibrous formation unlike the particles obtained from other methods. Also, higher population of fine particles could be observed from the images. The mean particle size was found to be 119 ± 51.6 µm with a maximum of 370 µm (Fig. 3.12). In addition to reduced particle size, size distribution of the particles was more uniform compared to those obtained from pulverization method. Although diverse particle size distribution allows cellular adhesion and growth [461], it has been shown that particles with uniform size distribution provide more controlled *in vivo* tissue development. For instance, use of ECM powder with diverse particle sizes in skin tissue engineering can cause the formation of meshes with gaps which results in noncontiguous tissue formation [462]. Based on these results, ECM particles obtained from grinding method were used for the further steps.

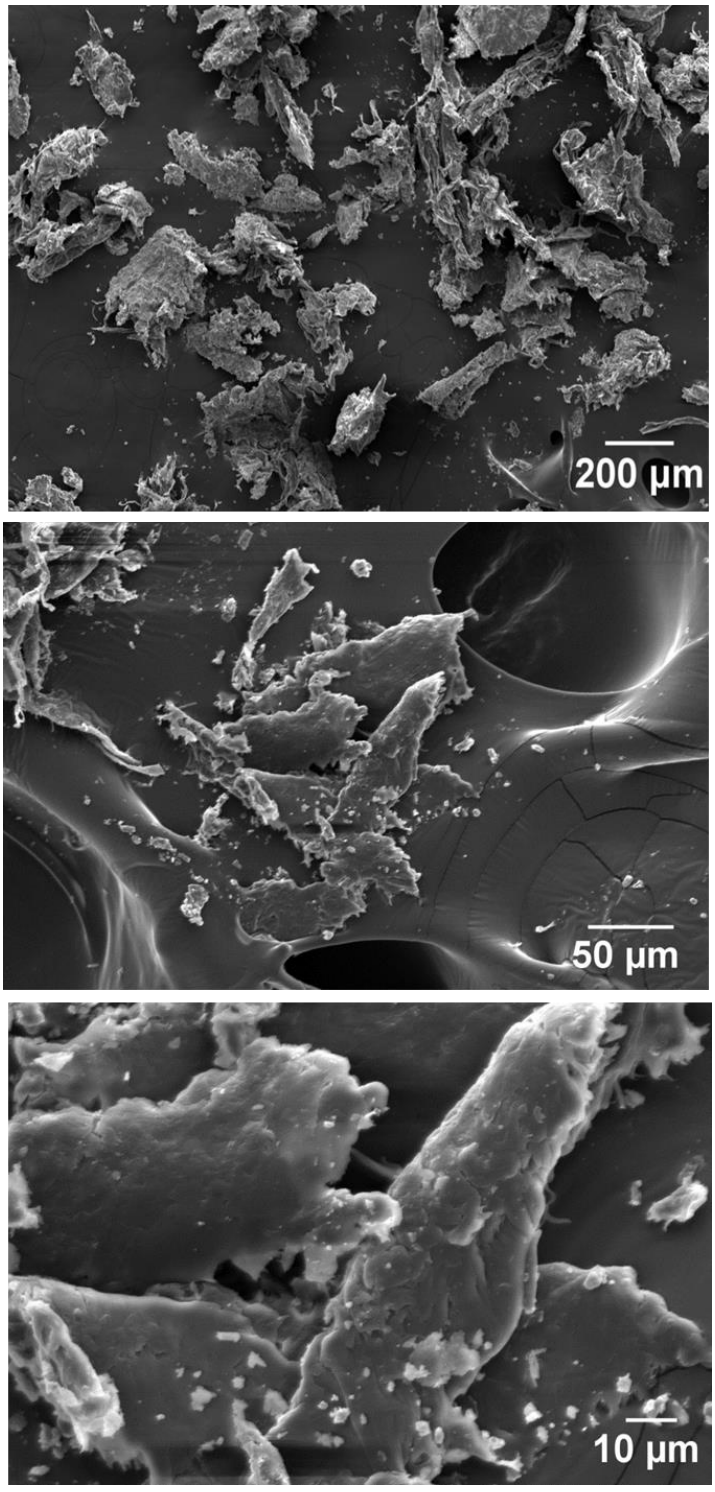

Figure 3.22 SEM images of WJ particles produced by grinding method. Particles showed irregular-shaped convoluted forms with low porous microstructure without a fibrous formation unlike the particles obtained from other methods.

3.3 Protein components of Gelatin and WJ supplemented Gelatin scaffold extracts

Gelatin and WJ supplemented gelatin scaffolds were evaluated by reverse-phase high-performance liquid chromatography (RP-HPLC) in order to detect and quantify the nature of the ECM components incorporated into the gelatin/WJ scaffold (Fig 3.23) The quantification was based on the released molecules from the scaffolds incubated in PBS over the period of 14 days. PBS extraction solutions showed similar profiles, even though there were several extra peaks for Wharton`s jelly in 17-23 min retention range, which may be attributed to the release of extra components derived from Wharton's jelly. However, ECM contains fibrous proteins such as collagen, fibrillin and fibronectin, which are cross-linked, making them insoluble. Thus, identification and evaluation of these proteins in ECM has proved challenging. Various protein extraction protocols have been developed. These methods typically involve a decellularization step followed by chaotrope extraction or dilution and digestion with LysC and/or Trypsin in preparation for Liquid Chromatograph (LC) analysis [463-465]. Biochemical methods have also been developed which use chemical digestion to solubilize and access highly insoluble ECM proteins of interest [466, 467].

Figure 3.23 RP-HPLC analysis of gelatin and WJ supplemented gelatin scaffold extracts

Protein component differentiation between Gelatin and Gelatin/Wj scaffolds was also studied under SDS/PAGE conditions at a molecular weight region ranged from 3 to 198 kD with 20 mg of total protein over the period of 1, 7 and 14 days PBS extraction (Fig 3.24). Over the time period of 1-14 days, both types of extracts were exhibited no time dependent variation in terms of band pattern. Also, in consideration of the type of extracts, no difference was observed between Gelatin and Gelatin/Wj scaffolds. Only one major band was detected at the point corresponding to 50 kD which is common for both type of samples. Gelatin consists of different compounds of α-chains (~100 kDa), β-chains (~240 kDa) and γ-chains (~ 400kDa) [468]. The presence of polypeptide bands with molecular weight less than α-chain in gelatin was attributed to the manufacturing conditions and the age of animal used [469]. Azira et. al [470] studied on the detection and differentiation of porcine and bovine skin derived gelatins added in processed foods using a combination method of SDS-PAGE and Principal Component Analysis (PCA). They detected 11 prominent bands which are approximately 125, 120, 114, 106, 96, 87, 83, 76, 70, 64 and 58 kDa on porcine skin derived gelatin.

Although our SDS-PAGE molecular weight region covers 100 kDa, related patterns were not observed for Gelatin or Gelatin/Wj extracts. In consideration of Wj, in similar studies, Wj derived ECM components have been identified by using SDS/PAGE such as fibronectin, collagen α-1 and some growth factors [471, 472]. Consequently, in terms of the both methods, HPLC and SDS/PAGE possible reason not to detect related proteins of gelatin and Wj could be explained by the low concentration of the protein because of the inefficient release conditions.

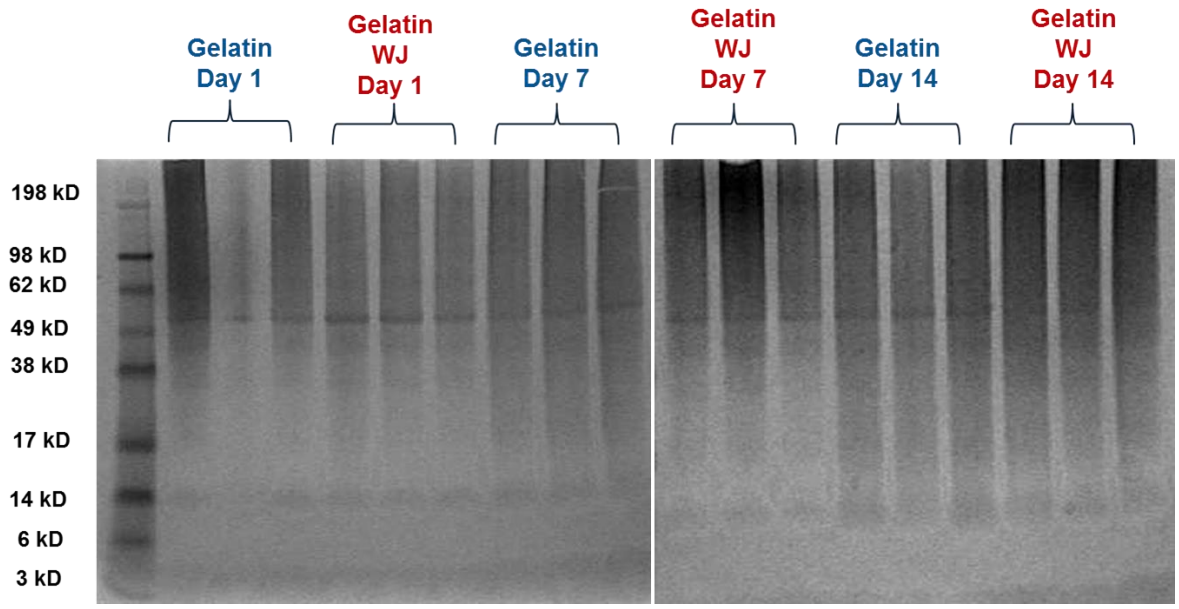

Figure 3.24 SDS/PAGE analyses of gelatin and WJ loaded gelatin foam extracts over the period of 1, 7 and 14 days.

3. 4 Characterization of GEL/ WJ composite foams

Figure 3.25 shows the macroscopic images of GEL/WJ colloidal gel before freeze-drying. Qualitatively, samples had a shape retention following the extrusion from the mold and maintained shape at room temperature following handling. Also, obtained composite exhibits homogenous particle dispersion along xy plane. In consideration of defined average particle size (119 ± 51.6 µm), it could be observed that there is not a significant

particle agglomeration. However, a time dependent phase separation was observed during the gelation of the samples resulting in heterogeneity in particle distribution along z-axis (figure not shown) which has been explained by the non-Brownian motion (unlike the nanoparticles) of micro particles suspended in a viscos media [473].

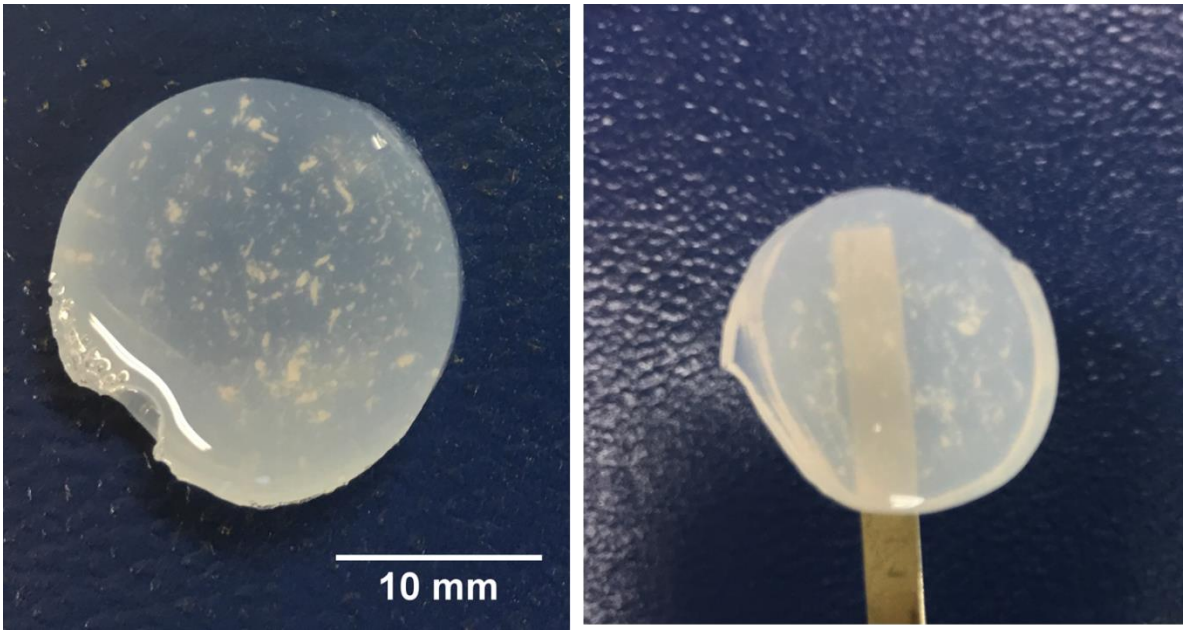

Figure 3.25 Macroscopic appearance of gelatin/WJ colloidal gel before freeze-drying. Samples had a shape retention following the extrusion from the mold and maintained shape at room temperature following handling.

Figure 3.26 shows the macroscopic images of GEL/WJ colloidal gel after freeze-drying. Material had a sponge like appearance with white color. After freeze-drying, the shape of the material was maintained but a decrease in volume, associated with the shrinkage was observed.

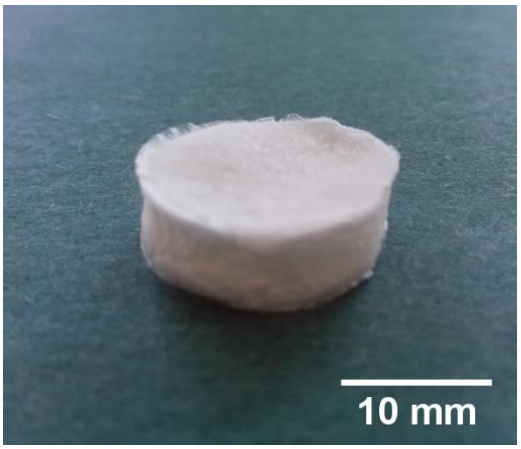

Figure 3.26 Macroscopic appearance of gelatin/WJ colloidal gel after freeze-drying. Material maintained its shape but a decrease in volume, associated with the shrinkage was observed.

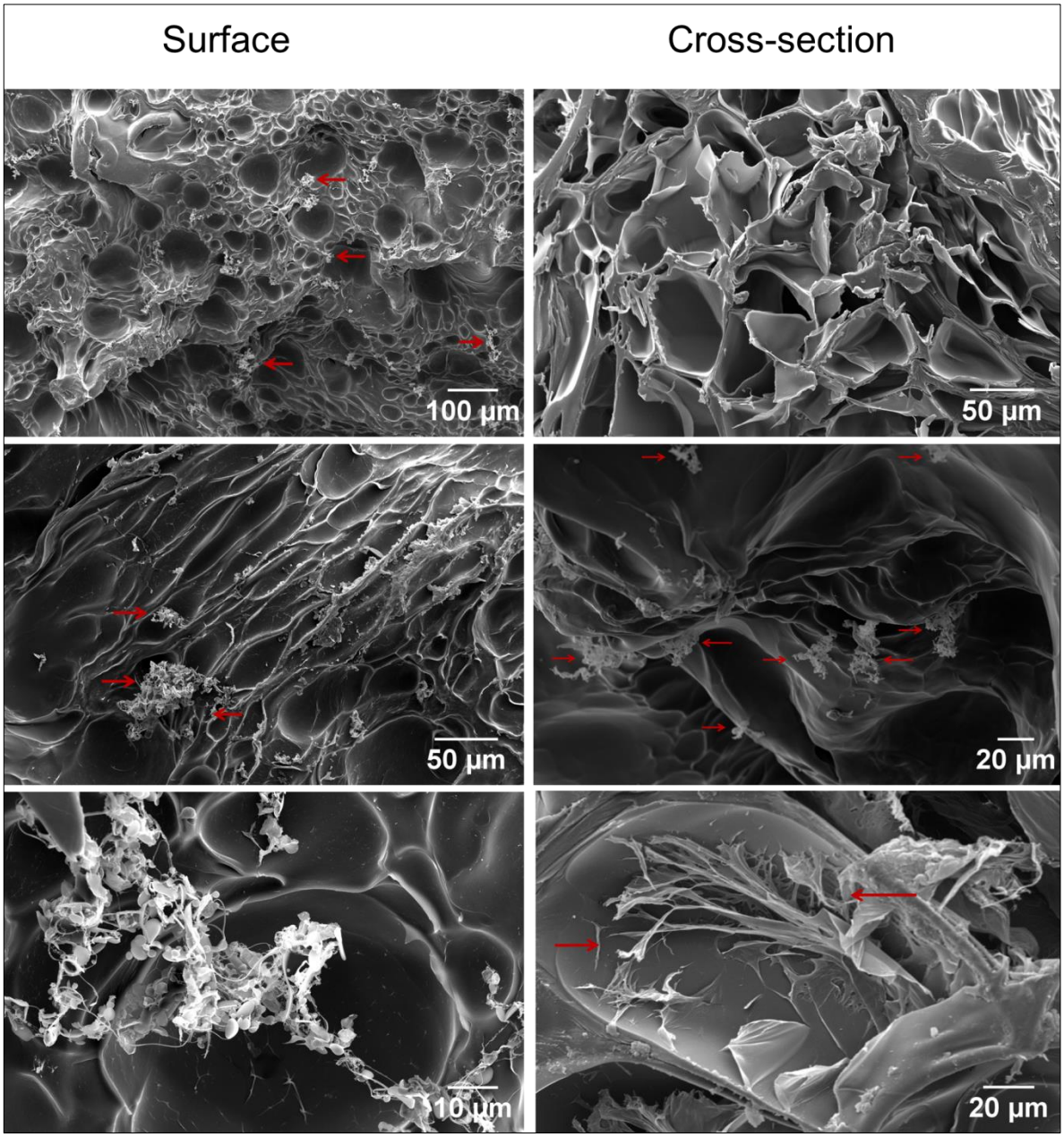

Figure 3.27 SEM images of Gel/WJ composite foams (surface). WJ particles attached and distributed around the scaffold.(Arrows represent WJ microparticles)

SEM images of Gel/WJ composite scaffold (Fig. 3.27) revealed that WJ particles attached and distributed around the scaffold. The size of the particles is consistent with the particle size distribution previously observed, indicating that the particles preserved their dispersed phase during freeze-drying.

Figure 3.28 shows the SEM images (a) and pore size distributions (b) of Gelatin (GEL) and Gelatin Wharton`s Jelly (GEL/WJ) composite foams. Pore size distribution results show that WJ addition to blank gelatin hydrogel had no significant effect on pore size of the scaffold. In consideration of similar studies subjected to ECM particle based scaffolds, increase in pore size with the addition of ECM particles has been explained by the crystallization of ice during freeze-drying [474, 475]; Pore size of a scaffold is mainly depended on the volume of ice crystals. Water distribution in the initial ECM may contribute to mass crystallization of ice in frozen material and mass crystallization of ice lead to the larger pore formation. As mentioned earlier, WJ fragments were dried by freeze-drying prior to grinding process. Thus, stability in pore size after WJ addition could be explained by the prevention of mass crystallization in WJ loaded gelatin scaffolds during freeze-drying. However, as observed in SEM images (Fig. 3.28 a), WJ loaded gelatin scaffold had a contracted pore formation. In similar studies, this contraction in pore morphology has been attributed to the particle size range of ECM material [456, 476]. For example, Almeida et al. produced porous scaffolds using slurries of coarse or fine porcine cartilage ECM with a mean particle size of 322 ±195 μm and 97± 26 μm, respectively. More homogenous and spherical pores (mean diameter: 65 ± 20 μm) were observed in the fine ECM scaffolds while less spherical pores and a wider distribution of pore sizes (mean diameter: 104 ± 49 μm) was observed in the coarse ECM scaffolds.

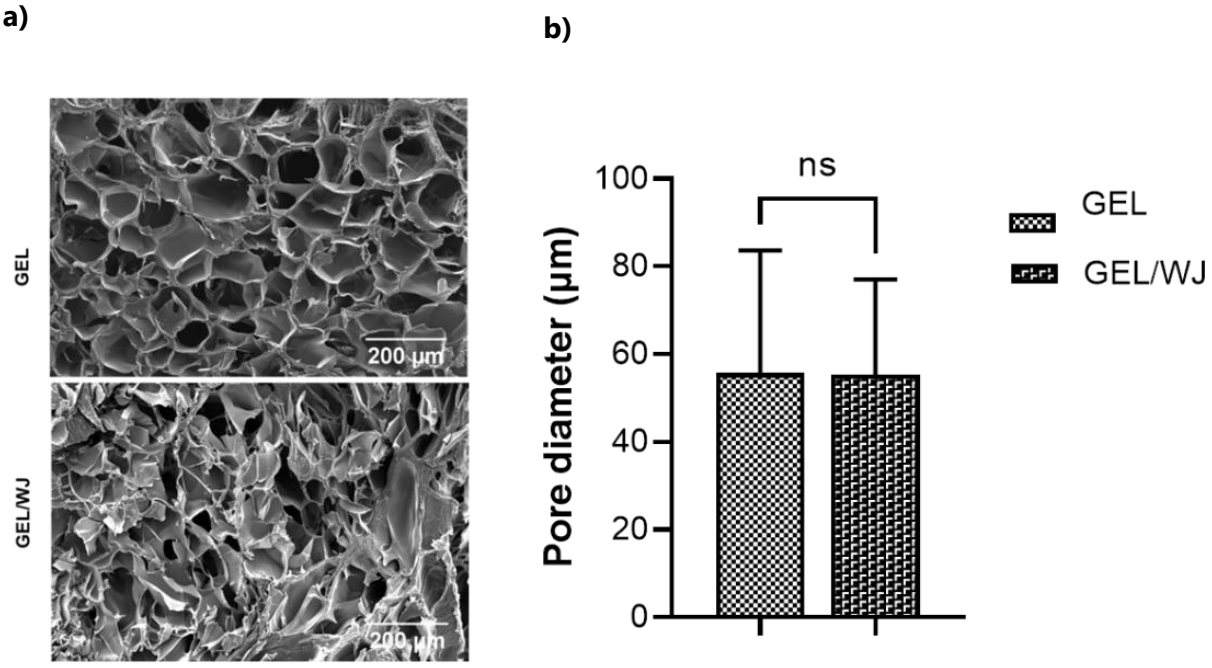

Figure 3.28 SEM images a) and b) pore size distributions of Gelatin (GEL) and Gelatin Wharton`s Jelly (GEL/WJ) composite foams. WJ particle addition had no significant effect on pore size of the scaffold.

3.4.1 THP-1 cell culture on GEL or GEL/WJ scaffold

In this work**,** THP-1 cell line was used as an *in vitro* cell model to study the monocyte /macrophage responses and possible effects from external stimuli in GEL and GEL/WJ scaffolds. THP-1 cell line is isolated from the peripheral blood of a 1-year old male patient suffering from acute monocytic leukemia [477]. These cells have been widely preferred to study human macrophage–biomaterial interactions as they are also in macrophage-like state. During inflammation, monocytes and not fully differentiated macrophages are recruited to the implant site, where they may differentiate into macrophages [478]. Here, for the characterization of the initial immune reaction in the presence and absence of WJ particles, human THP-1 monocytes have been seeded on the foams to mimic the arrival of

the circulation monocytes following implantation. Metabolic activity of seeded monocytes was evaluated over the time period of 1, 4 and 6 days (Fig. 3.29).

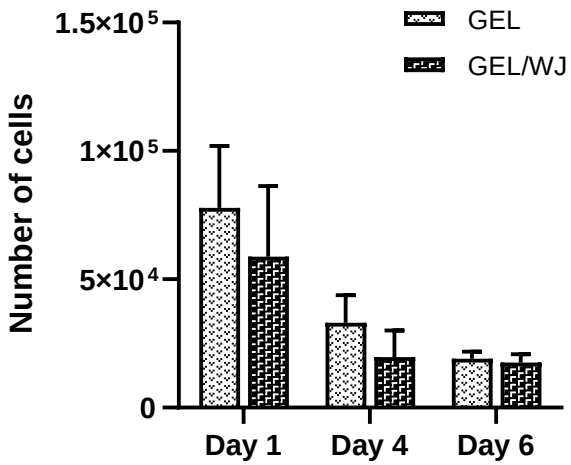

Figure 3.29 Metabolic activity of THP-1 monocytic cell line on GEL or GEL/WJ scaffold. Metabolic activity of monocytes incubated on GEL and GEL/WJ scaffolds decreased on the average at around % 60, 32 and 17 of that of cells cultured for 1, 4 and 6 day, respectively.

Metabolic activity of monocytes incubated on GEL and GEL/WJ scaffolds decreased on the average at around % 60, 32 and 17 of that of cells cultured for 1, 4 and 6 day, respectively. Also, no significant difference in metabolic activity was observed between the cells incubated on GEL or GEL/WJ scaffolds. SEM and Confocal imaging have been performed for detailed observation of the samples on day 1 and day 6. Figure 3.30 shows the SEM images of monocyte seeded GEL and GEL/WJ scaffolds. The monocyte attachment to the foam surfaces and penetration was minimal in both cases and the attached monocytes do not turn into macrophages and rest on the surface as evidenced by the decreasing metabolic activity. SEM images showed occasional attached monocytes, with no excessive clustering, or spreading which would be an indicator of increased interaction with the foams.

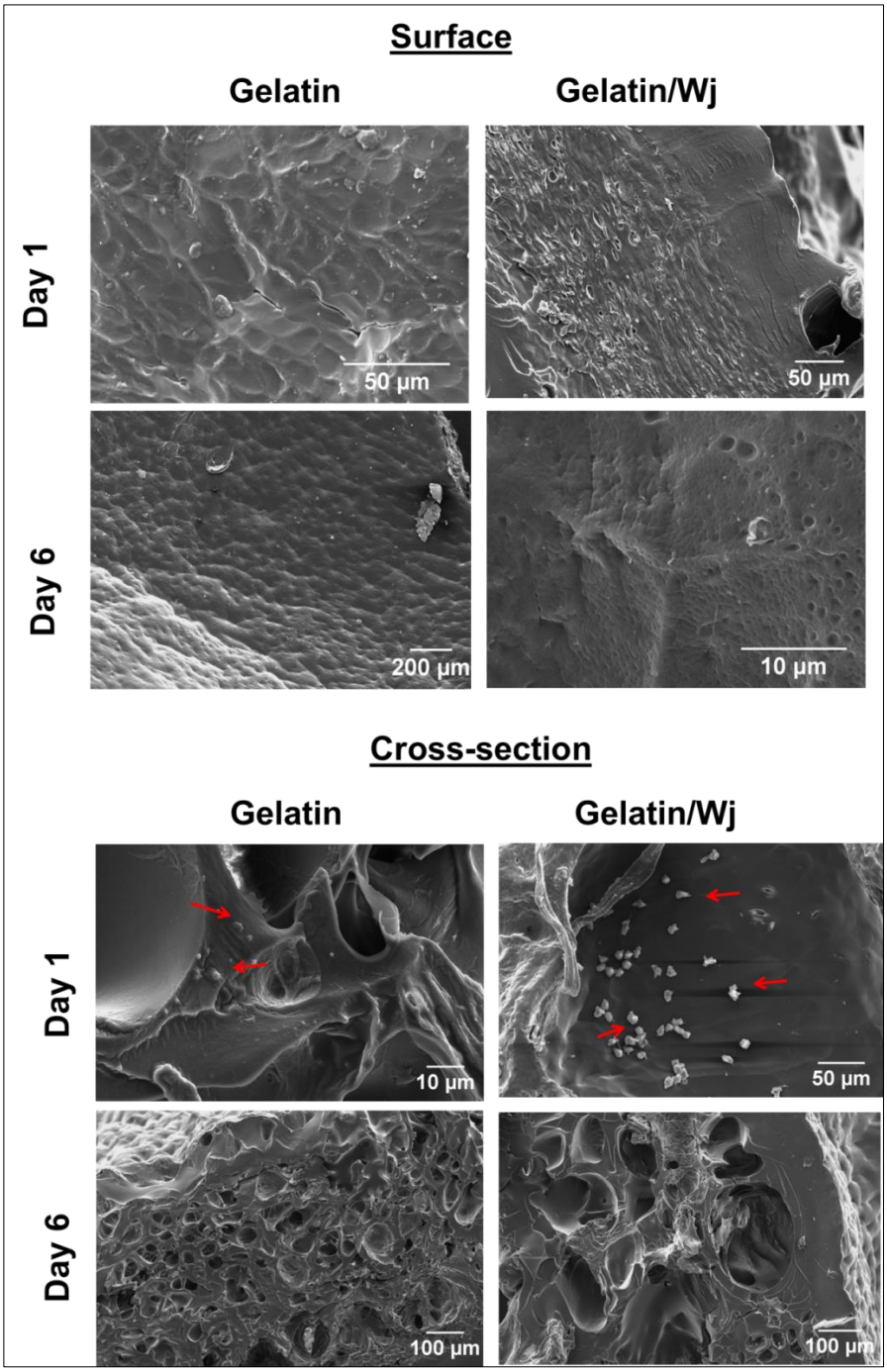

Figure 3.30 SEM images of THP-1 monocytes on gelatin (GEL) and WJ particle loaded gelatin (GEL/WJ) scaffolds at day 1and day 6 taken from surface and cross-section. Occasional attached monocytes, with no excessive clustering, or spreading were observed which would be an indicator of increased interaction with the foams. (Arrows represent THP-1 monocytes).

As a second step, macrophage response to the developed scaffolds has been examined. Macrophages have a key role in mediating tissue remodeling. By secreting chemokines and cytokines, they directly impact the overall response to the implanted biomaterial, whether a fibrous capsule formation or the resolution of the inflammatory process will take place [479]. Following the migration into the inflamed tissue, macrophages are activated to polarize two states related to their functional diversity: pro-inflammatory M1 and anti-inflammatory M2 [480]. M1 macrophages typically release high amounts of pro-inflammatory cytokines such as IL-1β, IL-8, and TNFα [481]. In context of an implanted biomaterial, M1 macrophage action is mandatory for wound healing and tissue regeneration. However, prolonged presence of M1 macrophages causes the formation of foreign body reaction (FBR), granuloma and fibrous encapsulation resulting in failure of biomaterial integration. In contrast, M2 macrophages release anti-inflammatory cytokines such as IL-10 and shows a high level of iron export which facilitates tissue remodeling [482]. M2 macrophages have different subsets including M2a, M2b and M2c. While M2a and M2b subsets have immune regulatory functions, M2c has a key role in suppression of inflammatory immune reactions and tissue remodeling [483]. These functions contribute to the vascularization of implanted biomaterial and inhibit the formation of fibrous tissue which improves the integration and the performance of the biomaterial to fulfill its aimed function [484]. Consequently, it has been suggested that a high M2:M1 ratio in proximity of an implanted biomaterial provides better constructive remodeling outcomes [485]. It is also established that the macrophages switch their polarization states depending on the micro-environmental conditions presented by biomaterials [486]. Chemical properties such as surface chemistry, ligand presentation and release of growth factors; Physical properties such as pore size, surface topography and substrate stiffness and temporal properties, such as degradation rates, all are the micro-environmental cues effecting macrophage behavior in terms of polarization state [480, 487].

In this work, to see the reaction of the differentiated innate immune cells to the developed foams, monocytes have been first differentiated into macrophages by PMA (50 ng/mL) and then seeded on the foams. Figure 3.31 shows the metabolic activity of macrophages seeded on GEL and GEL/WJ scaffolds at day 1, 4 and 6. If we consider the number of cells seeded on the scaffolds which was $11x10^4$ cells/scaffold, remaining cells detected at day 1 was

significantly lower which was in a range of $10x10^3$-25 $x10^3$ cells for both scaffold which can be attributed to the decreased attachment of the cells to the scaffolds. Also, at day 4, a significant difference was detected between two sets. If we consider that the macrophages do not divide, this difference can be explained by the lower affinity of macrophages to GEL scaffold which resulted in higher detachment of the cells. SEM images (Fig 3.32) showed that much less innate immune cells have attached on the surface, even though there is a statistically significant difference between the conditions, stemming from the increased amount of available ECM molecules in the presence of Wharton`s jelly. However, by day 6, there was no difference in the present macrophage numbers and in both cases they decreased showing a limited reaction to the foams by innate immune cells.

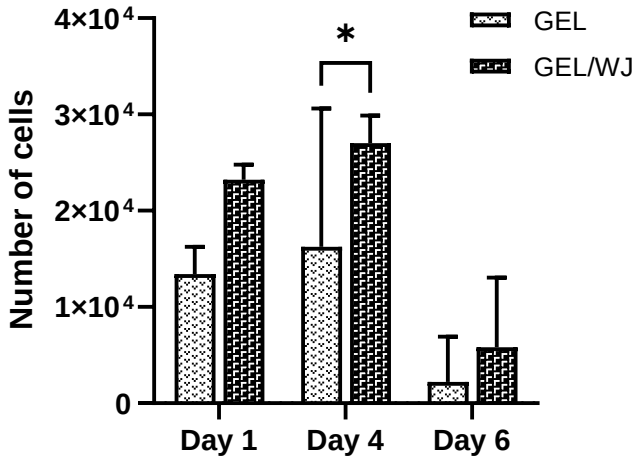

*Figure 3.31 Metabolic activity of THP-1 macrophage like cells on GEL and GEL/WJ scaffold (*p<0.05).*

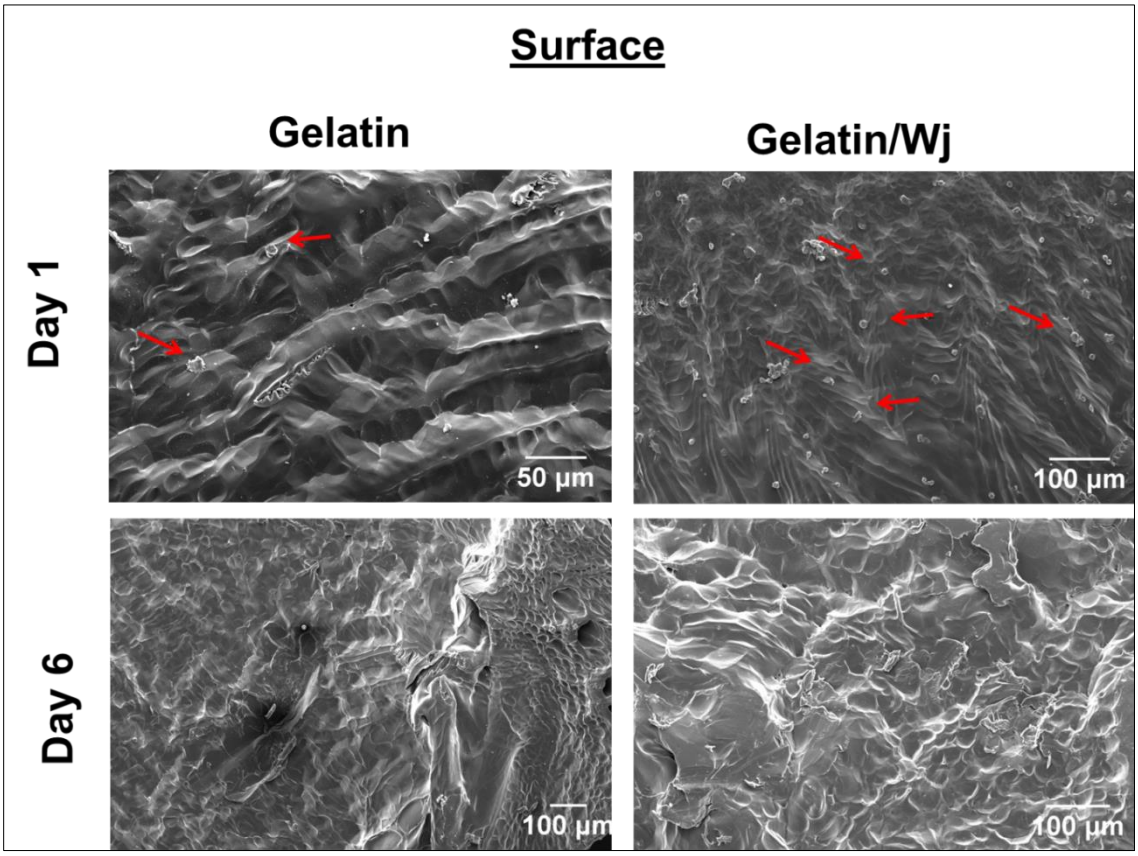

Figure 3.32 SEM surface images of THP-1 macrophage like cells on GEL and GEL/WJ scaffolds. (Arrows represent THP-1 macrophages.)

Figure 3.33 shows the 3D culture conditions at day 1 and day 6. Inconsistent with the viability results, higher number of cells were detected on Gelatin/Wj scaffold at day 1 which was around 1360 cells, while it was around 180 cells for Gelatin scaffold. However, at day 6, consistent with viability results, cell number significantly decreased particularly for Gel/Wj scaffold confirming the limited reaction to the foams by innate immune cells.

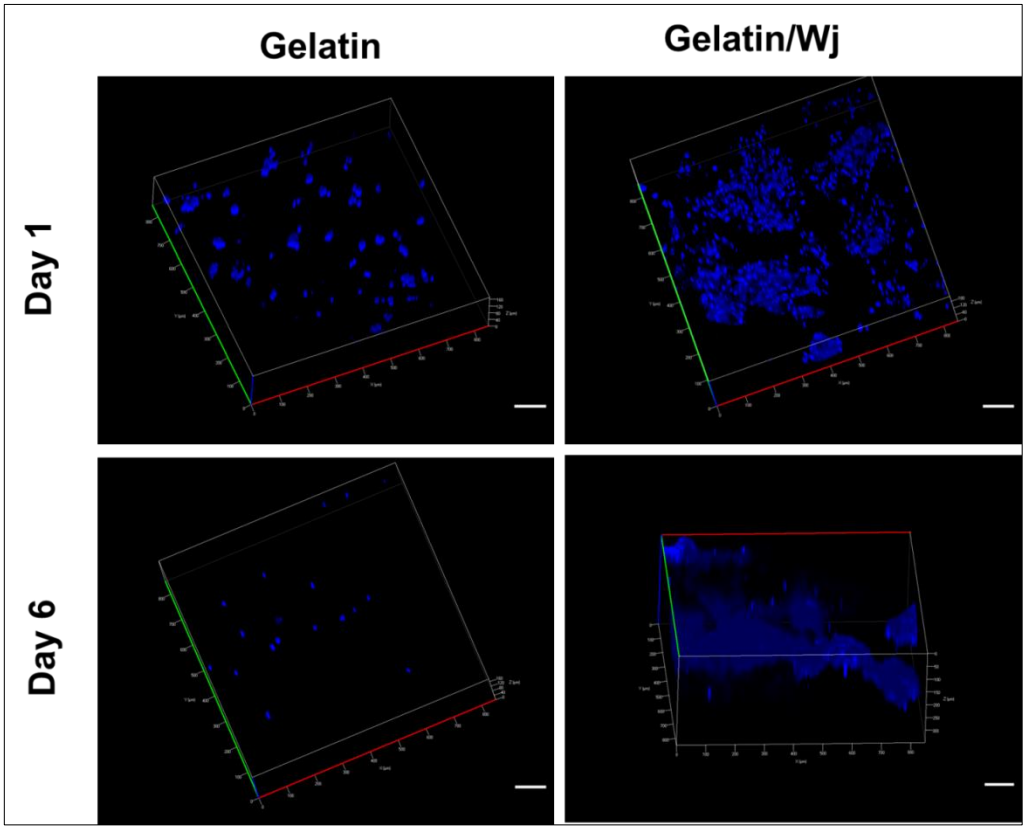

Figure 3.33 3D Confocal images at 20× magnification of DAPI (blue) staining of THP-1macrophage like cells on gelatin and WJ particle loaded gelatin scaffolds. Higher number of cells was detected on Gelatin/Wj scaffold at day 1. At day 6, cell number significantly decreased, particularly for Gel/Wj scaffold. (Scale bar: 100 µm).

3.4.2 HUCMSC culture on GEL or GEL/WJ scaffold

Gelatin and Gelatin/WJ scaffolds were also examined *in vitro* for cell response to evaluate the effect of WJ on HUCMSC proliferation using Alamar Blue cell viability assay. HUCMSCs cultured on gelatin scaffolds were used as control. Cell viability was assessed at 1, 4 and 6 day time points (Fig. 3.34 a). After 1 day of culture, no significant difference on cell viability was observed between the cells cultured on Gelatin and Gelatin/Wj scaffolds. At day 4, a significant increase in cell number was observed for both type of scaffolds comparing to day 1, indicating that WJ supplemented matrix allowed HUCMSC to proliferate at least as much as blank gelatin. After 6 days of culture, no difference was observed on cell viability for both of scaffolds comparing to day 4. In addition to this set of experiment, to observe if WJ has an effect on cell proliferation for a longer time course, 14 days, HUCMSC viability was assessed (Fig. 34.b). In this case, although no significant difference in viability was observed between the cells seeded on Gelatin and Gelatin/WJ, for each time point, a significant increase in cell number was observed for both scaffold types. Based on this observation, assessment of cell viability for a longer time period may provide more precise information to identify any variation in cell proliferation between two sets.

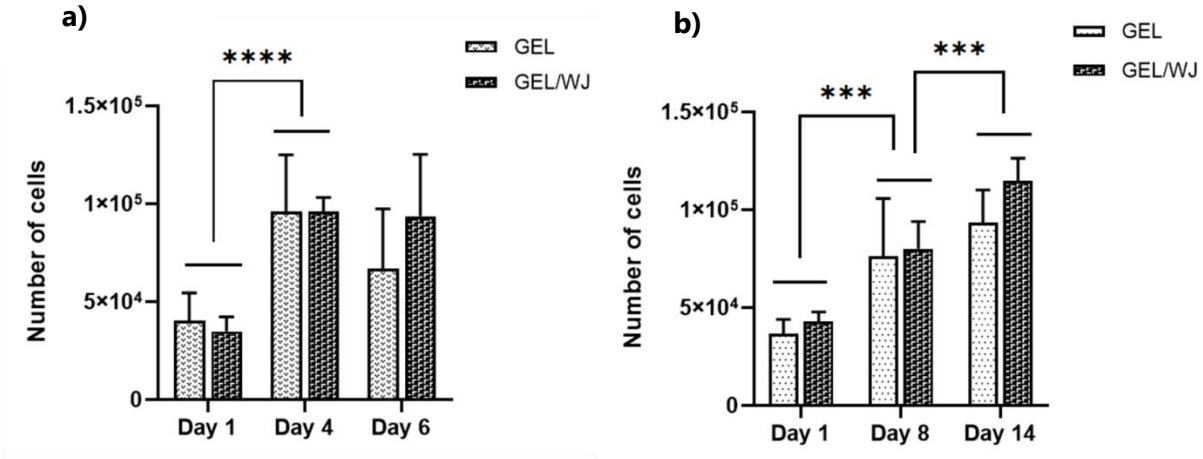

*Figure 3.34 Metabolic activities of HUCMSCs on GEL and GEL/WJ scaffolds over the time period of a) 6 days and b) 14 days. After 1 day of culture, no significant difference on cell viability was observed between the cells cultured on Gelatin and Gelatin/Wj scaffolds. (***p<0.001, ****p<0.0001).*

In addition to viability test, the first set of samples (Fig 3.34.a) was examined by Scanning electron microscopy and Laser Confocal Microscopy to evaluate the effect of WJ on adherence of HUCMSCs. Figure 3.35 shows the surface and cross-section SEM images of cell seeded Gelatin and Gelatin/Wj scaffolds at day 1 and day 6. Adhered cells were observed on the surface of both scaffolds. Gelatin/Wj scaffolds was sparse comparing to ones on Gelatin scaffold and also they present a fibroblast-like appearance. However, from the cross-section images of day 1, no cell was observed on both Gelatin and Gelatin/Wj scaffolds. At the 6th day of culture, on the surface of the scaffolds no cell was observable. Existing cell like circular formations on the surface of the scaffolds which were around 10 µm in diameter could be precipitates formed during sample preparation stage. Cross-section images also revealed that cells were not observable inside the scaffold.

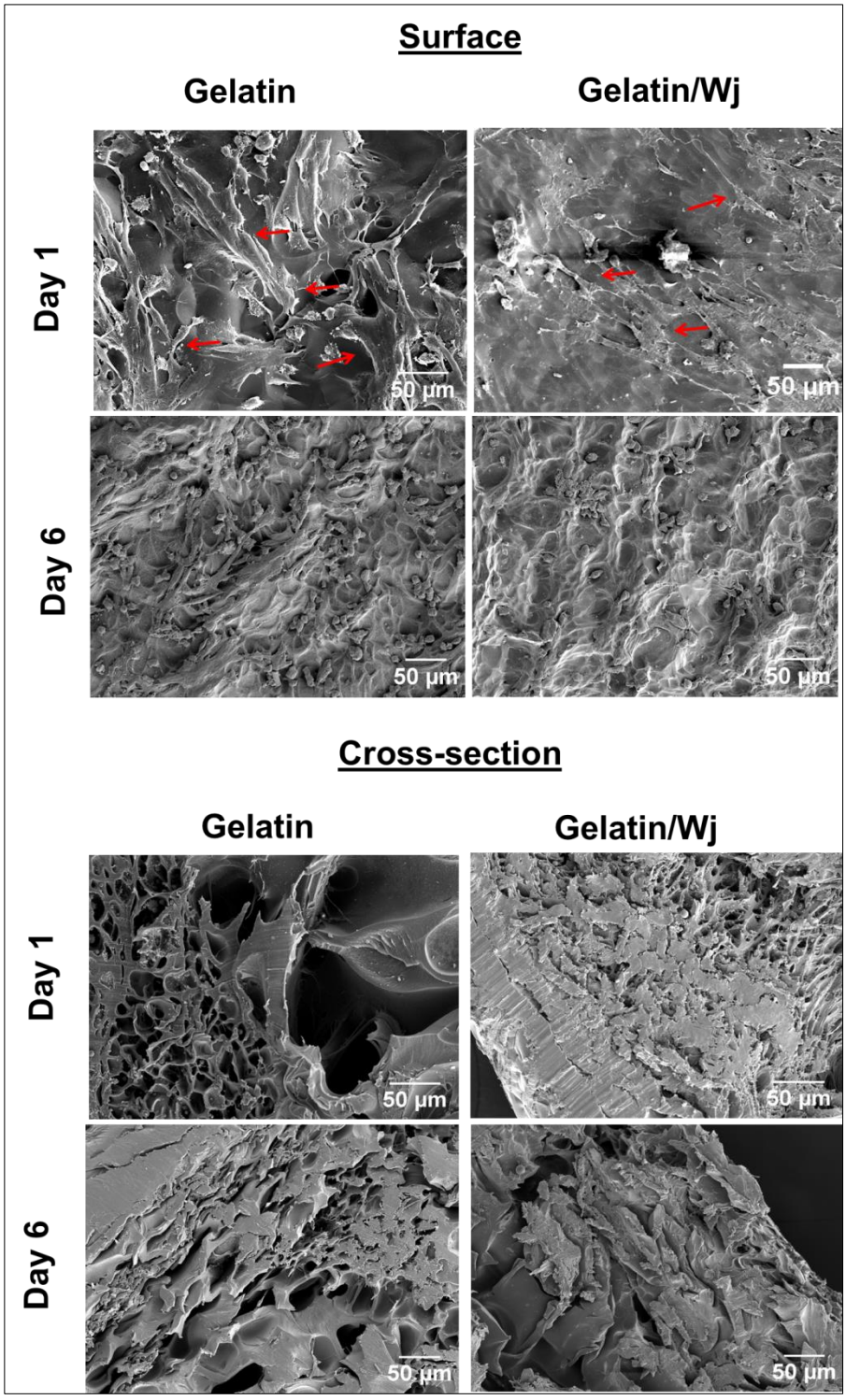

Figure 3.35 Surface and cross-section SEM microscopy of HUCMSCs on gelatin and WJ particle loaded gelatin scaffolds. (Arrows represent HUCMSCs).

Figure 3.36 shows the confocal microscopy images of HUCMSCs seeded on Gelatin and Gelatin/Wj scaffolds at day 1 and day 6. Images revealed that, cells had started to penetrate at day 1 on Gelatin and Gelatin/Wj scaffolds in a distance of 80 µm and 140 µm, respectively. Also at day 1, cell numbers on Gelatin and Gelatin/Wj scaffolds were found to be 39 and 106 respectively and at day 6, it was found to be as 10 and 73 for Gelatin and Gelatin/WJ scaffolds, respectively.

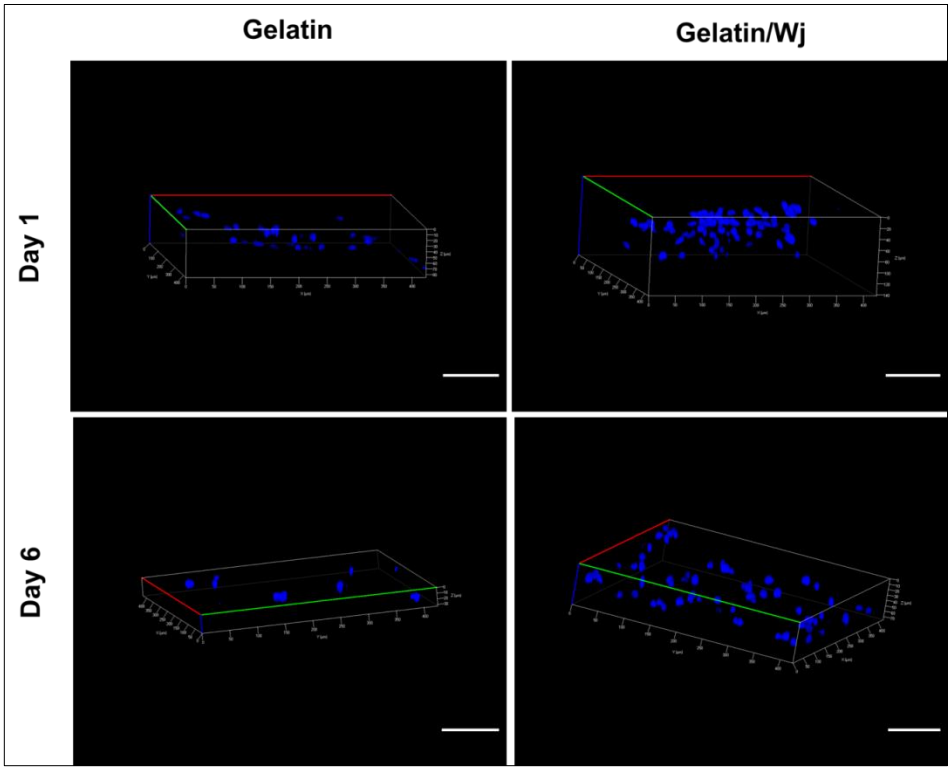

Figure 3.36 3D Confocal images at 20× magnification of DAPI (blue) staining of HUCMSCs on gelatin and WJ particle loaded gelatin foams. (Scale bar: 100 µm).

3.4.2.1 Paracrine activity of HUCMSCs seeded on Gelatin and Gelatin/Wj scaffolds

Mesenchymal stem cells respond to biochemical and structural cues presented by their surrounding microenvironment. These environmental cues affect their constitutive cytokines secretion/self-renewal/differentiation which contributing to tissue homeostasis [488]. Here, HUCMSCs cultured on Gelatin and Gelatin/Wj scaffolds have been assessed for their ability to release cytokines, as IL-6, IL-8 and vascular endothelial growth factor (VEGF) over the time periods of 1 and 7 days by ELISA (results should be evaluated as being aware of n=1). Cells cultured in tissue culture plate in culture medium were evaluated as control. At 1 day culture, IL-6 released from HUCMSCs seeded on GEL/Wj was nearly equal to the ones obtained from control and Gelatin samples. At 6 day culture, a sharp decrease has been identified on IL-6 release for all of the cells cultured on different conditions (Figure 3.37 a). While the IL-8 releases were nearly constant over the experimental time for control and Gelatin conditions, a slight increase was observable for the cells cultured on Gelatin/Wj scaffold (Figure 37 b). VEGF amount released at the 1st day of the culture was slightly higher for the cells cultured on Gelatin/Wj scaffold and at 6th day of culture VEGF release showed a sharp decrease for all the cells. (Figure 35 c). IL-6 was shown to be either a pro- or anti-inflammatory cytokine [489] and it plays a key role in wound healing by way of impaired angiogenesis, leukocyte recruitment and collagen deposition [490]. Lin et al. [491] reported that IL-6 knockout mice have delayed wound healing. . IL-8 has been shown to upregulate VEGF in endothelial cells [492] and BMMSCs via signaling pathways [493]. In consideration of obtained results show that Gelatin/Wj scaffold can be considered in terms of tissue regeneration, but further examinations are required at least for the reproducibility of the results.

.

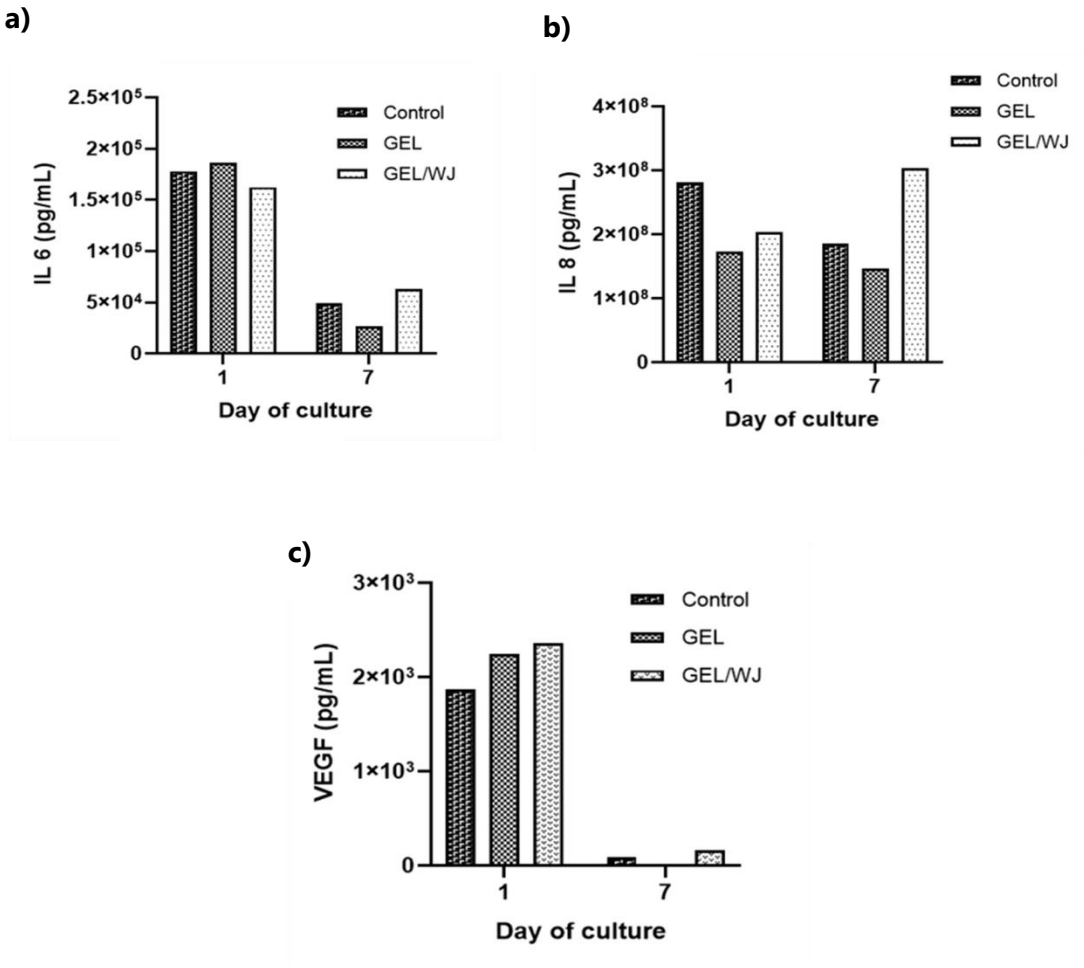

Figure 3.37 HUCMSCs paracrine activity over the time period of 1 and 7 days. Histograms of (a) IL-6, (b) IL-8 and (c) VEGF ELISA quantification,(n=1).

CHAPTER 4

CONCLUSIONS AND OUTLOOK

Tissue regeneration efficiency of Wharton`s Jelly derived ECM scaffolds were previously demonstrated. However, the main drawback of those scaffolds is limited availability and time consuming process conditions of the ECM material. Therefore, designing of composite tissue engineered materials containing an extracellular matrix and natural polymers is an alternative to create bioactive scaffolds. In this regard, here, we proposed a composite scaffold taking advantage of Wharton`s jelly as an ECM source and gelatin as a biocompatible, readily available and bioactive material.

In this study, we developed a gelatin based porous scaffolds supplemented with Wharton`s Jelly derived ECM micro-particles. Microbial transglutaminase has been used to crosslinked the scaffolds and five different gelatin concentrations, 1.4, 2.8, 5.6, 11.2, and 16.8 %, have been assessed for their pore size and porosity to define optimum gelatin- WJ formulation. The concentration of 5.6% both allowed a well-defined pore structure and a nearly 90% porosity, both were enabling features for cellular in-growth and scaffold remodeling. Hydrolytic and enzymatic degradation rates of 5.6 % crosslinked foam were in a proper range to provide structural integrity allowing tissue remodeling. In consideration of 5.6 % crosslinked gelatin formulation, TGA crosslinking had no cytotoxic effect on HUCMSc. Tannic acid has been incorporated to the crosslinked gelatin foams for antimicrobial and anti-biofilm purposes against Gram-positive and Gram-negative bacteria. However, incorporated amount of Tannic acid had a cytotoxic effect on HUCMSc. To reach a non-cytotoxic level, scaffold extracts obtained from consecutive days have been assessed for their cytotoxicity. Indirect cytotoxicity results showed that day 3 extract had no cytotoxic effect on cell viability. In addition, TA supplementation resulted in a significant decrease in pore size of the foams from 54.82 ± 27.5 to 32.84 ± 25.4. For defined gelatin TA formulation, prepared scaffold did not provide a complete bacterial inhibition, which was limited around 70 %.

After defining optimum Gelatin-TGA formulation, WJ particles have been loaded to the final structure. Wj particles varying in size and shape have been produced by using three different particularization methods. By grinding method, Wj particle size has been reduced till an average value of 119 ± 51.6 µm with a maximum of 370 µm which is suitable for induction of regeneration. In addition, obtained composite exhibited homogenous particle

dispersion and no significant difference has been observed on pore size before and after WJ addition. Protein components of gelatin and WJ loaded scaffolds were assessed by reverse-phase high-performance liquid chromatography and SDS/PAGE. However, for both of techniques, no difference in protein release between Gelatin and WJ loaded scaffolds was observed because of the insufficient denaturation of the proteins.

In vitro studies were carried out with THP-1 (human monocytic leukemia cell line) and human umbilical cord mesenchymal stem cells. THP-1 monocytes were used to assess the initial immune reaction in the presence and absence of WJ particles, mimicking the arrival of the circulating monocytes following implantation. SEM and viability results revealed that on the 6^{th} day of culture, for both type of scaffold, number of cells present and the viability were reduced due to the lack of adhesion showing that the both scaffold environment had no effect on monocytes to turn into macrophages. Also, macrophage response to the developed scaffolds was minimal at the 6^{th} day of culture showing that the limited reaction to the scaffolds by innate immune cells. However, to confirm this result, quantitative characterization methods such as ELISA should be performed to evaluate the cytokine release profile of the cells. Cell viability studies carried out with HUCMSCs revealed that WJ addition does not have a significant effect on cell proliferation. However, confocal laser microscopy image analysis showed that in case of the presence of WJ, more cells have been detected which showed higher penetration into the scaffold.

To sum up, here, we have demonstrated the feasibility of Whartons`s jelly microparticles in combination with gelatin as a porous 3D construct for possible tissue engineering applications. Also, Tannic acid-Gelatin interactions were partially characterized for future applications of tannic acid as an antimicrobial agent for the production of ECM derived tissue engineered scaffolds.

For this aim, as a future perspective, Wharton’s jelly/gelatin formulation should be optimized to strengthen the cell proliferation, which will be possible by increasing the amount of Wharton`s Jelly in the structure. Then, a proper Gelatin- Wharton`s Jelly -TA formulation should be considered which meets the both antimicrobial and biocompatible features. Also, in addition to the SEM and CLSM analysis, monocyte and macrophage behavior could be evaluated by assessing the cytokine release profiles of the cultured cells.

Annexe

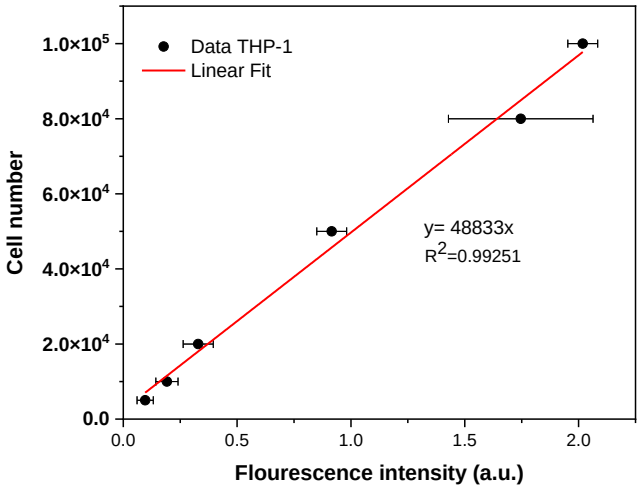

Figure 1 Calibration curve of Alamar blue assay for THP-1 macrophage like cells

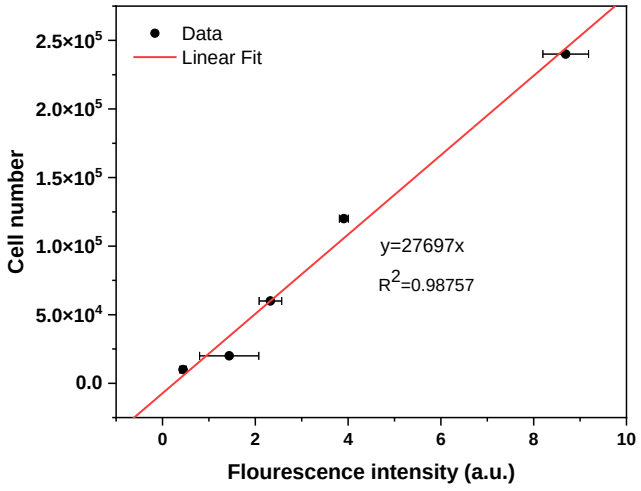

Figure 2 Calibration curve of Alamar blue assay for HUCMSCs

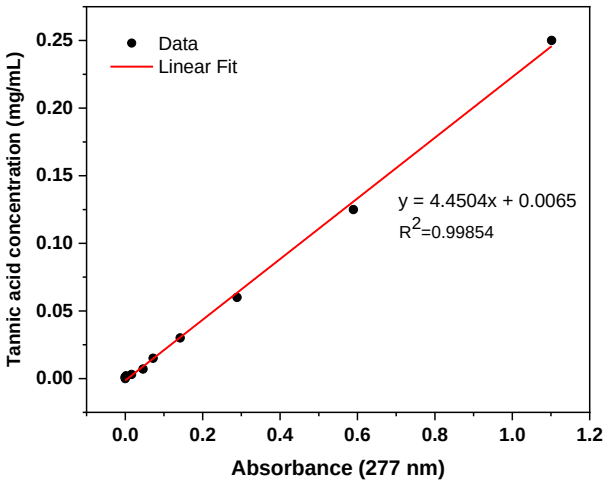

Figure 3 Calibration curve of Tannic acid concentration vs. absorbance

References

1. Langer, R. and J.P. Vacanti, *Tissue Engineering.* Science, 1993. **260**(5110): p. 920-926.
2. Persidis, A., *Tissue engineering.* Nature Biotechnology, 1999. **17**(5): p. 508-510.
3. Vacanti, J.P. and C.A. Vacanti, *Chapter 1 - The History and Scope of Tissue Engineering*, in *Principles of Tissue Engineering (Fourth Edition)*, R. Lanza, R. Langer, and J. Vacanti, Editors. 2014, Academic Press: Boston. p. 3-8.
4. *Organ Donation and Transplantation Statistics*. Available from: https://www.organdonor.gov/statistics-stories/statistics/data.html.
5. Langer, R. and J. Vacanti, *Tissue engineering.* Science, 1993. **260**(5110): p. 920-926.
6. Bancroft, G.N., et al., *Fluid flow increases mineralized matrix deposition in 3D perfusion culture of marrow stromal osteoblasts in a dose-dependent manner.* Proceedings of the National Academy of Sciences of the United States of America, 2002. **99**(20): p. 12600-12605.
7. Carrier, R.L., et al., *Cardiac tissue engineering: cell seeding, cultivation parameters, and tissue construct characterization.* Biotechnol Bioeng, 1999. **64**(5): p. 580-9.
8. Sikavitsas, V.I., G.N. Bancroft, and A.G. Mikos, *Formation of three-dimensional cell/polymer constructs for bone tissue engineering in a spinner flask and a rotating wall vessel bioreactor.* J Biomed Mater Res, 2002. **62**(1): p. 136-48.
9. Fortunato, T., P. De Bank, and G. Pula, *Vascular Regenerative Surgery: Promised Land for Tissue Engineers?* International Journal of Stem Cell Research and Transplantation, 2017: p. 268-276.
10. Yannas, I.V., et al., *Synthesis and characterization of a model extracellular matrix that induces partial regeneration of adult mammalian skin.* Proceedings of the National Academy of Sciences, 1989. **86**(3): p. 933-937.
11. Zhong, W., et al., *In vivo comparison of the bone regeneration capability of human bone marrow concentrates vs. platelet-rich plasma.* PloS one, 2012. **7**(7): p. e40833-e40833.
12. Atala, A., et al., *Tissue-engineered autologous bladders for patients needing cystoplasty.* Lancet, 2006. **367**(9518): p. 1241-6.
13. Delaere, P.R. and R. Hermans, *Clinical transplantation of a tissue-engineered airway.* The Lancet, 2009. **373**(9665): p. 717-718.
14. O'Brien, F.J., *Biomaterials & scaffolds for tissue engineering.* Materials Today, 2011. **14**(3): p. 88-95.
15. Nikolova, M.P. and M.S. Chavali, *Recent advances in biomaterials for 3D scaffolds: A review.* Bioactive Materials, 2019. **4**: p. 271-292.
16. Williams, D.F., *Tissue-biomaterial interactions.* Journal of Materials Science, 1987. **22**(10): p. 3421-3445.
17. Williams, D.F., *Definitions in Biomaterials, 4th ed.* Proceedings of a Consensus Conference of the European Society for Biomaterials, Chester, England, 1986.

18. Saleh, L.S. and S.J. Bryant, *In vitro and in vivo models for assessing the host response to biomaterials.* Drug Discovery Today: Disease Models, 2017. **24**: p. 13-21.
19. Anderson, J.M., *Biological Responses to Materials.* Annual Review of Materials Research, 2001. **31**(1): p. 81-110.
20. Ratner, B.D. and S.J. Bryant, *Biomaterials: Where We Have Been and Where We Are Going.* Annual Review of Biomedical Engineering, 2004. **6**(1): p. 41-75.
21. Gibon, E., et al., *The biological response to orthopedic implants for joint replacement. II: Polyethylene, ceramics, PMMA, and the foreign body reaction.* Journal of Biomedical Materials Research Part B: Applied Biomaterials, 2017. **105**(6): p. 1685-1691.
22. Salthouse, T.N., *Some aspects of macrophage behavior at the implant interface.* J Biomed Mater Res, 1984. **18**(4): p. 395-401.
23. Gordon, S. and F.O. Martinez, *Alternative Activation of Macrophages: Mechanism and Functions.* Immunity, 2010. **32**(5): p. 593-604.
24. Bystroňová, J., et al., *Creating a 3D microenvironment for monocyte cultivation: ECM-mimicking hydrogels based on gelatine and hyaluronic acid derivatives.* RSC Advances, 2018. **8**(14): p. 7606-7614.
25. Karp, R.D., et al., *Tumorigenesis by Millipore Filters in Mice: Histology and Ultrastructure of Tissue Reactions as Related to Pore Size2.* JNCI: Journal of the National Cancer Institute, 1973. **51**(4): p. 1275-1285.
26. Fukano, Y., et al., *Epidermal and dermal integration into sphere-templated porous poly(2-hydroxyethyl methacrylate) implants in mice.* J Biomed Mater Res A, 2010. **94**(4): p. 1172-86.
27. Madden, L.R., et al., *Proangiogenic scaffolds as functional templates for cardiac tissue engineering.* Proceedings of the National Academy of Sciences of the United States of America, 2010. **107**(34): p. 15211-15216.
28. Sussman, E.M., et al., *Porous implants modulate healing and induce shifts in local macrophage polarization in the foreign body reaction.* Ann Biomed Eng, 2014. **42**(7): p. 1508-16.
29. Ratner, B.D., *A pore way to heal and regenerate: 21st century thinking on biocompatibility.* Regenerative biomaterials, 2016. **3**(2): p. 107-110.
30. Babensee, J.E., et al., *Host response to tissue engineered devices.* Advanced Drug Delivery Reviews, 1998. **33**(1): p. 111-139.
31. Katti, D.S., et al., *Toxicity, biodegradation and elimination of polyanhydrides.* Adv Drug Deliv Rev, 2002. **54**(7): p. 933-61.
32. Biomater, B.-P.L.M.P., *Polymers in controlled drug delivery.* Med Plast Biomater, 1997. **4**: p. 34-44.
33. N. A. Peppas, L.B.-P. and *Drug Delivery Biomaterials*, in *Encyclopedia of Materials: Science and Technology* p. 2351-2355.
34. Vrana, N.E., et al., *EDC/NHS cross-linked collagen foams as scaffolds for artificial corneal stroma.* Journal of Biomaterials Science, Polymer Edition, 2007. **18**(12): p. 1527-1545.
35. Leong, K.F., et al., *Engineering functionally graded tissue engineering scaffolds.* Journal of the Mechanical Behavior of Biomedical Materials, 2008. **1**(2): p. 140-152.

36. *Stiffness — an unknown world of mechanical science?* Injury, 2000. **31**: p. 14-84.
37. Goulet, R.W.e.a., *Th e relationship between the structural and orthogonal compressive properties of trabecular bone.* J. Biomech., 1994. **27m** p. 375–389.
38. Ogden, G.A.H.W., *Biomechanics of Soft Tissue in Cardiovascular Systems*. 2003: Springer, Vienna.
39. Murugan, R. and S. Ramakrishna, *Development of nanocomposites for bone grafting.* Composites Science and Technology, 2005. **65**(15): p. 2385-2406.
40. Mandal, B.B. and S.C. Kundu, *Cell proliferation and migration in silk fibroin 3D scaffolds.* Biomaterials, 2009. **30**(15): p. 2956-2965.
41. Deb, P., et al., *Scaffold Development Using Biomaterials: A Review*. Materials Today: Proceedings, 2018. **5**(5, Part 2): p. 12909-12919.
42. Phelps, E.A. and A.J. Garcia, *Update on therapeutic vascularization strategies.* Regen Med, 2009. **4**(1): p. 65-80.
43. Ko, H.C., B.K. Milthorpe, and C.D. McFarland, *Engineering thick tissues--the vascularisation problem.* Eur Cell Mater, 2007. **14**: p. 1-18; discussion 18-9.
44. O'Brien, F.J., et al., *The effect of pore size on cell adhesion in collagen-GAG scaffolds.* Biomaterials, 2005. **26**(4): p. 433-41.
45. Murphy, C.M., M.G. Haugh, and F.J. O'Brien, *The effect of mean pore size on cell attachment, proliferation and migration in collagen-glycosaminoglycan scaffolds for bone tissue engineering.* Biomaterials, 2010. **31**(3): p. 461-6.
46. Baksh, D., J.E. Davies, and S. Kim, *Three-dimensional matrices of calcium polyphosphates support bone growth in vitro and in vivo.* Journal of Materials Science: Materials in Medicine, 1998. **9**(12): p. 743-748.
47. Akay, G., M.A. Birch, and M.A. Bokhari, *Microcellular polyHIPE polymer supports osteoblast growth and bone formation in vitro.* Biomaterials, 2004. **25**(18): p. 3991-4000.
48. Dhandayuthapani, B., et al., *Polymeric Scaffolds in Tissue Engineering Application: A Review*. International Journal of Polymer Science, 2011. **2011**: p. 290602.
49. Karageorgiou, V. and D. Kaplan, *Porosity of 3D biomaterial scaffolds and osteogenesis.* Biomaterials, 2005. **26**(27): p. 5474-91.
50. Loh, Q.L. and C. Choong, *Three-dimensional scaffolds for tissue engineering applications: role of porosity and pore size.* Tissue engineering. Part B, Reviews, 2013. **19**(6): p. 485-502.
51. *Freeze-Drying*, in *Ullmann's Encyclopedia of Industrial Chemistry*. p. 1-47.
52. Whang, K., et al., *A novel method to fabricate bioabsorbable scaffolds.* Polymer, 1995. **36**(4): p. 837-842.
53. Autissier, A., et al., *Fabrication of porous polysaccharide-based scaffolds using a combined freeze-drying/cross-linking process.* Acta Biomaterialia, 2010. **6**(9): p. 3640-3648.
54. O'Brien, F.J., et al., *Influence of freezing rate on pore structure in freeze-dried collagen-GAG scaffolds.* Biomaterials, 2004. **25**(6): p. 1077-1086.
55. Reneker, D.H. and I. Chun, *Nanometre diameter fibres of polymer, produced by electrospinning.* Nanotechnology, 1996. **7**(3): p. 216-223.
56. Lu, T., Y. Li, and T. Chen, *Techniques for fabrication and construction of three-dimensional scaffolds for tissue engineering.* International journal of nanomedicine, 2013. **8**: p. 337-350.

57. Pham, Q.P., U. Sharma, and A.G. Mikos, *Electrospun poly(epsilon-caprolactone) microfiber and multilayer nanofiber/microfiber scaffolds: characterization of scaffolds and measurement of cellular infiltration.* Biomacromolecules, 2006. **7**(10): p. 2796-805.
58. Faki, R., O. Gursoy, and Y. Yilmaz, *Effect of Electrospinning Process on Total Antioxidant Activity of Electrospun Nanofibers Containing Grape Seed Extract.* Open Chemistry, 2019. **17**(1): p. 912-918.
59. Rho, K.S., et al., *Electrospinning of collagen nanofibers: effects on the behavior of normal human keratinocytes and early-stage wound healing.* Biomaterials, 2006. **27**(8): p. 1452-61.
60. Lannutti, J., et al., *Electrospinning for tissue engineering scaffolds.* Materials Science and Engineering: C, 2007. **27**(3): p. 504-509.
61. Li, X., et al., *Preparation and characterization of PLLA/nHA nonwoven mats via laser melt electrospinning.* Materials Letters, 2012. **73**: p. 103-106.
62. Park, J.-S., et al., *Characterization and structure analysis of PLGA/collagen nanofibrous membranes by electrospinning.* Journal of Applied Polymer Science, 2012. **125**(S2): p. E595-E603.
63. Fang, J., et al., *Needleless Melt-Electrospinning of Polypropylene Nanofibres.* Journal of Nanomaterials, 2012. **2012**: p. 382639.
64. Zhang, J., et al., *Fabrication of three dimensional polymeric scaffolds with spherical pores.* Journal of Materials Science, 2006. **41**(6): p. 1725-1731.
65. *Biodegradable Polymer Scaffolds with Well-Defined Interconnected Spherical Pore Network.* Tissue Engineering, 2001. **7**(1): p. 23-33.
66. Shum, A.W.T., J. Li, and A.F.T. Mak, *Fabrication and structural characterization of porous biodegradable poly(dl-lactic-co-glycolic acid) scaffolds with controlled range of pore sizes.* Polymer Degradation and Stability, 2005. **87**(3): p. 487-493.
67. Draghi, L., et al., *Microspheres leaching for scaffold porosity control.* Journal of Materials Science: Materials in Medicine, 2005. **16**(12): p. 1093-1097.
68. Cima, A.G.M.G.S.J.P.V.R.S.L.L.G., *Biocompatible polymer membranes and methods of preparation of three dimensional membrane structures*, in *Google Patents, 1996*. 1996.
69. Bencherif, S.A., T.M. Braschler, and P. Renaud, *Advances in the design of macroporous polymer scaffolds for potential applications in dentistry.* J Periodontal Implant Sci, 2013. **43**(6): p. 251-261.
70. Ma, P.X., *Scaffolds for tissue fabrication.* Materials Today, 2004. **7**(5): p. 30-40.
71. Pezeshki Modaress, M., H. Mirzadeh, and M. Zandi, *Fabrication of a porous wall and higher interconnectivity scaffold comprising gelatin/chitosan via combination of salt-leaching and lyophilization methods.* Iranian Polymer Journal, 2012. **21**(3): p. 191-200.
72. Giordano, R.A., et al., *Mechanical properties of dense polylactic acid structures fabricated by three dimensional printing.* Journal of Biomaterials Science, Polymer Edition, 1997. **8**(1): p. 63-75.
73. Wang, H., et al., *Synthetic scaffold morphology controls human dermal connective tissue formation.* Journal of Biomedical Materials Research Part A, 2005. **74A**(4): p. 523-532.
74. Chen, F., J.J. Yoo, and A. Atala, *Acellular collagen matrix as a possible "off the shelf" biomaterial for urethral repair.* Urology, 1999. **54**(3): p. 407-10.

75. Piechota, H.J., et al., *IN VITRO FUNCTIONAL PROPERTIES OF THE RAT BLADDER REGENERATED BY THE BLADDER ACELLULAR MATRIX GRAFT.* The Journal of Urology, 1998. **159**(5): p. 1717-1724.
76. Ikada, Y., *Challenges in tissue engineering.* Journal of the Royal Society, Interface, 2006. **3**(10): p. 589-601.
77. Patience, C., Y. Takeuchi, and R.A. Weiss, *Infection of human cells by an endogenous retrovirus of pigs.* Nature Medicine, 1997. **3**(3): p. 282-286.
78. Heath, C.A., *Cells for tissue engineering.* Trends in Biotechnology, 2000. **18**(1): p. 17-19.
79. Schnabel, M., et al., *Dedifferentiation-associated changes in morphology and gene expression in primary human articular chondrocytes in cell culture.* Osteoarthritis and Cartilage, 2002. **10**(1): p. 62-70.
80. Tögel, F. and C. Westenfelder, *Adult bone marrow-derived stem cells for organ regeneration and repair.* Dev Dyn, 2007. **236**(12): p. 3321-31.
81. Raff, M., *Adult stem cell plasticity: fact or artifact?* Annu Rev Cell Dev Biol, 2003. **19**: p. 1-22.
82. Zakrzewski, W., et al., *Stem cells: past, present, and future.* Stem Cell Research & Therapy, 2019. **10**(1): p. 68.
83. Gancheva, M.R., et al., *Using Dental Pulp Stem Cells for Stroke Therapy.* Frontiers in Neurology, 2019. **10**(422).
84. Watt, F.M. and R.R. Driskell, *The therapeutic potential of stem cells.* Philosophical transactions of the Royal Society of London. Series B, Biological sciences, 2010. **365**(1537): p. 155-163.
85. Han, Y., et al., *Mesenchymal Stem Cells for Regenerative Medicine.* Cells, 2019. **8**(8): p. 886.
86. Dominici, M., et al., *Minimal criteria for defining multipotent mesenchymal stromal cells. The International Society for Cellular Therapy position statement.* Cytotherapy, 2006. **8**(4): p. 315-317.
87. Lin, C.-S., et al., *Is CD34 truly a negative marker for mesenchymal stromal cells?* Cytotherapy, 2012. **14**(10): p. 1159-1163.
88. Tsai, M.S., et al., *Isolation of human multipotent mesenchymal stem cells from second-trimester amniotic fluid using a novel two-stage culture protocol.* Human Reproduction, 2004. **19**(6): p. 1450-1456.
89. Kadar, K., et al., *Differentiation potential of stem cells from human dental origin - promise for tissue engineering.* J Physiol Pharmacol, 2009. **60 Suppl 7**: p. 167-75.
90. Gronthos, S., et al., *The STRO-1+ fraction of adult human bone marrow contains the osteogenic precursors.* Blood, 1994. **84**(12): p. 4164-73.
91. Gronthos, S., et al., *Surface protein characterization of human adipose tissue-derived stromal cells.* J Cell Physiol, 2001. **189**(1): p. 54-63.
92. Pittenger, M.F., et al., *Multilineage potential of adult human mesenchymal stem cells.* Science, 1999. **284**(5411): p. 143-7.
93. Mamidi, M.K., et al., *Comparative cellular and molecular analyses of pooled bone marrow multipotent mesenchymal stromal cells during continuous passaging and after successive cryopreservation.* J Cell Biochem, 2012. **113**(10): p. 3153-64.
94. Wagner, W., et al., *Comparative characteristics of mesenchymal stem cells from human bone marrow, adipose tissue, and umbilical cord blood.* Exp Hematol, 2005. **33**(11): p. 1402-16.

95. In 't Anker, P.S., et al., *Amniotic fluid as a novel source of mesenchymal stem cells for therapeutic transplantation.* Blood, 2003. **102**(4): p. 1548-9.
96. Huang, G.T., S. Gronthos, and S. Shi, *Mesenchymal stem cells derived from dental tissues vs. those from other sources: their biology and role in regenerative medicine.* J Dent Res, 2009. **88**(9): p. 792-806.
97. Schüring, A.N., et al., *Characterization of endometrial mesenchymal stem-like cells obtained by endometrial biopsy during routine diagnostics.* Fertility and Sterility, 2011. **95**(1): p. 423-426.
98. Jiao, F., et al., *Human mesenchymal stem cells derived from limb bud can differentiate into all three embryonic germ layers lineages.* Cell Reprogram, 2012. **14**(4): p. 324-33.
99. Ab Kadir, R., et al., *Characterization of mononucleated human peripheral blood cells.* ScientificWorldJournal, 2012. **2012**: p. 843843.
100. Raynaud, C.M., et al., *Comprehensive characterization of mesenchymal stem cells from human placenta and fetal membrane and their response to osteoactivin stimulation.* Stem Cells Int, 2012. **2012**: p. 658356.
101. Rotter, N., et al., *Isolation and characterization of adult stem cells from human salivary glands.* Stem Cells Dev, 2008. **17**(3): p. 509-18.
102. Bartsch, G., et al., *Propagation, expansion, and multilineage differentiation of human somatic stem cells from dermal progenitors.* Stem Cells Dev, 2005. **14**(3): p. 337-48.
103. Morito, T., et al., *Synovial fluid-derived mesenchymal stem cells increase after intra-articular ligament injury in humans.* Rheumatology (Oxford), 2008. **47**(8): p. 1137-43.
104. *Umbilical Cord Wharton's Jelly: A New Potential Cell Source of Mesenchymal Stromal Cells for Bone Tissue Engineering.* Tissue Engineering Part A, 2009. **15**(9): p. 2325-2334.
105. Baksh, D., R. Yao, and R.S. Tuan, *Comparison of proliferative and multilineage differentiation potential of human mesenchymal stem cells derived from umbilical cord and bone marrow.* Stem Cells, 2007. **25**(6): p. 1384-92.
106. Chen, Y., et al., *Mesenchymal stem cells: a promising candidate in regenerative medicine.* Int J Biochem Cell Biol, 2008. **40**(5): p. 815-20.
107. Ullah, I., R.B. Subbarao, and G.J. Rho, *Human mesenchymal stem cells - current trends and future prospective.* Bioscience reports, 2015. **35**(2): p. e00191.
108. Jiang, Y., et al., *Pluripotency of mesenchymal stem cells derived from adult marrow.* Nature, 2002. **418**(6893): p. 41-9.
109. Mackay, A.M., et al., *Chondrogenic differentiation of cultured human mesenchymal stem cells from marrow.* Tissue Eng, 1998. **4**(4): p. 415-28.
110. Akiyama, H., et al., *The transcription factor Sox9 has essential roles in successive steps of the chondrocyte differentiation pathway and is required for expression of Sox5 and Sox6.* Genes Dev, 2002. **16**(21): p. 2813-28.
111. Neve, A., A. Corrado, and F.P. Cantatore, *Osteoblast physiology in normal and pathological conditions.* Cell and Tissue Research, 2011. **343**(2): p. 289-302.
112. Almalki, S.G. and D.K. Agrawal, *Key transcription factors in the differentiation of mesenchymal stem cells.* Differentiation; research in biological diversity, 2016. **92**(1-2): p. 41-51.

113. Augello, A. and C. De Bari, *The regulation of differentiation in mesenchymal stem cells.* Hum Gene Ther, 2010. **21**(10): p. 1226-38.
114. Naghdi, M., et al., *Transdifferentiation of bone marrow stromal cells into cholinergic neuronal phenotype: a potential source for cell therapy in spinal cord injury.* Cytotherapy, 2009. **11**(2): p. 137-152.
115. Datta, I., et al., *Neuronal plasticity of human Wharton's jelly mesenchymal stromal cells to the dopaminergic cell type compared with human bone marrow mesenchymal stromal cells.* Cytotherapy, 2011. **13**(8): p. 918-32.
116. Barzilay, R., et al., *Lentiviral delivery of LMX1a enhances dopaminergic phenotype in differentiated human bone marrow mesenchymal stem cells.* Stem Cells Dev, 2009. **18**(4): p. 591-601.
117. Lee, K.-D., et al., *In vitro hepatic differentiation of human mesenchymal stem cells.* Hepatology, 2004. **40**(6): p. 1275-1284.
118. An, S.Y., et al., *Valproic acid promotes differentiation of hepatocyte-like cells from whole human umbilical cord-derived mesenchymal stem cells.* Tissue Cell, 2014. **46**(2): p. 127-35.
119. Criscimanna, A., et al., *In vitro generation of pancreatic endocrine cells from human adult fibroblast-like limbal stem cells.* Cell Transplant, 2012. **21**(1): p. 73-90.
120. Govindasamy, V., et al., *Differentiation of Dental Pulp Stem Cells into Islet-like Aggregates.* Journal of Dental Research, 2011. **90**(5): p. 646-652.
121. Kim, J., et al., *Human insulin secreted from insulinogenic xenograft restores normoglycemia in type 1 diabetic mice without immunosuppression.* Cell Transplant, 2012. **21**(10): p. 2131-47.
122. Baddoo, M., et al., *Characterization of mesenchymal stem cells isolated from murine bone marrow by negative selection.* J Cell Biochem, 2003. **89**(6): p. 1235-49.
123. Uccelli, A., L. Moretta, and V. Pistoia, *Immunoregulatory function of mesenchymal stem cells.* Eur J Immunol, 2006. **36**(10): p. 2566-73.
124. Riordan, N.H., et al., *Cord blood in regenerative medicine: do we need immune suppression?* Journal of Translational Medicine, 2007. **5**(1): p. 8.
125. Prabakar, K.R., et al., *Generation of glucose-responsive, insulin-producing cells from human umbilical cord blood-derived mesenchymal stem cells.* Cell Transplant, 2012. **21**(6): p. 1321-39.
126. González, M.A., et al., *Treatment of experimental arthritis by inducing immune tolerance with human adipose-derived mesenchymal stem cells.* Arthritis Rheum, 2009. **60**(4): p. 1006-19.
127. Alatyyat, S.M., et al., *Umbilical cord stem cells: Background, processing and applications.* Tissue and Cell, 2020. **65**: p. 101351.
128. Tuch, B., *Stem cells A clinical update.* Australian family physician, 2006. **35**: p. 719-21.
129. Evans, M.J. and M.H. Kaufman, *Establishment in culture of pluripotential cells from mouse embryos.* Nature, 1981. **292**(5819): p. 154-156.
130. Martin, G.R., *Isolation of a pluripotent cell line from early mouse embryos cultured in medium conditioned by teratocarcinoma stem cells.* Proc Natl Acad Sci U S A, 1981. **78**(12): p. 7634-8.

131. Thomson, J.A., et al., *Isolation of a primate embryonic stem cell line.* Proceedings of the National Academy of Sciences of the United States of America, 1995. **92**(17): p. 7844-7848.
132. Thomson, J.A., et al., *Embryonic stem cell lines derived from human blastocysts.* Science, 1998. **282**(5391): p. 1145-7.
133. Geens, M., et al., *Human embryonic stem cell lines derived from single blastomeres of two 4-cell stage embryos.* Human reproduction (Oxford, England), 2009. **24**(11): p. 2709-2717.
134. Landry, D.W. and H.A. Zucker, *Embryonic death and the creation of human embryonic stem cells.* The Journal of Clinical Investigation, 2004. **114**(9): p. 1184-1186.
135. Berthod, F., et al., *Optimization of thickness, pore size and mechanical properties of a biomaterial designed for deep burn coverage.* Clinical Materials, 1994. **15**(4): p. 259-265.
136. Bielby, R.C., et al., *In vitro differentiation and in vivo mineralization of osteogenic cells derived from human embryonic stem cells.* Tissue Eng, 2004. **10**(9-10): p. 1518-25.
137. Hwang, N.S., et al., *Effects of three-dimensional culture and growth factors on the chondrogenic differentiation of murine embryonic stem cells.* Stem Cells, 2006. **24**(2): p. 284-91.
138. Gerecht-Nir, S., et al., *Three-dimensional porous alginate scaffolds provide a conducive environment for generation of well-vascularized embryoid bodies from human embryonic stem cells.* Biotechnology and bioengineering, 2004. **88**: p. 313-20.
139. Lavon, N., O. Yanuka, and N. Benvenisty, *The effect of overexpression of Pdx1 and Foxa2 on the differentiation of human embryonic stem cells into pancreatic cells.* Stem Cells, 2006. **24**(8): p. 1923-30.
140. Baharvand, H., et al., *Differentiation of human embryonic stem cells into hepatocytes in 2D and 3D culture systems in vitro.* Int J Dev Biol, 2006. **50**(7): p. 645-52.
141. Teixeira, A.I., et al., *The effect of environmental factors on the response of human corneal epithelial cells to nanoscale substrate topography.* Biomaterials, 2006. **27**(21): p. 3945-54.
142. *In Vitro Differentiation and In Vivo Mineralization of Osteogenic Cells Derived from Human Embryonic Stem Cells.* Tissue Engineering, 2004. **10**(9-10): p. 1518-1525.
143. *Differentiation of Osteoblasts and in Vitro Bone Formation from Murine Embryonic Stem Cells.* Tissue Engineering, 2001. **7**(1): p. 89-99.
144. Hentze, H., R. Graichen, and A. Colman, *Cell therapy and the safety of embryonic stem cell-derived grafts.* Trends Biotechnol, 2007. **25**(1): p. 24-32.
145. Maherali, N., et al., *Directly reprogrammed fibroblasts show global epigenetic remodeling and widespread tissue contribution.* Cell Stem Cell, 2007. **1**(1): p. 55-70.
146. Zhou, Q., et al., *In vivo reprogramming of adult pancreatic exocrine cells to β-cells.* Nature, 2008. **455**(7213): p. 627-632.
147. Narsinh, K.H., et al., *Single cell transcriptional profiling reveals heterogeneity of human induced pluripotent stem cells.* J Clin Invest, 2011. **121**(3): p. 1217-21.

148. Nelakanti, R.V., N.G. Kooreman, and J.C. Wu, *Teratoma formation: a tool for monitoring pluripotency in stem cell research.* Curr Protoc Stem Cell Biol, 2015. **32**: p. 4a.8.1-4a.8.17.
149. Ferraro F., C.C.L., Scadden D. , *Adult Stem Cels and Their Niches.* The Cell Biology of Stem Cells. Advances in Experimental Medicine and Biology,Springer, Boston, MA, 2010. **695**.
150. Hodgkinson, T., X.F. Yuan, and A. Bayat, *Adult stem cells in tissue engineering.* Expert Rev Med Devices, 2009. **6**(6): p. 621-40.
151. Tuan, R.S., G. Boland, and R. Tuli, *Adult mesenchymal stem cells and cell-based tissue engineering.* Arthritis Res Ther, 2003. **5**(1): p. 32-45.
152. Pillow, R.P., et al., *Treatment of Bone-Marrow Failure by Isogeneic Marrow Infusion.* New England Journal of Medicine, 1966. **275**(2): p. 94-97.
153. Huard, J., B. Cao, and Z. Qu-Petersen, *Muscle-derived stem cells: potential for muscle regeneration.* Birth Defects Res C Embryo Today, 2003. **69**(3): p. 230-7.
154. Zuk, P.A., et al., *Human adipose tissue is a source of multipotent stem cells.* Molecular biology of the cell, 2002. **13**(12): p. 4279-4295.
155. Dowthwaite, G.P., et al., *The surface of articular cartilage contains a progenitor cell population.* J Cell Sci, 2004. **117**(Pt 6): p. 889-97.
156. Nishimura, K., et al., *Chondroprogenitor cells of synovial tissue.* Arthritis & Rheumatism, 1999. **42**(12): p. 2631-2637.
157. Nöth, U., et al., *Multilineage mesenchymal differentiation potential of human trabecular bone-derived cells.* J Orthop Res, 2002. **20**(5): p. 1060-9.
158. Crompton, M.J., et al., *Stem cells in gastrointestinal epithelium: numbers, characteristics and death.* Philosophical Transactions of the Royal Society of London. Series B: Biological Sciences, 1998. **353**(1370): p. 821-830.
159. Gage, F.H., *Mammalian Neural Stem Cells.* Science, 2000. **287**(5457): p. 1433-1438.
160. Nakahara, H., et al., *In vivo osteochondrogenic potential of cultured cells derived from the periosteum.* Clin Orthop Relat Res, 1990(259): p. 223-32.
161. Wickham, M.Q., et al., *Multipotent Stromal Cells Derived From the Infrapatellar Fat Pad of the Knee.* Clinical Orthopaedics and Related Research®, 2003. **412**: p. 196-212.
162. Gnecchi, M. and L.G. Melo, *Bone Marrow-Derived Mesenchymal Stem Cells: Isolation, Expansion, Characterization, Viral Transduction, and Production of Conditioned Medium*, in *Stem Cells in Regenerative Medicine*, J. Audet and W.L. Stanford, Editors. 2009, Humana Press: Totowa, NJ. p. 281-294.
163. Polak, J.M. and A.E. Bishop, *Stem cells and tissue engineering: past, present, and future.* Ann N Y Acad Sci, 2006. **1068**: p. 352-66.
164. Friedenstein, A.J., *Precursor cells of mechanocytes.* Int Rev Cytol, 1976. **47**: p. 327-59.
165. Hristov, M., W. Erl, and P.C. Weber, *Endothelial progenitor cells: mobilization, differentiation, and homing.* Arterioscler Thromb Vasc Biol, 2003. **23**(7): p. 1185-9.
166. Larochelle, A., et al., *Identification of primitive human hematopoietic cells capable of repopulating NOD/SCID mouse bone marrow: Implications for gene therapy.* Nature Medicine, 1996. **2**(12): p. 1329-1337.
167. Gronthos, S. and P.J. Simmons, *The biology and application of human bone marrow stromal cell precursors.* J Hematother, 1996. **5**(1): p. 15-23.

168. Marcacci, M., et al., *Stem cells associated with macroporous bioceramics for long bone repair: 6- to 7-year outcome of a pilot clinical study.* Tissue Eng, 2007. **13**(5): p. 947-55.
169. Guerrouahen, B.S., I. Al-Hijji, and A.R. Tabrizi, *Osteoblastic and vascular endothelial niches, their control on normal hematopoietic stem cells, and their consequences on the development of leukemia.* Stem cells international, 2011. **2011**: p. 375857-375857.
170. Warnke, P.H., et al., *Growth and transplantation of a custom vascularised bone graft in a man.* Lancet, 2004. **364**(9436): p. 766-70.
171. Vojtassák, J., et al., *Autologous biograft and mesenchymal stem cells in treatment of the diabetic foot.* Neuro Endocrinol Lett, 2006. **27 Suppl 2**: p. 134-7.
172. Kastrinaki, M., et al., *Functional, Molecular and Proteomic Characterization of Bone Marrow Mesenchymal Stem Cells in Rheumatoid Arthritis.* Annals of the Rheumatic Diseases, 2008. **67**(6): p. 741-749.
173. Rubio, D., et al., *Spontaneous Human Adult Stem Cell Transformation.* Cancer Research, 2005. **65**(8): p. 3035-3039.
174. Zuk, P.A., et al., *Human adipose tissue is a source of multipotent stem cells.* Mol Biol Cell, 2002. **13**(12): p. 4279-95.
175. Kakudo, N., et al., *Bone tissue engineering using human adipose-derived stem cells and honeycomb collagen scaffold.* J Biomed Mater Res A, 2008. **84**(1): p. 191-7.
176. Betre, H., et al., *Chondrocytic differentiation of human adipose-derived adult stem cells in elastin-like polypeptide.* Biomaterials, 2006. **27**(1): p. 91-99.
177. Nuti, N., et al., *Multipotent Differentiation of Human Dental Pulp Stem Cells: a Literature Review.* Stem Cell Rev Rep, 2016. **12**(5): p. 511-523.
178. Tatullo, M., et al., *Dental pulp stem cells: function, isolation and applications in regenerative medicine.* J Tissue Eng Regen Med, 2015. **9**(11): p. 1205-16.
179. Tatullo, M., et al., *Dental pulp stem cells: function, isolation and applications in regenerative medicine.* Journal of Tissue Engineering and Regenerative Medicine, 2015. **9**(11): p. 1205-1216.
180. Shi, S., et al., *The efficacy of mesenchymal stem cells to regenerate and repair dental structures.* Orthod Craniofac Res, 2005. **8**(3): p. 191-9.
181. Liu, H., S. Gronthos, and S. Shi, *[5] - Dental Pulp Stem Cells*, in *Methods in Enzymology*, I. Klimanskaya and R. Lanza, Editors. 2006, Academic Press. p. 99-113.
182. Gronthos, S., et al., *Postnatal human dental pulp stem cells (DPSCs) in vitro and in vivo*. Proceedings of the National Academy of Sciences, 2000. **97**(25): p. 13625-13630.
183. Shi, S. and S. Gronthos, *Perivascular niche of postnatal mesenchymal stem cells in human bone marrow and dental pulp.* J Bone Miner Res, 2003. **18**(4): p. 696-704.
184. Zhang, W., et al., *In vivo evaluation of human dental pulp stem cells differentiated towards multiple lineages.* Journal of Tissue Engineering and Regenerative Medicine, 2008. **2**(2-3): p. 117-125.
185. Shi, S., P.G. Robey, and S. Gronthos, *Comparison of human dental pulp and bone marrow stromal stem cells by cDNA microarray analysis.* Bone, 2001. **29**(6): p. 532-9.

186. Karaöz, E., et al., *Human dental pulp stem cells demonstrate better neural and epithelial stem cell properties than bone marrow-derived mesenchymal stem cells.* Histochem Cell Biol, 2011. **136**(4): p. 455-73.
187. Ranganathan, K. and V. Lakshminarayanan, *Stem cells of the dental pulp.* Indian J Dent Res, 2012. **23**(4): p. 558.
188. Zhang, Q., et al., *Mesenchymal stem cells derived from human gingiva are capable of immunomodulatory functions and ameliorate inflammation-related tissue destruction in experimental colitis.* Journal of immunology (Baltimore, Md. : 1950), 2009. **183**(12): p. 7787-7798.
189. Seo, B.M., et al., *Recovery of stem cells from cryopreserved periodontal ligament.* J Dent Res, 2005. **84**(10): p. 907-12.
190. Sonoyama, W., et al., *Mesenchymal stem cell-mediated functional tooth regeneration in swine.* PLoS One, 2006. **1**(1): p. e79.
191. Miura, M., et al., *SHED: Stem cells from human exfoliated deciduous teeth.* Proceedings of the National Academy of Sciences, 2003. **100**(10): p. 5807-5812.
192. Morsczeck, C., et al., *Isolation of precursor cells (PCs) from human dental follicle of wisdom teeth.* Matrix Biol, 2005. **24**(2): p. 155-65.
193. Ledesma-Martínez, E., V.M. Mendoza-Núñez, and E. Santiago-Osorio, *Mesenchymal Stem Cells Derived from Dental Pulp: A Review.* Stem Cells International, 2016. **2016**: p. 4709572.
194. Basegmez, C., L. Berber, and F. Yalcin, *Clinical and biochemical efficacy of minocycline in nonsurgical periodontal therapy: a randomized controlled pilot study.* J Clin Pharmacol, 2011. **51**(6): p. 915-22.
195. Research, N.I.o.D.a.C. *Periodontal Disease in Seniors (Age 65 and Over)*. Available from: https://www.nidcr.nih.gov/research/data-statistics/periodontal-disease/seniors.
196. Sharpe, P.T. and C.S. Young, *Test-tube teeth.* Sci Am, 2005. **293**(2): p. 34-41.
197. Yu, J., J. Shi, and Y. Jin, *Current approaches and challenges in making a bio-tooth.* Tissue Eng Part B Rev, 2008. **14**(3): p. 307-19.
198. Battistella, E., S. Mele, and L. Rimondini, *Dental Tissue Engineering: a New Approach to Dental Tissue Reconstruction*. 2010.
199. Abou Neel, E.A., et al., *Tissue engineering in dentistry.* Journal of Dentistry, 2014. **42**(8): p. 915-928.
200. Gonçalves, F., et al., *Combination of Bioactive Polymeric Membranes and Stem Cells for Periodontal Regeneration: In Vitro and In Vivo Analyses.* PLoS One, 2016. **11**(3): p. e0152412.
201. Khorsand, A., et al., *Autologous dental pulp stem cells in regeneration of defect created in canine periodontal tissue.* J Oral Implantol, 2013. **39**(4): p. 433-43.
202. Wang, J., et al., *The odontogenic differentiation of human dental pulp stem cells on nanofibrous poly(L-lactic acid) scaffolds in vitro and in vivo.* Acta Biomater, 2010. **6**(10): p. 3856-63.
203. Yang, X., et al., *The performance of dental pulp stem cells on nanofibrous PCL/gelatin/nHA scaffolds.* J Biomed Mater Res A, 2010. **93**(1): p. 247-57.
204. Clarke, D.L., et al., *Generalized potential of adult neural stem cells.* Science, 2000. **288**(5471): p. 1660-3.
205. Galli, R., et al., *Skeletal myogenic potential of human and mouse neural stem cells.* Nat Neurosci, 2000. **3**(10): p. 986-91.

206. Elhassani, S.B., *The umbilical cord: care, anomalies, and diseases.* South Med J, 1984. **77**(6): p. 730-6.
207. Nagamura-Inoue, T. and H. He, *Umbilical cord-derived mesenchymal stem cells: Their advantages and potential clinical utility.* World journal of stem cells, 2014. **6**(2): p. 195-202.
208. *In vitro growth of granulocytic colonies from circulating cells in human cord blood*. 1974.
209. Ghen, M.J., et al., *Potential clinical applications using stem cells derived from human umbilical cord blood.* Reprod Biomed Online, 2006. **13**(4): p. 562-72.
210. Majore, I., et al., *Growth and differentiation properties of mesenchymal stromal cell populations derived from whole human umbilical cord.* Stem Cell Rev Rep, 2011. **7**(1): p. 17-31.
211. Ishige, I., et al., *Comparison of mesenchymal stem cells derived from arterial, venous, and Wharton's jelly explants of human umbilical cord.* Int J Hematol, 2009. **90**(2): p. 261-269.
212. Mitchell, K.E., et al., *Matrix cells from Wharton's jelly form neurons and glia.* Stem Cells, 2003. **21**(1): p. 50-60.
213. Kita, K., et al., *Isolation and characterization of mesenchymal stem cells from the sub-amniotic human umbilical cord lining membrane.* Stem Cells Dev, 2010. **19**(4): p. 491-502.
214. Zebardast, N., D. Lickorish, and J.E. Davies, *Human umbilical cord perivascular cells (HUCPVC): A mesenchymal cell source for dermal wound healing.* Organogenesis, 2010. **6**(4): p. 197-203.
215. Bissell, M.J., H.G. Hall, and G. Parry, *How does the extracellular matrix direct gene expression?* J Theor Biol, 1982. **99**(1): p. 31-68.
216. Labat-Robert, J. and L. Robert, *Aging of the extracellular matrix and its pathology.* Exp Gerontol, 1988. **23**(1): p. 5-18.
217. Bosman, F.T. and I. Stamenkovic, *Functional structure and composition of the extracellular matrix.* J Pathol, 2003. **200**(4): p. 423-8.
218. Kim, S.H., J. Turnbull, and S. Guimond, *Extracellular matrix and cell signalling: the dynamic cooperation of integrin, proteoglycan and growth factor receptor.* J Endocrinol, 2011. **209**(2): p. 139-51.
219. Badylak, S.F., D.O. Freytes, and T.W. Gilbert, *Extracellular matrix as a biological scaffold material: Structure and function.* Acta Biomater, 2009. **5**(1): p. 1-13.
220. Rozario, T. and D.W. DeSimone, *The extracellular matrix in development and morphogenesis: a dynamic view.* Dev Biol, 2010. **341**(1): p. 126-40.
221. Engler, A.J., et al., *Matrix elasticity directs stem cell lineage specification.* Cell, 2006. **126**(4): p. 677-89.
222. Yi, S., et al., *Extracellular Matrix Scaffolds for Tissue Engineering and Regenerative Medicine.* Curr Stem Cell Res Ther, 2017. **12**(3): p. 233-246.
223. Yue, B., *Biology of the extracellular matrix: an overview.* J Glaucoma, 2014. **23**(8 Suppl 1): p. S20-3.
224. Daamen, W.F., et al., *Elastin as a biomaterial for tissue engineering.* Biomaterials, 2007. **28**(30): p. 4378-98.
225. Kular, J.K., S. Basu, and R.I. Sharma, *The extracellular matrix: Structure, composition, age-related differences, tools for analysis and applications for tissue engineering.* J Tissue Eng, 2014. **5**: p. 2041731414557112.

226. Singh, P., C. Carraher, and J.E. Schwarzbauer, *Assembly of fibronectin extracellular matrix.* Annual review of cell and developmental biology, 2010. **26**: p. 397-419.
227. Wu, C., et al., *Integrin activation and cytoskeletal interaction are essential for the assembly of a fibronectin matrix.* Cell, 1995. **83**(5): p. 715-24.
228. Timpl, R., et al., *Laminin--a glycoprotein from basement membranes.* J Biol Chem, 1979. **254**(19): p. 9933-7.
229. Rosso, F., et al., *From cell-ECM interactions to tissue engineering.* J Cell Physiol, 2004. **199**(2): p. 174-80.
230. Cohen, G.B., R. Ren, and D. Baltimore, *Modular binding domains in signal transduction proteins.* Cell, 1995. **80**(2): p. 237-48.
231. Ehrbar, M., et al., *Cell-Demanded Liberation of VEGF₁₂₁ From Fibrin Implants Induces Local and Controlled Blood Vessel Growth.* Circulation Research, 2004. **94**(8): p. 1124-1132.
232. Zisch, A.H., et al., *Covalently conjugated VEGF--fibrin matrices for endothelialization.* J Control Release, 2001. **72**(1-3): p. 101-13.
233. Hynes, R.O., *Integrins: A family of cell surface receptors.* Cell, 1987. **48**(4): p. 549-554.
234. Tzima, E., et al., *Activation of integrins in endothelial cells by fluid shear stress mediates Rho-dependent cytoskeletal alignment.* The EMBO Journal, 2001. **20**(17): p. 4639-4647.
235. Eble, J.A., et al., *The alpha 1 beta 1 integrin recognition site of the basement membrane collagen molecule [alpha 1(IV)]2 alpha 2(IV).* Embo j, 1993. **12**(12): p. 4795-802.
236. Chong, E.J., et al., *Evaluation of electrospun PCL/gelatin nanofibrous scaffold for wound healing and layered dermal reconstitution.* Acta Biomater, 2007. **3**(3): p. 321-30.
237. Belkin, A.M. and M.A. Stepp, *Integrins as receptors for laminins.* Microsc Res Tech, 2000. **51**(3): p. 280-301.
238. Shen, B., et al. *Integrin alpha11 is an Osteolectin receptor and is required for the maintenance of adult skeletal bone mass*. eLife, 2019. **8**, DOI: 10.7554/elife.42274.
239. Ayerst, B.I., C.L.R. Merry, and A.J. Day, *The Good the Bad and the Ugly of Glycosaminoglycans in Tissue Engineering Applications.* Pharmaceuticals (Basel, Switzerland), 2017. **10**(2): p. 54.
240. Klass, C.M., J.R. Couchman, and A. Woods, *Control of extracellular matrix assembly by syndecan-2 proteoglycan.* J Cell Sci, 2000. **113 (Pt 3)**: p. 493-506.
241. Baldwin, A.D. and K.L. Kiick, *Polysaccharide-modified synthetic polymeric biomaterials.* Biopolymers, 2010. **94**(1): p. 128-40.
242. Jeon, O., et al., *Affinity-based growth factor delivery using biodegradable, photocrosslinked heparin-alginate hydrogels.* J Control Release, 2011. **154**(3): p. 258-66.
243. Silva, S.S., J.F. Mano, and R.L. Reis, *Potential applications of natural origin polymer-based systems in soft tissue regeneration.* Crit Rev Biotechnol, 2010. **30**(3): p. 200-21.
244. Pieper, J.S., et al., *Development of tailor-made collagen-glycosaminoglycan matrices: EDC/NHS crosslinking, and ultrastructural aspects.* Biomaterials, 2000. **21**(6): p. 581-93.

245. Vigetti, D., et al., *Hyaluronan: biosynthesis and signaling.* Biochim Biophys Acta, 2014. **1840**(8): p. 2452-9.
246. Häcker, U., K. Nybakken, and N. Perrimon, *Heparan sulphate proteoglycans: the sweet side of development.* Nat Rev Mol Cell Biol, 2005. **6**(7): p. 530-41.
247. Bix, G., et al., *Endorepellin causes endothelial cell disassembly of actin cytoskeleton and focal adhesions through alpha2beta1 integrin.* The Journal of cell biology, 2004. **166**(1): p. 97-109.
248. Kalamajski, S. and A. Oldberg, *The role of small leucine-rich proteoglycans in collagen fibrillogenesis.* Matrix Biol, 2010. **29**(4): p. 248-53.
249. Mongiat, M., et al., *The protein core of the proteoglycan perlecan binds specifically to fibroblast growth factor-7.* J Biol Chem, 2000. **275**(10): p. 7095-100.
250. Kumbar, S.G., et al., *Electrospun nanofiber scaffolds: engineering soft tissues.* Biomed Mater, 2008. **3**(3): p. 034002.
251. Barnes, C.P., et al., *Nanofiber technology: designing the next generation of tissue engineering scaffolds.* Adv Drug Deliv Rev, 2007. **59**(14): p. 1413-33.
252. Bader, A., et al., *Tissue engineering of heart valves--human endothelial cell seeding of detergent acellularized porcine valves.* Eur J Cardiothorac Surg, 1998. **14**(3): p. 279-84.
253. Conklin, B.S., et al., *Development and evaluation of a novel decellularized vascular xenograft.* Med Eng Phys, 2002. **24**(3): p. 173-83.
254. Liem, P.H., et al., *Autologous skin reconstruction by combining epidermis and acellular dermal matrix tissue derived from the skin of giant congenital melanocytic nevi.* Journal of Artificial Organs, 2013. **16**(3): p. 332-342.
255. Hudson, T.W., S.Y. Liu, and C.E. Schmidt, *Engineering an improved acellular nerve graft via optimized chemical processing.* Tissue Eng, 2004. **10**(9-10): p. 1346-58.
256. Cartmell, J.S. and M.G. Dunn, *Effect of chemical treatments on tendon cellularity and mechanical properties.* J Biomed Mater Res, 2000. **49**(1): p. 134-40.
257. Gilbert, T.W., et al., *Production and characterization of ECM powder: implications for tissue engineering applications.* Biomaterials, 2005. **26**(12): p. 1431-5.
258. Jadalannagari, S., et al., *Decellularized Wharton's Jelly from human umbilical cord as a novel 3D scaffolding material for tissue engineering applications.* PLoS One, 2017. **12**(2): p. e0172098.
259. Dan, P., et al., *Human-derived extracellular matrix from Wharton's jelly: An untapped substrate to build up a standardized and homogeneous coating for vascular engineering.* Acta Biomaterialia, 2017. **48**: p. 227-237.
260. Beiki, B., B. Zeynali, and E. Seyedjafari, *Fabrication of a three dimensional spongy scaffold using human Wharton's jelly derived extra cellular matrix for wound healing.* Mater Sci Eng C Mater Biol Appl, 2017. **78**: p. 627-638.
261. Lutz, A.J., et al., *Double knockout pigs deficient in N-glycolylneuraminic acid and Galactose α-1,3-Galactose reduce the humoral barrier to xenotransplantation.* Xenotransplantation, 2013. **20**(1): p. 27-35.
262. Liguori, G.R., et al., *(*) Ethical Issues in the Use of Animal Models for Tissue Engineering: Reflections on Legal Aspects, Moral Theory, Three Rs Strategies, and Harm-Benefit Analysis.* Tissue Eng Part C Methods, 2017. **23**(12): p. 850-862.
263. Tamura, M., et al., *Wharton's Jelly Stem Cells as Agents for Cancer Therapy.* Open Tissue Eng. Regen. Med. J, 2010. **4**.

264. McELREAVEY, K.D., et al., *Isolation, culture and characterisation of fibroblast-like cells derived from the Wharton's jelly portion of human umbilical cord.* Biochemical Society Transactions, 1991. **19**(1): p. 29S-29S.
265. Kobayashi, K., T. Kubota, and T. Aso, *Study on myofibroblast differentiation in the stromal cells of Wharton's jelly: expression and localization of alpha-smooth muscle actin.* Early human development, 1998. **51**(3): p. 223-233.
266. Bańkowski, E., et al., *Collagen and glycosaminoglycans of Wharton's jelly and their alterations in EPH-gestosis.* European Journal of Obstetrics & Gynecology and Reproductive Biology, 1996. **66**(2): p. 109-117.
267. Sobolewski, K., et al., *Wharton's jelly as a reservoir of peptide growth factors.* Placenta, 2005. **26**(10): p. 747-52.
268. Edmondson, S.R., et al., *Epidermal homeostasis: the role of the growth hormone and insulin-like growth factor systems.* Endocr Rev, 2003. **24**(6): p. 737-64.
269. Yu, C., et al., *Role of fibroblast growth factor type 1 and 2 in carbon tetrachloride-induced hepatic injury and fibrogenesis.* Am J Pathol, 2003. **163**(4): p. 1653-62.
270. Shalitin, N., et al., *Expression of procollagen C-proteinase enhancer in cultured rat heart fibroblasts: Evidence for co-regulation with type I collagen.* Journal of Cellular Biochemistry, 2003. **90**(2): p. 397-407.
271. Geckil, H., et al., *Engineering hydrogels as extracellular matrix mimics.* Nanomedicine (Lond), 2010. **5**(3): p. 469-84.
272. Tayalia, P. and D.J. Mooney, *Controlled growth factor delivery for tissue engineering.* Adv Mater, 2009. **21**(32-33): p. 3269-85.
273. Reintjes, T., J. Tessmar, and A. Göpferich, *Biomimetic polymers to control cell adhesion.* Journal of Drug Delivery Science and Technology, 2008. **18**(1): p. 15-24.
274. Salbach, J., et al., *Regenerative potential of glycosaminoglycans for skin and bone.* J Mol Med (Berl), 2012. **90**(6): p. 625-35.
275. Unterman, S.A., et al., *Hyaluronic acid-binding scaffold for articular cartilage repair.* Tissue Eng Part A, 2012. **18**(23-24): p. 2497-506.
276. Tous, E., et al., *Influence of injectable hyaluronic acid hydrogel degradation behavior on infarction-induced ventricular remodeling.* Biomacromolecules, 2011. **12**(11): p. 4127-35.
277. Bańkowski, E., L. Romanowicz, and S. Jaworski, *Collagen of umbilical cord arteries and its alterations in EPH-gestosis.* J Perinat Med, 1993. **21**(6): p. 491-8.
278. Dawson, J.I., et al., *Clay Gels For the Delivery of Regenerative Microenvironments.* Advanced Materials, 2011. **23**(29): p. 3304-3308.
279. Freytes, D.O., et al., *Biaxial strength of multilaminated extracellular matrix scaffolds.* Biomaterials, 2004. **25**(12): p. 2353-61.
280. Badylak, S.F., et al., *Small intestinal submucosa as a large diameter vascular graft in the dog.* J Surg Res, 1989. **47**(1): p. 74-80.
281. Badylak, S.F., et al., *The use of xenogeneic small intestinal submucosa as a biomaterial for Achilles tendon repair in a dog model.* J Biomed Mater Res, 1995. **29**(8): p. 977-85.
282. Xu, Y., et al., *Nanofibrillar Decellularized Wharton's Jelly Matrix for Segmental Tracheal Repair.* Advanced Functional Materials, 2020. **30**(14): p. 1910067.
283. Franc, S., et al., *Microfibrillar composition of umbilical cord matrix: characterization of fibrillin, collagen VI and intact collagen V.* Placenta, 1998. **19**(1): p. 95-104.

284. Lin, L., et al., *Nanofibrous Wharton's jelly scaffold in combination with adipose-derived stem cells for cartilage engineering.* Materials & Design, 2020. **186**: p. 108216.
285. Stocco, E., et al., *Tailored PVA/ECM scaffolds for cartilage regeneration.* Biomed Res Int, 2014. **2014**: p. 762189.
286. Xia, D., et al., *Tissue-engineered trachea from a 3D-printed scaffold enhances whole-segment tracheal repair in a goat model.* J Tissue Eng Regen Med, 2019. **13**(4): p. 694-703.
287. Herrero-Mendez, A., et al., *HR007: a family of biomaterials based on glycosaminoglycans for tissue repair.* J Tissue Eng Regen Med, 2017. **11**(4): p. 989-1001.
288. Nekanti, U., et al., *Long-term expansion and pluripotent marker array analysis of Wharton's jelly-derived mesenchymal stem cells.* Stem Cells Dev, 2010. **19**(1): p. 117-30.
289. Troyer, D.L. and M.L. Weiss, *Wharton's jelly-derived cells are a primitive stromal cell population.* Stem Cells, 2008. **26**(3): p. 591-9.
290. Marino, L., et al., *Mesenchymal Stem Cells from the Wharton’s Jelly of the Human Umbilical Cord: Biological Properties and Therapeutic Potential.* International Journal of Stem Cells, 2019. **12**(2): p. 218-226.
291. Fu, Y.S., et al., *Conversion of human umbilical cord mesenchymal stem cells in Wharton's jelly to dopaminergic neurons in vitro: potential therapeutic application for Parkinsonism.* Stem Cells, 2006. **24**(1): p. 115-24.
292. Kuroda, Y., et al., *Mesenchymal Stem Cells and Umbilical Cord as Sources for Schwann Cell Differentiation: their Potential in Peripheral Nerve Repair.* Open Tissue Eng. Regen. Med. J, 2010. **4**.
293. Du, T., et al., *Human Wharton's jelly-derived mesenchymal stromal cells reduce renal fibrosis through induction of native and foreign hepatocyte growth factor synthesis in injured tubular epithelial cells.* Stem Cell Res Ther, 2013. **4**(3): p. 59.
294. Moodley, Y., et al., *Human umbilical cord mesenchymal stem cells reduce fibrosis of bleomycin-induced lung injury.* Am J Pathol, 2009. **175**(1): p. 303-13.
295. I, S., *Cell Therapy for the Treatment of Metabolic Liver Disease: An Update on the Umbilical Cord Derived Stem Cells Candidates.* The Open Tissue Engineering and Regenerative Medicine Journal, 2011. **4**: p. 48-53.
296. Millán-Rivero, J.E., et al., *Silk fibroin scaffolds seeded with Wharton's jelly mesenchymal stem cells enhance re-epithelialization and reduce formation of scar tissue after cutaneous wound healing.* Stem Cell Research & Therapy, 2019. **10**(1): p. 126.
297. Chen, X., et al., *Chondrogenic differentiation of umbilical cord-derived mesenchymal stem cells in type I collagen-hydrogel for cartilage engineering.* Injury, 2013. **44**(4): p. 540-549.
298. Jamalpoor, Z., et al., *In vitro interaction of human Wharton's jelly mesenchymal stem cells with biomimetic 3D scaffold.* Journal of Biomedical Materials Research Part A, 2019. **107**(6): p. 1166-1175.
299. Li, P., et al., *Promoting the recovery of injured liver with poly (3-hydroxybutyrate-co-3-hydroxyvalerate-co-3-hydroxyhexanoate) scaffolds loaded with umbilical cord-derived mesenchymal stem cells.* Tissue Eng Part A, 2015. **21**(3-4): p. 603-15.

300. Chen, G.P., T. Ushida, and T. Tateishi, *Scaffold design for tissue engineering.* Macromolecular Bioscience, 2002. **2**(2): p. 67-77.
301. Burg, K.J., S. Porter, and J.F. Kellam, *Biomaterial developments for bone tissue engineering.* Biomaterials, 2000. **21**(23): p. 2347-59.
302. Yannas, I.V., *Classes of materials used in medicine: natural materials," in Biomaterials Science—An Introduction toMaterials in Medicine.* Elsevier Academic Press, 2004: p. 127–136.
303. Gomes, M., et al., *Chapter 6 - Natural Polymers in tissue engineering applications*, in *Tissue Engineering*, C.v. Blitterswijk, et al., Editors. 2008, Academic Press: Burlington. p. 145-192.
304. Broderick, E.P., et al., *Enzymatic stabilization of gelatin-based scaffolds.* Journal of Biomedical Materials Research Part B: Applied Biomaterials, 2005. **72B**(1): p. 37-42.
305. Argüelles-Monal, W.M., et al., *Chitosan Derivatives: Introducing New Functionalities with a Controlled Molecular Architecture for Innovative Materials.* Polymers, 2018. **10**(3): p. 342.
306. Chaffey, N., *Alberts, B., Johnson, A., Lewis, J., Raff, M., Roberts, K. and Walter, P. Molecular biology of the cell. 4th edn.* Annals of Botany, 2003. **91**(3): p. 401-401.
307. van der Rest, M. and R. Garrone, *Collagen family of proteins.* Faseb j, 1991. **5**(13): p. 2814-23.
308. Prockop, D.J. and K.I. Kivirikko, *Collagens: molecular biology, diseases, and potentials for therapy.* Annu Rev Biochem, 1995. **64**: p. 403-34.
309. Ma, L., et al., *Collagen/chitosan porous scaffolds with improved biostability for skin tissue engineering.* Biomaterials, 2003. **24**(26): p. 4833-4841.
310. Liu, T., et al., *Nanofibrous collagen nerve conduits for spinal cord repair.* Tissue Eng Part A, 2012. **18**(9-10): p. 1057-66.
311. Cui, Y., et al., *Collagen scaffolds modified with CNTF and bFGF promote facial nerve regeneration in minipigs.* Biomaterials, 2014. **35**(27): p. 7819-27.
312. Inzana, J.A., et al., *3D printing of composite calcium phosphate and collagen scaffolds for bone regeneration.* Biomaterials, 2014. **35**(13): p. 4026-34.
313. Chen, G., L. Yang, and Y. Lv, *Cell-free scaffolds with different stiffness but same microstructure promote bone regeneration in rabbit large bone defect model.* J Biomed Mater Res A, 2016. **104**(4): p. 833-41.
314. Gigante, A., et al., *Purified collagen I oriented membrane for tendon repair: an ex vivo morphological study.* J Orthop Res, 2013. **31**(5): p. 738-45.
315. Yunoki, S., et al., *A novel fabrication method to create a thick collagen bundle composed of uniaxially aligned fibrils: an essential technology for the development of artificial tendon/ligament matrices.* J Biomed Mater Res A, 2015. **103**(9): p. 3054-65.
316. Lee, S.J., et al., *Development of a composite vascular scaffolding system that withstands physiological vascular conditions.* Biomaterials, 2008. **29**(19): p. 2891-2898.
317. Liu, T., et al., *Endothelialization of implanted cardiovascular biomaterial surfaces: The development from in vitro to in vivo.* Journal of Biomedical Materials Research Part A, 2014. **102**(10): p. 3754-3772.

318. Lynn, A., I.V. Yannas, and W. Bonfield, *Antigenicity and immunogenicity of collagen.* Journal of biomedical materials research. Part B, Applied biomaterials, 2004. **71**: p. 343-54.
319. Schmitt, F.O., et al., *THE ANTIGENICITY OF TROPOCOLLAGEN.* Proceedings of the National Academy of Sciences of the United States of America, 1964. **51**(3): p. 493-497.
320. Furthmayr, H., W. Beil, and R. Timpl, *Different antigenic determinants in the polypeptide chains of human collagen.* FEBS Lett, 1971. **12**(6): p. 341-344.
321. Zata, H., C. Prahasanti, and K. Shafira, *Collagen from marine source for regenerative therapy: A literature review*. Vol. 2314. 2020. 050017.
322. Djagny, K.B., Z. Wang, and S. Xu, *Gelatin: A Valuable Protein for Food and Pharmaceutical Industries: Review.* Critical Reviews in Food Science and Nutrition, 2001. **41**: p. 481 - 492.
323. Gómez-Guillén, M.C., et al., *Functional and bioactive properties of collagen and gelatin from alternative sources: A review.* Food Hydrocolloids, 2011. **25**(8): p. 1813-1827.
324. Frazier, S.D. and W.V. Srubar, *Evaporation-based method for preparing gelatin foams with aligned tubular pore structures.* Materials Science & Engineering C-Materials for Biological Applications, 2016. **62**: p. 467-473.
325. Damrongsakkul, S., et al., *Enzymatic hydrolysis of rawhide using papain and neutrase.* Journal of Industrial and Engineering Chemistry, 2008. **14**(2): p. 202-206.
326. Wahab, R. and N. Mahat, *Protocols and Methods for Developing Green Immobilized Nanobiocatalysts for Esterification Reactions*. 2016.
327. Kariduraganavar, M.Y., A.A. Kittur, and R.R. Kamble, *Chapter 1 - Polymer Synthesis and Processing*, in *Natural and Synthetic Biomedical Polymers*, S.G. Kumbar, C.T. Laurencin, and M. Deng, Editors. 2014, Elsevier: Oxford. p. 1-31.
328. Gioffrè, M., et al., *Role of pH on stability and mechanical properties of gelatin films.* Journal of Bioactive and Compatible Polymers, 2012. **27**(1): p. 67-77.
329. S.M. Lien, L.Y.K., T.J. Huang,, 2009. **5**: p. 670-679.
330. Jaipan, P., A. Nguyen, and R.J. Narayan, *Gelatin-based hydrogels for biomedical applications.* MRS Communications, 2017. **7**(3): p. 416-426.
331. MacQueen, L.A., et al., *Muscle tissue engineering in fibrous gelatin: implications for meat analogs.* npj Science of Food, 2019. **3**(1): p. 20.
332. Lewis, P.L., R.M. Green, and R.N. Shah, *3D-printed gelatin scaffolds of differing pore geometry modulate hepatocyte function and gene expression.* Acta Biomaterialia, 2018. **69**: p. 63-70.
333. Chong, E.J., et al., *Evaluation of electrospun PCL/gelatin nanofibrous scaffold for wound healing and layered dermal reconstitution.* Acta Biomaterialia, 2007. **3**(3): p. 321-330.
334. Chang, C.-H., et al., *Gelatin–chondroitin–hyaluronan tri-copolymer scaffold for cartilage tissue engineering.* Biomaterials, 2003. **24**(26): p. 4853-4858.
335. J.Y. Lai, Y.T.L., Biomacromolecules 2010. **11**: p. 1387–1397.
336. X.H. Liu, P.X.M., Biomaterials, 2009. **30**: p. 4094–4103.
337. P.A Salerno, E.N., S. Di Maio, Iannace, J. Cell. Plast., 2009. **45** p. 103–117.
338. Van Vlierberghe, S., et al., *Porous Gelatin Hydrogels: 1. Cryogenic Formation and Structure Analysis.* Biomacromolecules, 2007. **8**(2): p. 331-337.

339. Bhattacharya, A., P. Sood, and V. Citovsky, *The roles of plant phenolics in defence and communication during Agrobacterium and Rhizobium infection.* Mol Plant Pathol, 2010. **11**(5): p. 705-19.
340. D'Archivio, M., et al., *Polyphenols, dietary sources and bioavailability.* Ann Ist Super Sanita, 2007. **43**(4): p. 348-61.
341. Tanaka, T., Y. Matsuo, and Y. Saito, *Solubility of Tannins and Preparation of Oil-Soluble Derivatives.* J Oleo Sci, 2018. **67**(10): p. 1179-1187.
342. Song, J.E., et al., *Quercetin Inlaid Silk Fibroin/Hydroxyapatite Scaffold Promotes Enhanced Osteogenesis.* ACS Applied Materials & Interfaces, 2018. **10**(39): p. 32955-32964.
343. Nathan, C. and A. Cunningham-Bussel, *Beyond oxidative stress: an immunologist's guide to reactive oxygen species.* Nature Reviews Immunology, 2013. **13**(5): p. 349-361.
344. Gao, X., et al., *Polyphenols as a versatile component in tissue engineering.* Acta Biomaterialia, 2021. **119**: p. 57-74.
345. Chen, Y., et al., *Antioxidant activities and emulsifying properties of porcine plasma protein hydrolysates modified by oxidized tannic acid and oxidized chlorogenic acid.* Process Biochemistry, 2019. **79**: p. 105-113.
346. Aewsiri, T., et al., *Emulsifying Property and Antioxidative Activity of Cuttlefish Skin Gelatin Modified with Oxidized Linoleic Acid and Oxidized Tannic Acid.* Food and Bioprocess Technology, 2013. **6**(4): p. 870-881.
347. Thi, P.L., et al., *In situ forming and reactive oxygen species-scavenging gelatin hydrogels for enhancing wound healing efficacy.* Acta Biomaterialia, 2020. **103**: p. 142-152.
348. Daglia, M., *Polyphenols as antimicrobial agents.* Curr Opin Biotechnol, 2012. **23**(2): p. 174-81.
349. Della Valle, C., et al., *American Academy of Orthopaedic Surgeons Clinical Practice Guideline on: The Diagnosis of Periprosthetic Joint Infections of the Hip and Knee.* JBJS, 2011. **93**(14): p. 1355-1357.
350. Levin, P.A. and E.R. Angert, *Small but Mighty: Cell Size and Bacteria.* Cold Spring Harbor perspectives in biology, 2015. **7**(7): p. a019216-a019216.
351. Singh, B., et al., *Human pathogens utilize host extracellular matrix proteins laminin and collagen for adhesion and invasion of the host.* FEMS Microbiology Reviews, 2012. **36**(6): p. 1122-1180.
352. Stewart, P.S. and J. William Costerton, *Antibiotic resistance of bacteria in biofilms.* The Lancet, 2001. **358**(9276): p. 135-138.
353. Miklasińska-Majdanik, M., et al., *Phenolic Compounds Diminish Antibiotic Resistance of Staphylococcus Aureus Clinical Strains.* International journal of environmental research and public health, 2018. **15**(10): p. 2321.
354. Leekha, S., C.L. Terrell, and R.S. Edson, *General principles of antimicrobial therapy.* Mayo Clinic proceedings, 2011. **86**(2): p. 156-167.
355. Gurtner, G.C., et al., *Wound repair and regeneration.* Nature, 2008. **453**(7193): p. 314-321.
356. Eming, S.A., P. Martin, and M. Tomic-Canic, *Wound repair and regeneration: Mechanisms, signaling, and translation.* Science Translational Medicine, 2014. **6**(265): p. 265sr6-265sr6.

357. Ikigai, H., et al., *Bactericidal catechins damage the lipid bilayer.* Biochimica et Biophysica Acta (BBA) - Biomembranes, 1993. **1147**(1): p. 132-136.
358. Stapleton, P.D., et al., *Anti-Staphylococcus aureus activity and oxacillin resistance modulating capacity of 3-O-acyl-catechins.* International Journal of Antimicrobial Agents, 2004. **24**(4): p. 374-380.
359. Taguri, T., T. Tanaka, and I. Kouno, *Antibacterial Spectrum of Plant Polyphenols and Extracts Depending upon Hydroxyphenyl Structure.* Biological and Pharmaceutical Bulletin, 2006. **29**(11): p. 2226-2235.
360. Field, J.A. and G. Lettinga, *Toxicity of Tannic Compounds to Microorganisms*, in *Plant Polyphenols: Synthesis, Properties, Significance*, R.W. Hemingway and P.E. Laks, Editors. 1992, Springer US: Boston, MA. p. 673-692.
361. Chung, K.T., Z. Lu, and M.W. Chou, *Mechanism of inhibition of tannic acid and related compounds on the growth of intestinal bacteria.* Food and Chemical Toxicology, 1998. **36**(12): p. 1053-1060.
362. Pandey, A. and P.S. Negi, *Phytochemical composition, in vitro antioxidant activity and antibacterial mechanisms of Neolamarckia cadamba fruits extracts.* Natural Product Research, 2018. **32**(10): p. 1189-1192.
363. Ma, L., et al., *Development of Molecularly Imprinted Polymers To Block Quorum Sensing and Inhibit Bacterial Biofilm Formation.* ACS Applied Materials & Interfaces, 2018. **10**(22): p. 18450-18457.
364. Reitzer, F., et al., *Use of Gelatin as Tannic Acid Carrier for Its Sustained Local Delivery.* Pharmaceutical Frontiers, 2020. **2**(1): p. e200002.
365. Ninan, N., et al., *Antibacterial and Anti-Inflammatory pH-Responsive Tannic Acid-Carboxylated Agarose Composite Hydrogels for Wound Healing.* ACS Applied Materials & Interfaces, 2016. **8**(42): p. 28511-28521.
366. Sungur, S. and A. Uzar, *Investigation of complexes tannic acid and myricetin with Fe(III).* Spectrochim Acta A Mol Biomol Spectrosc, 2008. **69**(1): p. 225-9.
367. Dabbaghi, A., et al., *Synthesis of bio-based internal and external cross-linkers based on tannic acid for preparation of antibacterial superabsorbents.* Polymers for Advanced Technologies, 2019. **30**(11): p. 2894-2905.
368. Liu, R., et al., *Synthesis of New Biobased Antibacterial Methacrylates Derived from Tannic Acid and Their Application in UV-Cured Coatings.* Industrial & Engineering Chemistry Research, 2014. **53**(27): p. 10835-10840.
369. Umashankar, P.R., P.V. Mohanan, and T.V. Kumari, *Glutaraldehyde treatment elicits toxic response compared to decellularization in bovine pericardium.* Toxicol Int, 2012. **19**(1): p. 51-8.
370. Perrotta, I., et al., *New evidence for a critical role of elastin in calcification of native heart valves: immunohistochemical and ultrastructural study with literature review.* Histopathology, 2011. **59**(3): p. 504-513.
371. MATHEIS, G. and J.R. WHITAKER, *MODIFICATION OF PROTEINS BY POLYPHENOL OXIDASE AND PEROXIDASE AND THEIR PRODUCTS.* Journal of Food Biochemistry, 1984. **8**(3): p. 137-162.
372. Rawel, H.M., J. Kroll, and U.C. Hohl, *Model studies on reactions of plant phenols with whey proteins.* Food / Nahrung, 2001. **45**(2): p. 72-81.
373. Ozdal, T., E. Capanoglu, and F. Altay, *A review on protein–phenolic interactions and associated changes.* Food Research International, 2013. **51**(2): p. 954-970.

374. Rawel, H.M., K. Meidtner, and J. Kroll, *Binding of Selected Phenolic Compounds to Proteins.* Journal of Agricultural and Food Chemistry, 2005. **53**(10): p. 4228-4235.
375. Robbins, R.J., *Phenolic acids in foods: an overview of analytical methodology.* J Agric Food Chem, 2003. **51**(10): p. 2866-87.
376. Strauss, G. and S.M. Gibson, *Plant phenolics as cross-linkers of gelatin gels and gelatin-based coacervates for use as food ingredients.* Food Hydrocolloids, 2004. **18**(1): p. 81-89.
377. Zhang, X., et al., *Chemical Modification of Gelatin by a Natural Phenolic Cross-linker, Tannic Acid.* Journal of Agricultural and Food Chemistry, 2010. **58**(11): p. 6809-6815.
378. Guarino, V., et al., *Polylactic acid fibre-reinforced polycaprolactone scaffolds for bone tissue engineering.* Biomaterials, 2008. **29**(27): p. 3662-3670.
379. Maspero, F.A., et al., *Resorbable defect analog PLGA scaffolds using CO2 as solvent: Structural characterization.* Journal of Biomedical Materials Research, 2002. **62**(1): p. 89-98.
380. Ghasemi-Mobarakeh, L., D. Semnani, and M. Morshed, *A novel method for porosity measurement of various surface layers of nanofibers mat using image analysis for tissue engineering applications.* Journal of Applied Polymer Science, 2007. **106**(4): p. 2536-2542.
381. Mayer, R.P. and R.A. Stowe, *Mercury porosimetry—breakthrough pressure for penetration between packed spheres.* Journal of Colloid Science, 1965. **20**(8): p. 893-911.
382. Hu, Y., et al., *Fabrication of poly(alpha-hydroxy acid) foam scaffolds using multiple solvent systems.* J Biomed Mater Res, 2002. **59**(3): p. 563-72.
383. Ma, J., C. Wang, and K.W. Peng, *Electrophoretic deposition of porous hydroxyapatite scaffold.* Biomaterials, 2003. **24**(20): p. 3505-10.
384. Li, W.J., et al., *Electrospun nanofibrous structure: a novel scaffold for tissue engineering.* J Biomed Mater Res, 2002. **60**(4): p. 613-21.
385. León y León, C.A., *New perspectives in mercury porosimetry.* Advances in Colloid and Interface Science, 1998. **76-77**: p. 341-372.
386. Shi, G., et al., *Fabrication and biocompatibility of cell scaffolds of poly(L-lactic acid) and poly(L-lactic-co-glycolic acid).* Polymers for Advanced Technologies, 2002. **13**(3-4): p. 227-232.
387. Zhang, Y. and M. Zhang, *Synthesis and characterization of macroporous chitosan/calcium phosphate composite scaffolds for tissue engineering.* J Biomed Mater Res, 2001. **55**(3): p. 304-12.
388. Zhao, F., et al., *Preparation and histological evaluation of biomimetic three-dimensional hydroxyapatite/chitosan-gelatin network composite scaffolds.* Biomaterials, 2002. **23**(15): p. 3227-34.
389. Park, S.-N., et al., *Characterization of porous collagen/hyaluronic acid scaffold modified by 1-ethyl-3-(3-dimethylaminopropyl)carbodiimide cross-linking.* Biomaterials, 2002. **23**(4): p. 1205-1212.
390. Damien, E., et al., *A preliminary study on the enhancement of the osteointegration of a novel synthetic hydroxyapatite scaffold in vivo.* J Biomed Mater Res A, 2003. **66**(2): p. 241-6.

391. Nazarov, R., H.-J. Jin, and D.L. Kaplan, *Porous 3-D Scaffolds from Regenerated Silk Fibroin.* Biomacromolecules, 2004. **5**(3): p. 718-726.
392. Barry, J.J., et al., *Porous methacrylate scaffolds: supercritical fluid fabrication and in vitro chondrocyte responses.* Biomaterials, 2004. **25**(17): p. 3559-68.
393. Bartoš, M., T. Suchý, and R. Foltán, *Note on the use of different approaches to determine the pore sizes of tissue engineering scaffolds: what do we measure?* BioMedical Engineering OnLine, 2018. **17**(1): p. 110.
394. SCHLADITZ, K., *Quantitative micro-CT.* Journal of Microscopy, 2011. **243**(2): p. 111-117.
395. Ho, S.T. and D.W. Hutmacher, *A comparison of micro CT with other techniques used in the characterization of scaffolds.* Biomaterials, 2006. **27**(8): p. 1362-76.
396. Zidek, J., et al., *Accurate micro-computed tomography imaging of pore spaces in collagen-based scaffold.* Journal of Materials Science: Materials in Medicine, 2016. **27**(6): p. 110.
397. Sell, S., et al., *Scaffold permeability as a means to determine fiber diameter and pore size of electrospun fibrinogen.* J Biomed Mater Res A, 2008. **85**(1): p. 115-26.
398. Kolb, H.E., et al., *A critical analysis of capillary flow porometry with regard to ist application to non-woven fibrous filter media*. 2018, Vortrag gehalten auf International Conference and Exhibition for Filtration and Separation Technologies (FILTECH 2018), Köln, Deutschland, 13.–15. März 2018.
399. Erbe, F., *Die Bestimmung der Porenverteilung nach ihrer Größe in Filtern und Ultrafiltern.* Kolloid-Zeitschrift, 1933. **63**(3): p. 277-285.
400. Laemmli, U.K., *Cleavage of Structural Proteins during the Assembly of the Head of Bacteriophage T4.* Nature, 1970. **227**(5259): p. 680-685.
401. Smith, J.R., et al., *Standardizing Umbilical Cord Mesenchymal Stromal Cells for Translation to Clinical Use: Selection of GMP-Compliant Medium and a Simplified Isolation Method.* Stem Cells Int, 2016. **2016**: p. 6810980.
402. Dollinger, C., et al., *Controlling Incoming Macrophages to Implants: Responsiveness of Macrophages to Gelatin Micropatterns under M1/M2 Phenotype Defining Biochemical Stimulations.* Advanced Biosystems, 2017. **1**(6): p. 1700041.
403. *Biological evaluation of medical devices* in *Part 5:Tests for in vitro cytotoxicity*.
404. Vennat, E., et al., *Demineralized dentin 3D porosity and pore size distribution using mercury porosimetry.* Dent Mater, 2009. **25**(6): p. 729-35.
405. Celikkin, N., et al., *Gelatin methacrylate scaffold for bone tissue engineering: The influence of polymer concentration.* Journal of Biomedical Materials Research Part A, 2018. **106**(1): p. 201-209.
406. Yang, L., et al., *Influence of lyophilization factors and gelatin concentration on pore structures of atelocollagen/gelatin sponge biomaterial.* Dent Mater J, 2017. **36**(4): p. 429-437.
407. Sultana Phd Ceng Csci, N., M. Hassan, and M. Lim, *Fabrication and Characterization of Polymer and Composite Scaffolds Using Freeze-Drying Technique*. 2015. p. 45-60.
408. Hou, Q., D.W. Grijpma, and J. Feijen, *Preparation of interconnected highly porous polymeric structures by a replication and freeze-drying process.* Journal of Biomedical Materials Research Part B: Applied Biomaterials, 2003. **67B**(2): p. 732-740.

409. Woinet, B., J. Andrieu, and M. Laurent, *Experimental and theoretical study of model food freezing. Part I. Heat transfer modelling.* Journal of Food Engineering, 1998. **35**(4): p. 381-393.
410. Enrione, J., et al., *Designing a gelatin/chitosan/hyaluronic acid biopolymer using a thermophysical approach for use in tissue engineering.* Bioprocess and Biosystems Engineering, 2013. **36**(12): p. 1947-1956.
411. Zhang, F., et al., *Fabrication of gelatin–hyaluronic acid hybrid scaffolds with tunable porous structures for soft tissue engineering.* International Journal of Biological Macromolecules, 2011. **48**(3): p. 474-481.
412. Kang, X., et al., *Adipogenesis of murine embryonic stem cells in a three-dimensional culture system using electrospun polymer scaffolds.* Biomaterials, 2007. **28**(3): p. 450-458.
413. Kasten, P., et al., *Porosity and pore size of beta-tricalcium phosphate scaffold can influence protein production and osteogenic differentiation of human mesenchymal stem cells: an in vitro and in vivo study.* Acta Biomater, 2008. **4**(6): p. 1904-15.
414. Cho, S.-W., et al., *Smooth muscle-like tissues engineered with bone marrow stromal cells.* Biomaterials, 2004. **25**(15): p. 2979-2986.
415. Belyadi, H., E. Fathi, and F. Belyadi, *Chapter Eight - Hydraulic fracturing chemical selection and design*, in *Hydraulic Fracturing in Unconventional Reservoirs (Second Edition)*, H. Belyadi, E. Fathi, and F. Belyadi, Editors. 2019, Gulf Professional Publishing. p. 107-120.
416. Krokida, M.K., V.T. Karathanos, and Z.B. Maroulis, *Effect of freeze-drying conditions on shrinkage and porosity of dehydrated agricultural products.* Journal of Food Engineering, 1998. **35**(4): p. 369-380.
417. Zhao, X., et al., *Controlling the Pore Structure of Collagen Sponge by Adjusting the Cross-Linking Degree for Construction of Heterogeneous Double-Layer Bone Barrier Membranes.* ACS Applied Bio Materials, 2020. **3**(4): p. 2058-2067.
418. Vrana, N.E., et al., *Development of a reconstructed cornea from collagen-chondroitin sulfate foams and human cell cultures.* Invest Ophthalmol Vis Sci, 2008. **49**(12): p. 5325-31.
419. McKegney, M., I. Taggart, and M.H. Grant, *The influence of crosslinking agents and diamines on the pore size, morphology and the biological stability of collagen sponges and their effect on cell penetration through the sponge matrix.* J Mater Sci Mater Med, 2001. **12**(9): p. 833-44.
420. Long, H., et al., *PreparSation and characteristics of gelatin sponges crosslinked by microbial transglutaminase.* PeerJ, 2017. **5**.
421. Yang, G., et al., *Assessment of the characteristics and biocompatibility of gelatin sponge scaffolds prepared by various crosslinking methods.* Sci Rep, 2018. **8**(1): p. 1616.
422. Arfat, Y.A., et al., *Thermo-mechanical, rheological, structural and antimicrobial properties of bionanocomposite films based on fish skin gelatin and silver-copper nanoparticles.* Food Hydrocolloids, 2017. **62**: p. 191-202.
423. Bahmanzadeh, S., T. Ruzgas, and J. Sotres, *Proteolytic degradation of gelatin-tannic acid multilayers.* Journal of Colloid and Interface Science, 2018. **526**: p. 244-252.

424. Cao, N., Y. Fu, and J. He, *Mechanical properties of gelatin films cross-linked, respectively, by ferulic acid and tannin acid.* Food Hydrocolloids, 2007. **21**(4): p. 575-584.
425. Ruiz, J., A. Mantecón, and V. Cádiz, *States of water in poly(vinyl alcohol) derivative hydrogels.* Journal of Polymer Science Part B: Polymer Physics, 2003. **41**(13): p. 1462-1467.
426. Cushing, M.C. and K.S. Anseth, *Materials science. Hydrogel cell cultures.* Science, 2007. **316**(5828): p. 1133-4.
427. Khetan, S., et al., *Degradation-mediated cellular traction directs stem cell fate in covalently crosslinked three-dimensional hydrogels.* Nat Mater, 2013. **12**(5): p. 458-65.
428. Chen, Y.C., et al., *Functional Human Vascular Network Generated in Photocrosslinkable Gelatin Methacrylate Hydrogels.* Adv Funct Mater, 2012. **22**(10): p. 2027-2039.
429. Henderson, J.A., X. He, and E. Jabbari, *Concurrent differentiation of marrow stromal cells to osteogenic and vasculogenic lineages.* Macromol Biosci, 2008. **8**(6): p. 499-507.
430. Thompson, P.A., et al., *Effusion-associated anaplastic large cell lymphoma of the breast: time for it to be defined as a distinct clinico-pathological entity.* Haematologica, 2010. **95**(11): p. 1977-9.
431. Kang, H.G., S.Y. Kim, and Y.M. Lee, *Novel porous gelatin scaffolds by overrun/particle leaching process for tissue engineering applications.* J Biomed Mater Res B Appl Biomater, 2006. **79**(2): p. 388-97.
432. Schultz, K.M. and K.S. Anseth, *Monitoring degradation of matrix metalloproteinases-cleavable PEG hydrogels via multiple particle tracking microrheology.* Soft Matter, 2013. **9**(5): p. 1570-1579.
433. West, J.L. and J.A. Hubbell, *Polymeric Biomaterials with Degradation Sites for Proteases Involved in Cell Migration.* Macromolecules, 1999. **32**(1): p. 241-244.
434. Yang, G., et al., *Enzymatically crosslinked gelatin hydrogel promotes the proliferation of adipose tissue-derived stromal cells.* PeerJ, 2016. **4**: p. e2497.
435. Muller, C., et al., *Polyarginine Decorated Polydopamine Nanoparticles With Antimicrobial Properties for Functionalization of Hydrogels.* Frontiers in Bioengineering and Biotechnology, 2020. **8**(982).
436. Ciftci, S., et al., *Double thin film-based sandwich-cell carrier design for multicellular tissue engineering.* Materials & Design, 2016. **95**.
437. Wang, Y., et al., *Differences in cytocompatibility between collagen, gelatin and keratin.* Mater Sci Eng C Mater Biol Appl, 2016. **59**: p. 30-34.
438. Li, M., et al., *Electrospinning polyaniline-contained gelatin nanofibers for tissue engineering applications.* Biomaterials, 2006. **27**(13): p. 2705-2715.
439. Stevens, K.R., et al., *In vivo biocompatibility of gelatin-based hydrogels and interpenetrating networks.* J Biomater Sci Polym Ed, 2002. **13**(12): p. 1353-66.
440. Yang, G., et al., *Assessment of the characteristics and biocompatibility of gelatin sponge scaffolds prepared by various crosslinking methods.* Scientific Reports, 2018. **8**(1): p. 1616.
441. Ulubayram, K., et al., *Cytotoxicity evaluation of gelatin sponges prepared with different cross-linking agents.* J Biomater Sci Polym Ed, 2002. **13**(11): p. 1203-19.

442. DM, O.H., et al., *Characterization of a microbial transglutaminase cross-linked type II collagen scaffold.* Tissue Eng, 2006. **12**(6): p. 1467-74.
443. Kobayashi, K., et al., *Molecular cloning of the transglutaminase gene from Bacillus subtilis and its expression in Escherichia coli.* Biosci Biotechnol Biochem, 1998. **62**(6): p. 1109-14.
444. Yung, C.W., et al., *Transglutaminase crosslinked gelatin as a tissue engineering scaffold.* J Biomed Mater Res A, 2007. **83**(4): p. 1039-1046.
445. Glasstone, S., *Textbook of Physical Chemistry.* Macmillan and CO. Ltd. London, 1948. **Second ed.**
446. Chase, P.B., T.M. Denkinger, and M.J. Kushmerick, *Effect of viscosity on mechanics of single, skinned fibers from rabbit psoas muscle.* Biophysical journal, 1998. **74**(3): p. 1428-1438.
447. Cala, O., et al., *The Colloidal State of Tannins Impacts the Nature of Their Interaction with Proteins: The Case of Salivary Proline-Rich Protein/Procyanidins Binding.* Langmuir, 2012. **28**(50): p. 17410-17418.
448. Gime?nez-Marti?n, E., O.A.O. Ontiveros, and M. Espinosa-Jime?nez, *Improvement in Acrylic Fibres Dyeing*. 2011.
449. Tanimura, S., et al., *Suppression of tumor cell invasiveness by hydrolyzable tannins (plant polyphenols) via the inhibition of matrix metalloproteinase-2/-9 activity.* Biochem Biophys Res Commun, 2005. **330**(4): p. 1306-13.
450. Sakagami, H., et al., *Induction of apoptosis by flavones, flavonols (3-hydroxyflavones) and isoprenoid-substituted flavonoids in human oral tumor cell lines.* Anticancer Res, 2000. **20**(1a): p. 271-7.
451. Yang, L.L., C.Y. Lee, and K.Y. Yen, *Induction of apoptosis by hydrolyzable tannins from Eugenia jambos L. on human leukemia cells.* Cancer Lett, 2000. **157**(1): p. 65-75.
452. Chen, X., et al., *Tannic acid is an inhibitor of CXCL12 (SDF-1alpha)/CXCR4 with antiangiogenic activity.* Clinical cancer research : an official journal of the American Association for Cancer Research, 2003. **9**: p. 3115-23.
453. Cass, C.A. and K.J. Burg, *Tannic acid cross-linked collagen scaffolds and their anti-cancer potential in a tissue engineered breast implant.* J Biomater Sci Polym Ed, 2012. **23**(1-4): p. 281-98.
454. Borges, A., et al., *Antibacterial activity and mode of action of ferulic and gallic acids against pathogenic bacteria.* Microb Drug Resist, 2013. **19**(4): p. 256-65.
455. Lowy, F.D., *Staphylococcus aureus infections.* N Engl J Med, 1998. **339**(8): p. 520-32.
456. Zhai, C., et al., *The effect of cartilage extracellular matrix particle size on the chondrogenic differentiation of bone marrow mesenchymal stem cells.* Regen Med, 2019. **14**(7): p. 663-680.
457. Maroudas, N.G., *Anchorage dependence: Correlation between amount of growth and diameter of bead, for single cells grown on individual glass beads.* Experimental Cell Research, 1972. **74**(2): p. 337-342.
458. Gao, H., P.S. Ayyaswamy, and P. Ducheyne, *Dynamics of a microcarrier particle in the simulated microgravity environment of a rotating-wall vessel.* Microgravity Sci Technol, 1997. **10**(3): p. 154-65.

459. Yang, Q., et al., *A cartilage ECM-derived 3-D porous acellular matrix scaffold for in vivo cartilage tissue engineering with PKH26-labeled chondrogenic bone marrow-derived mesenchymal stem cells.* Biomaterials, 2008. **29**(15): p. 2378-87.
460. Almeida, H.V., et al., *Coupling Freshly Isolated CD44(+) Infrapatellar Fat Pad-Derived Stromal Cells with a TGF-β3 Eluting Cartilage ECM-Derived Scaffold as a Single-Stage Strategy for Promoting Chondrogenesis.* Adv Healthc Mater, 2015. **4**(7): p. 1043-53.
461. Edgar, L., et al., *Utility of extracellular matrix powders in tissue engineering.* Organogenesis, 2018. **14**(4): p. 172-186.
462. Zuo, H., et al., *Regeneration of mature dermis by transplanted particulate acellular dermal matrix in a rat model of skin defect wound.* J Mater Sci Mater Med, 2012. **23**(12): p. 2933-44.
463. Schiller, H.B., et al., *Time- and compartment-resolved proteome profiling of the extracellular niche in lung injury and repair.* Molecular Systems Biology, 2015. **11**(7): p. 819.
464. Naba, A., K.R. Clauser, and R.O. Hynes, *Enrichment of Extracellular Matrix Proteins from Tissues and Digestion into Peptides for Mass Spectrometry Analysis.* Journal of visualized experiments : JoVE, 2015(101): p. e53057-e53057.
465. Ma, F., et al., *Surfactant and Chaotropic Agent Assisted Sequential Extraction/On-Pellet Digestion (SCAD) for Enhanced Proteomics.* J Proteome Res, 2018. **17**(8): p. 2744-2754.
466. Epstein, E.H., Jr. and N.H. Munderloh, *Isolation and characterization of CNBr peptides of human (alpha 1 (III))3 collagen and tissue distribution of (alpha 1 (I))2 alpha 2 and (alpha 1 (III))3 collagens.* Journal of Biological Chemistry, 1975. **250**(24): p. 9304-9312.
467. Barrett, A.S., et al., *Hydroxylamine Chemical Digestion for Insoluble Extracellular Matrix Characterization.* Journal of Proteome Research, 2017. **16**(11): p. 4177-4184.
468. Weber, P., H. Steinhart, and A. Paschke, *Characterization, antigenicity and detection of fish gelatine and isinglass used as processing aids in wines.* Food Additives & Contaminants: Part A, 2010. **27**(3): p. 273-282.
469. Cole, C.G.B.a.R., J. J, *The presence of polypeptide bands with molecular weight less than α-chain in PSS gelatin were in good agreement with Cole and Roberts* Journal of Leather Technologists and Chemists 1996. **80**: p. 136-141.
470. Tukiran, N., I. Amin, and Y. Man, *Differentiation of bovine and porcine gelatins in processed products via sodium dodecyl sulphate-polyacrylamide gel electrophoresis (SDS-PAGE) and principal component analysis (PCA) techniques.* international food research journal, 2012. **19**: p. 1175-1180.
471. Beiki, B., B. Zeynali, and E. Seyedjafari, *Fabrication of a three dimensional spongy scaffold using human Wharton's jelly derived extra cellular matrix for wound healing.* Materials Science and Engineering: C, 2017. **78**: p. 627-638.
472. Hellewell, A., S. Rosini, and J. Adams, *A Rapid, Scalable Method for Isolation, Functional Study and Analysis of Cell-Derived Extracellular Matrix.* Journal of Visualized Experiments, 2017. **2017**.

473. Uma, B., et al., *Nanoparticle Brownian motion and hydrodynamic interactions in the presence of flow fields.* Physics of fluids (Woodbury, N.Y. : 1994), 2011. **23**(7): p. 73602-7360215.
474. Deville, S., et al., *Freezing as a path to build complex composites.* Science, 2006. **311**(5760): p. 515-8.
475. Mandal, B.B. and S.C. Kundu, *Cell proliferation and migration in silk fibroin 3D scaffolds.* Biomaterials, 2009. **30**(15): p. 2956-65.
476. Almeida, H.V., et al., *Coupling Freshly Isolated CD44(+) Infrapatellar Fat Pad-Derived Stromal Cells with a TGF-β3 Eluting Cartilage ECM-Derived Scaffold as a Single-Stage Strategy for Promoting Chondrogenesis.* Advanced healthcare materials, 2015. **4**(7): p. 1043-1053.
477. Tsuchiya, S., et al., *Establishment and characterization of a human acute monocytic leukemia cell line (THP-1).* Int J Cancer, 1980. **26**(2): p. 171-6.
478. Franz, S., et al., *Immune responses to implants – A review of the implications for the design of immunomodulatory biomaterials.* Biomaterials, 2011. **32**(28): p. 6692-6709.
479. Sridharan, R., et al., *Biomaterial based modulation of macrophage polarization: a review and suggested design principles.* Materials Today, 2015. **18**(6): p. 313-325.
480. Mantovani, A., et al., *Macrophage plasticity and polarization in tissue repair and remodelling.* The Journal of Pathology, 2013. **229**(2): p. 176-185.
481. Mantovani, A., et al., *The chemokine system in diverse forms of macrophage activation and polarization.* Trends Immunol, 2004. **25**(12): p. 677-86.
482. Koh, T.J. and L.A. DiPietro, *Inflammation and wound healing: the role of the macrophage.* Expert Reviews in Molecular Medicine, 2011. **13**: p. e23.
483. Martinez, F.O., et al., *Macrophage activation and polarization.* Frontiers in Bioscience-Landmark, 2008. **13**(2): p. 453-461.
484. Mosser, D.M. and J.P. Edwards, *Exploring the full spectrum of macrophage activation.* Nature Reviews Immunology, 2008. **8**(12): p. 958-969.
485. Brown, B.N., et al., *Macrophage phenotype as a predictor of constructive remodeling following the implantation of biologically derived surgical mesh materials.* Acta Biomaterialia, 2012. **8**(3): p. 978-987.
486. Adutler-Lieber, S., et al., *Engineering of synthetic cellular microenvironments: Implications for immunity.* Journal of Autoimmunity, 2014. **54**: p. 100-111.
487. Brown, B.N., et al., *Macrophage polarization: An opportunity for improved outcomes in biomaterials and regenerative medicine.* Biomaterials, 2012. **33**(15): p. 3792-3802.
488. Lo, Y.-P., et al., *Three-dimensional spherical spatial boundary conditions differentially regulate osteogenic differentiation of mesenchymal stromal cells.* Scientific Reports, 2016. **6**(1): p. 21253.
489. Scheller, J., et al., *The pro- and anti-inflammatory properties of the cytokine interleukin-6.* Biochim Biophys Acta, 2011. **1813**(5): p. 878-88.
490. Lin, C.S., G. Lin, and T.F. Lue, *Allogeneic and xenogeneic transplantation of adipose-derived stem cells in immunocompetent recipients without immunosuppressants.* Stem Cells Dev, 2012. **21**(15): p. 2770-8.
491. Lin, Z.Q., et al., *Essential involvement of IL-6 in the skin wound-healing process as evidenced by delayed wound healing in IL-6-deficient mice.* J Leukoc Biol, 2003. **73**(6): p. 713-21.

492. Martin, D., R. Galisteo, and J.S. Gutkind, *CXCL8/IL8 stimulates vascular endothelial growth factor (VEGF) expression and the autocrine activation of VEGFR2 in endothelial cells by activating NFkappaB through the CBM (Carma3/Bcl10/Malt1) complex.* J Biol Chem, 2009. **284**(10): p. 6038-42.
493. Hou, Y., et al., *IL-8 enhances the angiogenic potential of human bone marrow mesenchymal stem cells by increasing vascular endothelial growth factor.* Cell Biol Int, 2014. **38**(9): p. 1050-9.